CRYPTIC ANTIMICROBIAL PEPTIDES HIDDEN IN PROTEIN PRECURSORS: IDENTIFICATION OF NOVEL BIOACTIVE MOLECULES

Rosa Gaglione

Dottorato in Scienze Biotecnologiche 29° ciclo

Università di Napoli Federico II

Dottorato in Scienze Biotecnologiche 29° ciclo

Università di Napoli Federico II

CRYPTIC ANTIMICROBIAL PEPTIDES HIDDEN IN PROTEIN PRECURSORS: IDENTIFICATION OF NOVEL BIOACTIVE MOLECULES

Rosa Gaglione

Dottorando: Rosa Gaglione

Relatore: Prof.ssa Renata Piccoli

Correlatore: Dott.ssa Angela Arciello

Coordinatore: Prof. Giovanni Sannia

A coloro che hanno
sempre creduto in me,
ancor prima che ci credessi io:
la mia famiglia.

INDEX

ABSTRACT

Antibiotics are the mainstay in treatment of bacterial infections. However, resistance to antibacterial treatments has been rising since the 1970s, causing serious problems in the treatment and control of infectious diseases. Antibiotic resistance is now considered as one of the major global health threats of the 21st century in that the worldwide use of antibiotics is predicted to increase by more than 65% in the coming decades due to the increasing demand for meat and shift in agriculture practices in developing countries. New antibacterial drugs are urgently needed, but only three antibacterial drugs have been brought to the market since 1999 and very few new antibiotics are currently in development. This has prompted the search for alternatives to conventional antibiotics. Multiple alternative anti-infective strategies are being investigated, including vaccines, probiotics and phage therapy. Other promising alternatives to antibiotics are host defense peptides (HDPs), an important component of the first line of defense against infection, found in all multicellular organisms. HDPs are seen as true multifunctional peptides with activities as diverse as chemotaxis, inhibition of LPS-induced inflammation, modulation of leukocyte differentiation and promotion of wound healing. Interestingly, novel functions of these peptides are still being described to date. Many human proteins with functions not necessarily related to host defense behave as sources of HDPs. Some examples are lactoferrin, lysozyme and thrombin. Since these peptides are hidden in large proteins, they can be defined as “cryptic”. In order to identify by a rational approach further human proteins carrying cryptic HDPs, we recently developed an *in-silico* screening method to localize antimicrobial regions hidden inside the primary structure of precursor proteins. A wide list of potential new antimicrobial peptides was obtained by applying this method to about 4,000 human extracellular proteins.
The main aim of this PhD project was the identification of interesting potential HDPs, to develop novel bioactive peptides. Firstly, we developed a novel and cost-effective method to produce recombinant HDPs, based on the use a cheap and efficient medium to be employed in an auto-inducing fermentation process. Furthermore, to avoid HDPs toxicity towards bacterial host, a novel fusion system based on a carrier protein (derived from a *Rana pipiens* ribonuclease) was used. Once optimized the production system, a broad characterization of two novel recombinant peptides, previously identified in human Apolipoprotein B (ApoB), was performed. We demonstrated that both peptides are endowed with a significant antimicrobial activity towards Gram-negative and Gram-positive strains, and are able to prevent biofilm formation in several strains at concentrations lower than those required to directly kill planktonic bacterial cells. Moreover, ApoB-derived peptides were found to be endowed with anti-inflammatory properties as well as the ability to promote wound healing in keratinocytes. In addition, two further cryptic HDPs have been structurally and functionally characterized. One of these HDPs has been identified in human 11-hydroxysteroid dehydrogenase-1 β-like, the other represents the first HDP from an archaeal protein, the transcription factor Stf76 encoded by the hybrid plasmid-virus pSSVx from *Sulfolobus islandicus.* By means of a multidisciplinary approach including biochemical, cellular biology and spectroscopic techniques, the action mechanism of both peptides has been elucidated, and intriguing results have been obtained by testing their immunomodulatory and anti-cancer activities. Hence, the *in silico*-derived panel of potential HDPs is a rich source of peptides with pharmacologically relevant properties.

RIASSUNTO

Negli ultimi decenni lo smisurato ed incauto uso di antibiotici per fini terapeutici, agro-alimentari e veterinari ha determinato la progressiva diffusione di ceppi batterici resistenti agli antibiotici convenzionali. Si è stimato che più del 70% delle infezioni batteriche che colpiscono gli esseri umani sono caratterizzate da fenomeni di resistenza ai farmaci, ciò che le rende un grave problema per la salute umana, come evidenziato nel rapporto dell'Agenzia Mondiale della Sanità (2015). Negli ultimi decenni a suscitare maggiore preoccupazione sono stati i ceppi resistenti alla meticillina o alla vancomicina appartenenti al genere *Staphylococcus* oltre che batteri Gram-negativi appartenenti ai generi *Escherichia*, *Pseudomonas* e *Acinetobacter*.
Tale fenomeno ha stimolato un'intensa ricerca di nuove classi di antibiotici che garantisca un'efficacia duratura nel tempo. Di recente, l'interesse scientifico si è focalizzato sui cosiddetti cAMPs (*cationic Anti Microbial Peptides*), peptidi dotati di un'attività antimicrobica ad ampio spettro, dal momento che sono attivi contro batteri Gram-positivi e Gram-negativi, ma anche contro funghi, virus e protozoi. Tali peptidi sono prodotti da un'ampia gamma di organismi tra cui batteri, piante, insetti, anfibi e mammiferi. L'ampia distribuzione dei cAMPs sia nel regno animale che vegetale ha fatto ipotizzare un loro ruolo fondamentale nel successo evolutivo degli organismi multicellulari; essi, infatti, sono considerati una delle più antiche "armi" della risposta immunitaria innata. Inizialmente identificati sulla base della loro attività antimicrobica ad ampio spettro, essi hanno suscitato sempre più attenzione anche per gli interessanti ruoli fisiologici che rivestono nella modulazione della risposta immunitaria. Per tale motivo sono oggi definiti, in senso più ampio, peptidi della difesa dell'ospite (*Host Defense Peptides*, HDPs). Tutti i peptidi antimicrobici naturali hanno origine da precursori proteici in seguito a modifiche post-traduzionali comprendenti quasi sempre un evento proteolitico e, in alcuni casi, glicosilazione e amidazione carbossi-terminale.
La maggior parte dei peptidi antimicrobici appartiene ad una delle seguenti classi strutturali: (i) peptidi con struttura ad alfa-elica, privi di residui di cisteina; (ii) peptidi globulari con struttura beta stabilizzata da ponti disolfurici intramolecolari; (iii) peptidi caratterizzati da un'insolita abbondanza di specifici amminoacidi, quali istidina, glicina, prolina o triptofano. Nonostante la struttura primaria e secondaria e la lunghezza (12-50 amminoacidi) dei peptidi antimicrobici naturali possano essere molto diverse, essi condividono proprietà chimico-fisiche, quali la carica netta positiva (compresa tra +2 e +7 a pH 7) conferita dalla presenza di un elevato numero di residui basici e l'esposizione di regioni idrofobiche. Tali proprietà sono alla base del loro peculiare meccanismo d'azione. Infatti, la principale differenza tra gli HDPs e la maggior parte degli antibiotici convenzionali risiede nel "bersaglio molecolare" della loro azione. Gli antibiotici convenzionali agiscono su specifiche macromolecole (ribosomi, enzimi, DNA), mentre i peptidi antimicrobici agiscono a livello delle membrane batteriche (interna e/o esterna). Le basi molecolari del meccanismo di azione degli HDPs non sono del tutto chiare, sebbene si ritenga che le due caratteristiche molecolari comuni a tutti gli HDPs, cationicità ed anfipaticità, siano alla base della loro attività biologica. In particolare, evidenze sperimentali indicano che l'interazione primaria tra i peptidi e le cellule bersaglio è mediata dalla carica netta dei peptidi e che la loro selettività di azione sia da attribuire alla differente composizione delle membrane cellulari procariotiche ed eucariotiche.

La membrana batterica presenta, infatti, un'elevata percentuale di fosfolipidi acidi su entrambi i lati, quali cardiolipina e fosfatidilglicerolo, che conferiscono una carica negativa a queste superfici. Anche nel caso dei batteri Gram-negativi, la membrana più esterna è carica negativamente, dal momento che contiene lipopolissaccaridi anionici (LPS). Nel caso della membrana plasmatica delle cellule eucariotiche, invece, i fosfolipidi carichi negativamente sono quasi sempre localizzati sulla superficie interna, mentre sulla superficie esterna sono presenti fosfolipidi zwitterionici, quali fosfatidilcolina e fosfatidiletanolammina. Inoltre, la membrana delle cellule eucariotiche è ricca di colesterolo che, conferendole rigidità, la rende non suscettibile all'attacco dei peptidi.
Diversi modelli sono stati proposti per spiegare l'attività biologica dei peptidi antimicrobici, i quali sono in grado di instaurare una interazione elettrostatica con i fosfolipidi anionici della membrana batterica e di adottare poi una conformazione anfipatica che consente loro di inserirsi nella membrana. Si innescano così una serie di eventi che compromettono le funzioni fisiologiche della membrana (alterazioni di fluidità, di spessore, di permeabilità selettiva, ecc.). Alcuni peptidi, tuttavia, sono in grado di esplicare un meccanismo di azione differente e, una volta attraversata la membrana, attaccano bersagli intracellulari. È questo il caso della buforina II, in grado di legare il DNA.
Tra i modelli proposti per spiegare il meccanismo di azione dei cAMPs, il modello "*barrel-stave*" prevede che le regioni idrofobiche del peptide interagiscano con le catene idrocarburiche dei fosfolipidi di membrana formando un poro, la cui superficie interna è costituita dalle regioni idrofiliche del peptide. Tale modello si applica solo ad un numero di casi molto ristretto. Vi è poi il modello "*toroidal*" o "*worm-hole*" che sembra rappresentare il meccanismo di azione della maggior parte dei peptidi. Tale modello prevede l'associazione dei peptidi con i gruppi esposti dei fosfolipidi di membrana, ciò che provoca una curvatura del doppio strato lipidico a livello del poro. In questo caso, quindi, la superficie interna del canale sarà costituita sia dai peptidi sia dai gruppi esposti dei fosfolipidi di membrana. Un altro modello, noto come "*carpet*", prevede che i peptidi si dispongano parallelamente alla superficie della membrana rivestendola come un "tappeto". Una volta che la concentrazione dei peptidi ha superato un valore soglia, essi determinano poi la distruzione della membrana grazie alla formazione di micelle o piccoli aggregati peptidolipidici. Le modalità con cui i peptidi antimicrobici attraversano la capsula polisaccaridica della membrana esterna dei batteri Gram-negativi o la parete di peptidoglicano dei Gram-positivi restano, invece, ancora ignote.
Grazie al peculiare meccanismo di azione dei cAMPs, è improbabile che i batteri possano sviluppare una completa resistenza ai peptidi; ciò, infatti, richiederebbe un sostanziale cambiamento nella composizione di membrana ed implicherebbe "costi" metabolici troppo elevati per i batteri. Basti pensare che le membrane batteriche sono coinvolte in ruoli metabolici fondamentali, quali le catene di trasporto degli elettroni e la produzione di ATP.
Oltre all' attività antimicrobica diretta, gli HDPs fungono anche da molecole ponte tra i meccanismi dell'immunità innata e quella acquisita. Alcuni noti peptidi antimicrobici umani, come *α*- e *β*-defensine ed LL-37, l'unica catelicidina umana, oltre ad essere efficaci come antimicrobici, sono anche dotati di diverse proprietà immunomodulanti. Ad esempio, essi sono in grado di reclutare le cellule effettrici dell'immunità innata nei siti di infezione (chemiotassi dei macrofagi) ed attivare le cellule specializzate coinvolte nei meccanismi dell'immunità adattativa (cellule dendritiche immature, cellule T immature). Inoltre, alcuni peptidi cationici sono stati proposti come agenti

antitumorali, in virtù del loro ridotto peso molecolare, della struttura relativamente semplice, del basso rischio di indurre resistenza e della specificità di azione verso le cellule tumorali stesse. Il carattere cationico e anfipatico dei peptidi gli consente, infatti, di legare ed invadere le cellule tumorali, portando alla rapida distruzione delle membrane e alla fuoriuscita del contenuto intracellulare, con conseguente attivazione dei meccanismi che mediano la morte cellulare. Essi possono anche funzionare in sinergia con i farmaci anti-cancro convenzionali e/o con altre potenziali molecole antitumorali, contribuendo a migliorare l'esito della terapia.

Ogni specie possiede una specifica ed ampia collezione di peptidi antimicrobici, il cui ruolo è quello di difendere l'organismo dai microbi con cui potrebbe entrare in contatto. Questi peptidi sono localizzati principalmente nei tessuti bersaglio dell'attacco dei microbi, quali gli epiteli. Le piante producono varie classi di peptidi antimicrobici, inclusi i membri della famiglia delle defensine e le tionine. Anche nelle piante, gli HDPs sono costitutivamente presenti in organi sensibili ad infezioni (principalmente fiore e seme), ma la loro espressione può anche essere indotta in seguito all'attacco di un patogeno, in un primo momento nel sito di infezione e successivamente in maniera sistemica. Gli organismi invertebrati, quali insetti e molluschi, sono privi di immunità adattativa e devono quindi disporre di un'efficiente immunità innata. Negli insetti, l'espressione di peptidi antimicrobici è inducibile nel corpo grasso (l'equivalente funzionale del fegato), il quale secerne HDPs nell'emolinfa circolante. L'espressione dei peptidi antimicrobici è, invece, costitutiva nelle cellule epiteliali. Nei molluschi, gli HDPs sono prodotti nelle cellule del sangue e sono presenti ad elevate concentrazioni nell'organismo anche in assenza di uno stimolo esterno. I mammiferi dispongono di un vasto repertorio di peptidi antimicrobici, caratterizzato da uno specifico *pattern* di espressione. La loro espressione può essere, infatti, costitutiva o, più frequentemente, indotta da infiammazioni, danni o lesioni. I peptidi sono, in genere, prodotti come *cocktails* ed ogni tessuto possiede il proprio archivio di differenti peptidi che si delinea sulla base delle specifiche condizioni fisiologiche.

I prototipi umani di HDPs sono le defensine e le catelicidine, principalmente prodotte dai leucociti e dalle cellule epiteliali. Le defensine sono caratterizzate da una struttura prevalentemente β, dalla presenza di 6 ponti disolfurici e da una carica netta positiva. Esse si suddividono in 2 principali sub-famiglie: α- e β-defensine. Entrambe sono dotate di un'attività antibatterica ad ampio spettro e di attività antifungina ed antivirale, associate ad un'efficiente attività immunomodulatoria. Un'altra nota classe di HDPs umani è rappresentata dalle catelicidine, ampiamente diffuse nei mammiferi. Nell'uomo è presente una sola catelicidina a struttura α-elicoidale (LL-37), derivata dal processamento proteolitico della proteasi 3 dei neutrofili. LL-37 svolge numerose funzioni immunomodulatorie e gioca, infatti, un ruolo chiave nella salute umana.

Diversi HDPs umani, inoltre, giocano un ruolo di difesa chiave a livello della pelle. Tra questi, si annoverano la dermicidina e la psoriasina. La prima è costitutivamente secreta dalle ghiandole sudoripare e conserva la sua attività antimicrobica anche ad elevate concentrazioni saline o a bassi valori di pH. La psoriasina è stata isolata per la prima volta dai cheratinociti dell'epidermide psoriasica. In tale condizione patologica, la psoriasina ed altri peptidi antimicrobici sono prodotti ad alti livelli. Ciò spiega la bassa predisposizione dei pazienti affetti da psoriasi alle infezioni della pelle. Negli individui sani, la psoriasina è prodotta principalmente in aree della pelle ad alta densità batterica, quali le parti superiori dei follicoli del capello, il naso e il palmo della mano. Tale peptide presenta siti di legame per gli ioni zinco e calcio e attacca specificamente *E. coli* flagellato mediante un meccanismo non

membranolitico. Questa specificità di azione esemplifica l'abilità del sistema immunitario innato di discriminare tra microrganismi potenzialmente dannosi e commensali. In alternativa, la psoriasina è anche in grado di formare pori nella membrana di batteri Gram-positivi. Tale attività è risultata fortemente dipendente dal valore di pH, essendo ottimale ad un valore di pH al di sotto di 6, caratteristico della pelle umana.

Negli ultimi anni in letteratura sono state descritte numerose proteine eucariotiche con funzioni non strettamente legate alla difesa dell'ospite, ma che agiscono da "contenitori" o "vettori" di peptidi antimicrobici. Secondo un modello molto suggestivo, quando tali proteine vengono a contatto con i batteri, l'azione delle proteasi batteriche, eventualmente combinata a quella di proteasi dell'ospite, consentirebbe il rilascio di regioni che, una volta libere dai vincoli conformazionali della proteina nativa, diventerebbero dei veri e propri HDPs.

Uno degli esempi meglio descritti in letteratura è rappresentato dalla lattoferrina, una glicoproteina dei mammiferi presente soprattutto nel latte materno, ma anche in altre secrezioni, quali lacrime e saliva. La lattoferrina appartiene alla famiglia della transferrina ed esplica la sua attività antimicrobica agendo come potente chelante del ferro, un nutriente essenziale per i microrganismi. La lattoferrina possiede anche un'attività antimicrobica non correlata alla chelazione del ferro, destinata principalmente a proteggere i neonati dalle infezioni del sistema digerente. Nello stomaco del neonato, infatti, tale proteina viene idrolizzata dalla pepsina, ciò che determina il rilascio di un peptide di 25 residui amminoacidici denominato "lactoferricina", il quale rappresenta un potente peptide antimicrobico. La lactoferricina è un antimicrobico più attivo di quanto non lo sia la lattoferrina stessa e i peptidi da essa derivati esplicano anche un'azione antivirale nelle fasi precoci dell'infezione. È stato, inoltre, dimostrato che tali peptidi svolgono un'azione antitumorale, dal momento che promuovono l'apoptosi nelle cellule cancerose.

Un altro esempio ben noto in letteratura è rappresentato dal lisozima di pollo (*Gallus gallus*), una proteina dotata di una potente attività antimicrobica, dal momento che è in grado di idrolizzare il peptidoglicano e quindi di danneggiare la parete dei batteri, principalmente di quelli Gram-positivi. Diversi studi hanno dimostrato che la denaturazione termica della proteina ne abolisce l'attività enzimatica, ma non quella antimicrobica. Studi successivi hanno dimostrato, inoltre, che vari peptidi rilasciati dall'azione della pepsina sul lisozima si comportano come HDPs.

Anche numerosi membri della superfamiglia delle ribonucleasi (RNasi) da vertebrati sono risultati dotati di attività battericida non dipendente dalla loro attività catalitica o dalla loro struttura tridimensionale. Gli esempi meglio noti sono la ribonucleasi ECP (*Eosinophil Cationic Protein*), la RNasi A-2 da linfociti di pollo e le RNasi Zf-1, -2 e -3 da *Zebrafish* (*Danio rerio*). Sia nel caso dell'ECP che della RNasi A-2, è stato dimostrato che corti frammenti (10-30 amminoacidi) possiedono un'attività antimicrobica simile a quella della proteina nativa. Nel caso della RNasi Zf-3, l'attività antimicrobica è risultata associata alla regione C-terminale della proteina, la quale viene rilasciata in seguito ad un evento proteolitico operato dalla proteasi della membrana esterna degli enterobatteri (OmpT).

Preliminarmente alle attività descritte nel presente progetto di dottorato, è stato sviluppato dal Dott. Notomista un metodo bioinformatico che consente di localizzare regioni antimicrobiche in precursori proteici e di fornire una predizione quantitativa dell'attività antibatterica ad esse associata. Ciò ha consentito di identificare con un approccio razionale peptidi "criptici" presenti nel secretoma umano. Sono state così

analizzate circa 4,000 proteine extracellulari umane ed è stata creata una lista di potenziali HDPs.
Il presente progetto di dottorato si colloca in una vasta linea di ricerca il cui obiettivo principale è la produzione e la caratterizzazione dei più interessanti HDPs identificati mediante metodo bioinformatico. I primi HDPs ad essere prodotti commercialmente come agenti anti-infettivi, sono state le gramicidine prodotte da *Bacillus brevis* che sono state utilizzate come antibiotici per applicazioni topiche. Altri esempi sono rappresentati da peptidi approvati nell'industria alimentare come conservanti naturali o integratori alimentari, come la nisina, approvato dal 1969 e la lattoferrina aggiunto alla formula del latte per neonati. Il fine ultimo di questo progetto è, quindi, quello di selezionare candidati ideali per lo sviluppo di nuovi agenti antimicrobici ed anti-infiammatori per uso topico, impiegabili nel trattamento di ferite chirurgiche, ulcere cutanee e delle mucose o nell'industria alimentare come conservanti alimentari. In tale contesto, l'Apolipoproteina B (ApoB) è stata identificata come un nuovo precursore proteico di HDPs umani. In particolare, sono state identificate due brevi sequenze amminoacidiche dalla putativa azione antimicrobica (regione 887-922), denominate $ApoB_L$ ed $ApoB_S$ per indicare, rispettivamente, una porzione lunga (*long*) di 37 amminoacidi ed una corta (*short*) di 25 amminoacidi. Nel corso del presente progetto di ricerca, questi due nuovi HDPs sono stati caratterizzati per la loro attività antimicrobica, anti-biofilm, anti-infiammatoria, la loro capacità di agire in sinergia con gli antibiotici convenzionali e l'EDTA e la loro attività di wound healing. Inoltre, è stata condotta una caratterizzazione strutturale e funzionale del primo HDP identificato in una proteina archeobatterica (una *DNA-binding protein* da *Sulfolobus islandicus*) e di un peptide identificato nella 11 beta-idrossisteroide deidrogenasi umana. Per entrambi i peptidi, è stata effettuata un'approfondita caratterizzazione chimico-fisica ed è stata dimostrata un'attività antibatterica ad ampio spettro. Sono state, inoltre, messe in evidenza interessanti capacità immunomodulanti e antitumorali.
Gli obiettivi del presente progetto di dottorato possono essere riassunti in due punti fondamentali:
1) ottimizzazione di un sistema di espressione ricombinante di peptidi antimicrobici, ciò che ha previsto la messa a punto di una strategia fermentativa su larga scala da impiegare a livello industriale per la produzione di peptidi antimicrobici di interesse biotecnologico;
2) la caratterizzazione funzionale completa di peptidi HDPs identificati mediante metodo bioinformatico, quali due HDPs identificati nell'Apolipoproteina B umana e due nuovi HDPs identificati, rispettivamente, nel fattore di trascrizione Stf76 di *Sulfolobus islandicus* e nella 11 beta-idrossisteroide deidrogenasi umana.
Lo sviluppo di un sistema di espressione di peptidi tossici in *E. coli* può rappresentare una valida ed economica alternativa alle strategie di sintesi chimica attualmente disponibili. Per tale motivo, in prima battuta, si è proceduto ad ottimizzare le condizioni colturali di *E. coli* puntando sullo sviluppo di un mezzo di coltura costituito da componenti economici e facilmente reperibili. Dal momento che la procedura sperimentale prevede l'accumulo della proteina di interesse nei corpi di inclusione, è stato messo a punto un mezzo di coltura ricco e quindi in grado di sostenere la formazione di grandi quantità di biomassa. È stata, inoltre, privilegiata una fonte di carbonio economica, quale il triptone. L'impiego di glucosio ha anche consentito di minimizzare l'espressione basale nella fase di crescita delle cellule batteriche. E' stata anche messa a punto una procedura di auto-induzione, basata sull'impego di lattosio quale valida ed economica alternativa all'IPTG, come riportato

in letteratura per l'espressione eterologa di geni clonati in vettori pET per fermentazioni *fed-batch* in sistemi "*high-cell density*".
Nell'ottica di rendere il processo economico ed applicabile su larga scala, va anche segnalata l'economicità della strategia di purificazione del costrutto chimerico di interesse. Infatti, la presenza di un sito amminoacidico acido labile Asp-Pro, interposto tra la proteina *carrier* (onconasi) ed il peptide di interesse, consente di ottenere un'efficiente separazione mediante idrolisi acida selettiva, evitando così l'impiego di costose proteasi, ciò che è classicamente previsto in tali strategie sperimentali.
La caratterizzazione funzionale completa dei peptidi oggetto del presente progetto di dottorato, ha riguardato l'analisi delle loro proprietà antimicrobiche, anti-biofilm ed immunomodulanti ed è stata in parte svolta durante il periodo di ricerca (6 mesi) nel gruppo diretto dal Prof. Henk P. Haagsman, presso la *Faculty of Veterinary Medicine, Utrecht University, The Netherlands*. L'esperienza di tale gruppo nel campo della caratterizzazione dei peptidi bioattivi è ben nota. I risultati ottenuti hanno mostrato che i peptidi in esame sono dotati di attività antimicrobica ad ampio spettro. È risultato, inoltre, molto interessante che i peptidi siano risultati in grado di esplicare attività anti-biofilm a concentrazioni significativamente più basse di quelle necessarie per ottenere effetti su cellule batteriche allo stato planctonico. Ciò riveste particolare importanza se si considera che l'80% delle malattie infettive croniche umane sono causate da batteri patogeni capaci di formare biofilm. Solo agenti battericidi in grado di agire in maniera specifica su cellule in stato stazionario o in lenta divisione, quali gli HDPs, possono risultare in grado di eradicare completamente il biofilm. In tale contesto appaiono fortemente promettenti "terapie combinate" basate sulla somministrazione di formulazioni di peptidi e antibiotici convenzionali. Allo scopo di valutare l'efficacia di tale approccio combinatorio, sono stati condotti studi di sinergia utilizzando combinazioni dei peptidi in esame con i più noti antibiotici convenzionali. Sono stati così dimostrati effetti sinergici sulla maggioranza dei ceppi saggiati, inclusi ceppi caratterizzati da un fenotipo di resistenza agli antibiotici classici.
Nel complesso, i dati sperimentali ottenuti danno rilevanza all'effettivo impiego di questi peptidi per svariate applicazioni in ambito biotecnologico. Gli HDPs, infatti, trovano già impiego nell'industria alimentare come conservanti alimentari o come arma per abbattere l'impiego di antibiotici in allevamenti a scopo alimentare. Basti pensare alla nisina o alla lattoferrina presente nel latte in polvere. Inoltre, in ambito cosmetico, numerosi studi riportano dati sul loro potenziale quali componenti di formulazioni ad uso topico. Per quanto riguarda l'ambito clinico, ad oggi, numerosi HDPs sono in fase di studio pre-clinico e clinico, quale valida alternativa agli antibiotici convenzionali.

CHAPTER 1

General Introduction

Rosa Gaglione

Department of Chemical Sciences, PhD in Biotechnology

University of Naples "Federico II", Napoli, Italy

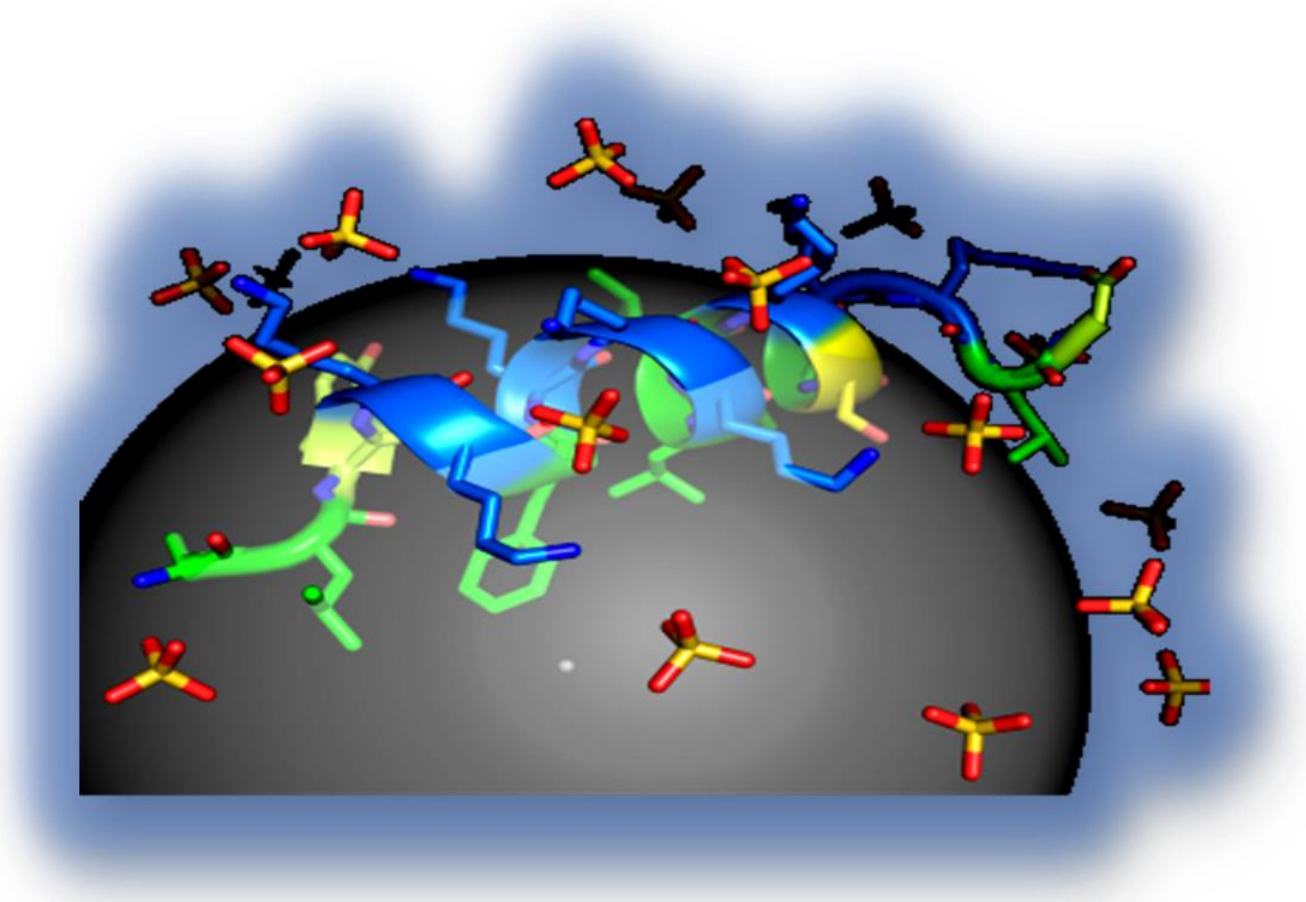

Antibiotic Resistance

The discovery of penicillin opened a new era in the treatment of infectious diseases, which was described as the “golden age” of antibiotic research (1940–1962) [1]. This was rapidly followed by the discovery of other antimicrobials, including widely used antibiotics, such as streptomycin, chloramphenicol, and tetracycline. For the first time, many common bacterial diseases could be cured. The first antibiotics played a crucial role in the treatment and prevention of infections during World War II [2]. Antibiotics were so successful that they were considered the ultimate cure, the “miracle drugs” that the medical world was craving. As a result of the initial success of antibiotics, bacterial diseases were naively considered to be permanently defeated. However, the excessive and unneeded use of antibiotics led to the development of more and more pathogenic bacteria resistant to their inhibitory effects [3]. Hence, despite their initial effectiveness, most antibiotics have a limited life, and their efficacy is compromised by the selection of pathogens endowed with intrinsic or acquired resistance mechanisms [4]. Currently, antimicrobial resistance threatens the effective prevention and treatment of an ever-expanding range of infections. It is an increasingly serious threat to global public health that requires immediate action, since it affects all parts of the world as new resistance mechanisms emerge and rapidly spread around the globe [5].

To clarify the molecular bases of the development of antibiotic resistance phenotype, in recent years, scientists focused their attention on the comprehension of the intra- and inter-cellular processes that govern bacterial ecology. Far from being isolated cells, bacteria might be more appropriately viewed as disseminated multicellular organisms, whose interactions are mediated by complex cell-cell signaling [6, 7]. Cell-cell interactions can lead to the formation of spatially complex matrices composed by polysaccharide and extracellular DNA, and embedding bacterial cells that consequently form a biofilm community [8]. In this scenario, to combat bacterial infections, a deeper understanding of bacteria intracellular genetics and biochemistry is needed, as well as the comprehension of biofilm effects on antibiotic uptake and resistance (Figure 1).

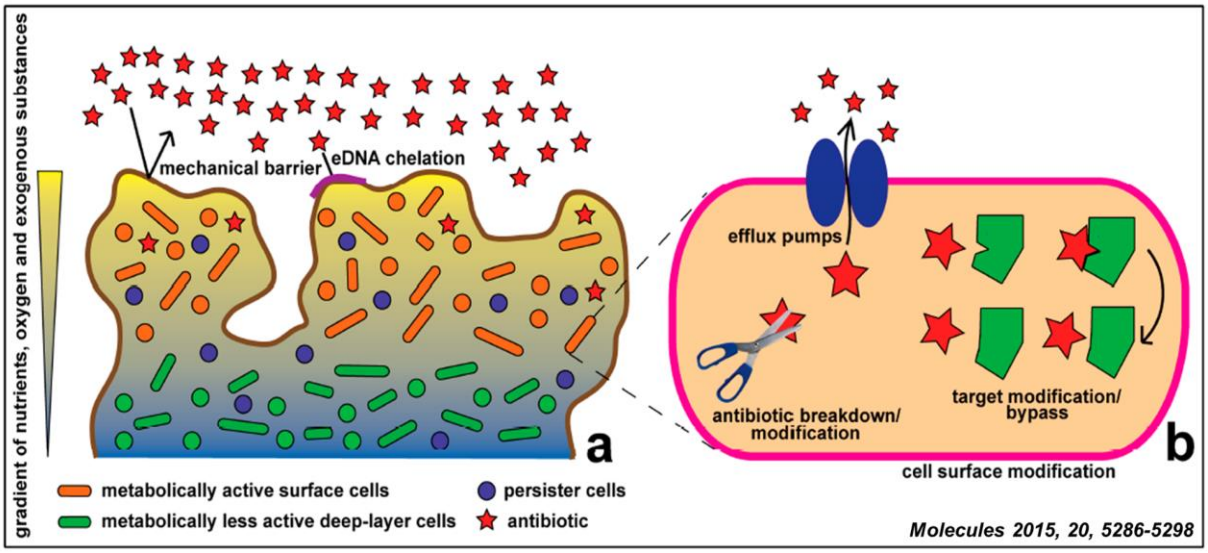

Figure 1: Schematic rapresentation of antiobiotic resistance development in the case of bacteria embedded in a biofilm structure (a), and in the case of planktonic cells (b).

Resistance phenotype in planktonic bacterial cells

Historically, research activities aimed at the comprehension of the molecular bases of antibiotic resistance development have been carried out at the level of single planktonic cells, and have led to the identification of the following mechanisms: inactivation of drugs *via* hydrolysis (*e.g.*, *via* β-lactamase) or modification (*e.g.*, aminoglycoside resistance); alteration of cellular targets that become unrecognizable to the drug (*e.g.*, by DNA gyrase mutation in fluoroquinolone resistance); by the development of permeation barriers, preventing drug access to the target (*e.g.*, the Gram-negative outer membrane); and by the active efflux of drugs out of the cell *via* membrane-bound efflux transporters [9, 10] (Figure 1). The development of cellular resistance is generally the result of endogenous genes mutations, or is due to the transfer of resistance determinants from other microorganisms. Recent advances in genomics and metagenomics have revealed that many natural ecosystems contain a large number of genes whose functions can be co-opted to confer resistance to antimicrobials [11-14]. These genes are collectively known as the resistome [15, 16]. The resistome concept is anthropocentric, since the original functions of resistome genes were probably not related to the development of antibiotic resistance phenotypes. However, the resistome concept is certainly useful, since it underscores the role of environmental bacteria in supplying resistance genes to pathogens [17]. Moreover, the finding that genes able to confer resistance phenotypes may be recovered from extreme environments that have not been in contact with humans, such as the deep subsurface [18], ice [19], and permafrost [20], further suggests that these genes have natural roles not related to antibiotic resistance phenotype. This is indeed the case of multi-drug transporters, which might have evolved as transporters for naturally occurring substrates, serving as mechanisms to pump toxins out from cells, and their consequent ability to transport also antibiotics might have been fortuitous [21]. “Resistance” genes during the pre-antibiotic era were probably chromosomal, and encoded physiologically relevant functions. In the post-antibiotic era, resistome genes might have been laterally transferred to a new host where their original biochemical and genetic functions were adopted to develop antibiotic resistance [22]. Over the last fifty years, research has mainly focused on clinical aspects of antibiotic resistance, while the possible original functions of resistance genes have been largely overlooked. The deep comprehension of the original roles of these resistome elements may aid the development of successful strategies to fight infections caused by antibiotic resistant pathogens.

Resistance phenotype in bacterial communities

Bacterial communities can exhibit tolerance to environmental stress that single cells cannot, and this tolerance might be crucial for the development of resistance phenotype. It has been reported that microbes in a biofilm community gain additional antibiotic resistance that can be up to 1,000 times higher than that gained by the corresponding planktonic cells [23]. Community level resistance adds to the cellular level resistance, thus greatly enhancing the overall antibiotic resistance of the microbial community. [24, 25]. Bacteria aggregates in biofilm are exposed to nutrient and oxygen gradients that may lead to heterogeneity. In fact, cells in the deeper layers of biofilms may have a slower metabolism, being locally adapted to the low levels of nutrients and oxygen, with respect to the more metabolically active surface cells. This, in turn, can lead to significant differences in resistance phenotypes exhibited by these subpopulations in response to antimicrobial treatment [26]. A large percentage (80%) of bacterial infections is complicated by biofilms involvement [27].

As a consequence, guidelines for antibiotic use based on studies on planktonic cells might not be appropriate. Biofilm-specific resistance mechanisms, which are distinct from the well characterized resistance mechanisms developed at the level of single cells, may act in an orchestrated manner to confer high levels of antibiotic resistance in biofilm communities. Components of the biofilm matrix form a mechanical shield that acts to inhibit the effect of antibiotics. The Pel (extracellular polysaccharide) and Psl (membrane polysaccharide) components, produced in *Pseudomonas aeruginosa* biofilms, contribute to antibiotic resistance. In fact, Pel deficient mutants were found to be more susceptible to aminoglycoside antibiotics tobramycin and gentamicin, with respect to the wild type strain [28, 29]. Extracellular DNA (eDNA) forms part of biofilm matrices, and may play a key role in biofilm antibiotic resistance. Since eDNA is negatively charged, it might act as a chelator of cationic antimicrobials [30] it can also act as a shield against aminoglycosides [31]. Bacteria can also become highly resistant to antibiotics when they experience nutrient limitation in growth media [32]. In fact, the starvation-induced stringent (SOS) response has been found to be implicated in enhanced biofilm-specific resistance towards various classes of antibiotics in the case of *P. aeruginosa* and *E. coli* strains [33]. A further phenomenon that greatly contributes to antibiotic resistance in biofilms is the emergence of persister cells [34], which adopt a slow or non-growing phenotype, and become highly resistant to environmental stresses, including antibiotic challenge. Furthermore, persister cells may survive even when the rest of the community has perished, thus creating reservoirs of surviving cells that are able to regrow and cause relapsing infections [35]. Metabolic quiescence is indeed a strategy to tolerate antibiotic exposure [36].

Synergism between resistance mechanisms

It has also to be highlighted that, despite the inherent differences regarding the nature and mechanisms of cellular and community resistance, they are indeed synergistic. The biofilm mode of life, besides providing resistance at a community level, can also promote resistance at the level of single cells. Biofilm communities have a greatly enhanced mutation rate (up to 100 times higher with respect to planktonic cells) [37], which inevitably leads to faster development of antibiotic resistant mutants. Moreover, in biofilm communities, different microbial organisms are in close proximity, and there is an abundance of eDNA, what likely facilitates horizontal gene transfer, and acquisition and spread of resistance determinants. Indeed, it has been shown that biofilms may constitute specific foci of genetic adaptation and evolution, leading to the selection of subpopulations with a greater ability to acquire antibiotic resistance [38, 39]. Furthermore, traditional mechanisms of resistance development at a single cell level may also act in a biofilm-specific manner. For example, an up-regulation of certain pumps specialized in drug efflux is observed in *P. aeruginosa* and *E. coli* [40, 41] biofilms even without an antibiotic challenge, suggesting a physiological role of these pumps in the biofilm mode of life.

As a consequence of this complex picture, the increased use of antibiotics in clinical practice was soon followed by the emergence of antibiotic resistance phenotypes (Figure 2). Indeed, resistance development was observed in target organisms within a few years from the introduction of antibiotics into medical practice [42]. Within seven years from penicillin first use, 50% of hospital *Staphylococcus aureus* isolates were resistant [43], and they represent hidden backbone of advanced medical care, such as surgical procedures, transplant and geriatric medicine, critical care and cancer chemotherapy [44].

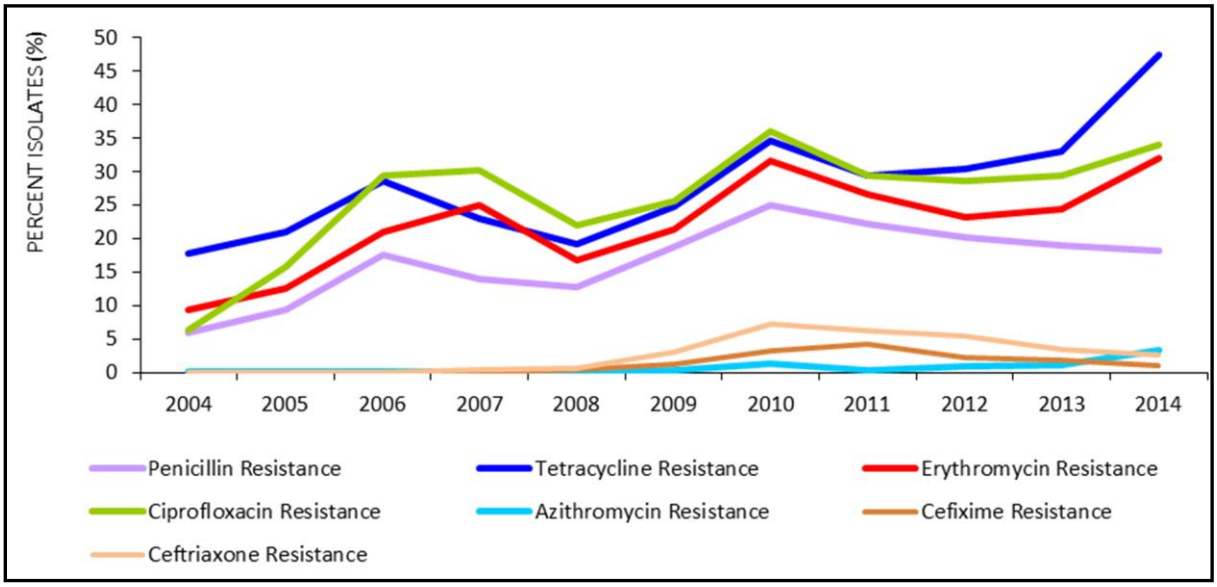

Figure 2: Monitoring the emergence of antibiotic resistance in the last decade.

Unfortunately, despite the desperate need for new antibiotics, there has been little investment into novel antibiotics discovery by the pharmaceutical industry, largely because financial returns are likely to be limited. Development of antibiotics faces stringent government regulations that can delay new drugs entering the market [45]. The time between the initial discovery of a compound and its market entry takes about 10 years on average. This means that antibiotics launched today are the products of drug discovery projects initiated a decade ago [46]. In 1980, there were more than 25 pharmaceutical companies in the USA with active antibacterial drug discovery programmes [47]; today only a few of the largest companies remain active in the field. As a consequence, during the last two decades, a substantial gap in the discovery of antibacterial drugs has been created, which is responsible for the current lack of newly approved systemic antibacterial agents (Figure 3).

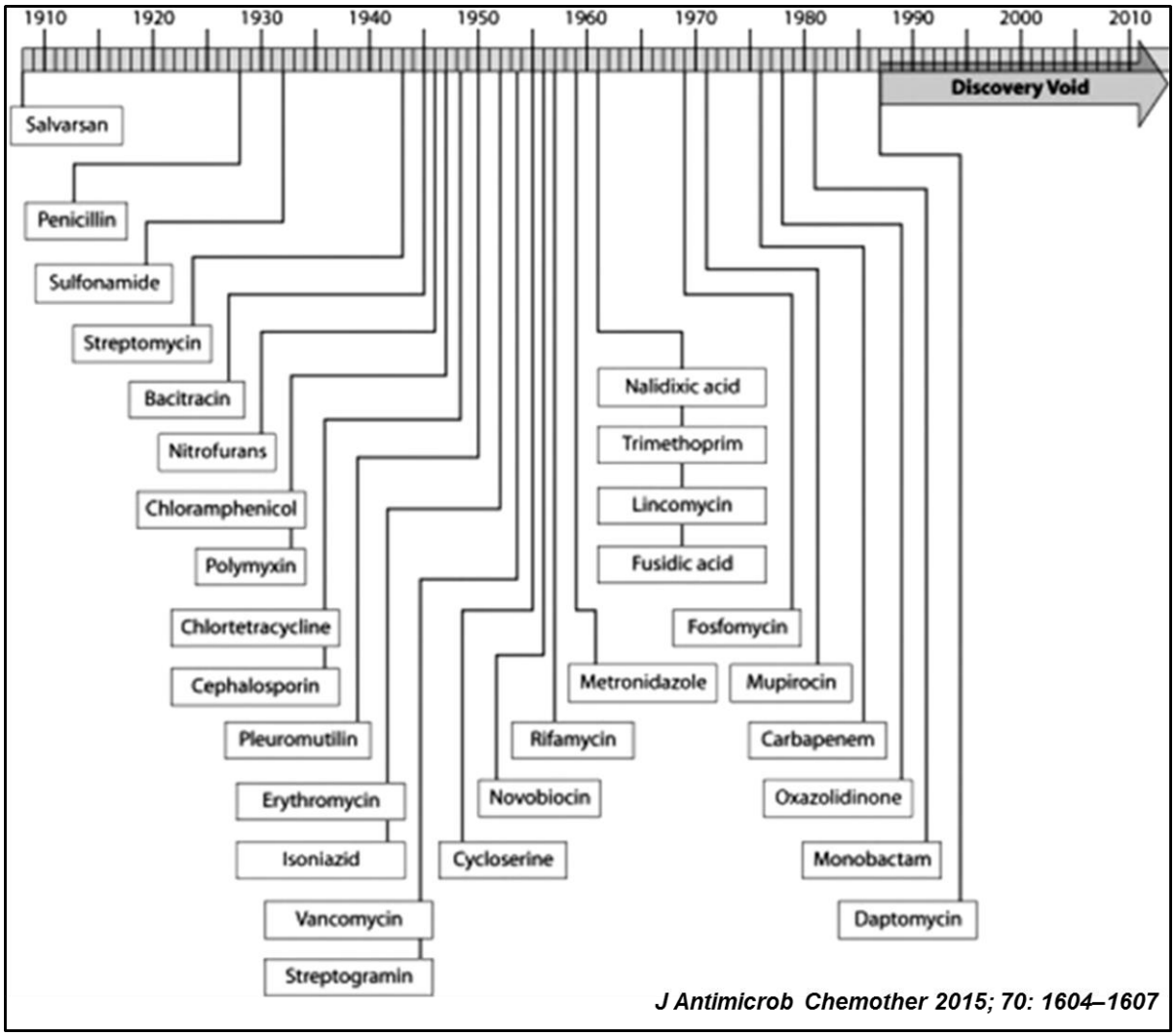

Figure 3: Schematic representation of the 'discovery void'.

This makes the search for novel antimicrobial therapies and approaches imperative. In this scenario, the exploitation of the broad antimicrobial and immunomodulatory properties of naturally occurring Host Defence Peptides (HDPs), first called Anti-Microbial Peptides (AMPs), has attracted considerable attention.

Host Defence Peptides

Host defense peptides are evolutionarily conserved molecules of the innate immune system. They are produced by all complex animals, insects and plants, and generally have modest direct activity against a broad range of microorganisms including bacteria, viruses, fungi, and protozoa [48, 49]. Remarkably, there are more than 2,600 known natural peptides with very diverse sequences and structures [50]. Naturally occurring HDPs can vary in size, ranging from 12 to 50 (or more) amino acids, are generally cationic owing to the presence of high levels of lysine and arginine residues, and contain about 50% hydrophobic amino acids [51]. These properties allow them to interact with membranes, and, in some cases, to penetrate cell membranes. HDPs are classified into four major classes based on their structures: *β-sheet* (for example, human α and β defensins), *α-helical* (for example, LL-37, magainins and mellitin), *loop peptides* with one disulfide bridge (for example, bactenecin), and peptides enriched in specific amino acids as proline, tryptophan,

histidine or glycine without a well-defined structure (for example, indolicidin) [52]. They associate preferentially with membranes of bacteria-like composition (*i.e.*, negatively charged) in model systems, and many peptides are able to translocate into host cells.

Several models have been proposed to explain HDPs mechanism of action, such as *carpet model*, *barrel-stave model*, the *toroidal-pore model*, and the *detergent-type mechanism*. In the case of *carpet model*, peptides assemble on the surface of target membranes, and disrupt them [53]. In the *barrel-stave model*, peptides are believed to insert into target membranes and to aggregate, thus forming a traditional ion-channel pore. In the case of *toroidal-pore model*, instead, peptides are believed to locate close to membrane phospholipids head groups, with an initial orientation parallel to that of lipid bilayer surface. In this orientation, helices hydrophilic sides are exposed to the hydrophilic membrane head groups, whereas helices hydrophobic faces are buried into membrane hydrophobic core. When peptide concentration reaches a critical value, peptides aggregation occurs, thus determining membrane curvature and toroidal-pores formation [54]. Finally, in the *detergent-type mechanism,* peptides are believed to first assemble on the surface of target membranes, as in the carpet and toroidal-pore models, then they aggregate, thus reaching a high local concentration. HDPs amphipathic nature allows them to behave as detergents and to disrupt lipid membrane into small fragments, such as bicelles or micelles [55] (Figure 4).

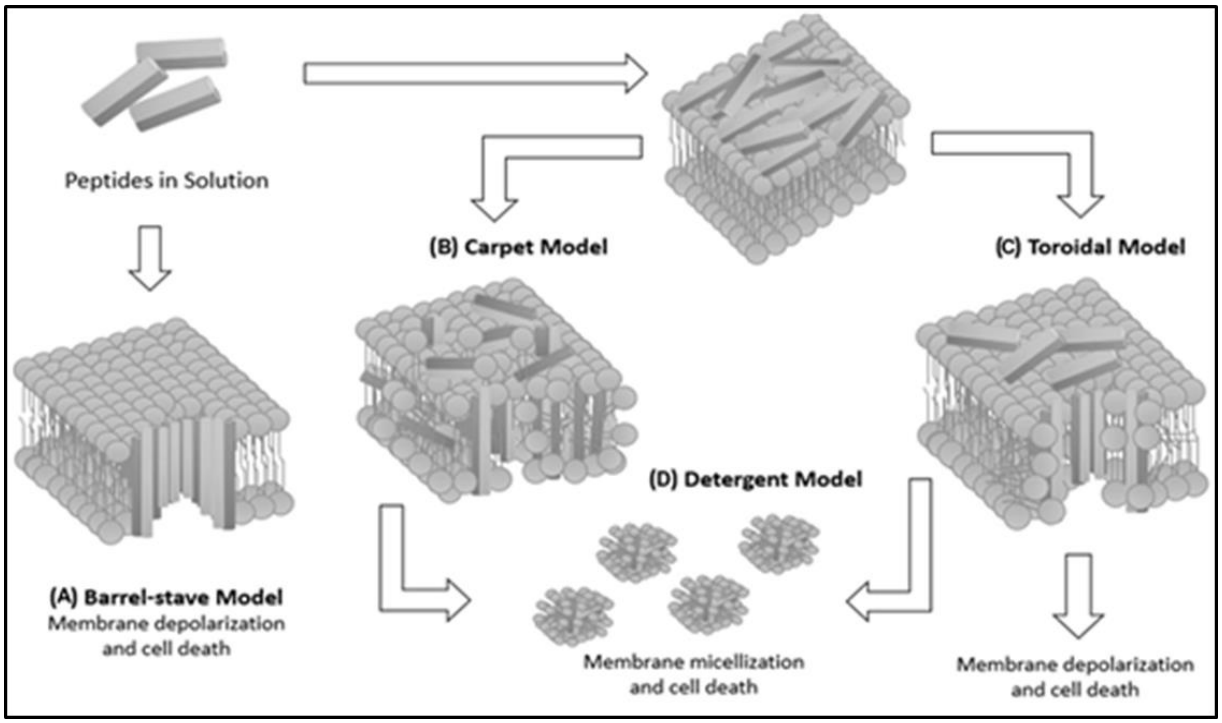

Figure 4: Schematic representation of models proposed to explain HDPs mechanism of action.

It has been suggested that peptides tend to translocate intracellularly in bacteria owing to the presence of a large electrical potential gradient of about 120 mV [56]. Their direct antimicrobial mechanism of action against bacteria often involves multiple different targets including bacterial membrane, essential processes that utilize membrane-associated intermediates, such as cell wall peptidoglycan

biosynthesis and possibly cell division, or essential biomolecules, such as cytosolic RNA, DNA, proteins, and/or enzymes/chaperones. Given to this broad range of targets, HDPs induction of resistance mechanisms in bacteria is improbable [57].
Recent studies have demonstrated that antimicrobial peptides are endowed with a wide range of activities in modulating the functions of host cells and tissues as part of natural host defences, which has led to the depiction of these peptides as Host Defence Peptides rather than antimicrobial peptides to better define their multifaceted roles as immunomodulatory mediators and, under some circumstances, antimicrobial agents. This concept mainly derived from the observation that many HDPs lose their antimicrobial potency under physiological conditions, whereas their immunomodulatory activities can be detected both in tissue cultures and *in vivo* [58]. Moreover, it was demonstrated that a synthetic HDP modelled on bovine bactenecin, although completely lacking direct antibacterial activity *in vitro*, protected mice from infection *in vivo* [59]. This clearly indicated that its anti-infective properties are mainly associated to its ability to modulate the immune response. Nowadays, the ability of HDPs to act as modulators of the immune response and immune cell signalling has been extensively studied, and their role in innate and adaptive immunity is becoming increasingly appreciated [60].

HDPs immunomodulatory activity

HDPs are much more than simple immunomodulators acting through a single receptor or a linear signalling pathway of the immune system. This complexity has become clearly evident by the analysis of the protein–protein interaction network of the human cathelicidin LL-37 [61].
Natural and powerful immune functions of HDPs have been also transferred to synthetic peptide analogues, such as the innate defense regulators (IDRs), which are conceptually based on natural peptides. IDRs protective effects have been demonstrated in mouse models upon infection with *Staphylococcus aureus* including *MRSA*, *vancomycin-resistant enterococci* (VRE), *Plasmodium berghei*, multi-drug-resistant *Mycobacterium tuberculosis*, and *herpes simplex virus* [62-67].
HDPs and IDRs immunomodulatory activities include the ability to modulate pro- and anti-inflammatory responses through signaling pathways alteration, the ability to directly and indirectly recruite effector cells (phagocytes), the enhancement of extracellular and intracellular bacterial killing, the promotion of polarized dendritic cell maturation and macrophage differentiation, and the modulation of wound repair, apoptosis, and pyroptosis (Figure 5) [68-76].

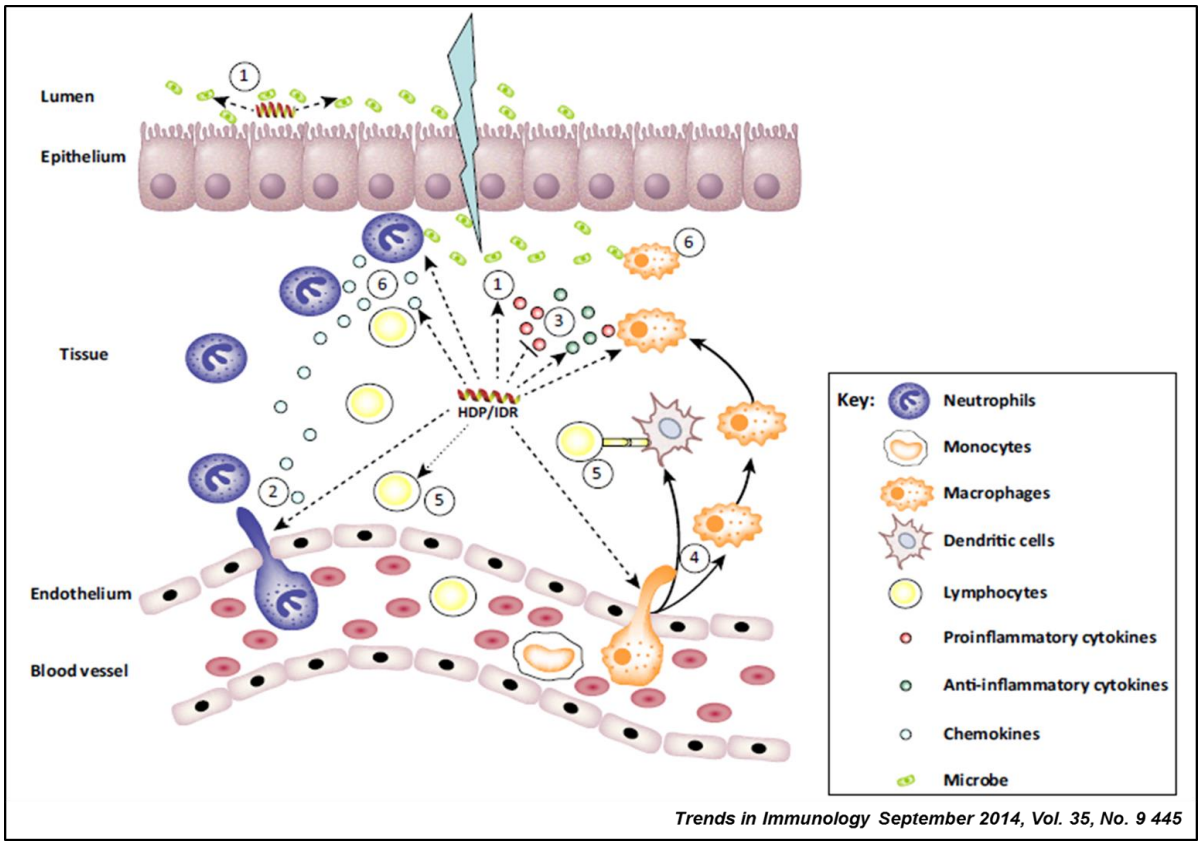

Figure 5: HDPs and IDRs immune functions. HDPs, once released at high concentrations by epithelial cells and immune cells, might exert direct antimicrobial or anti-biofilm activity against invading bacteria (1). At lower concentrations, HDPs might indirectly or directly promote the recruitment of immune cells, such as neutrophils and monocytes (2), suppress the induced production of proinflammatory cytokines, such as tumor necrosis factor (TNF)-α, interleukin-6 (IL-6), and IL-8, and enhance the production of anti-inflammatory mediators including IL-10 and chemokines (monocyte chemotactic protein 1, MCP-1) (3), induce macrophage and dendritic cells differentiation and activation (4), leading to the modulation of adaptive immunity and inducing the recruitment of T cells, and (5) regulate specific cell activities including autophagy and the formation of neutrophil extracellular traps (NETs) (6).

In humans, HDPs are produced by a variety of immune cells of hematopoietic and epithelial origin (Table 1) [77]. Among human HDPs, six are classified as α-defensins; four out of them are produced and stored in the secretory granules of neutrophils (human neutrophil peptides, HNPs), whereas two are expressed as pro-peptides in granules of Paneth cells. When stimulated by pro-inflammatory molecules, both neutrophils and Paneth cells degranulate, releasing α-defensins into the local environment.
Human β-defensins (HBDs), instead, play a major role in preventing the colonization of microbes, such as bacteria, viruses, parasites, and fungi, on epithelial surfaces. Some β-defensins are constitutively produced. This is the case of human β-defensin 1 (HβD-1), which is predominantly released by keratinocytes, since it represents a constitutive defense. Other β-defensins, such as HBD2-4, are produced by the mucosal, gastrointestinal, and urogenital epithelia, and their production is induced by

pro-inflammatory stimuli, such as lipopolysaccharide (LPS) and tumor necrosis factor α (TNF-α) [78].
A very well studied human HDP is a cathelicidin precursor, hCAP-18, which is processed by serine protease 3 to generate α-helical LL-37, a 37-amino acid linear peptide [79]. LL-37 has been identified in many cells, tissues, and organs, as well as on the mucosa, and in secretions. Moreover, during infections and inflammatory processes, neutrophils degranulation determines the release of relatively high levels of LL-37 into the local environment. LL-37 has been found to be endowed with a broad range of immunomodulatory functions *in vivo*, including the direct and indirect recruitment of neutrophils, monocytes, and T cells, as well as a very strong anti-endotoxin activity [80, 81]. Individuals with Kostmann disease are LL-37 deficient, and present a significantly reduced production of human neutrophil peptide (HNP). It has been found that they exhibit an increased susceptibility to severe periodontal diseases, what demonstrates the key role played by these peptides in host defense [82].

HDP	Produced by	Acts on
α-Defensins	Neutrophils, Paneth cells	Epithelial cells, monocytes
β-Defensins	Neutrophils, epithelial cells (keratinocytes)	Monocytes, dendritic cells, T cells
LL-37	Neutrophils, monocytes, mast cells, epithelial cells	Neutrophils, monocytes, macrophages, dendritic cells, T cells, mast cells, epithelial cells, vascular endothelium, mesenchymal stromal cells

Table 1. Human HDPs: sites of production and specific targets.

Anti-biofilm peptides: their potential as broad-spectrum agents
In recent years, various approaches to treat bacterial biofilm infections (*e.g.*, quorum sensing antagonists, antibodies, anti-adhesion strategies, bacteriophages, *etc.*) have been developed [83]. A promising and efficient alternative strategy might be represented, indeed, by cationic and amphipathic HDPs endowed with anti-biofilm activity [84]. One of the first successes in the field was obtained by demonstrating that human cathelicidin LL-37 is able to inhibit *Pseudomonas aeruginosa* biofilm formation at concentrations significantly lower than those required to kill planktonic organisms [85, 86]. Starting from this observation, it was demonstrated that anti-biofilm peptides represent a distinct subset of peptides with an amino acidic composition similar to those of conventional HDPs, but with a structure-function relationship different from that of classical antimicrobial peptides [87]. Indeed, structure-function relationship studies have excluded significant overlaps between anti-biofilm and antimicrobial (*vs*. planktonic bacteria) activities, and it was demonstrated that organisms completely resistant to antibiotic peptides may be efficiently treated with anti-biofilm peptides [88]. Therefore, it is possible to generate novel anti-biofilm peptides able to: (i) kill multiple species of bacteria growing in biofilms, including major clinically-relevant antibiotic resistant Gram-negative and Gram-positive bacteria, (ii) synergistically act in combination with conventional antibiotics on multiple species, and (iii) affect biofilm infections in animal models.
In this scenario, combination therapy approaches based on the concomitant administration of anti-biofilm peptides and conventional antibiotics offer a very promising and powerful weapon to treat both biofilms and dispersed infections, thereby forming the basis for novel and efficacy adjuvant therapies [89].

HDPs applications

HDPs applications span from pharmaceutical industry to food industry. HDPs are gaining attention mainly as antimicrobial alternative weapons, food preservatives and as immune defense regulators. Some HDPs are already in phase II or III of clinical trial as antimicrobials, mainly for topical applications [90-95]. The first HDPs to be commercially manufactured as anti-infective agents were gramicidins produced by *Bacillus brevis* [96], which were used as antibiotics for topical applications. Among HDP-based compounds in advanced stages of development as anti-infective drugs, it is worth mentioning Locilex for the treatment of diabetic foot ulcers, and OP-145 against chronic bacterial middle-ear infections [97]. Other examples are represented by peptides approved in food industry as natural preservatives or dietary supplements, such as nisin, approved since 1969 [98], and lactoferrin added to infant milk formula [99].

Currently, antimicrobial peptides application in the medical field is still one of the most interesting perspectives. The ability of HDPs to modulate the innate immune system has also made them promising candidates as vaccine adjuvants [100]. In fact, it was demonstrated that human neutrophil defensins can enhance both humoral and cell-mediated antigen specific immune response in murine models [101].

Moreover, since HDPs dysregulation is often associated to disease states, these molecules have been proposed as biomarkers for specific disorders. This was found to be particularly useful to identify patients with underlying bacterial infections, whose diagnosis would have otherwise taken a longer time. For example, urinary levels of specific HDPs have been found to be substantially increased in patients presenting infections of the urinary tract [102]. HDPs have also been identified as biomarkers in cancer. In fact, serum levels of specific HDPs were found to be elevated in patients with colon cancer, a phenomenon that was proposed as a specific marker for cancer diagnosis [103].

In the literature, new HDPs activities are continuously identified, a clear indication that the interest in these molecules continues to grow. A recent example is represented by the discovery of a new HDP from earthworms, that exerted neurotropic activity in mouse neural stem cells and a protective effect in a mouse model of Parkinson disease [104]. Another recent study describes a novel bone-forming cell phenotype that was generated by differentiating blood-derived monocytes in the presence of the HDP LL-37. The authors suggest that these cells, which were named monoosteophils, might potentially be used to enhance the repair of broken bones or even to treat osteoporosis [105, 106].

On the basis of these observations, it is probable that, in the next future, further interesting applications might be envisaged for this promising class of biomolecules.

“Cryptic” HDPs

It has been reported that many proteins whose functions are not necessarily related to host defense can act as sources of HDPs. Some examples are haemoglobin, thrombin, lactoferrin, lysozyme, histone-like proteins and vertebrate secretory ribonucleases [107-108]. This is also the case of apolipoproteins, proteins commonly known for their role in lipid transport into blood. In fact, it has been reported that Apoliporotein B [109] and Apolipoprotein E [110] contain hidden HDPs. Since these peptides are hidden within the sequences of precursor proteins, they have been defined “cryptic” peptides. Based on this observation, human proteome could be fascinatingly seen as a yet unexplored source of bioactive peptides with potential pharmacological applications. This has also led to the formulation of a very

interesting hypothesis asserting that multicellular eukaryotes, have developed a panel of “AMP-Releasing Proteins” (AMPRPs), which release active peptides only after a partial proteolytic processing operated by bacterial and/or host proteases [111]. As a consequence of this, bacterial strains that secrete proteases as a weapon against antimicrobial peptides would kill themselves by releasing “cryptic” HDPs from their precursor proteins.
The identification and localization of a cryptic peptide inside its precursor protein is often carried out either through the analysis of peptide fragments generated by proteases, or by synthesizing a set of overlapping peptides, which cover the entire sequence of the protein of interest. Such experimental procedures are expensive and time-consuming. Hence, the development of faster bioinformatics approaches, capable of highlighting the presence of a putative antimicrobial region in a precursor protein, would prove extremely useful.

Aims of the Thesis

The overall aim of the present research project is the identification and characterization of cryptic HDPs hidden in protein precursors by using a novel bioinformatics method, which was recently developed by Dr. Notomista [112]. This method, based on a set of scoring functions, allows a semi-quantitative prediction of the antibacterial activity of specific amino acidic sequences contained in a precursor protein. Once set up, the method was validated by analyzing the sequences of known HDP-Releasing proteins (HDP-RPs), and it was found to a powerful tool to identify novel HDP-RPs. An important advantage of the recently developed method is that it includes some strain-specific parameters, thus offering the possibility to predict HDP efficacy on any desired bacterial strain.
Once identified, human HDPs described in the present Thesis were recombinantly produced in *Escherichia coli* host. This allowed the setting up of a cost-effective production procedure, whose development represents the first aim accomplished in the present research work, which is described in **Chapter 2**. This aspect is particularly interesting since, although chemical synthesis is very efficient and represents the most popular strategy to produce peptides, it is a complex and costly process. Hence, it is well suited to obtain small amounts of peptides, but it could be rather expensive when peptides longer than 30 amino acids or high quantities of peptides are required [113].
The second aim of the present Thesis is reported in **Chapter 3**, where the production and the characterization of two novel bioactive HDPs identified in human Apolipoprotein B is reported.
Chapter 4 mainly focuses on the structural and functional characterization of two novel cryptic host defense peptides. The first one was identified in human 11-hydroxysteroid dehydrogenase-1 β-like, whereas the second one was identified in the transcription factor, Stf76, encoded by pSSVx, a hybrid plasmid-virus from the archaeon *Sulfolobus islandicus.*
A general discussion on the main findings and conclusions derived from the present research work is reported in **Chapter 5.**

References

1) Singh, S.B. Foundation in natural products. Biochem. Pharmacol. 2006, 71, 1006–1015.
2) Lerner, P.I. Producing penicillin. N. Engl. J. Med. 2004, 351, 524.
3) Barriere, S.L. Clinical, economic and societal impact of antibiotic resistance. Expert Opin. Pharmacother. 2015, 16, 151–153.
4) Alanis, A.J. Resistance to antibiotics: Are we in the post-antibiotic era? Arch. Med. Res. 2005, 36, 697–705.
5) World Health Organization. Antimicrobial Resistance: Global Report on Surveillance; World Health Organization: Geneva, Switzerland, 2014.
6) Nadell, C.D. The sociobiology of biofilms. FEMS Microbiol. Rev. 2009, 33, 206–224.
7) Camilli, A. Bacterial small-molecule signaling pathways. Science 2006, 311, 1113–1116.
8) Flemming, H.C. The biofilm matrix. Nat. Rev. Microbiol. 2010, 8, 623–633.
9) Nikaido, H. Multiple antibiotic resistance and efflux. Curr. Opin. Microbiol. 1998, 1, 516–523.
10) Paulsen, I.T. Multidrug efflux pumps and resistance: Regulation and evolution. Curr. Opin. Microbiol. 2003, 6, 446–451.
11) Martinez, J.L. What is a resistance gene? Ranking risk in resistomes. Nat. Rev. Microbiol. 2015, 13, 116–123.
12) Perry, J.A. Forces shaping the antibiotic resistome. Bioessays 2014, 36, 1179–1184.
13) D'Costa, V.M. Sampling the antibiotic resistome. Science 2006, 311, 374–377.
14) Sommer, M.O.A. Functional characterization of the antibiotic resistance reservoir in the human microflora. Science 2009, 325, 1128–1131.
15) Wright, G.D. The antibiotic resistome: The nexus of chemical and genetic diversity. Nat. Rev. Microbiol. 2007, 5, 175–186.
16) Wright, G.D. Antibiotic resistance in the environment: A link to the clinic? Curr. Opin. Microbiol. 2010, 13, 589–594.
17) Gillings, M.R. Evolutionary consequences of antibiotic use for the resistome, mobilome, and microbial pangenome. Front. Microbiol. 2013, 4, doi:10.3389/fmicb.2013.00004.
18) Brown, M.G. Antibiotic resistance in bacteria isolated from the deep terrestrial subsurface. Microb. Ecol. 2009, 57, 484–493.
19) Miteva, V.I. Phylogenetic and physiological diversity of microorganisms isolated from a deep greenland glacier ice core. Appl. Environ. Microbiol. 2004, 70, 202–213.
20) D'Costa, V.M.L. Antibiotic resistance is ancient. Nature 2011, 477, 457–461.
21) Paulsen, I.T. Proton-dependent multidrug efflux systems. Microbiol. Rev. 1996, 60, 575–608.
22) Debabov, D. Antibiotic resistance: Origins, mechanisms, approaches to counter. Appl. Biochem. Microbiol. 2013, 49, 665–671.
23) Ceri, H. The calgary biofilm device: New technology for rapid determination of antibiotic susceptibilities of bacterial biofilms. J. Clin. Microbiol. 1999, 37, 1771–1776.
24) Romero, D. Amyloid fibers provide structural integrity to Bacillus subtilis biofilms. Proc. Natl. Acad. Sci. USA 2010, 107, 2230–2234.
25) Whitchurch, C.B. Extracellular DNA required for bacterial biofilm formation. Science 2002, 295, 1487.
26) De la Fuente-Núñez, C. Bacterial biofilm development as a multicellular adaptation: Antibiotic resistance and new therapeutic strategies. Curr. Opin. Microbiol. 2013, 16, 580–589.
27) Costerton, J.W. Bacterial biofilms: A common cause of persistent infections. Science 1999, 284, 1318–1322.
28) Khan, W. Aminoglycoside resistance of Pseudomonas aeruginosa biofilms modulated by extracellular polysaccharide. Int. Microbiol. 2010, 13, 207–212.
29) Yang, L. Distinct roles of extracellular polymeric substances in Pseudomonas aeruginosa biofilm development. Environ. Microbiol. 2011, 13, 1705–1717.
30) Mulcahy, H. Extracellular DNA chelates cations and induces antibiotic resistance in Pseudomonas aeruginosa biofilms. PLoS Pathog. 2008, 4, e1000213.
31) Chiang, W.C. Extracellular DNA shields against aminoglycosides in Pseudomonas aeruginosa biofilms. Antimicrob. Agents Chemother. 2013, 57, 2352–2361.
32) Nguyen, D. Active starvation responses mediate antibiotic tolerance in biofilms and nutrient-limited bacteria. Science 2011, 334, 982–986.
33) Bernier, S.P. Starvation, together with the sos response, mediates high biofilm-specific tolerance to the fluoroquinolone ofloxacin. PLoS Genet. 2013, 9, e1003144.
34) Lewis, K. Multidrug tolerance of biofilms and persister cells. Curr. Top. Microbiol. Immunol. 2008, 322, 107–131.

35) Mulcahy, L.R. Emergence of Pseudomonas aeruginosa strains producing high levels of persister cells in patients with cystic fibrosis. J. Bacteriol. 2010, 192, 6191–6199.
36) Fridman, O. Optimization of lag time underlies antibiotic tolerance in evolved bacterial populations. Nature 2014, 513, 418–421.
37) Conibear, T.C.R. Role of mutation in Pseudomonas aeruginosa biofilm development. PLoS One 2009, 4, e6289.
38) Blázquez, J. Hypermutation as a factor contributing to the acquisition of antimicrobial resistance. Clin. Infect. Dis. 2003, 37, 1201–1209.
39) Macía, M.D. Hypermutation is a key factor in development of multiple-antimicrobial resistance in Pseudomonas aeruginosa strains causing chronic lung infections. Antimicrob. Agents Chemother. 2005, 49, 3382–3386.
40) Zhang, L. Involvement of a novel efflux system in biofilm-specific resistance to antibiotics. J. Bacteriol. 2008, 190, 4447–4452.
41) Lynch, S.V. A. Role of the rapA gene in controlling antibiotic resistance of Escherichia coli biofilms. Antimicrob. Agents Chemother. 2007, 51, 3650–3658.
42) Scheffler, R.J. Antimicrobials, drug discovery, and genome mining. Appl. Microbiol. Biotechnol. 2013, 97, 969–978.
43) Wenzel, R.P. The antibiotic pipeline—Challenges, costs, and values. N. Engl. J. Med. 2004, 351, 523–526.
44) Yoshikawa TT. Antimicrobial resistance and aging: beginning of the end of the antibiotic era? J Am Geriatr Soc 2002; 50 Suppl 7: 226–9.
45) Livermore, D.M. The need for new antibiotics. Clin. Microbiol. Infec. Suppl. 2004, 10, 1–9. Koehn, F.E.; Carter, G.T. The evolving role of natural products in drug discovery. Nat. Rev. Drug Discov. 2005, 4, 206–220.
46) Boucher HW. Progress—development of new drugs active against Gram-negative bacilli: an update from the Infectious Diseases Society of America. Clin Infect Dis 2013; 56: 1685–94.
47) Zasloff, M. Antimicrobial peptides of multicellular organisms. Nature 2002, 415, 389–395.
48) Phoenix, D.A. Antimicrobial Peptides: Their History, Evolution, and Functional Promiscuity, Wiley, 2013.
49) Wang, G. APD3: the antimicrobial peptide database as a tool for research and education. Nucleic Acids Res. 2016, 44, D1087–D1093.
50) Hancock, R.E. Trends Biotechnol. 1998, 16, 82–88.
51) Hancock R.E. Antimicrobial and host-defense peptides as new anti-infective therapeutic strategies. Nat Biotechnol. 2006 Dec;24(12):1551-7.
52) Oren, Z. Mode of action of linear amphipathic *α*-helical antimicrobial peptides. Biopolymers. 1998;47(6):451-63.
53) Stella, L. Alamethicin interaction with lipid membranes: a spectroscopic study on synthetic analogues. Chem Biodivers. 2007 Jun;4(6):1299-312.
54) Dürr U.H.N. LL-37, the only human member of the cathelicidin family of antimicrobial peptides. Biochim Biophys Acta. 2006 Sep;1758(9):1408-25.
55) Spindler, E.C. Deciphering the mode of action of the synthetic antimicrobial peptide Bac8c. Antimicrob. Agents Chemother. 2012, 55, 1706–1716
56) Fjell, C.D. Designing antimicrobial peptides: form follows function. Nat. Rev. Drug Discov. 2012, 11, 37–51
57) Hilchie, A. L. Immune modulation by multifaceted cationic host defence (antimicrobial) peptides. Nat. Chem. Biol. 2013, 9, 761–768.
58) Scott, M. G. An anti-infective peptide that selectively modulates the innate immune response. Nat. Biotechnol. 2007, 25, 465–472.
59) Mansour, S. C. Host defence peptides: front-line immunomodulators. Trends Immunol. 2014, 35, 443–450.
60) Hancock Robert E. W. The immunology of host defence peptides: beyond antimicrobial activity. Nature Reviews Immunology, 2016, Vol. 16, 321-334
61) Nijnik, A. Synthetic cationic peptide IDR-1002 provides protection against bacterial infections through chemokine induction and enhanced leukocyte recruitment. J. Immunol. 2010, 184, 2539–2550.
62) Scott, M.G. An anti-infective peptide that selectively modulates the innate immune response. Nat. Biotechnol. 2007, 25, 465–472.
63) Achtman, A.H. Effective adjunctive therapy by an innate defense regulatory peptide in a preclinical model of severe malaria. Sci. Transl. Med. 2012, 4(135):135ra64.

64) Steinstraesser, L. Innate defense regulator peptide 1018 in wound healing and wound infection. PLoS ONE. 2012, 7, e39373.

65) Shestakov, A. Synthetic analogues of bovine bactenecin dodecapeptide reduce herpes simplex virus type 2 infectivity in mice. Antiviral Res. 2013, 100, 455–459.

66) Bolouri, H. Innate defense regulator peptide 1018 protects against perinatal brain injury. Ann. Neurol. 2014, 75, 395–3410.

67) Mookherjee, N. Modulation of the TLR-mediated inflammatory response by the endogenous human host defense peptide LL-37. J. Immunol. 2006, 176, 2455–2464.

68) Tjabringa, G.S. Human cathelicidin LL-37 is a chemoattractant for eosinophils and neutrophils that acts via formyl-peptide receptors. Int. Arch. Allergy Immunol. 2006, 140, 103–112.

69) Nijnik, A. Signaling pathways mediating chemokine induction in keratinocytes by cathelicidin LL-37 and flagellin. J. Innate Immun. 2012, 4, 377–386.

70) Mantovani, A. Neutrophils in the activation and regulation of innate and adaptive immunity. Nat. Rev. Immunol. 2011, 11, 519–531.

71) Niyonsaba, F. The innate defense regulator peptides IDR- HH2, IDR-1002, and IDR-1018 modulate human neutrophil functions. J. Leukoc. Biol. 2013, 94, 159–170.

72) Davidson, D.J. The cationic antimicrobial peptide LL-37 modulates dendritic cell differentiation and dendritic cell-induced T cell polarization. J. Immunol. 2004, 172, 1146–1156.

73) Heilborn, J.D. The cathelicidin anti-microbial peptide LL- 37 is involved in re-epithelialization of human skin wounds and is lacking in chronic ulcer epithelium. J. Invest. Dermatol. 2003,120, 379–389.

74) Barlow, P.G. The human cathelicidin LL-37 preferentially promotes apoptosis of infected airway epithelium. Am. J. Respir. Cell Mol. Biol. 2010, 43, 692–702.

75) Hu, Z. Antimicrobial cathelicidin peptide LL-37 inhibits the LPS/ATP-induced pyroptosis of macrophages by dual mechanism. PLoS ONE 2014, 9, e85765.

76) Hilchie, A.L. Immune modulation by multifaceted cationic host defense (antimicrobial) peptides. Nat. Chem. Biol. 2013, 9, 761–768.

77) Arnett, E. The multifaceted activities of mammalian defensins. Curr. Pharm. Des. 2011, 17, 4254–4269.

78) Sorensen, O.E. Human cathelicidin, hCAP-18, is processed to the antimicrobial peptide LL-37 by extracellular cleavage with proteinase 3. Blood. 2001, 97, 3951–3959.

79) Fukumoto, K. Effect of antibacterial cathelicidin peptide CAP18/LL-37 on sepsis in neonatal rats. Pediatr. Surg. Int. 2005, 21, 20–24.

80) De, Y. LL-37, the neutrophil granule- and epithelial cell-derived cathelicidin, utilizes formyl peptide receptor-like 1 (FPRL1) as a receptor to chemoattract human peripheral blood neutrophils, monocytes, and T cells. J. Exp. Med. 2000, 192, 1069–1074.

81) Putsep, K. Deficiency of antibacterial peptides in patients with morbus Kostmann: an observation study. Lancet. 2002, 360, 1144–1149.

82) Lynch A.S. New antibiotic agents and approaches to treat biofilm associated infections. Expert Opin Ther Pat. 2010, 20:1373-1387.

83) Hancock R.E.W. Antimicrobial and host-defense peptides as new anti-infective therapeutic strategies. Nat Biotechnol. 2006, 24:1551-1557.

84) Overhage J. Human host defense peptide LL-37 prevents bacterial biofilm formation. Infect Immun. 2008, 76:4176-4182.

85) Dean S.N. Susceptibility of Pseudomonas aeruginosa biofilm to alpha-helical peptides: D-enantiomer of LL-37. Front Microbiol. 2011, 2:128.

86) de la Fuente-Nunez C. Inhibition of bacterial biofilm formation and swarming motility by a small synthetic cationic peptide. Antimicrob Agents Chemother. 2012, 56:2696-2704.

87) de la Fuente-Nunez C. D-enantiomeric peptides that eradicate wild-type and multidrug-resistant biofilms and protect against lethal Pseudomonas aeruginosa infections. Chem Biol. 2015, 22:196-205.

88) Pletzer D. Anti-biofilm peptides: Potential as broad spectrum agents. J. Bacteriol. 2016, DOI: 10.1128/JB.00017-16

89) Yeung A.T. Multifunctional cationic host defence peptides and their clinical applications. Cell Mol Life Sci. 2011, Jul;68(13):2161-76.

90) Zasloff, M. Antimicrobial peptides of multicellular organism. Nature. 2002. 415:389-95.

91) Hancock R.E. Cationic peptides: a new source of antibiotics. Trends Biotechnol.1998, Feb;16(2):82-8.

92) Harris F. Anionic antimicrobial peptides from eukaryotic organisms. Curr Protein Pept Sci. 2009;10(6):585-606.
93) Maróti G. Natural roles of antimicrobial peptides in microbes, plants and animals. Res Microbiol. 2011, May;162(4):363-74.
94) Hancock R.E. Antimicrobial and host-defense peptides as new antiinfective therapeutic strategies. Nat Biotechnol. 2006, Dec;24(12):1551-7.
95) Nakatsuji T. Antimicrobial peptides: old molecules with new ideas. J Invest Dermatol. 2012, Mar;132(3 Pt 2):887-95. 20
96) Fox, J. L. Antimicrobial peptides stage a comeback. Nat. Biotech. 2013, 31, 379-382.
97) Narayana, J. L. Antimicrobial peptides: Possible anti-infective agents. Peptides. 2015, 72, 88-94.
98) Delves-Broughton J. Applications of the bacteriocin, nisin. Antonie Van Leeuwenhoek. 1996, 69(2):193-202.
99) Lönnerdal B. Infant formula and infant nutrition: bioactive proteins of human milk and implications for composition of infant formulas. Am J Clin Nutr. 2014, Mar;99(3):712S-7S.
100) Yeung A.T. Multifunctional cationic host defence peptides and their clinical applications. Cell Mol Life Sci. 2011, Jul;68(13):2161-76.
101) Lillard J.W. Mechanisms for induction of acquired host immunity by neutrophil peptide defensins Proc Natl Acad Sci U S A. 1999, 96(2): 651–656.
102) Caterino J. M. A Prospective, observational pilot study of the use of urinary antimicrobial peptides in diagnosing emergency department patients with positive urine cultures. Acad. Emerg. Med. 2015, 22, 1226–1230.
103) Albrethsen, J. Human neutrophil peptides 1, 2 and 3 are biochemical markers for metastatic colorectal cancer. Eur. J. Cancer. 2006, 42, 3057–3064.
104) Kim, D. H. Antimicrobial peptide, lumbricusin, ameliorates motor dysfunction and dopaminergic neurodegeneration in a mouse model of parkinson's disease. J. Microbiol. Biotechnol. 2015, 25, 1640–1647.
105) Zhang, Z. Generation of novel bone forming cells (monoosteophils) from the cathelicidinderived peptide LL-37 treated monocytes. PLoS ONE. 2010, 5, e13985.
106) Rosenberg HF. RNase A ribonucleases and host defense: an evolving story, 2008. J Leukoc Biol. 2008, May;83(5):1079-87.
107) Boix E. Structural determinants of the eosinophil cationic protein antimicrobial activity. Biol Chem. 2012, Aug;393(8):801-15.
108) Huang Y.C. The flexible and clustered lysine residues of human ribonuclease 7 are critical for membrane permeability and antimicrobial activity. J Biol Chem. 2007, Feb 16;282(7):4626-33.
109) Kelly B.A. Anti-infective activity of apolipoprotein domain derived peptides in vitro: identification of novel antimicrobial peptides related to apolipoprotein B with anti-HIV activity. BMC Immunol. 2010, Mar 18;11:13. doi: 10.1186/1471-2172-11-13.
110) Dobson C.B. The receptor binding region of human apolipoprotein E has direct anti-infective activity. J Infect Dis. 2006, Feb 1;193(3):442-50.
111) D'Alessio G. Denatured bactericidal proteins: active per se, or reservoirs of active peptides? FEBS Letters. 2011, 585:2403-2404.
112) Pane K. Antimicrobial potency of cationic antimicrobial peptides can be predicted from their amino acid composition: application to the detection of "cryptic" antimicrobial peptides. Theorical Biology (2017) doi: http://dx.doi.org/10.1016/j.jtbi.2017.02.012.
113) Chandrudu S. Chemical methods for peptide and protein production. Molecules. 2013, Apr 12;18(4):4373-88.

CHAPTER 2

Development of a simple and cost-effective strategy to produce recombinant HDPs in Escherichia coli

Rosa Gaglione

Department of Chemical Sciences, PhD in Biotechnology

University of Naples "Federico II", Napoli, Italy

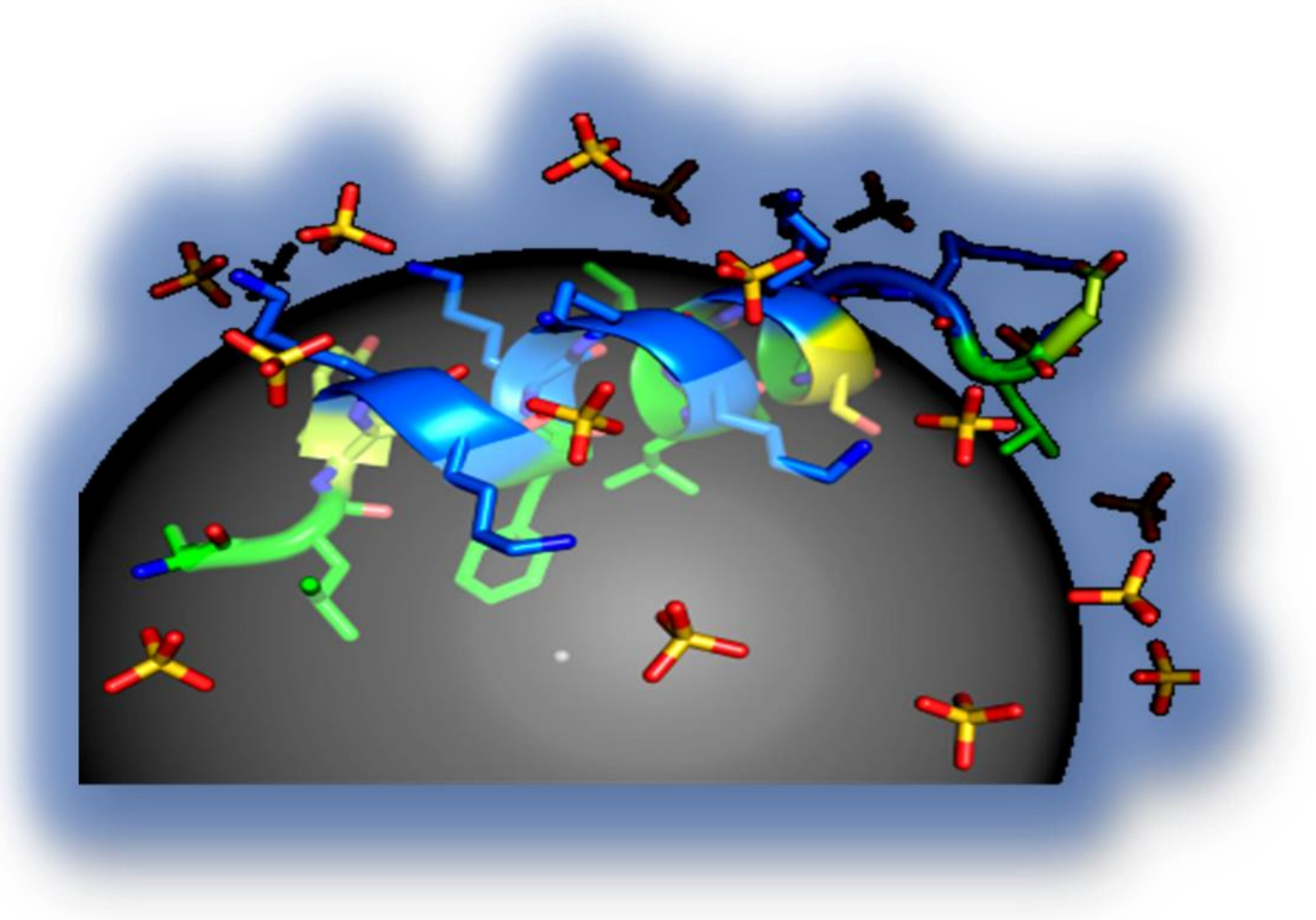

1. Introduction

Both basic research and clinical applications require high quality peptides to be readily available in a cost-effective manner. This is the case of antimicrobial peptides (AMPs), also referred to as host defense peptides (HDPs), in order to account for their immunomodulatory properties. HDPs are short cationic molecules produced by virtually all living organisms. So far, more than 2,500 HDPs have been identified, which exhibit a wide range of biological activities from direct killing of invading pathogens to modulation of immunity and other biological responses of the host [1]. Due to their functional properties, HDPs potential applications range from biomedical therapies to food industry and agriculture field. In general, HDPs isolation from natural sources is a labor intensive and time-consuming process, not suitable to obtain peptides in large amounts. On the other hand, chemical synthesis, although very efficient, is a complex and costly process [2]. For this reason, it is well suited to obtain small amounts of peptides, but it could be rather expensive when peptides longer than 30 amino acids or high quantities of peptide are required. Therefore, it is not an ideal platform for large-scale peptide production. In this scenario, recombinant DNA technology provides an economical means for peptide manufacture. Indeed, many AMPs have been successfully obtained through recombinant production in various heterologous hosts [3]. Among these, *Escherichia coli* has been the most widely used host to produce recombinant peptides [4]. However, it has to be considered that recombinant production of peptides entails several difficulties [3, 5-7]. Firstly, the peptides' antibacterial nature makes them potentially fatal to the producing host. Secondly, the peptides' small size and cationic property make them highly susceptible to proteolytic degradation, with consequent low yields. A strategy that effectively overcomes both obstacles is peptide fusion to a carrier protein. By using this strategy, the peptide of interest can be released from the carrier by enzymatic or chemical cleavage at a specific site around the carrier-peptide junction. In general, enzymatic cleavage has been found to be less efficient than chemical proteolysis to obtain pure peptides [6]. The fusion design mimics the peptide precursor structure, since the carrier protein plays a similar role as the peptide natural pro-segment, thus protecting the host from the toxic peptide and the peptide from bacterial proteases [8]. Recently, we described the rational development of a new carrier protein for high yield production of recombinant peptides in *E. coli* [9-11]. The denatured form of Onconase (ONC), a RNase from *Rana pipiens* [12], is a very well suited partner, since it can be expressed at very high levels in inclusion bodies (about 200–250 mg/L in Terrific Broth), it is a very small protein (104 aa) thus allowing high yields of the peptides upon chemical cleavage, and its solubility is pH dependent (the denatured protein is soluble only at pH<4.0) thus allowing the purification of peptides soluble at pH 7.0 by selective precipitation of the carrier. Moreover, the chimeric construct has been designed to contain a His tag sequence, positioned between the ONC and the peptide moieties, suitable for an easy purification of the chimeric construct, a flexible linker (Gly-Thr-Gly), and a dipeptide (Asp-Pro), which is cleaved in mild acidic conditions thus allowing the release of the peptide from the carrier [9-11]. Carrier mutations were designed to minimize undesired cleavage events by removing all the potential unwanted cleavage sites, and to reduce the possibility of intra-chain disulfides formation without affecting expression levels of the fusion protein, its propensity to form inclusion bodies in *E. coli* and to aggregate at pH 7.0, since this feature is crucial to remove the carrier after the chemical cleavage by means of a simple centrifugation step [9]. The optimized procedure allows the purification of about 10 mg of pure peptide from 1 L of bacterial

culture [11]. Here, we describe the development of a novel growth medium and a scaling up of the present strategy, in order to set up a cost-effective and competitive procedure to produce large amounts of peptides needed for both basic research and industrial applications. To perform this optimization, a good starting point was represented by the simplicity and limited costs of the previously set up production protocol. The necessity to design a novel growth medium derives from the observation that LB growth medium, which is the most commonly used medium for culturing *E. coli*, although easy to make, rich in nutrients and with an optimal osmolarity for *E. coli* growth at early log phase, is generally responsible for a stop of bacterial cell growth at relatively low densities. This is mainly due to the presence of scarce amounts of carbohydrates (and other utilizable carbon sources) and divalent cations [13]. Not surprisingly, when the amount of peptone or yeast extract is increased, higher cell densities are reached [14]. By the same way, divalent cation supplementation ($MgSO_4$ in the millimolar range) results in higher cell growth. Glucose supplementation is, instead, of limited help because acid generation by glucose metabolism overwhelms the limited buffer capacity of LB, at least in shake flasks where pH control can be laborious [15,16]. If culture acidification poses a problem, the media can be buffered with phosphate salts at 50 mM. Indeed, this is the case of 2x YT, TB (Terrific Broth) and SB (Super Broth) media, which have been shown to be superior to LB for reaching higher cell densities [17]. The novel culture medium, here developed, is composed by cheap components, readily available and containing defined amounts of each compound. We also set up an auto-induction procedure with the ultimate goal of scaling up an efficient and commercially competitive production strategy. The proposed experimental strategy has been successfully applied to GKY20 peptide, a short cationic antimicrobial peptide derived from the C-terminus of human thrombin [9] and to two novel HDPs identified in an isoform of human Apolipoprotein B (residues 887-922), and recently characterized for their biological activities [11]. Since the peptides GKY20, ApoB887-923, and ApoB887-911, upon cleavage of the chimeric construct in mild acidic conditions, are released with an additional proline residue at the N-terminus, they were here named r(P)GKY20, r(P)ApoB$_L$, and r(P)ApoB$_S$, respectively.

2. Materials and Methods

2.1 Bacterial strains, plasmids and bacterial culture media

E. coli BL21(DE3) and *E. coli* BL21(DE3) pLysS strains, purchased from AMS Biotechnology, were used as host organisms for the expression of recombinant constructs ONC-r(P)GKY20, ONC-r(P)ApoB$_L$, ONC-r(P)ApoB$_S$ and His$_6$-Apolipoprotein AI (ApoAI). To produce recombinant constructs ONC-r(P)GKY20, ONC-r(P)ApoB$_L$ and ONC-r(P)ApoB$_S$ in bacterial cells, the cDNAs encoding the antimicrobial peptides were cloned in pET-22b(+) expression vector purchased from Novagen. In the case of His$_6$-ApoAI, pET-20b(+) expression vector purchased from Novagen has been used. Bacterial cultures were carried out accordingly to Sambrook [18]. All the reagents were purchased from Sigma-Aldrich, unless differently specified.

2.2 Shake flask expression

Competent bacterial cells were transformed with ~80 ng of recombinant plasmid, and incubated for 30 min on ice. Following the addition of 1 mL of LB medium, cells were incubated for 60 min at 37°C and then centrifuged at 12,000 rpm for 20 min at 4°C. Medium (1 mL) was then removed, and the cell pellet was dissolved in the remaining

solution (about 100 µL) and added to medium containing the appropriate antibiotic. Bacterial cells were then incubated over-night at 37°C on a shaker. *E. coli* BL21(DE3) cells, individually transformed with recombinant pET-22b(+) expression vectors containing the sequence encoding ONC-r(P)ApoB$_L$, ONC-r(P)ApoB$_S$ or ONC-r(P)GKY20, were incubated over-night at 37°C in 50 mL of medium supplemented with ampicillin (0.1 mg/mL). Following over-night incubation, cell cultures were diluted 1:20 in 1 L of complete medium. Cultures were incubated at 37°C up to OD_{600nm} of 3–4. Expression of recombinant constructs was then induced by addition of IPTG (isopropyl-β-D-thiogalactopyranoside) at a final concentration of 0.7 mM. To verify recombinant constructs expression, aliquots of bacterial cells (corresponding to 0.125 OD_{600nm}) were taken before induction and at the end of the expression procedure, solubilized in lysis buffer (0.125 M Tris-HCl pH 6.8, 2% SDS, 10% glycerol) and analyzed by 15% SDS-PAGE.

2.3 Bioreactor cultivation

Bioreactor cultivation was performed in a BioFlo 3000 system from New Brunswick. This instrumentation is endowed with a 5 L vessel, temperature control by a heating sleeve and an integrated cooling system, monitoring of airflow rate, monitoring of pH values and dissolved O_2 levels through specific probes (Mettler Toledo). The medium in bioreactor (3 L) was inoculated with *E. coli* BL21(DE3) or *E. coli* BL21(DE3)pLysS cells, previously transformed with recombinant vectors, and incubated over-night at 37°C in 150 mL of antibiotic-supplemented medium ($OD_{600\ nm}$ = 2-4). In order to ensure aerobic growth conditions along the entire fermentation process, dissolved oxygen levels were automatically adjusted through control of both airflow and stirring speed. Sterile antifoam A emulsion (Sigma-Aldrich) was manually added (0.01% v/v final concentration) under aseptic conditions prior to over-night incubation. To avoid undesired growth of contaminant bacterial cells upon ampicillin degradation, antibiotic was regularly added to bacterial cells at a rate of 100 mg/h by using a fermenter peristaltic pump. Along the whole fermentation process, the stirring speed was kept constant at 300 rpm, with an air flow rate of 10 cm^3/sec. The temperature was kept constant at 37 °C. When bacterial culture in bioreactor reached $OD_{600\ nm}$ of about 3-5, protein expression was induced by 0.7 mM IPTG added by using a fermenter peristaltic pump. The time of 30 min after IPTG addition was defined as the starting time (t = 0 h). In the case of auto-inducing expression procedure, instead, the time of 30 min after bacteria inoculation into the bioreactor was defined as the starting time (t = 0 h). Bioreactor cultivation was carried out for a total time of 24 h.

2.4 Biomass determination

In the case of both shake flask and bioreactor cultivations, samples OD measurements at 600 nm were performed on triplicates by using a Shimadzu Photometer UV-2600. For OD measurements, samples were diluted in complete medium. For cell dry weight determination, samples (25 mL) were harvested, centrifuged for 20 min at 6,000 rpm, and washed with 0.9% NaCl for three times. Afterwards, samples were dried over-night at 80 °C, and lyophilized before weighing.

2.5 Analyses of recombinant constructs expression levels

In the case of both shake flask and bioreactor cultivations, at established time intervals, bacterial aliquots (corresponding to 0.125 OD_{600nm}) were withdrawn and solubilized in lysis buffer (0.125 M Tris-HCl pH 6.8 containing 2% SDS and 10%

glycerol), in order to determine recombinant constructs expression levels by 15% SDS-PAGE.
Protein bands intensity was detected by densitometric analyses performed by using a ChemiDoc Imaging System (Bio-Rad). In order to estimate recombinant constructs expression levels, the intensity of protein bands with the expected electrophoretic mobility was evaluated by densitometric analyses and referred to a calibration curve obtained by analyzing increasing defined amounts of bovine serum albumin (BSA).

2.6 Techno-economic analysis

The determination of production strategy costs was performed by implementing the process sections in Superpro Designer 9.0 (Intelligen Inc.). We performed mass and energy balances, in order to evaluate chemicals demand, electricity consumption and utilities duties for each unit operation. Figure 1 reports the flow chart of the process, consisting of three sections: fermentation, recombinant constructs extraction and purification. Step 1 (fermentation) consists of pre-culture carried out in shake flasks, bioreactor cultivation and bacterial culture harvesting carried out by centrifugation. Step 2 (extraction) consists of four washing-centrifugation steps according to Katia P. *et al* [9] Step 3 (purification) is performed by expanded bed chromatography followed by dialysis, chimercic construct controlled hydrolysis, onconase precipitation, peptide lyophilization and further solubilization in an appropriate buffer.
The chosen scenario describes, as first, the costs to produce 100 mg peptide per batch, then ten times scaling up simulating the case of a small-medium enterprise. Italy was chosen as location to fix the costs for labor, electricity and other utilities, as reported in Table 1.
Capital (CAPEX) and Operating Expenditures (OPEX) were calculated according to the procedure reported in Table 2. The overall Lang factor for the process is about 8, which is in line with indications for high value products derived from production in bacteria [19]. Chemicals costs were obtained by bulk quotations gently provided by Sigma-Aldrich, Panreac Applichem and GE Healthcare Biosciences (Table 3). A detailed batch schedule has been implemented with operations associated to each unit, accordingly to the procedure reported in Figure 2. Major equipment depreciament has been evaluated by assuming 10 years lifetime of the process with an interest rate of 8%. We considered 330 days production per year to evaluate maintenance.
Production process was initially fixed at a lab scale, *i.e.* at a working fermenter volume of 5 L, and then scaled up to 50 L for future scenarios. Fermenter costs were scaled up accordingly to power law exponents suggested by Kalk and Langlykke (1986) [20]. Costs of other equipments were scaled up accordingly to the model provided by SuperPro Designer, whereas wastewater treatment was fixed to 0.4 € m^{-3} [19]. Since all the process is carried out under batchwise conditions, the labor demand was always fixed to 1 direct labor hour per hour for all the procedures described in each step.

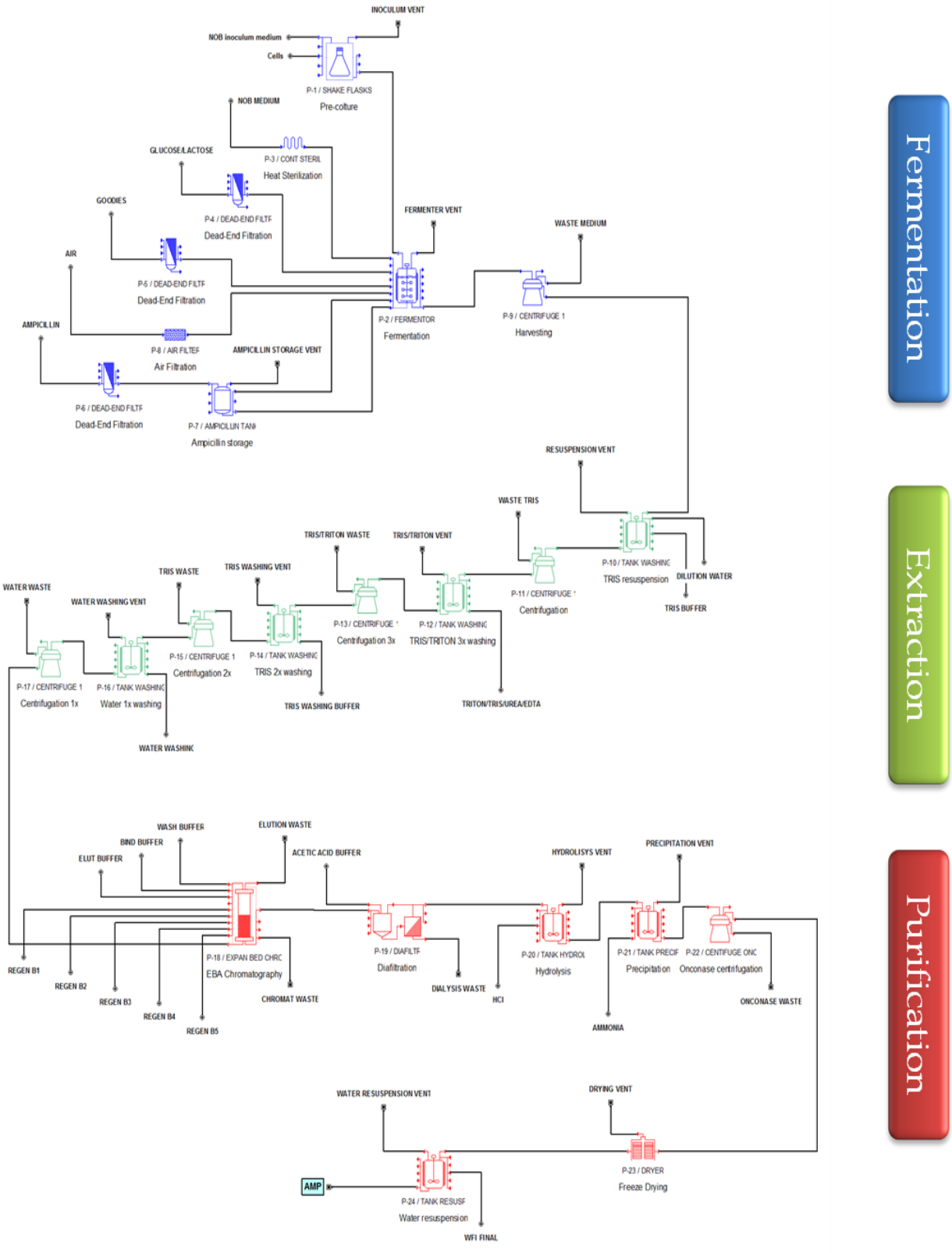

Fermentation

Extraction

Purification

Figure 1. Flow chart illustrating the production process.

	Unit cost
Operator labor	26.3 € hr^{-1} *
Electricity	0.16 € kWh^{-1} **
Freon	0.18 € MT^{-1} ***
Chilled water	0.49 € MT^{-1} ***
Hot water	0.062 € MT^{-1} ***
Steam	14.8 € MT^{-1} ***

Table 1. Unit costs of electricity, labor and utilities referred to the Italian scenario of industrial production.

*source: Bureau of Labor Statistic - www.bls.gov
**source: Eurostat - http://ec.europa.eu/eurostat/statistics-explained/index.php/Energy_price_statistics
***source: Data are taken from SuperPro databank and linearly scaled by ratio of electricity cost in US and in Italy

			Cultivation
TOTAL CAPITAL INVESTMENT	Direct Cost (DC)	Major equipment cost	MEC
		Installation costs	50% MEC
		Instrumentation and control	50% MEC
		Piping	30% MEC
		Insulation	3% MEC
		Electrical	20% MEC
		Buildings	100% MEC
		Land improvements	15% MEC
		Service facilities	70% MEC
	Indirect Cost (IC)	Construction expenses	25% DC
		Engineering and supervision	35% DC
	Other Cost (OC)	Contractor's fee	5% (DC+IC)
		Contingency (Major equipment)	10% (DC+IC)
	Direct fixed capital cost (DFC)		DC+IC+OC
	Working capital		OPEX first month of operation
	Start-up and validation		5% DFC
	Total capital investment		DFC + working capital + Start-up and validation
CAPEX	Depreciation		(DC+IC+OC)/10 years
	Interest		8% of depreciation
	Property tax		2% of depreciation+interest
	Insurance		1% of depreciation+interest
	Purchase tax		5% of depreciation+interest
OPEX	Energy		Calculated from MEC consumption
	Labour		Salaries + Employer's contribution (40%)+Operating Supplies (10%)+Supervision (20%)+Administration(60%)
	Raw materials		Calculated from mass balances
	Utilities		Calculated from MEC consumption and mass balances
	Laboratory/Quality control/Quality assurance		15% Labour cost
	Wastewater treatment		Calculated from mass balances
	Consumables		Calculated from MEC design
	Others	Maintenance	6% DFC
		Operating supplies	0.4% (Electricity + Raw materials + Utilities)
		Contingencies	15% (Raw materials + Utilities)
		Overheads	55% (Labour + Maintenance)

Table 2. CAPEX and OPEX evaluation.

Tryptone	Euro 94,35 (1 kg)
Betaine	Euro 29.80 (50 gr)
Ammonia	Euro 31,3 (5 L)
Citric acid	Euro 26,10 (1 kg)
Kh_2po_4	Euro 28,70 (500 gr)
K_2hpo	Euro 83,34 (500 gr)
C-goodies:	
· $MgSO_4$	Euro 76,59 (500 gr)
· $FeSO_4$ * 7 H2O	Euro 18,40 (250 gr)
· MgO	Euro 66,60 (250 gr)
· $CaCO_3$	Euro 55,50 (500 gr)
· $ZnSO_4$ * 7 H_2O	Euro 44,40 (100 gr)
· $MnSO_4$ * 1 H_2O	Euro 44,82 (100 gr)
· $CuSO_4$	Euro 45,60 (100 gr)
· $CoSO_4$ * H_2O	Euro 52,83 (100 gr)
· H_3Bo_3	Euro 56,60 (500 gr)
· $NiCl_2$	Euro 64,44 (100 gr)
· Na_2MoO_4	Euro 43,02 (100 gr)
Ampicillin	Euro 42,21 (5 gr)
Glucose	Euro 67,32 (1kg)
Lactose	Euro 35,01 (500 gr)
Glycerol	Euro 51,4 (2,5 L)
Trizma	Euro 109 (500 gr)
Hcl	Euro 20,20 (1 L)
Edta	Euro 39,78 (500 gr)
Triton x-100	Euro 109 (500 gr)
Urea	Euro 27,60 (1 kg)
Resin Ni-sepharose	Euro 299 (25 mL)
Acetic acid	Euro 20,07 (1 L)
Guanidine hydrochloride	Euro 123,40 (1 kg)
Sodium acetate	Euro 52,11 (250 gr)
NaH_2PO_4•H2O	Euro 38 (1 kg)
Na_2HPO_4	Euro 109 (500 gr)
Nacl	Euro 84,15 (1 kg)
Imidazolo	Euro 55,98 (100 gr)
$NiSO_4$	Euro 52,29 (10 gr)

Table 3. Chemical costs; source: Sigma-Aldrich, Panreac Applichem and GE Healthcare Biosciences.

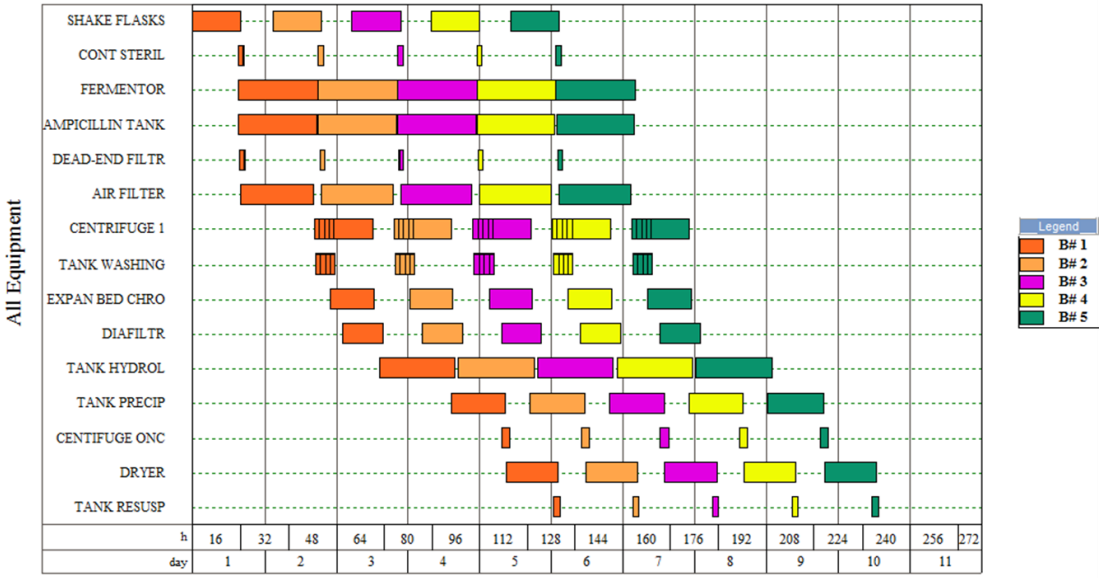

Figure 2. Detailed schedule of the operations within the whole production process.

3. Results

3.1 Bacterial growth medium design

We developed a novel semi-defined rich medium, named NoB medium, with the aim to obtain high cell densities and significantly higher expression levels of recombinant peptides and proteins. NoB medium composition is reported in Table 4. As it can be noticed, this medium is composed by cheap components, readily available and containing defined amounts of each compound. In particular, yeast extract, which is commonly employed as a source of exogenous factors essential for microorganism growth, has been replaced by known growth factors, in order to obtain a chemically defined medium rather than a complex crude extract whose composition varies not only depending on the manufacturer but also from batch to batch of the same manufacturer [21]. In NoB medium, yeast extract has been prevalently substituted with tryptone, which has a defined amino acidic composition, since it derives from bovine casein hydrolysis. As different batches of tryptone can contain different amounts of lactose, we added 4 g/L glucose to NoB medium (Table 4), in order to avoid undesired basal induction of recombinant protein expression. Glucose, in fact, acts as a repressor of lac promoter and prevents expression induction in the absence of IPTG. NoB medium also contains a mixture of salts providing optimal amounts of required metals (e.g. Mg, Ca, Zn, Fe, Mn, Cu, etc.), usually acting as cofactors for essential enzymatic reactions. Glycerol (1.2%) was added as main carbon source. Ammonium citrate was added to NoB medium both as a source of inorganic nitrogen and as an additional buffer system. Furthermore, since citrate acts as a chelating agent, its presence is fundamental to avoid transition metal cations precipitation. Finally, since *E. coli* is able to synthesize betaine from choline, a component likely present in yeast extract but not in tryptone, betaine was added to NoB medium, as this compound is one of the best osmolytes for *E. coli* [22].

ORGANIC COMPONENTS	CONCENTRATION
Industrial Tryptone	34 g/L
Betaine	0.12 g/L
NH_3	0.075%
Citric Acid	3 g/L
Glycerol	1.2%
Glucose	4 g/L
BUFFER COMPONENTS	**CONCENTRATION**
KH_2PO_4	23 g/L
K_2HPO_4	125 g/L
C-Goodies	0.5%
C-GOODIES SALTS	**CONCENTRATION**
$MgSO_4$	30.1 g/L
$FeSO_4$ * 7 H2O	4.75 g/L
MgO	5.4 g/L
$CaCO_3$	1.0 g/L
$ZnSO_4$ * 7 H_2O	0.72 g/L
$MnSO_4$ * 1 H_2O	0.56 g/L
$CuSO_4$	0.125 g/L
$CoSO_4$ * H_2O	0.14 g/L
H_3BO_3	0.03 g/L
$NiCl_2$	0.004 g/L
Na_2MoO_4	0.006 g/L
HCl 37%	24.5 mL/L

Table 4. NoB medium composition.

To verify NoB medium efficiency for *E. coli* culturing and recombinant proteins production, we first performed a comparison between TB and NoB media in shake flasks cultures. To this purpose, we used *E. coli* BL21(DE3) strain as a host to

produce recombinant bioactive peptides r(P)GKY20, r(P)ApoB$_L$, and r(P)ApoB$_S$. Since peptides are expressed in bacterial cells as fusion proteins with onconase (ONC), the chimeric constructs have been here named ONC-r(P)GKY20, ONC-r(P)ApoB$_L$, and ONC-r(P)ApoB$_L$, respectively. To perform a comparison between TB and NoB media, bacterial cells, transformed with pET recombinant plasmids, were grown in 50 mL of medium containing 100 μg/mL ampicillin, at 37°C over-night. Bacterial cultures were then used to inoculate 1 L of ampicillin containing medium. Glucose at a final concentration of 4 g/L was added to bacterial culture to limit undesired basal protein expression before induction with IPTG. Culture was then incubated at 37°C up to OD_{600nm} of 1-3.5. Expression of recombinant constructs was induced by addition of IPTG (isopropyl-β-D-thiogalactopyranoside) at a final concentration of 0.7 mM. Cells were harvested after over-night induction by centrifugation and lysed in order to analyze recombinant constructs expression by 15% SDS-PAGE (Figure 3-5, a and b). We found that, in the case of NoB medium, significantly higher expression levels were reached in the case of ONC-r(P)ApoB$_L$ and ONC-r(P)ApoB$_S$ recombinant constructs (Figure 3 and 4, d and e, and Table 4). In particular, expression levels were found to be 1.5 times and 1.6 times higher in NoB medium than in TB medium in the case of ONC-r(P)ApoB$_L$ and ONC-r(P)ApoB$_S$ recombinant constructs, respectively (Table 4). In the case of ONC-r(P)GKY20 construct, instead, effects of NoB medium on the expression levels were found to be slight. Furthermore, in all the cases, we observed a strong decrease of undesired basal expression in NoB medium with respect to TB medium (Figure 3-5). It has also to be noticed that we observed faster growth kinetics in NoB medium with respect to TB medium. In fact, by monitoring biomass increase on the bases of $OD_{600\ nm}$ values, we observed that at early stationary phase, the moment selected for IPTG addition, higher cell densities were achieved in NoB medium with respect to TB medium. In Table 4, results of typical experiments are reported.

3.2 Setting up of an auto-induction protocol

To further improve and to significantly lower the costs of the production procedure, we decided to set up an auto-induction protocol. To do this, we first developed an auto-inducing medium characterized by a well-balanced combination of different carbon sources and other essential nutrients, allowing cultures to grow to high cell densities, thus supporting the expression at high levels of the target chimeric proteins. Indeed, NoB medium was conceived to already possess the mineral salt formulation required for a successful auto-induction procedure [23]. Hence, to set up an efficient auto-induction protocol, NoB medium was supplemented with 0.4 % (54 mM) glycerol and 1.92 g/L (5.6 mM) lactose [14]. Glucose was kept constant at a concentration of 0.5 g/L (2.8 mM) along the whole auto-induction expression procedure [14], in order to promote fast cellular growth in the early stages of the culture, while also preventing uptake and metabolism of inducing sugar (lactose). By this way, lactose is consumed after glucose exhaustion, with a consequent automatic induction of recombinant protein expression under the control of T7 promoter. In fact, *E. coli* has specific preferences with respect to alternative carbon sources, and can switch between them in a certain order (diauxic shift) [23]. Glucose is used as *E. coli* primary carbon source, since it efficiently inhibits the intake and metabolism of alternative sugars, such as lactose. Once glucose is fully metabolized, *E. coli* switches relatively fast to the use of lactose. By this way, unlike experimental procedures based on the use of IPTG, induction of protein expression is automatic and, consequently, bacterial cell growth does not need to be monitored. Furthermore,

to achieve sustained bacterial growth during the induction phase, glycerol is provided in auto-inducing media together with lactose [14, 24, 25]. NoB medium, containing the above reported doses of glucose, glycerol and lactose, has been here named auto-inducing NoB medium. As first, we set up the auto-induction procedure. To do this, bacterial cells were transformed with pET recombinant plasmids, and grown in 50 mL of classical NoB medium containing 100 µg/mL ampicillin, at 37°C over-night. Bacterial cultures were then used to inoculate 1 L of ampicillin containing auto-inducing NoB medium. Culture was then incubated at 37°C for 24 h, in order to allow automatic induction of chimeric proteins expression. Following incubation, cells were harvested by centrifugation and lysed in order to analyze recombinant constructs expression by 15% SDS-PAGE (Figure 3-5 c). We observed significantly higher expression levels of all the constructs under test (Figure 3-5 c, and Table 4), which were found to be about 1.5 times higher than those observed in NoB medium under IPTG induction (Table 4). However, it has to be noticed that saturation densities ($OD_{600\ nm}$ values at the end of the experiment) were found to be significantly lower than those observed in the classical induction protocol (NoB with the addition of IPTG). This is in agreement with previous findings indicating that, in shake flask cultivations, lactose auto-induction generally occurs in the active growth phase, with a possible consequent inactivation of bacterial cell growth [23].

TB medium (induction by IPTG 0.7 mM)			
Recombinant construct	Expression level (g/L)	$OD_{600\ nm}$ before induction	Final $OD_{600\ nm}$
ONC-r(P)ApoB$_L$	0.51	3.2	5.7
ONC-r(P)ApoB$_S$	0.66	2.8	7
ONC-r(P)GKY20	0.44	3.4	6.6
NoB medium (induction by IPTG 0.7 mM)			
Recombinant construct	Expression level (g/L)	$OD_{600\ nm}$ before induction	Final $OD_{600\ nm}$
ONC-r(P)ApoB$_L$	0.80	4.6	9.5
ONC-r(P)ApoB$_S$	1.07	4.3	9.1
ONC-r(P)GKY20	0.50	5	8.3
auto-inducing NoB mediun			
Recombinant construct	Expression level (g/L)	Final $OD_{600\ nm}$	
ONC-r(P)ApoB$_L$	1.25	5.2	
ONC-r(P)ApoB$_S$	2.05	4	
ONC-r(P)GKY20	1.03	2.7	

Table 4. Expression levels of recombinant ONC-r(P)ApoB$_L$, ONC-r(P)ApoB$_S$ and ONC-r(P)GKY20 in TB medium, NoB medium and auto-inducing NoB medium.

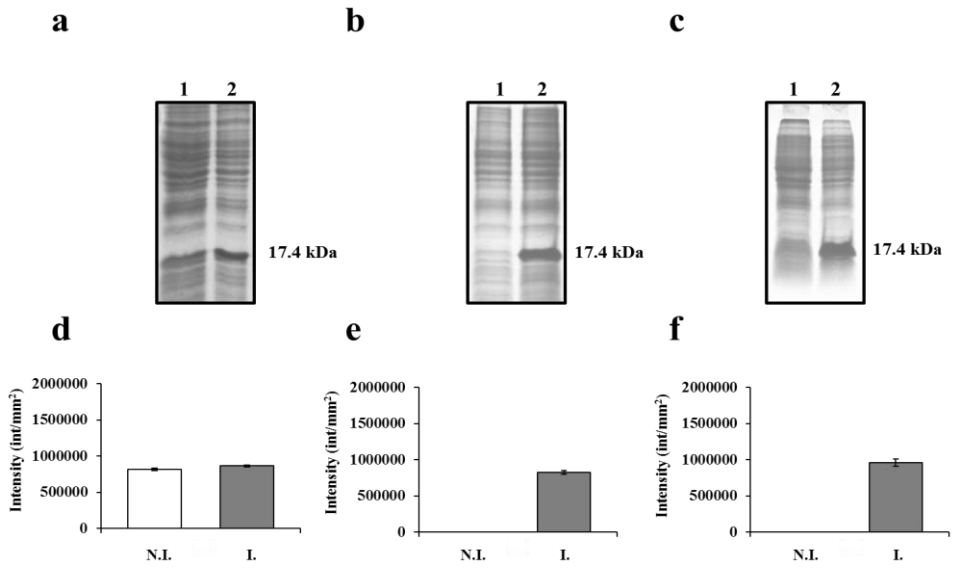

Figure 3. Analysis by SDS-PAGE of total proteins extracted from not induced and induced bacterial cells transformed with pET recombinant plasmid encoding ONC-r(P)ApoB$_L$ construct (a, b, c). Densitometric analyses of protein bands with a molecular weight corresponding to that of ONC-r(P)ApoB$_L$ construct (17.4 kDa) are reported as histograms (d, e, f). Analysis of protein expression was per formed in TB medium upon IPTG induction (a, d), in NoB medium upon IPTG induction (b, e), and in auto-inducing NoB medium (c, f).

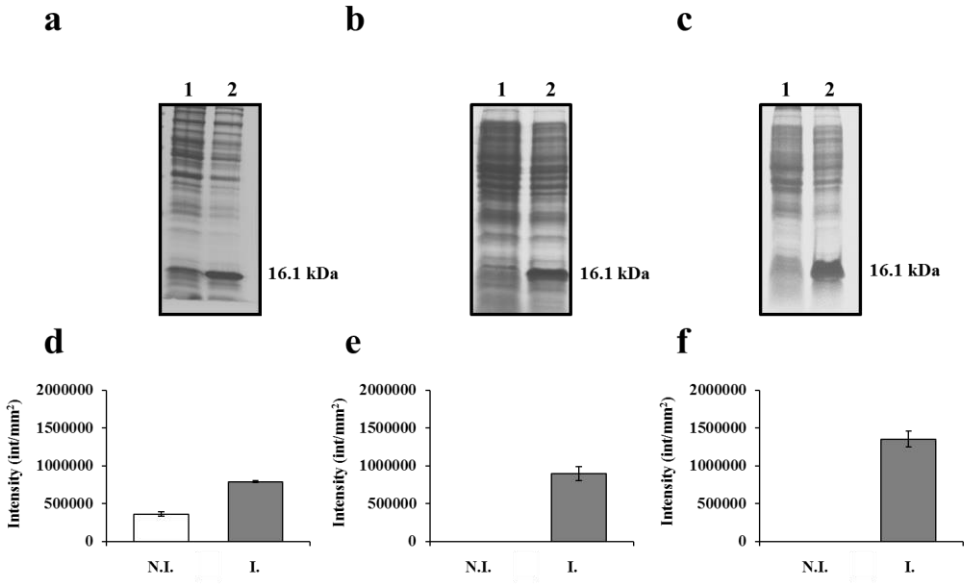

Figure 4. Analysis by SDS-PAGE of total proteins extracted from not induced and induced bacterial cells transformed with pET recombinant plasmid encoding ONC-r(P)ApoBs construct (a, b, c). Densitometric analyses of protein bands with a molecular weight corresponding to that of ONC-r(P)ApoBs construct (16.1 kDa) are reported as histograms (d, e, f). Analysis of protein expression was per formed in TB medium upon IPTG induction (a, d), in NoB medium upon IPTG induction (b, e), and in auto-inducing NoB medium (c, f).

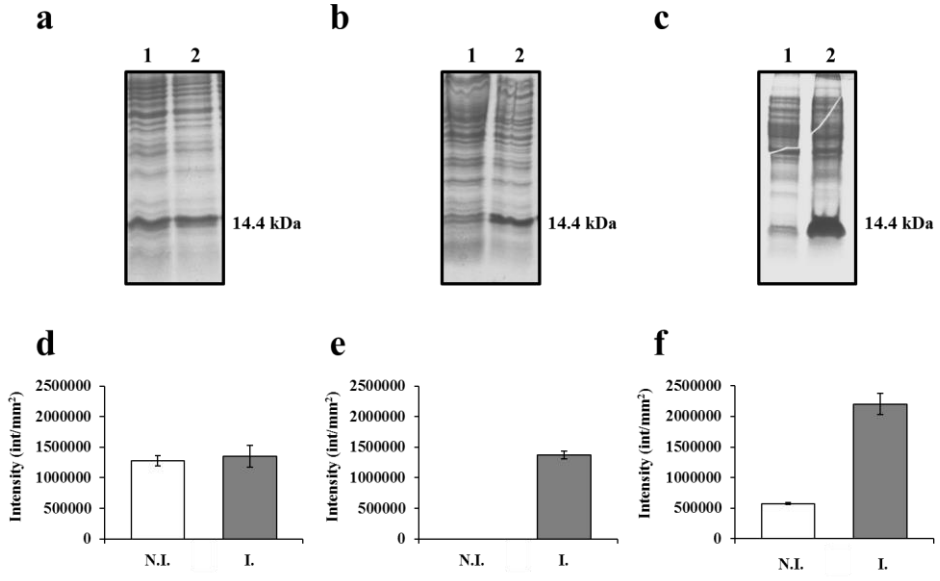

Figure 5. Analysis by SDS-PAGE of total proteins extracted from not induced and induced bacterial cells transformed with pET recombinant plasmid encoding ONC-r(P)GKY20 construct (a, b, c). Densitometric analyses of protein bands with a molecular weight corresponding to that of ONC-r(P)GKY20 construct (14.4 kDa) are reported as histograms (d, e, f). Analysis of protein expression was per formed in TB medium upon IPTG induction (a, d), in NoB medium upon IPTG induction (b, e), and in auto-inducing NoB medium (c, f).

3.3 Scaling up of the production procedure

To scale up the production procedure and to evaluate its efficacy on a larger scale, we set up a fermentation process by using a 5 L fermenter. As first, we optimized the production procedure by using classical NoB medium and IPTG induction, and then we compared recombinant constructs expression yields to those obtained in auto-inducing NoB medium to set up a competitive and cost-effective process. To this purpose, transformed bacterial cells were inoculated into 150 mL of classical NoB medium containing 100 µg/mL of ampicillin and 4 g/L glucose, and incubated at 37°C over-night. Bacterial cultures were then diluted into 3 L (dilution 1:20 v/v) of NoB medium in a 5 L batch reactor. Since in stirred bioreactors generally a higher gas–liquid oxygen transfer is achieved than in shake flasks [23], oxygen was not expected to be a limiting factor. The oxygen saturation was maintained above 60% throughout the cultivation. Along the fermentation process, the stirring speed was kept constant at 300 rpm, with an air flow rate of 10 cm^3/sec. To overcome advantages associated to ampicillin degradation, the antibiotic was added to bacterial cells at a rate of 100 mg/h by using a fermenter peristaltic pump. In fact, a fundamental problem associated with the use of ampicillin resistance as a selection mechanism is the rapid degradation of the antibiotic by the extracellular enzyme β-lactamase [26, 27]. For the BL21(DE3) host strain containing the pET-type vectors, the half-life of 100 µg/mL ampicillin is reported to be 30 min for mid-log phase cells grown in a fermenter [28]. By regularly adding ampicillin, we were able to prevent undesired plasmid loss, with a consequent improvement of expression yields. Fermentation process was carried out at 37°C up to OD_{600nm} of about 4. At this stage, expression of recombinant constructs was induced by addition of 0.7 mM IPTG. Fermentation was carried out for 24 h. At the end of the fermentation process, cells were collected by using a peristaltic pump, harvested by centrifugation, and lysed in order to analyze recombinant constructs expression by 15% SDS-PAGE (Figure 6-8). In all the cases, recombinant expression of chimeric constructs began at about 2-4 h after IPTG addition, reaching a maximum at 8 h (Figure 6-8 a, c, e). Moreover, in all the cases, protein expression yields were found to be significantly higher than those observed in shake flask cultures carried out in classical NoB medium upon IPTG induction (Figure 6-8 e, and Tables II and III). Saturation densities ($OD_{600\ nm}$ values at the end of fermentation process) were found, instead, to be similar to those obtained in shake flasks cultures. Biomass was monitored on the basis of cell dry weight and represented as a curve (Figure 6-8 e), which was found to have a shape similar to that of the curve representing recombinant chimeric constructs production yields (Figure 6-8 e).

Once verified the validity of the experimental strategy on a larger scale, we applied it to the auto-induction procedure, in order to develop a cost-effective production process to be used on an industrial scale. To this purpose, we performed the same experimental procedure described above with the only exception that *E. coli* BL21(DE3) cells, once transformed with recombinant pET-22b(+) expression vectors, were incubated over-night at 37°C in 150 mL of NoB medium supplemented with ampicillin (0.1 mg/mL), but lacking glucose, glycerol and lactose. Following over-night incubation, cell cultures were diluted 1:20 (v/v) in 3 L of auto-inducing NoB medium in a 5 L batch reactor.

NoB medium (induction by IPTG 0.7 mM)			
Recombinant construct	Expression level (g/L)	$OD_{600\ nm}$ before induction	Final $OD_{600\ nm}$
ONC-r(P)$ApoB_L$	2.36	3	8
ONC-r(P)$ApoB_S$	1.44	5	7.9
ONC-r(P)GKY20	1.17	4	6
auto-inducing NoB mediun			
Recombinant construct	Expression level (g/L)	Final $OD_{600\ nm}$	
ONC-r(P)$ApoB_L$	3.1	10.5	
ONC-r(P)$ApoB_S$	2.5	12	
ONC-r(P)GKY20	2	6	

Table 5. Expression levels of recombinant ONC-r(P)$ApoB_L$, ONC-r(P)$ApoB_S$ and ONC-r(P)GKY20 in NoB medium and auto-inducing NoB medium.

At this point, experimental conditions identical to those described above were applied, with the only exception of IPTG addition, since recombinant expression of chimeric constructs was automatically induced by lactose present in the medium. At defined time intervals, bacterial aliquots (corresponding to 0.125 OD_{600nm}) were withdrawn and lysed to determine recombinant constructs expression levels by 15% SDS-PAGE (Fig. 4-6 b, d, f). Recombinant expression of chimeric constructs was found to begin at 4h, indicating that, at this time, glucose probably decreases, and lactose begins to be metabolized, with a consequent inducing effect. In our experimental conditions, expression levels were found to reach a maximum level at 24 h. In all the cases, we observed recombinant constructs expression levels significantly higher than those obtained either in the same experimental conditions by using classical NoB medium (Fig. 4-6) or in shake flasks cultures by using auto-inducing NoB medium (Table 5). Similar results were also obtained by analyzing saturation densities ($OD_{600\ nm}$ values at the end of fermentation process), which were found to be higher than those obtained in the same experimental conditions by using classical NoB medium under IPTG induction for all the constructs, with the exception of ONC-r(P)GKY20. In the last case, in fact, biomass growth was found to be similar in both condition in batch reactor.

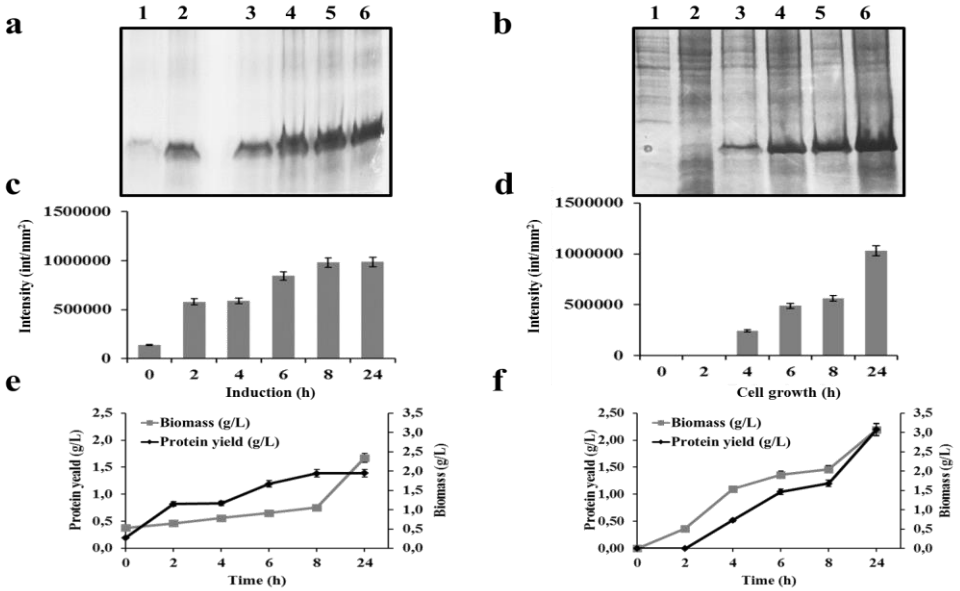

Figure 6. Analysis by SDS-PAGE of total proteins extracted from bacterial cells transformed with pET recombinant plasmid encoding ONC-r(P)ApoB$_L$ construct (a, b). Samples were collected at different time intervals along the fermentation process in batch reactor. In a, not induced cells (lane 1), cells upon 2h induction (lane 3), cells upon 4 h induction (lane 4), cells upon 8 h induction (lane 5), cells upon 24 h induction (lane 6). In b, cells at time 0 (lane 1), cells upon 2h growth (lane 3), cells upon 4 h growth (lane 4), cells upon 8 h growth (lane 5), cells upon 24 h growth (lane 6). Densitometric analyses of protein bands with a molecular weight corresponding to that of ONC-r(P)ApoB$_L$ construct (17.4 kDa) are reported as histograms (c, d). Chimeric construct expression levels (g/L) and biomass (cell dry weight, g/L) are reported in e and f. Analyses are representative of fermentation processes carried out either in classical NoB medium (a, c, e) or in auto-inducing NoB medium (b, d, f).

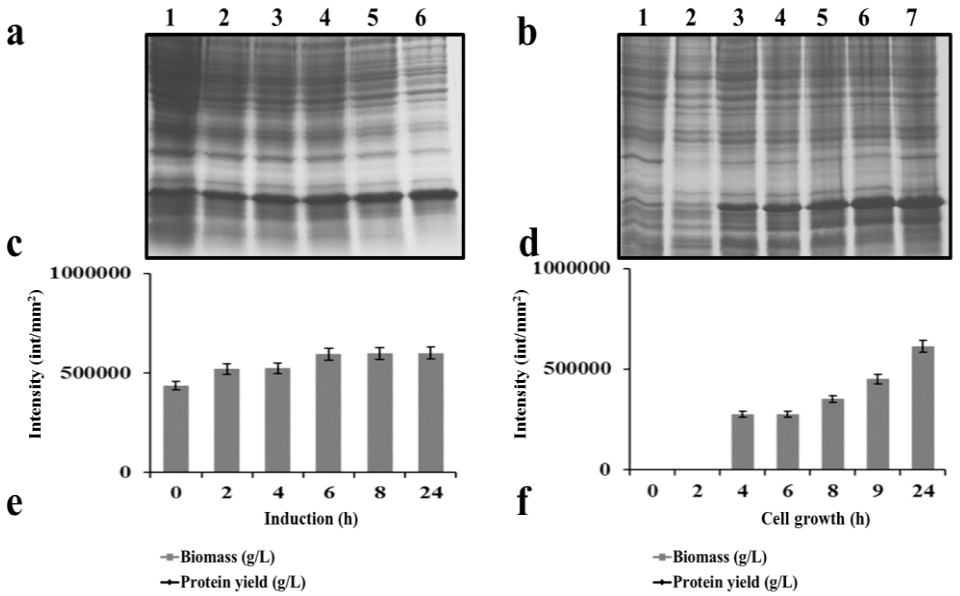

Figure 7. Analysis by SDS-PAGE of total proteins extracted from bacterial cells transformed with pET recombinant plasmid encoding ONC-r(P)ApoBs construct (a, b). Samples were collected at different time intervals along the fermentation process in batch reactor. In a, not induced cells (lane 1), cells upon 2h induction (lane 3), cells upon 4 h induction (lane 4), cells upon 8 h induction (lane 5), cells upon 9 h induction (lane 6), cells upon 24 h induction (lane 7). In b, cells at time 0 (lane 1), cells upon 2h growth (lane 3), cells upon 4 h growth (lane 4), cells upon 8 h growth (lane 5), cells upon 9 h growth (lane 6), cells upon 24 h growth (lane 7). Densitometric analyses of protein bands with a molecular weight corresponding to that of ONC-r(P)ApoBs construct (16.1 kDa) are reported as histograms (c, d). Chimeric construct expression levels (g/L) and biomass (cell dry weight, g/L) are reported in e and f. Analyses are representative of fermentative processes carried out either in classical NoB medium (a, c, e) or in auto-inducing NoB medium (b, d, f).

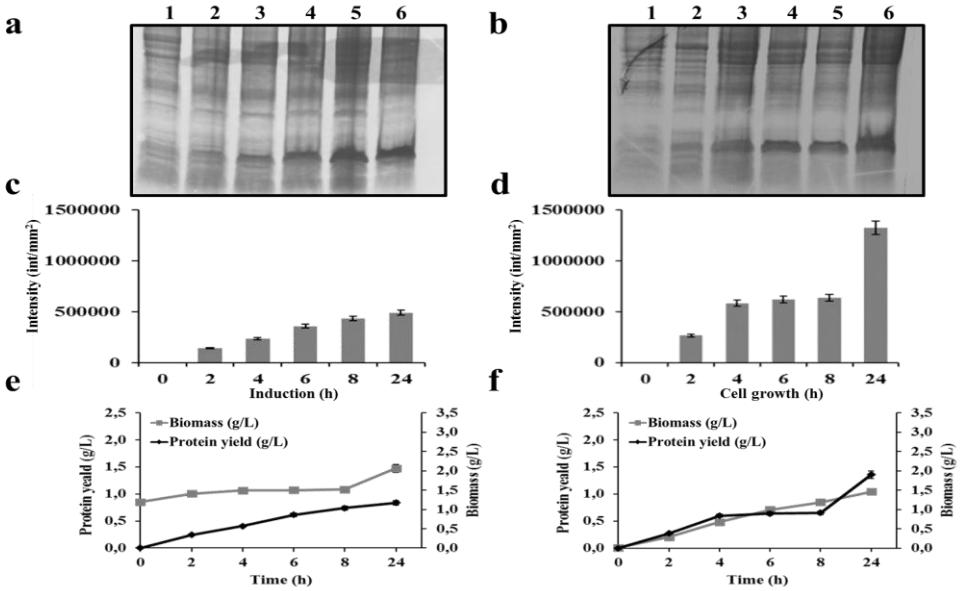

Figure 8. Analysis by SDS-PAGE of total proteins extracted from bacterial cells transformed with pET recombinant plasmid encoding ONC-r(P)GKY20 construct (a, b). Samples were collected at different time intervals along the fermentation process in batch reactor. In a, not induced cells (lane 1), cells upon 2h induction (lane 3), cells upon 4 h induction (lane 4), cells upon 8 h induction (lane 5), cells upon 24 h induction (lane 6). In b, cells at time 0 (lane 1), cells upon 2h growth (lane 3), cells upon 4 h growth (lane 4), cells upon 8 h growth (lane 5), cells upon 24 h growth (lane 6). Densitometric analyses of protein bands with a molecular weight corresponding to that of ONC-r(P)GKY20 construct (14.4 kDa) are reported as histograms (c, d). Chimeric construct expression levels (g/L) and biomass (cell dry weight, g/L) are reported in e and f. Analyses are representative of fermentation processes carried out either in classical NoB medium (a, c, e) or in auto-inducing NoB medium (b, d, f).

3.4 Cost estimation of HDPs production from lab to larger scales

The procedure to isolate pure recombinant HDPs has been previously described [9]. Briefly, upon recovery from inclusion bodies, the chimeric protein is purified by nickel affinity chromatography. The peptide is then released from the carrier onconase by a cleavage in mild acidic conditions. Since the carrier is insoluble at neutral or alkaline pH, the peptide is isolated from insoluble components by repeated cycles of centrifugation, and finally lyophilized (Figure 9). By using this experimental procedure, we obtained peptides 99% pure with a yield of 20-25 mg/L of bacterial culture. To determine yield, the purified peptide was weighed on a fine scale after lyophilization. However, analyses revealed that residual salts bound to the peptide significantly affect weight determination [29]. Indeed, when salts were removed by size-exclusion chromatography, peptides yield was found to be lowered to about 10-12 mg /L of bacterial culture.

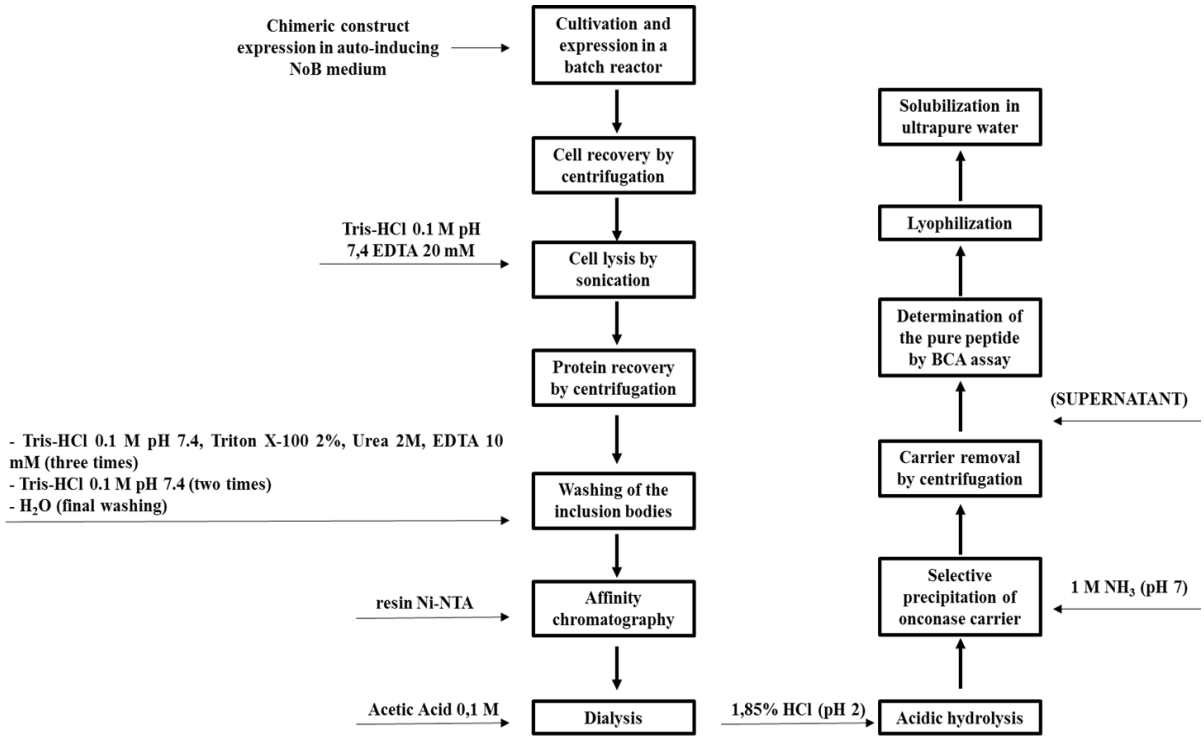

Figure 9. Block flow diagram describing the production and purification process of recombinant HDPs.

Figure 10 reports the breakdown of peptide unit costs (€/mg) as a function of the production scale expressed as mg/batch. It has to be emphasized that, at a lab scale (5 L fermenter), the cost is of about 250 €/mg and it is mainly affected by the labor costs and by the capital investment, such as main equipment costs and additional fixed costs required to maintain equipment. When production scale increases to 200, 500 or 1,000 mg/batch, the unit cost strongly decreases to 136, 65 and 42 €/mg, respectively. It has to be noticed that, in the last case, labor and chemical costs are the only relevant factors, which is typical of a production scale [19].

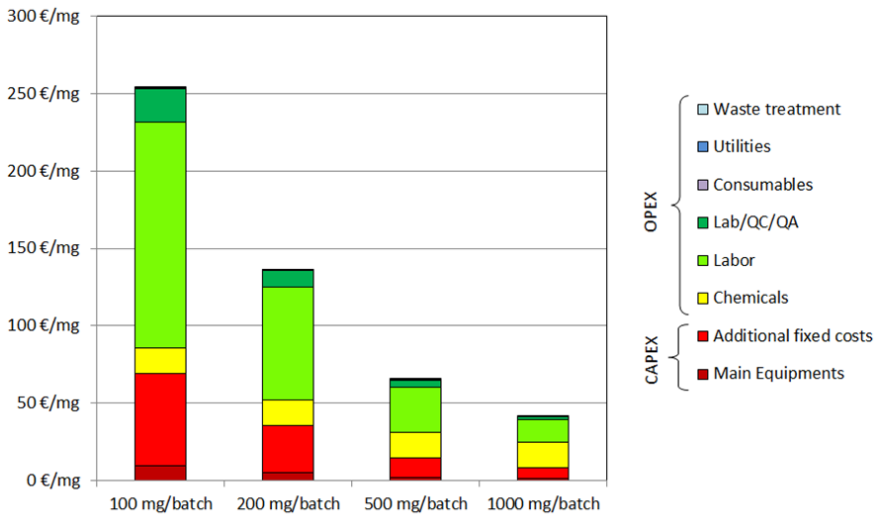

Figure 10. Breakdown of peptide unit production costs as a function of the production scale.

In order to identify process possible bottlenecks, costs have also been analysed by considering the contribution from each step of the process (fermentation, extraction and purification) (Figure 11). It has to be noticed that more than the half of the costs derives from the final purification step and that this contribution increases by increasing the production scale. Moreover, labor costs, instead, decrease by increasing the production scale, which further indicates that chemicals cost has a predominant effect. Indeed, the demand for chemicals, mainly guanidine, required to denature inclusion bodies and to perform expanded bed chromatography strongly affects the overall process costs.

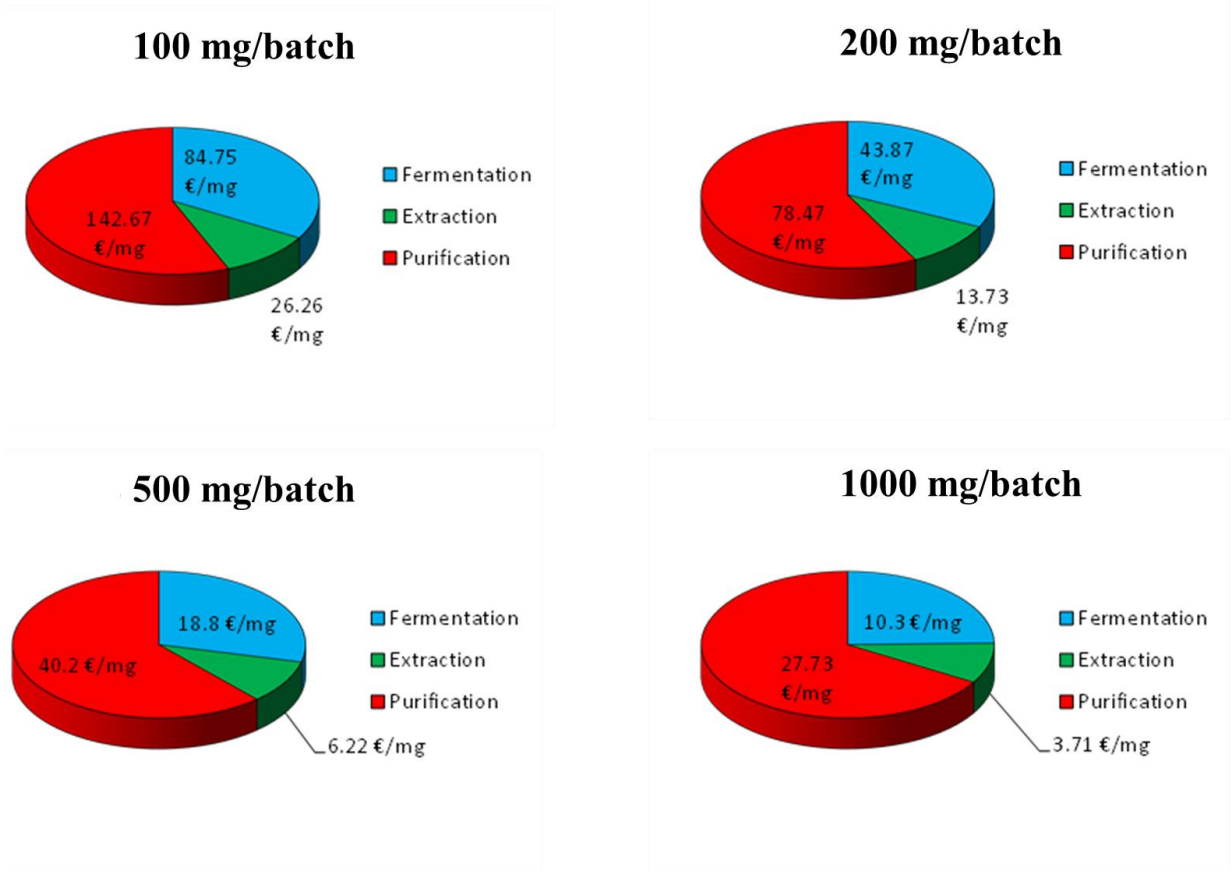

Figure 11. Impact of production process steps (fermentation, extraction and purification) on peptide unit production costs.

4. Discussion

Due to the current trend of reduction in the potency of commonly used antibiotics, there is an urgent demand for novel antimicrobials. Among these, HDPs are gaining great interest [30], since they generally do not lead to selection of resistant strains.

In general, HDPs isolation from natural sources is a labor intensive and time-consuming process, not suitable to obtain peptides in large amounts. On the other hand, chemical synthesis, although very efficient, is a complex and costly process [31]. In this scenario, to explore the pharmaceutical and therapeutic potential of antimicrobial peptides, a cost-effective and scalable method to produce active and effective HDPs is required. Procedures to express HDPs as recombinant peptides have encountered difficulties associated to their cytotoxicity to the bacterial host. As a consequence, difficulties to scale up the production process and peptide low yields upon purification represent main limitations [32-34]. Successful strategies are

generally based on the fusion of HDPs to carrier proteins. However, even when successful peptide expression was realized, further processing of fusion proteins, often requiring chemicals or costly enzymes, and multiple purification steps are responsible for low purification yields, with a consequent significant increase of production costs.

Here, we describe a cost-effective procedure to produce high amounts of three different HDPs [9-11]. The strategy is mainly based on the fusion of the HDP of interest to a convenient carrier, *i.e.* onconase from *Rana pipiens*, which has been previously optimized to ensure high expression levels of chimeric constructs [9]. To improve the production procedure, here, we also designed a novel cheap medium, named NoB medium, consisting of cheap components, readily available and containing precise amounts of each compound. The newly set up production procedure was also efficiently scaled up and the costs were significantly lowered by developing a successful auto-inducing procedure.

LB growth medium is the most commonly used medium for culturing *E. coli*, since it is easy to make, it is rich in nutrients, and its osmolarity is optimal for growth at early log phase. All these features make it adequate for protein production and compensate for the fact that it is not the best option to achieve high cell density cultures. In fact, although LB is a rich medium, bacterial cell growth usually stops at a relatively low density. This happens because LB contains scarce amounts of carbohydrates (and other utilizable carbon sources) and divalent cations [13]. Not surprisingly, when the amount of peptone or yeast extract is increased, higher cell densities are reached [14]. By the same way, divalent cation supplementation ($MgSO_4$ in the millimolar range) results in higher cell growth. Glucose supplementation is, instead, of limited help because acid generation by glucose metabolism overwhelms the limited buffer capacity of LB, at least in shake flasks where pH control can be laborious [15, 16]. Based on these observations, we developed a novel medium, which was found to support significantly higher cell densities and recombinant expression levels with respect to conventional culture media.

Furthermore, we also set up an auto-inducing expression protocol based on the concomitant presence of glucose, glycerol and lactose as carbon sources in the culture medium. By this way, recombinant constructs expression was found to be mediated by a common and cheap sugar, such as lactose, instead of IPTG, which might result too expensive for industrial purposes, even if generally required at sub millimolar concentrations [35-37]. Indeed, IPTG substitution was found to have several advantages, since this compound is not innocuous for bacterial cells and was found to have negative effects on bacterial cell growth [38-41]. It has also to be highlighted that auto-inducing procedure was found to support significantly higher yields of target constructs and cell biomass, with respect to conventional procedures based on IPTG mediated induction. The auto-induction procedure was also scaled up by using a 5 L fermenter system in which aerobic growth conditions were preserved by maintaining O_2 at 60% of saturation during the entire fermentation process. Moreover, to overcome disadvantages associated to ampicillin degradation, the antibiotic was regularly added to bacterial cells at a rate of 100 mg/h by using a fermenter peristaltic pump. Under these experimental conditions, expression levels of recombinant constructs were found to be significantly higher than those obtained in shake flask cultures, thus suggesting that the herein developed procedure might be successfully applied at an industrial scale. A further main advantage of the set-up procedure is the possibility to separate the peptide of interest from its carrier protein

by mild acidic conditions because of the presence of a dipeptide Asp-Pro between the peptide and the onconase moieties. By this way, it has been possible to avoid the use specific enzymes [42], which would have made the process too expensive and not suitable for industrial purposes.
Finally, to demonstrate the general validity of the set-up production strategy and its applicability to recombinant soluble proteins expressed in *E. coli*, we applied the auto-inducing protocol in NoB medium to the production of recombinant Apolipoprotein AI (ApoAI). The sequence encoding this protein was contained in the plasmid pET20b(+), and the protein was routinely expressed as soluble in *E. coli* BL21(DE3)pLysS cells [42]. When ApoAI expression and production were carried out by using the herein developed procedure, we found that the soluble protein expression levels were significantly higher in auto-inducing NOB medium (Figure 12) with respect to classical NOB medium under IPTG induction (data not shown). It has to be underlined that, in the case of soluble ApoAI recombinant expression, highest expression levels were observed after 8 h from the beginning of the fermentation process, with a slight decrease after 24 h, in agreement with data attesting ApoAI instability in bacterial expression systems [42]. However, the higher expression levels observed by applying this procedure with respect to conventional methods represent a fundamental feature attesting the general validity of the herein proposed procedure.

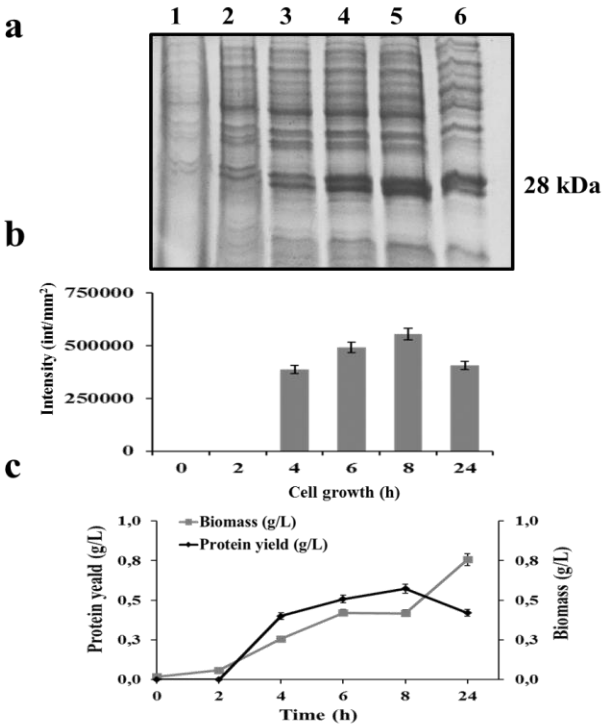

Figure 12. Analysis by SDS-PAGE of total proteins extracted from bacterial cells transformed with pET recombinant plasmid encoding ApoAI (a). Samples were collected at different time intervals along the fermentation process in batch reactor. In a, not induced cells (lane 1), cells upon 2h induction (lane 3), cells upon 4 h induction (lane 4), cells upon 8 h induction (lane 5), cells upon 24 h induction (lane 6). Densitometric analyses of protein bands with a molecular weight corresponding to ApoAI construct (28 kDa) are reported as histograms (b). Chimeric construct expression levels (g/L) and biomass (cell dry weight, g/L) are reported in c. Analyses

are representative of fermentation processes carried out in auto-inducing NoB medium.

In conclusion, along this Thesis project, we set up a cost-effective large-scale production system, which was found to be also successfully applicable to soluble proteins, and to provide expression levels significantly higher than those obtained with conventional protocols. Since the protocol to purify HDPs was previously optimized and found to provide high yields of pure peptides through a rapid one-step purification procedure, it is tempting to speculate that this optimized procedure might be successfully scaled up at an industrial scale in that increasing the production scale at 200, 500 and 1,000 mg/batch, unit costs strongly decreased. Hence, it represents a cost-effective and competitive strategy to produce the high amounts of peptides required for basic and clinical research.

5. References

1) Hancock R.E.W. The immunology of host defence peptides: beyond antimicrobial activity. 2006, Nature Reviews Immunology 16:321–334.

2) Andersson L. Large-scale synthesis of peptides. 2000, Biopolymers 55:227–250.

3) Ingham A.B. Recombinant production of antimicrobial peptides in heterologous microbial systems. 2007, Biotechnol. Appl. Biochem. 47:1–9.

4) Li Y. RAPD: a database of recombinantly-produced antimicrobial Peptides. 2008, FEMS Microbiol. Lett. 289:126–129.

5) Zorko M. Production of recombinant antimicrobial peptides in bacteria. 2010, Methods Mol Biol. 618:61–76.

6) Li Y. Recombinant production of antimicrobial peptides in Escherichia coli: a review. 2011, Protein Expr Purif. 80:260–267.

7) Li Y. Carrier proteins for fusion expression of antimicrobial peptides in Escherichia coli. 2009, Biotechnol Appl Biochem. 54:1–9.

8) Vassilevski A.A. Antimicrobial peptide precursor structures suggest effective production strategies. Recent Pat. 2008, Inflamm. Allergy Drug Discov. 2:58–63.

9) Pane K. Rational Design of a Carrier Protein for the Production of Recombinant Toxic Peptides in Escherichia coli. 2016, PLoS One 11:e0146552.

10) Pane K. A new cryptic cationic antimicrobial peptide from human apolipoprotein E with antibacterial activity and immunomodulatory effects on human cells. 2016, FEBS J. 283: 2115-2131.

11) Gaglione R. Novel human bioactive peptides identified in apolipoprotein B: evaluation of their therapeutic potential. 2017, Biochem Pharmacol. doi: 10.1016/j.bcp.2017.01.009.

12) Notomista E. Effective expression and purification of recombinant onconase, an antitumor protein. 1999, FEBS Lett. 463:211–215.

13) Sezonov G. Escherichia coli physiology in Luria-Bertani broth. 2007, J Bacteriol. 189:8746-8749.

14) Studier FW. Protein production by auto-induction in high density shaking cultures. 2005, Protein Expr Purif. 41:207-234.

15) Weuster-Botz D. Parallel substrate feeding and pH-control in shaking-flasks. 2001, Biochem Eng J. 7:163-170.

16) Scheidle M. Controlling pH in shake flasks using polymer-based controlled-release discs with pre-determined release kinetics. 2011, BMC Biotechnol. 11:25.

17) Madurawe R.D. A recombinant lipoprotein antigen against Lyme disease expressed in E. coli: fermentor operating strategies for improved yield. 2000, Biotechnol Prog. 16:571-576.

18) Green M.R. Molecular Cloning: A Laboratory Manual. 2012, 4th ed: Cold Spring Harbor laboratory Pess.

19) Heinzle E. Development of Sustainable Bioprocesses Modeling and Assessment. 2006, John Wiley & Sons, Ltd.

20) Langlykke AF. Microbial process translation-laboratory to pilot plant at the Frederick Cancer Research Center. Recent Results Cancer Res. 1978;63:85-98.

21) Huang C.J. Industrial production of recombinant therapeutics in Escherichia coli and its recent advancements. 2012, J Ind Microbiol Biotechnol. 39:383-399.

22) Sleator R.D. Bacterial osmoadaptation: the role of osmolytes in bacterial stress and virulence. 2002, FEMS Microbiol Rev. 26:49-71.
23) Mayer S. Lactose autoinduction with enzymatic glucose release: characterization of the cultivation system in bioreactor. 2014, Protein Expr Purif. 94:67-72.
24) Blommel P. Fox B. Enhanced bacterial protein expression during auto-induction obtained by alteration of Lac repressor dosage and medium composition. Biotechnology Progress. 2007, 23, no. 3: 585–598.
25) Fischer D. The general sigma factor rS of Escherichia coli is induced during the diauxic shift from glucose to lactose. 1998, J. Bacteriol. 180(23): 6203–6206.
26) Neubauer P. Maximizing the expression of a recombinant gene in Escherichia coli by manipulation of induction time using lactose as inducer. 1992, Appl Microbiol Biotechnol. Mar;36(6):739-44.
27) Jung G. High-cell density fermentation studies of recombinant Escherichia coli strains expressing human interleukin-1 beta. 1988, Ann Inst Pasteur Microbiol. Jan-Feb;139(1):129-46.
28) Hoffman Brian J. Lactose fed-batch overexpression of recombinant metalloproteins in E. coli BL21(DE3): process control yielding high levels of metal-incorporated, soluble protein. 1995, Protein expression and purification. 6, 646-654.
29) Bommarius B. Cost-effective Expression and Purification of Antimicrobial and Host Defense Peptides in Escherichia coli. 2010, Peptides 31(11): 1957–1965.
30) Brogden K. A. Antimicrobial peptitdes: pore formers or metabolic inhibitors in bacteria? 2005, Nat. Rev. Microbiol. 3(3): 238-50.
31) Chen Y.Q. Expression of a cytotoxic cationic antibacterial peptide in Escherichia coli using two fusion partners. 2008, Protein Expr Purif;57:303– 311.
32) Piers K.L. Recombinant DNA procedures for producing small antimicrobial cationic peptides in bacteria. 1993, Gene 134:7–13.
33) Zhang L. Determinants of recombinant production of antimicrobial cationic peptides and creation of peptide variants in bacteria. 1998, Biochem Biophys Res Commun; 247:674–680.
34) Tripathi N.K. High Yield Production of Heterologous Proteins with Escherichia coli. 2009, Defence Science Journal. Vol. 59, No. 2, pp. 137-146.
35) Xu P. Modular optimization of multi-gene pathways for fatty acids production in E. coli. 2013, Nat. Commun. 4: 1409.
36) Leonard E. Engineering central metabolic pathways for high-level flavonoid production in Escherichia coli. 2007, Appl. Environ. Microbiol. 73: 3877–3886.
37) Anthony J.R. Optimization of the mevalonate-based isoprenoid biosynthesis pathway in Escherichia coli for production of the anti-malarian drug precursor amorpha-4,11-diene. 2009, Metab. Eng.; 11: 13–19.
38) Kosinski M.J. Isopropyl-β-D-thiogalactopyranoside influences the metabolism of Escherichia coli. 1992, Appl. Microbiol. Biotechnol. 36: 782–784.
39) Andrews K.J. Selective disadvantage of non-functional protein synthesis in Escherichia coli. 1976, J. Mol. Evol. 8: 317–328.
40) Malakar P. Effect of substrate and IPTG concentrations on the burden to growth of Escherichia coli on glycerol due to the expression of Lac proteins. 2012, Appl. Microbiol. Biotechnol. 93: 2543–2549.
41) Zhou Q.F. High-level production of a novel antimicrobial peptide perinerin in Escherichia coli by fusion expression. 2007, Curr Microbiol;54:366–370.
42) Ryan R.O. Optimized bacterial expression of human apolipoprotein A-I. 2003, Protein Expr Purif. 27(1):98-103.

CHAPTER 3

Novel human bioactive peptides identified in Apolipoprotein B: evaluation of their therapeutic potential

Rosa Gaglione

Department of Chemical Sciences, PhD in Biotechnology

University of Naples "Federico II", Napoli, Italy

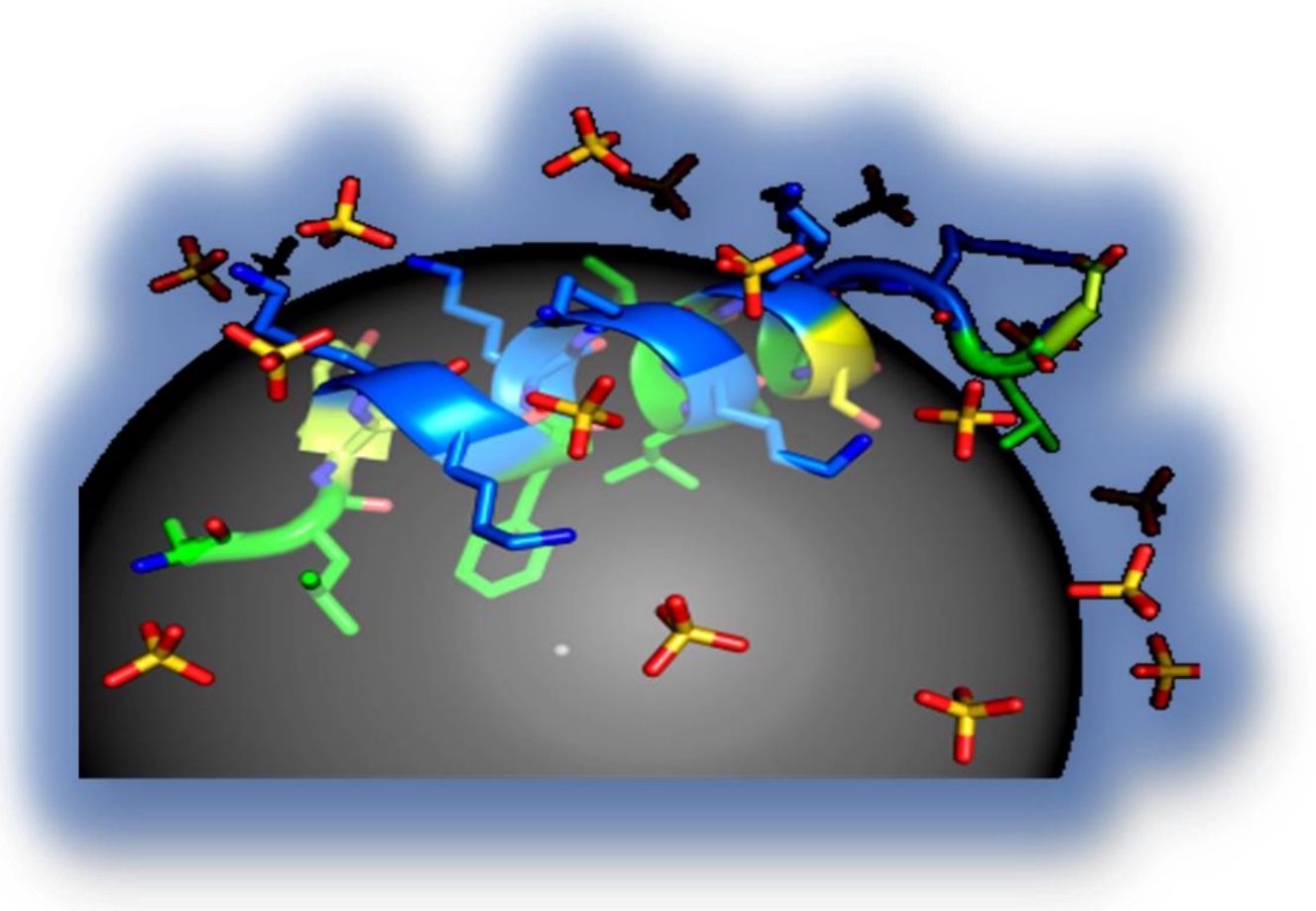

1. Introduction

Apolipoproteins, the main protein components of plasma lipoproteins, are a source of bioactive peptides. Reports have shown that peptides derived from the cationic receptor binding region of Apolipoprotein E (ApoE141-149) are endowed with broad anti-infective activity [1]. Apolipoprotein B (ApoB) also contains two LDL (low-density lipoprotein) receptor binding domains, namely region A (ApoB3147-3157) and region B (ApoB3359-3367). Region B, more uniformly conserved across species and primarily involved in receptor binding, has been found to be endowed with a significant antiviral activity [1]. Moreover, peptides derived from ApoB have been already used in vaccine preparations to treat atherosclerosis [2]. When ApoE deficient mice have been immunized with ApoB661–680 and ApoB3136–3155 peptides, a significant increase of the levels of peptide-specific immunoglobulins was detected accompanied by a concomitant increase of secreted interleukin-10 (IL-10) levels, with no effect on IFN-γ expression levels, thus indicating that ApoB derived peptides are able to modulate the immune response [2].

Recently, our group developed an *in silico* method [3] to identify HDPs in protein precursors and to predict quantitatively their antibacterial activity. This method assigns to any given peptide an antimicrobial score, called “absolute score” (AS), on the basis of net charge, hydrophobicity and length of the peptide and of two bacterial strain-dependent weight factors defining the contribution of charge and hydrophobicity to the antimicrobial activity. We demonstrated that AS is directly proportional to the antimicrobial activity of HDPs expressed as Log(1,000/MIC), where MIC is the minimal inhibitory concentration of the peptide. Score values lower than 6.5 are considered not significant as they correspond to predicted MIC values higher than 200 μM, while for score values higher than about 10 the linear relationship is no longer valid, and an increase in the score does not necessarily correspond to a concomitant increase in the antimicrobial activity. To analyse a protein potentially bearing hidden antimicrobial regions, the AS values of all the peptides of the desired length contained in a precursor protein can be plotted as a function of peptide sequence and length, thus obtaining an accurate map of the antimicrobial activity determinants. This method allows the identification of novel HDPs within the sequence of known proteins (“cryptic” HDPs), as demonstrated by the identification of a novel cationic HDP endowed with antibacterial and immunomodulatory activities in human ApoE [3], and in the transcription factor Stf76 from the archaeon *Sulfolobus islandicus*. In the last case, peptide VLL-28 represents the first antimicrobial peptide derived from an archaeal protein [4].

We applied our *in silico* analysis method to a human Apolipoprotein B (ApoB) isoform [5, 6]. In Figure 1, the isometric plot of region 882-929 of this ApoB variant is shown. An absolute maximum, corresponding to region 887-922 (AS = 12.0), and a relative maximum, corresponding to residues 887-909 (AS = 10.6), are shown (Figure 1). Even if several ApoB functional regions have already been analysed, and in some cases biologically active peptides were obtained [1, 2], to the best of our knowledge, this is the first report identifying ApoB region 887-922 as a source of HDPs. Here, we report the recombinant production and characterization of two variants of the putative HDP identified by our bioinformatics method in human ApoB, *i.e.* peptides ApoB887-923 and ApoB887-911. Both peptides include at the C-terminal side one (as in the case of ApoB887-923), or two (as in the case of ApoB887-911) small uncharged residues (serine, glycine or threonine), which are not present in the regions highlighted in the AS plot (Figure 1). These residues have been arbitrarily included to avoid that the negatively charged C-terminus of the peptide is adjacent to the

antimicrobial region. The sequence of peptide r(P)ApoB$_L$ is PHVALKPGKLKFIIPSPKRPVKLLSGGNTLHLVSTTKT, while that of peptide r(P)ApoB$_S$ is PHVALKPGKLKFIIPSPKRPVKLLSG.
To evaluate the therapeutic potential of these peptides, we analysed their structure, antimicrobial and anti-biofilm activities, the ability to act in synergy with conventional antibiotics, their anti-inflammatory and wound healing properties, and their possible toxic effects on eukaryotic cells.

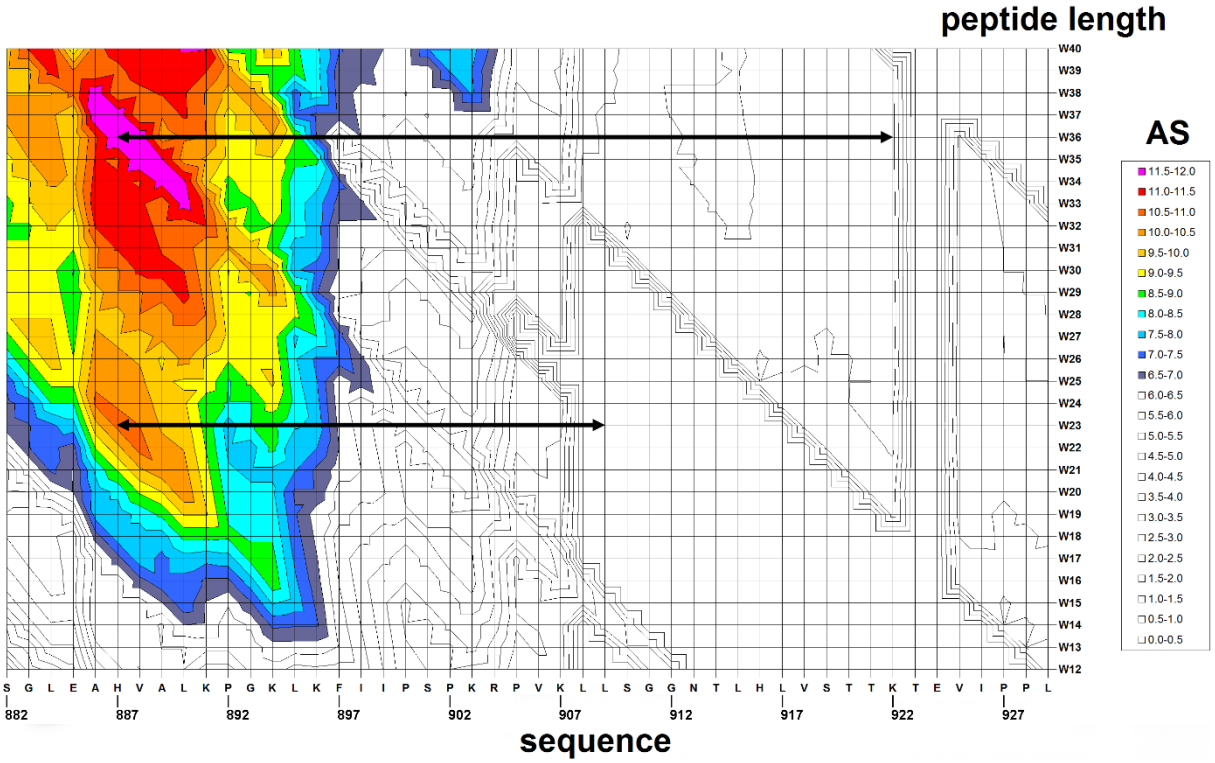

Figure 1. Isometric plot showing the absolute score values (AS) of peptides with a length ranging from 12 to 40 residues (W12-W40) in the region 882-929 of ApoB. Colors were used to highlight AS values higher than 6.5, and corresponding to predicted MIC values on *S. aureus* lower than 200 µM.

2. Materials and methods

2.1. Bacterial strains and growth conditions

Eight bacterial strains were used in the present study, *i.e. E. coli* ATCC 25922, methicillin-resistant *Staphylococcus aureus* (MRSA WKZ-2), *Salmonella enteriditis* 706 RIVM, *Bacillus globigii* TNO BM013, *Bacillus licheniformis* ATTC 21424, *Staphylococcus aureus* ATTC 29213, *Pseudomonas aeruginosa* ATCC 27853, and *Pseudomonas aeruginosa* PAO1. All bacterial strains were grown in Muller Hinton Broth (MHB, Becton Dickinson Difco, Franklin Lakes, NJ) and on Tryptic Soy Agar (TSA; Oxoid Ltd., Hampshire, UK). In all the experiments, bacteria were inoculated and grown over-night in MHB at 37 °C. The next day, bacteria were transferred to a fresh MHB tube and grown to mid-logarithmic phase.

2.2. Cell culture

Murine RAW 264.7 cells, malignant SVT2 murine fibroblasts (BALBc 3T3 cells transformed by SV40 virus), parental murine BALBc 3T3 cells, and human HeLa and HaCaT cells were from ATCC, Manassas, VA. Cells were cultured in Dulbecco's

modified Eagle's medium (Sigma Aldrich, Milan, Italy), supplemented with 10% foetal bovine serum (HyClone, GE Healthcare Lifescience, Chicago, IL) and antibiotics, in a 5% CO_2 humidified atmosphere at 37 °C.

2.3. Synthetic peptides

CATH-2 peptide was obtained from CPC Scientific Inc. (Sunnyvale, USA), and LL-37 peptide was from Sigma Aldrich, Milan, Italy.

2.4. Expression ad isolation of recombinant ApoB derived peptides

Expression and isolation of recombinant peptides was carried out as previously described by Pane K. et al [7] and in the Chapter 2.

2.5. Mass spectrometry analyses

Matrix-assisted laser desorption/ionization mass spectrometry (MALDI-MS) was carried out on a 4,800 Plus MALDI TOF/TOF mass spectrometer (Applied Biosystems, Framingham, MA) equipped with a nitrogen laser (337 nm). The peptide samples (1 mL) were mixed (1:1, v/v) with a 10 mg/mL solution of a-cyano-4-hydroxycinnamic acid in acetonitrile/50mM citrate buffer (70:30 v/v). Mass calibration was performed using external peptide standards purchased from Applied Biosystems. Spectra were acquired using 5,000 shots/spectrum in a mass (m/z) range of 1,000–5,000 amu and raw data were analysed using Data Explorer Software provided by the manufacturer.

2.6. Circular dichroism spectroscopy

CD experiments were performed on a Jasco J-815 circular dichroism spectropolarimeter, calibrated for intensity with ammonium [D10] camphorsulfonate ($[\Theta_{290.5}]$ = 7,910 deg cm^2 $dmol^{-1}$). The cell path length was 0.01 cm. CD spectra were collected at 25 °C in the 190-260 nm (far-UV) at 0.2 nm intervals, with a 20 nm/min scan rate, 2.5 nm bandwidth and a 16 sec response. Spectra are reported in terms of mean residue ellipticity, calculated by dividing the total molar ellipticity by the number of amino acids in the molecule. Each spectrum was corrected by subtracting the background, and reported without further signal processing. Lyophilized peptides were dissolved in ultra-pure water (Romil, Waterbeach, Cambridge, GB) at a concentration of 100 µM, determined on the basis of peptide dry weight and BCA assay (ThermoFisher Scientific, Waltham, MA). CD spectra of the peptides were collected in the absence or in the presence of increasing concentrations of trifluoroethanol (TFE, Sigma Aldrich, Milan, Italy), SDS (Sigma Aldrich, Milan, Italy) or lipopolysaccharide (LPS) from *E. coli* 0111:B4 strain (Sigma Aldrich, Milan, Italy). CD spectra were corrected by subtracting every time the contribution of the compound under test at any given concentration. CD spectra deconvolution was performed by using the program PEPFIT, that is based on peptide-derived reference spectra [8], in order to estimate secondary structure contents. A Microsoft Excel-ported version of PEPFIT was used for convenience [9].

2.7. Measurement of IL-6 release

IL-6 levels were determined by ELISA assay (DuoSet ELISA kits, R&D Systems, Minneapolis, MN) following the manufacturer's instructions. Briefly, RAW 264.7 cells (5×10^4) were seeded into 96-well microtiter plates, and grown to semi-confluency. After 24 h, the culture medium was replaced with fresh medium containing the peptides under test (5 or 20 µM) in the presence or in the absence of LPS from

Salmonella Minnesota (50 ng/mL, Sigma Aldrich, Milan, Italy) for 24 h at 37 °C. When the protective effect of peptides was evaluated, cells were pre-incubated with the peptides under test (5 or 20 μM) for 2 h at 37 °C. Following treatment, cells were washed three times with PBS prior to incubation with LPS (50 ng/mL) for further 24 h at 37 °C. In each case, at the end of incubation, the culture supernatants were collected, and centrifuged at 5,000 rpm for 3 min at room temperature, in order to remove cell debris. Samples were then analysed by reading absorbance values at 450 nm using 550 nm as a reference wavelength at an automatic plate reader (FLUOstar Omega, BMG LABTECH, Ortenberg, Germany).

2.8. Determination of NO production

To determine the levels of NO released by RAW 264.7 cells, a colorimetric assay based on the use of Griess reagent (Sigma Aldrich, Milan, Italy) was performed. The levels of nitrite (NO^{2-}) in cell supernatants were determined on the basis of a reference curve obtained by testing increasing concentrations (from 1 to 50 μM) of sodium nitrite dissolved in water. Briefly, cell culture supernatants were mixed with equal volumes of 1% sulphanilamide dissolved in 2.5% phosphoric acid, and incubated for 5 min at room temperature. Samples were then diluted 1:1 (v/v) with 0.1% N-(1-naphthyl) ethylenediamine dihydrochloride, and incubated for further 5 min at room temperature. Absorbance values were then determined at 520 nm using an automatic plate reader (FLUOstar Omega, BMG LABTECH, Ortenberg, Germany).

2.9. Antimicrobial activity assay

The antimicrobial activity of ApoB derived peptides was tested towards eight bacterial strains, *i.e. E. coli* ATCC 25922, methicillin-resistant *Staphylococcus aureus* (MRSA WKZ-2), *Salmonella enteriditis* 706 RIVM, *Bacillus globigii* TNO BM013, *Bacillus licheniformis* ATCC 21424, *Staphylococcus aureus* ATCC 29213, *Pseudomonas aeruginosa* ATCC 27853, and *Pseudomonas aeruginosa* PAO1. In each case, bacteria were grown to mid-logarithmic phase in MHB at 37 °C. Cells were then diluted to $2x10^6$ CFU/mL in Nutrient Broth (Difco, Becton Dickinson, FranklinLakes, NJ) containing increasing amounts of either r(P)$ApoB_L$ or r(P)$ApoB_S$ peptide (0.625 – 40 μM). In each case, starting from a peptide stock solution, two-fold serial dilutions were sequentially carried out, accordingly to broth microdilution method [10]. Following over-night incubation, MIC_{100} values were determined as the lowest peptide concentration responsible for no visible bacterial growth.

2.10. Killing kinetics studies

To kinetically analyse bacterial killing by ApoB derived peptides, experiments were performed on *E. coli* ATTC 25922 and *Bacillus licheniformis* ATTC 21424 strains. To this purpose, bacteria were grown over-night in MHB medium, then diluted in fresh MHB, and incubated at 37 °C until logarithmic phase of growth was reached. Bacteria were then diluted to $4×10^6$ CFU/mL in a final volume of 150 μL of Nutrient Broth 0.5X (Difco, Becton Dickinson, Franklin Lakes, NJ), and mixed with the peptide under test (1:1 v/v). For each strain, increasing concentrations of peptide were analysed (ranging from 0 to 20 μM or from 0 to 10 μM in the case of *E. coli* ATTC 25922 and *Bacillus licheniformis* ATTC 21424 strains, respectively. At defined time intervals, samples (20 μL) were serially diluted (from 10- to 10,000-fold), and 100 μL of each dilution were plated on TSA. Following an incubation of 16 h at 37 °C, bacterial colonies were counted.

2.11. Synergy evaluation

Synergism between ApoB derived peptides and antimicrobial agents was assessed by the so called “checkerboard” assay against *S. aureus* MRSA WKZ-2, *E. coli* ATCC 25922, *P. aeruginosa* ATCC 27853, *P. aeruginosa* PAO1, and *S. aureus* ATCC 29213. To this purpose, ApoB derived peptides were tested in combination with EDTA or antibiotics, such as ciprofloxacin, colistin, erythromycin, kanamycin sulfate, and vancomycin. All these antimicrobial agents were from Sigma Aldrich, Milan, Italy. Two-fold serial dilutions of each ApoB derived peptide and each antimicrobial agent were tested in combination on each strain tested. To do this, we tested peptide concentrations ranging from 0 to 20 μM. Compound concentrations tested on each strain are reported in Table 1. The fractional inhibitory concentration (FIC) index was calculated as follows: $FIC_A + FIC_B$, where FIC_A = MIC of drug A in combination/MIC of drug A alone, and FIC_B = MIC of drug B in combination/MIC of drug B alone. FIC indexes ≤ 0.5 were classified as synergism, whereas FIC indexes between 0.5 and 4 were associated to additive or “no interaction” effects [11]. Antagonism is usually associated to a FIC index > 4.

	S. aureus **ATCC 29213**	***S. aureus*** **MRSA WKZ-2**	***P. aeruginosa*** **ATCC 27853**	***P. aeruginosa*** **PAO1**	***E. coli*** **ATCC 25922**
Ciprofloxacin	0-0,5 μg/mL	0-1 μg/mL	0-2 μg/mL	0-1 μg/mL	0-0,03 μg/mL
Colistin	0-8 μg/mL	0-8 μg/mL	0-4 μg/mL	0-4 μg/mL	0-8 μg/mL
Erythromycin	0-4 μg/mL	0-4 μg/mL	0-16 μg/mL	0-128 μg/mL	0-128 μg/mL
Vancomycin	0-0,25 μg/mL	0-0,5 μg/mL	0-32 μg/mL	0-4 μg/mL	0-0,25 μg/mL
Kanamycin	0-0,5 μg/mL	0-0,125 μg/mL	0-64 μg/mL	0-8 μg/mL	0-0,125 μg/mL
EDTA	0-24,53 μg/mL	0-49,07 μg/mL	0-392,5 μg/mL	0-196,2 μg/mL	0-98,14 μg/mL

Table 1. Range of antimicrobial agent concentrations tested for combination therapy analyses. Based on bacterial strain susceptibility, different concentrations of each compound were used in combination with ApoB derived peptides (0- 20 μM) to evaluate synergistic effects.

2.12. Anti-biofilm activity

Anti-biofilm activity of ApoB derived peptides was tested on *S. aureus* MRSA WKZ-2, *E. coli* ATCC 25922, *P. aeruginosa* ATCC 27853, and *P. aeruginosa* PAO1 strains. Bacteria were grown over-night in MHB (Becton Dickinson Difco, Franklin Lakes, NJ), and then diluted to 1×10^8 CFU/mL in BM2 medium [12] containing increasing peptide concentrations (0 - 1 μM). Incubations with the peptides were carried out either for 4 h, in order to test peptide effects on biofilm attachment, or for 24 h, in order to test peptide effects on biofilm formation. When peptide effects on pre-formed biofilm were evaluated, bacterial biofilms were formed for 24 h at 37 ˚C, and then treated with increasing concentrations (0 - 1 μM) of the peptides. In all the cases, at the end of the incubation, the crystal violet assay was performed. To do this, the planktonic culture was removed from the wells, which were washed three times with sterile PBS prior to staining with 0.04% crystal violet (Sigma Aldrich, Milan, Italy) for 20 min. The colorant excess was eliminated by three successive washes with sterile PBS. Finally, the crystal violet was solubilised with 33% acetic acid and samples optical absorbance values were determined at 630 nm by using a microtiter plate reader (FLUOstar Omega, BMG LABTECH, Germany). To determine the percentage of viable bacterial cells inside the biofilm structure, upon biofilm disruption with 0,1% Triton X-100 (Sigma Aldrich, Milan, Italy), bacterial cells were ten-fold diluted on solid TSA and incubated for 16 h at 37 °C. Once evaluated the number of colony forming

units, bacterial cell survival was calculated as follows: ($CFU_{in\ treated\ sample}/CFU_{in\ untreated\ sample}$) ×100.
Biofilm cultivation in flow chambers was performed in minimal medium (BM_2) for 48 h at 37°C. Once biofilm was grown, samples were treated with 1 µM of each peptide for 24 h at 37 °C. Biofilms were then stained by using SYTO-9 dye to stain live biofilm cells (green signal) and propidium iodide, a normally cell-impermeable dye, to stain dead cells (red signal). Samples were examined by wide-field fluorescence microscopy. Prior to the analysis, silicone tubing was autoclaved, and the system was assembled and sterilized by pumping 0.5% hypochlorite at 6 rpm for 1 h by using a Watson Marlow 205S peristaltic pump. The system was then rinsed at 6 rpm with sterile water for 30 min, and then with medium for further 30 min. Flow chambers were then inoculated by injecting with a syringe mid-log culture diluted to an OD_{600} of 0.02 (400 µL). Chambers were then left in the absence of flow for 2 h. Afterwards, the medium was pumped through the system at a constant rate of 0.75 rpm (3.6 mL/h). Analyses were performed by using a Leica DMI 4000 B wide-field fluorescence microscope equipped with the following filter sets: Ex 490/20-Em 525/36 for the acquisition of green signal and Ex 555/25-Em 605/52 for the acquisition of red signal. Quorum Angstrom Optigrid (MetaMorph) acquisition software was used. Images were obtained with a 63× objective. Deconvolution was performed by using Huygens Essential (Scientific Volume Imaging B.V.), and three-dimensional (3D) reconstructions were generated using the Imaris software package (Bitplane AG).

2.13. Cytotoxicity assays

Cytotoxic effects of ApoB derived peptides on RAW 264.7 cells were determined by using the cell proliferator reagent WST-1(Roche Applied Science, Mannheim, Germany). To this purpose, RAW 264.7 cells were plated into 96-well plates at a density of 5×10^4 cells in 100 µL medium per well, and incubated over-night at 37 °C. Afterwards, cells were treated with increasing concentrations (0 - 20 µM) of the peptides for 24 h at 37 °C. Following incubation, peptide-containing medium was removed, and 100 µL of fresh medium containing 10% WST-1 reagent was added to each well. Following an incubation of 30 min at 37 °C in the dark, sample absorbance values were measured at 450 nm using 650 nm as a reference wavelength at a microtiter plate reader (FLUOstar Omega, BMG LABTECH, Germany).
Cytotoxic effects of peptides on the viability of malignant SVT2 murine fibroblasts, parental murine BALBc 3T3 fibroblasts, human HeLa cells, and human HaCaT keratinocytes were determined by using the 3-(4,5-dimethylthiazol-2-yl)-2,5-diphenyltetrazolium bromide (MTT) assay (Sigma Aldrich, Milan, Italy), as previously described [13]. Briefly, cells were seeded into 96-well plates at a density of 5×10^3/well in 100 µL medium per well, and incubated over-night at 37 °C. Afterwards, cells were treated with increasing concentrations (0 - 20 µM) of the peptides under test for 24 h at 37 °C. Following incubation, the peptide-containing medium was removed, and 100 µL of MTT reagent, dissolved in DMEM without phenol red (Sigma Aldrich, Milan, Italy), were added to the cells (100 µL/well) at a final concentration of 0.5 mg/mL. After 4 h at 37 °C, the culture medium was removed and the resulting formazan salts were dissolved by the addition of isopropanol containing 0.1 N HCl (100 µL/well). Absorbance values of blue formazan were determined at 570 nm using an automatic plate reader (Microbeta Wallac 1420, Perkin Elmer).
In all the cases, cell survival was expressed as the percentage of viable cells in the presence of the peptide under test, with respect to control cells grown in the absence of the peptide.

2.14. Haemolytic activity

The release of haemoglobin from mouse erythrocytes was used as a measure for the haemolytic activity of ApoB derived peptides. To do this, EDTA anti-coagulated mouse blood was centrifuged for 10 min at 800 x g at 20 °C, in order to obtain red blood cells (RBCs), which were washed three times, and 200-fold diluted in PBS. Subsequently, 75 µL aliquots of RBCs were added to 75 µL peptide solutions (final concentration ranging from 0 to 20 µM) in 96-well microtiter plates, and the mixture was incubated for 1 h at 37 °C. Following the incubation, the plate was centrifuged for 10 min at 1,300 × g at 20 °C, and 100 µL supernatant of each well were transferred to a new 96-well plate. Absorbance values were determined at 405 nm by using an automatic plate reader (FLUOstar Omega, BMG LABTECH, Germany), and the percentage of haemolysis was calculated by comparison with the control samples containing no peptide (negative control) or 0.2% (v/v) Triton X-100 (positive control, complete lysis). Haemolysis (%) = [($Abs_{405\ nm}$ peptide − $Abs_{405\ nm}$ negative control)/$Abs_{405\ nm}$ 0.2% Triton − $Abs_{405\ nm}$ negative control)] × 100.

2.15. Wound healing assay

Wound heling activity of r(P)$ApoB_L$ peptide was evaluated *in vitro* as previously described [14]. Human HaCaT keratinocytes were seeded into 12-well plates at a density of 6.3 x 10^5 cells/well in 1 mL medium per well. Following an incubation of 24 h at 37 °C, cells were pre-treated with 3 µM mitomycin C for 30 min, in order to inhibit cell proliferation [15]. Cell monolayers were then wounded with a pipette tip to remove cells from a specific region of the monolayer. The culture medium was then removed and the cells were washed twice with PBS. Cells were then incubated with fresh culture medium containing increasing concentrations of r(P)$ApoB_L$ peptide (0 – 0.5 – 10 – 20 µM). Wound closure was then followed by multiple field time-lapse microscopy (TLM) experiments, using an inverted microscope (Zeiss Axiovert 200, Carl Zeiss, Germany) equipped with an incubator to control temperature, humidity and CO_2 percentage [16, 17]. Images were iteratively acquired in phase contrast with a CCD video camera (Hamamatsu Orca AG, Japan) by using a 10x objective. The microscope was also equipped with a motorized stage and focus control (Marzhauser, Germany) enabling automated positioning of the acquired samples. The workstation was controlled through a homemade software in Labview. Each cell sample was analysed in duplicate, and in any case at least two fields of view were selected. Since three independents experiments were carried out, from 4 to 12 independent fields of view were analysed for each sample. The delay between consecutive imaging of the same field of view was set to 15 min. The wound closure dynamics were quantified by using a homemade automated image analysis software, that allowed to measure the size of the wound area for each time point (A). For each field of view, determined values were normalized with respect to the value of the wound area at time 0 (A_0), and plotted as function of time. After an initial lag phase, the wound area was found to decrease with a constant velocity [18, 19]. By reporting A/A_0 values as a function of time, a linear decrease was observed for A/A_0 values lower than 0.8 (Figure 7b). For each sample, the lag time t_L was calculated as the time required to obtain an initial wound closure corresponding to A/A_0=0.8. Being R^2 typically higher than 0.98, the linear range of the curve was fitted, and the slope (-α) was considered a measure of the wound closure velocity. The values of wound closure velocity obtained for each field of view from three independent experiments were averaged (α), and normalized with respect to the value of the corresponding

control sample (α_{contr}). For each peptide concentration tested, α/α_{contr} values obtained from three independent experiments were averaged and the standard error of the mean was calculated to account for reproducibility [20].

2.16. Statistical analyses

Statistical analysis was performed by the Student's t-Test. Significant differences were indicated as *($p < 0.05$), **($p < 0.01$) or ***($p < 0.001$).

3. Results

3.1. Recombinant production of ApoB derived peptides

Expression of HDPs in bacterial cells can be deleterious to the host due to their toxicity. For this reason, we used a procedure to produce HDPs as fusion proteins with onconase (ONC), a frog ribonuclease that mediates the delivery to inclusion bodies very efficiently, as previously described [3, 6], thus avoiding toxicity problems. DNA sequences encoding peptide ApoB887-923 or peptide ApoB887-911, synthesized by MWG Biotech in conformity with the *E. coli* codon usage, were cloned into the expression vector pET22b(+), downstream to a sequence encoding a mutated form of ONC. As described in Chapter 2, the resulting fusion proteins contain a His tag sequence, positioned between the ONC and the peptide moieties, suitable for easily purify the fusion protein, a flexible linker (Gly-Thr-Gly), and a dipeptide (Asp-Pro), which is cleaved in mild acidic conditions thus allowing the release of the peptide from the carrier. Since the carrier is insoluble at neutral or alkaline pH, ApoB derived peptides were isolated from insoluble components by repeated cycles of centrifugation, and finally lyophilized. Peptides purity was checked by SDS/PAGE and matrix assisted laser desorption ionisation (MALDI) mass spectrometry analyses. Recombinant peptides were found to be 99% pure. Molecular mass values of ApoB887-923 and ApoB887-911 were found to be 4,072.3 Da (Theoretical MH^+ 4,072.7) and 2,820.9 Da (Theoretical MH^+ 2,820.2), respectively, values which are in agreement with the expected molecular weight of the peptides including a Pro residue due to the cleavage of the Asp-Pro bond. The final yield of peptides ApoB887-923 and ApoB887-911, here named r(P)ApoB$_L$ and r(P)ApoB$_S$, was about 7 and 4 mg/L of bacterial culture, respectively.

3.2. Conformational analyses of r(P)ApoB$_L$ and r(P)ApoB$_S$ peptides by Far-UV circular dichroism

To analyse the secondary structure of recombinant ApoB derived peptides, we performed Far-UV CD spectra, and found that both peptides are largely unstructured in pure water (Figure 2a and b). We also evaluated the effects of membrane-mimicking agents, such as TFE and SDS at micellar concentrations, on peptide conformation. We found that r(P)ApoB$_L$ secondary structure shifts mainly towards an α-helical conformation in the presence of a membrane-mimicking agent, and only a partial (<10%) increase in β-strand content is observed (Table 2). This is clearly evidenced by the presence of two broad minima at around 208 and 222 nm, and a maximum at <200 nm (Figure 2a). A similar behavior has been described for different HDPs [24, 42, 43], and suggests that r(P)ApoB$_L$ peptide is prone to assume a specific ordered conformation when interacting with membrane-mimicking agents. Similar effects, even if significantly less pronounced, were observed in the case of r(P)ApoB$_S$ peptide (Figure 2b and Table 2). No appreciable β-strand formation was observed for this peptide, probably indicating that, in the r(P)ApoB$_L$ peptide, β-strand propensity is mainly localized in the C-terminus region.

We also analysed by CD spectroscopy the effects of the endotoxin LPS (lipopolysaccharide), the predominant glycolipid in the outer membrane of Gram-negative bacteria [44], on peptide conformation (Figure 2c and d and Table 2). When r(P)ApoB$_L$ secondary structure was analysed in the presence of increasing concentrations (from 0.1 to 0.8 mg/mL) of *E. coli* LPS, the progressive appearance of a maximum at approximately 200 nm and of a minimum at approximately 218 nm suggested that the peptide tends to assume prevalently a β-strand conformation, probably induced by its interaction with LPS (Figure 2c and Table 2). As expected on the basis of previous analyses, indicating no β-strand structure in r(P)ApoB$_S$, no significant effects were observed in the case of r(P)ApoB$_S$ (Figure 2d and Table 2) under the experimental conditions tested.

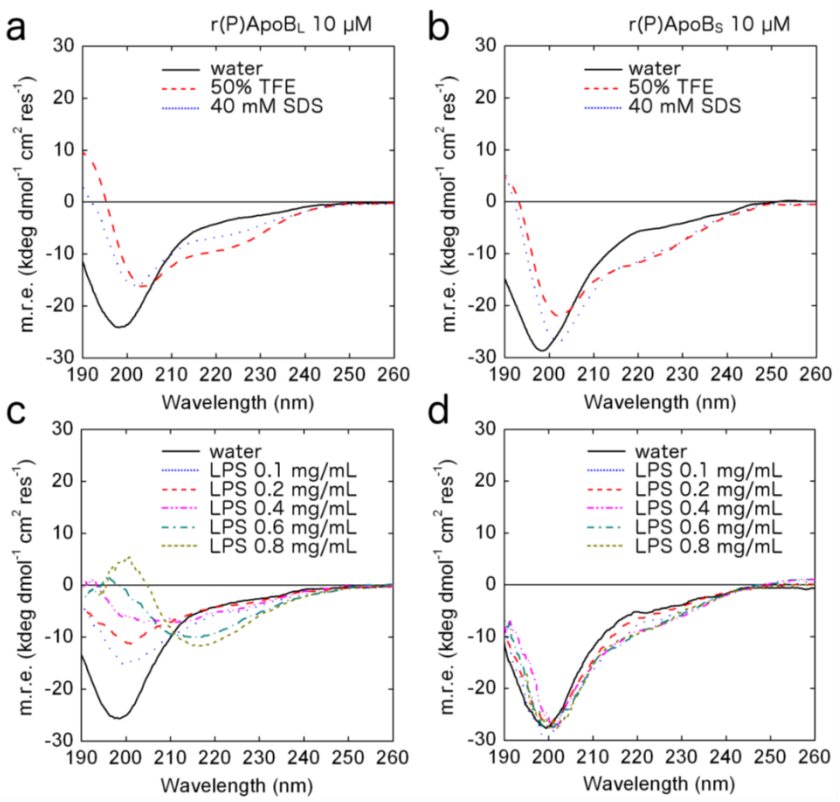

Figure 2. Far-UV CD spectra of recombinant peptides r(P)ApoB$_L$ (a, b) and r(P)ApoB$_S$ (c, d) at a concentration of 10 μM in the presence of the membrane-mimicking agents TFE or SDS at micellar concentrations (a, b), or in the presence of increasing concentrations of LPS (c, d).

	H_2O			TFE		
	α-helix (%)	β-strand (%)	random coil (%)	α-helix (%)	β-strand (%)	random coil (%)
r(P)ApoB$_L$	5	12	83	26	18	56
r(P)ApoB$_S$	7	3	90	26	0	74
	SDS			LPS		
	α-helix (%)	β-strand (%)	random coil (%)	α-helix (%)	β-strand (%)	random coil (%)
r(P)ApoB$_L$	17	21	62	11	64	25
r(P)ApoB$_S$	29	3	68	18	2	80

Table 2. Secondary structure content of ApoB derived peptides in water and in the presence of trifluoroethanol (TFE), sodium dodecyl sulfate (SDS), or lipopolysaccharide (LPS), calculated by means of PEPFIT program.

3.3. Analysis of the immunomodulatory activity of r(P)ApoB$_L$ and r(P)ApoB$_S$ peptides

Based on CD analyses, we hypothesized that an interaction between r(P)ApoB$_L$ peptide and LPS occurs. Since it is widely reported that HDPs are able to mitigate the pro-inflammatory effects induced by endotoxins [24], we tested the anti-inflammatory properties of ApoB derived peptides by monitoring their effects on LPS induced interleukin-6 (IL-6) release, as well as on nitric oxide (NO) release in murine macrophages (RAW 264.7 cell line). In fact, it is known that, upon activation by internal and external stimuli, macrophages produce and secrete various endogenous inflammatory mediators, such as nitric oxide (NO) and pro-inflammatory cytokines, including interleukin-6 [25, 26].

To test the effects of ApoB derived peptides on the release of IL-6, ELISA assays were performed on LPS stimulated RAW 264.7 cells. As shown in Figure 3a and b, a significant release of IL-6 was observed in control cells incubated with LPS from *Salmonella Minnesota* (50 ng/mL). When murine macrophages were incubated with LPS (50 ng/mL) in the presence of either r(P)ApoB$_L$ (Figure 3a) or r(P)ApoB$_S$ (Figure 3b) peptide, a strong decrease of IL-6 release was observed with respect to LPS induced control cells. Moreover, we found that both peptides have a significant protective effect on LPS stimulated RAW 264.7 cells. In fact, when macrophages were pre-treated for 2 h with either r(P)ApoB$_L$ or r(P)ApoB$_S$ peptide and then incubated for further 24 h with LPS, a significant decrease of IL-6 release was observed (Figure 3a and b).

Similar results were observed when the effects of ApoB derived peptides were tested on NO release (Figure 3c and d). Also in this case, following co-incubation of cells with LPS from *Salmonella Minnesota* and either r(P)ApoB$_L$ or r(P)ApoB$_S$ peptide, a significant attenuation of NO release with respect to control cells was detected (Figure 3c and d). However, in this case, it has to be noticed that a significant effect

of peptides on NO release was observed only at the highest peptide concentration tested (20 µM), while at 5 µM concentration both peptides were found to be almost ineffective (Figure 3c and d). However, when RAW 264.7 cells were pre-treated for 2 h with 5 or 20 µM of either r(P)ApoB$_L$ or r(P)ApoB$_S$ peptide and subsequently stimulated for 24 h with LPS (50 ng/mL), the reduction of NO release was observed even at 5 µM peptide concentration (Figure 3c and d), thus confirming the protective effect of both peptides on LPS stimulated RAW 264.7 cells.

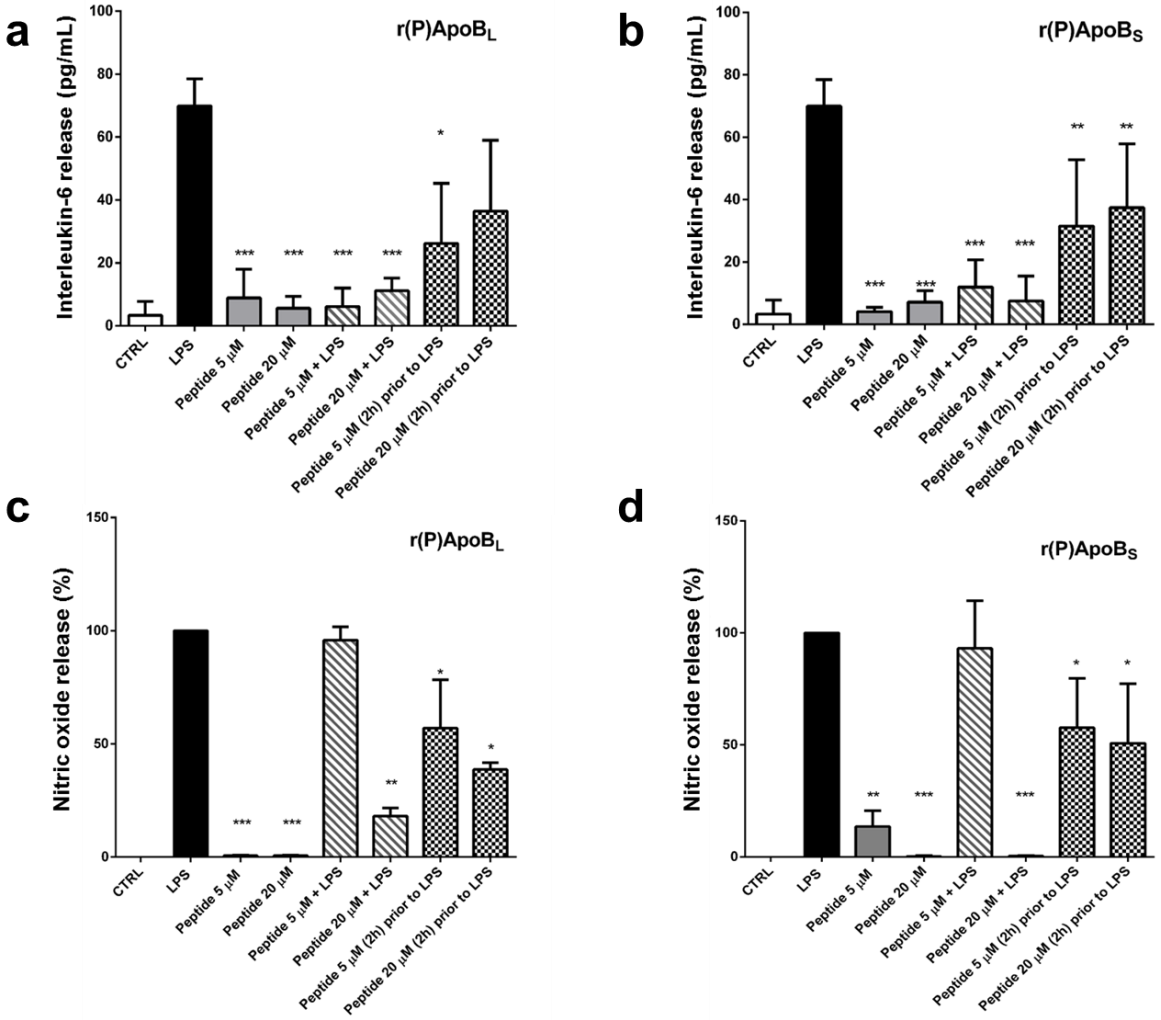

Figure 3. Effects of ApoB derived peptides on the release of IL-6 (a, b) and NO (c, d) in mouse macrophages RAW 264.7 stimulated with LPS (50 ng/mL) from Salmonella Minnesota. The effects of r(P)ApoB$_L$ (a, c) and r(P)ApoB$_S$ (b, d) peptides were evaluated either by co-incubating cells with peptides (5 or 20 µM) and LPS (oblique grey lanes) or by treating cells with the peptides (5 or 20 µM) for 2 h at 37 °C prior to incubation with LPS (chessboard bars). The results were compared to those obtained in the case of control untreated cells (white bars), cells stimulated with the LPS alone (black bars), or cells incubated with tdifferent concentrations (5 or 20 µM) of peptide (grey bars). Data represent the mean (± standard deviation, SD) of at least three independent experiments, each one carried out with triplicate determinations.

3.4. Antimicrobial activity of r(P)ApoB$_L$ and r(P)ApoB$_S$ peptides

The antibacterial activity of recombinant ApoB derived peptides was determined by measuring their MIC_{100} values on a panel of Gram-negative and Gram-positive bacterial strains (Table 3). A significant antimicrobial activity of r(P)$ApoB_L$ and r(P)$ApoB_S$ peptides was detected towards four out of eight strains tested, *i.e. E. coli* ATCC 25922, *P. aeruginosa* PAO1, *B. globigii* TNO BM013, and *B. licheniformis* 21424, for which almost identical MIC_{100} values were calculated for both ApoB derived peptides. Notably, MIC_{100} values were found to be comparable, or even significantly lower than those determined when control cathelidin-2 (CATH-2), a known HDP from chicken [48], was tested (Table 3). These data indicate that r(P)$ApoB_L$ and r(P)$ApoB_S$ peptides are endowed with a broad-range antimicrobial activity, being effective on both Gram-negative and Gram-positive bacterial strains. On the other hand, ApoB derived peptides were found to be ineffective towards *P. aeruginosa* ATCC 27853, methicillin-resistant *S. aureus* (MRSA WKZ-2), and *S. aureus* ATTC 29213 (Table 3), while, in the case of *S. enteriditis* 706 RIVM, a significant antibacterial effect was elicited only by r(P)$ApoB_L$ peptide.
To analyse the kinetic of peptides bactericidal activity, kinetic killing curves were obtained by treating *E. coli* ATTC 25922 and *B. licheniformis* ATTC 21424 strains, highly susceptible to both peptides (Table 3), with increasing concentrations of either r(P)$ApoB_L$ or r(P)$ApoB_S$ for different times (0-180 min). We found that, at the highest peptide concentrations tested (5-10 µM), *B. licheniformis* cells were killed within 10 min, while at the lowest peptide concentrations (1.25-2.5 µM) the same effect was obtained within 30 min (Figure 4a and c). When peptides were tested on *E. coli* ATTC 25922 at high concentrations (5-10-20 µM), bacterial cells were killed within 120 min, while at the lowest peptide concentration (2.5 µM) the same effect was obtained within 180 min (Figure 4c and d).

	MIC_{100} (µM)		
	r(P)$ApoB_L$	r(P)$ApoB_S$	CATH-2
Gram-negative strains			
Escherichia coli ATCC 25922	10	10	10
Pseudomonas aeruginosa ATCC 27853	> 40	> 40	10
Pseudomonas aeruginosa PAO1	20	20	20
Salmonella enteriditis 706 RIVM	10	> 40	10
Gram-positive strains			
Staphilococcus aureus MRSA WKZ-2	> 40	> 40	10
Bacillus globigii TNO BMO13	5	2.5	5
Bacillus licheniformis ATCC 21424	1.25	1.25	20
Staphylococcus aureus ATCC 29213	> 40	> 40	10

Table 3. Minimum Inhibitory Concentration (MIC, µM) values determined for r(P)$ApoB_L$ and r(P)$ApoB_S$ peptides tested on a panel of Gram-positive and Gram-negative bacterial strains. Chicken CATH-2 peptide was used as a positive control. Values were obtained from a minimum of three independent experiments.

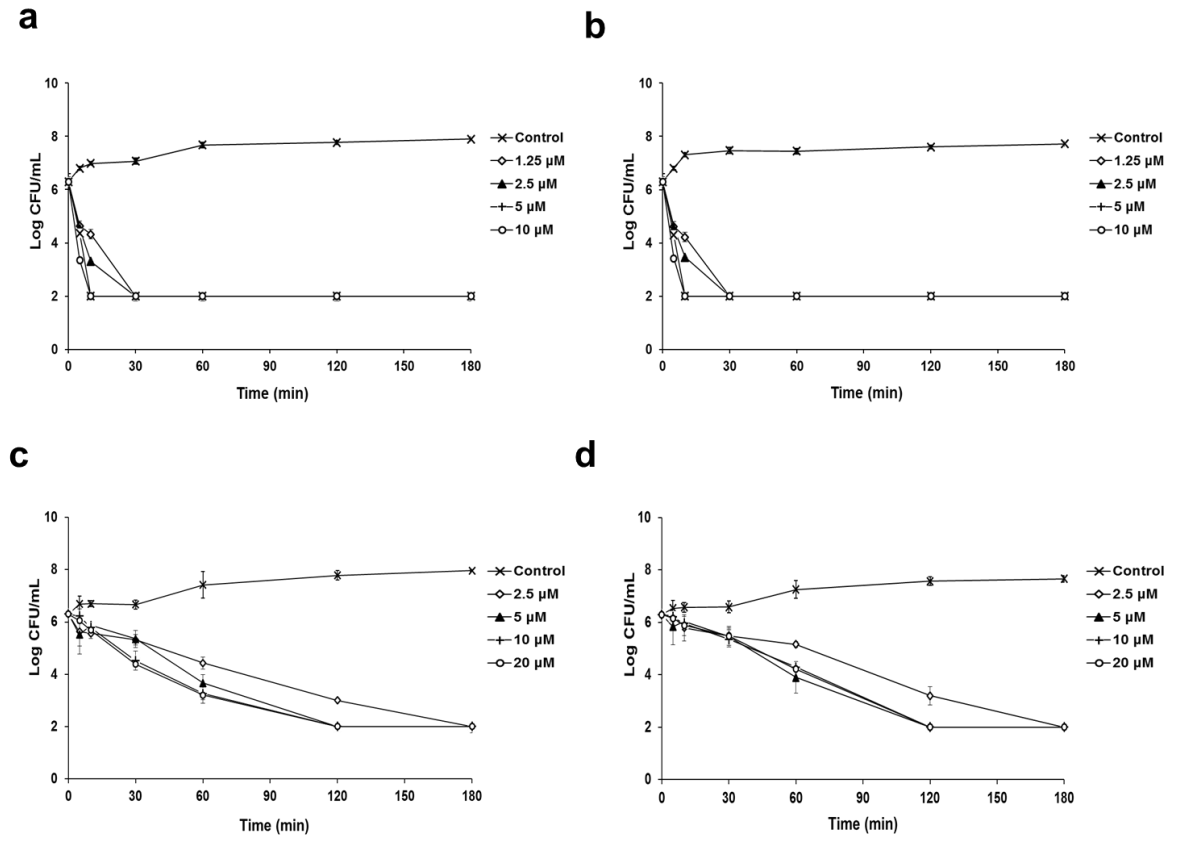

Figure 4. Time killing curves obtained by incubating *Bacillus licheniformis* ATTC 21424 (a, b) and *E. coli* ATTC 25922 (c, d) strains with increasing concentrations of r(P)ApoB$_L$ (a, c) or r(P)ApoB$_S$ (b, d) peptides for different lengths of time. Data represent the mean (± standard deviation, SD) of at least three independent experiments, each one carried out with triplicate determinations.

3.5. Combination therapy analyses

To potentiate the antimicrobial efficacy of recombinant ApoB derived peptides for therapeutic purposes, especially against *P. aeruginosa* and *S. aureus* strains, we carried out combination therapy analyses by concomitantly administrating peptides and antibiotics in various combinations to bacteria. One of the best-known test to evaluate synergism between two compounds is the so called “chequerboard” experiment, in which a two-dimensional array of serial concentrations of test compounds is used as the basis for calculation of a fractional inhibitory concentration (FIC) index to demonstrate that paired combinations of agents can exert inhibitory effects that are more than the sum of their effects alone [11]. It is generally accepted that FIC indexes ≤ 0.5 are indicative of “synergy”; FIC indexes comprised between > 0.5 and 4.0 are, instead, associated to “additive” or “no interaction” effects, whereas FIC indexes > 4.0 are indicative of “antagonism” [11].

As reported in Table 4, all the combinations tested were found to be effective, either with additive or synergistic effects between peptides and antibiotics. Notably, no FIC indexes higher than 2 were measured.

The most potent combinations were obtained in the presence of EDTA, which was selected for its ability to affect bacterial outer membrane permeability, thus sensitizing bacteria to a number of antibiotics [18-30]. Very pronounced synergistic

effects were observed for both ApoB derived peptides in combination with EDTA on *S. aureus* MRSA WKZ-2 and both *P. aeuroginosa* strains.
Both peptides were found to act synergistically with (i) ciprofloxacin on all the strains tested (Table 4); (ii) colistin on all the strains tested, except for *S. aureus* ATTC 29213 (Table 4); (iii) vancomycin on *S. aureus* MRSA WKZ-2, *P. aeruginosa* strains and *E. coli* ATTC 25922 (Table 4); (iv) erythromycin on *P. aeruginosa* ATCC 27853 (Table 4). In the latter case, a FIC index of 0.38 and 0.17 for r(P)ApoB$_L$ and r(P)ApoB$_S$ peptides, respectively, was obtained. In the case of kanamycin, the response varied depending on the peptide and the specific bacterial strain. In fact, r(P)ApoB$_L$ was found to act synergistically with this antibiotic prevalently on Gram-negative bacteria, particularly on the *P. aeruginosa* strains, whereas r(P)ApoB$_S$ peptide was found to be very active in the presence of kanamycin against both *S. aureus* strains as well as against *P. aeruginosa* PAO1 strain (FIC indexes < 0.4).
It should be emphasized that combinations of ApoB derived peptides with antibiotics or EDTA were found to have a strong antimicrobial activity even towards strains on which the peptides alone were found to be ineffective, such as both *S. aureus* strains and *P. aeruginosa* ATCC 27853 (Table 3). Notably, we did not observe any antagonistic interactions between the peptides and the antimicrobials.

Bacterial strains	Antibiotic	ΣFICI[a]	
		r(P)ApoB$_L$	r(P)ApoB$_S$
Methicillin resistant *S. aureus MRSA WKZ-2*	Ciprofloxacin	0,328	0,365
	Colistin	0,340	0,350
	Erythromycin	1,094	1,375
	Vancomycin	0,425	0,316
	Kanamycin	2,000	0,387
	EDTA	0,278	0,360
***S. aureus* ATTC 29213**	Ciprofloxacin	0,340	0,413
	Colistin	1,049	1,024
	Erythromycin	1,049	1,146
	Vancomycin	1,049	1,097
	Kanamycin	1,049	0,352
	EDTA	1,049	0,351
***P. aeruginosa* ATCC 27853**	Ciprofloxacin	0,347	0,328
	Colistin	0,267	0,255
	Erythromycin	0,389	0,170
	Vancomycin	0,379	0,306
	Kanamycin	0,479	1,030
	EDTA	0,333	0,089
***P. aeruginosa* PAO1**	Ciprofloxacin	0,396	0,444
	Colistin	0,144	0,266
	Erythromycin	0,569	0,556
	Vancomycin	0,500	0,486
	Kanamycin	0,507	0,389
	EDTA	0,396	0,438
***E. coli* ATCC 25922**	Ciprofloxacin	0,363	0,442
	Colistin	0,438	0,292
	Erythromycin	1,243	1,292
	Vancomycin	0,428	0,426
	Kanamycin	0,603	0,572
	EDTA	0,729	0,750

Table 4. Fractional inhibitory concentration (FIC) indexes determined for r(P)ApoB$_L$ and r(P)ApoB$_S$ peptides tested in combination with antibiotics or EDTA on Gram-positive and Gram-negative bacterial strains. Indexes were obtained from a minimum of three independent experiments, each one carried out with triplicate determinations.

3.6. Anti-biofilm activity of r(P)ApoB$_L$ and r(P)ApoB$_S$ peptides

Anti-biofilm peptides represent a very promising approach to treat biofilm-related infections and have an extraordinary ability to interfere with various stages of the biofilm growth mode [31]. To test whether recombinant ApoB derived peptides are endowed with anti-biofilm activity, we performed experiments on different bacterial strains, such as *E. coli* ATCC 25922, Pseudomonas aeruginosa PAO1, *Pseudomonas aeruginosa* ATCC 27853, and methicillin resistant *Staphylococcus aureus* MRSA WKZ-2 in BM_2 medium. The same experiments were also performed using LL-37 control peptide, that is a human antimicrobial peptide known to have a significant anti-biofilm activity against multidrug-resistant bacterial strains [32]. We also tested for the first-time CATH-2 anti-biofilm activity. Three different approaches were followed. At first, we tested the peptide effects on biofilm attachment. To do this, the bacterial culture, following over-night growth, was diluted in BM2 medium containing increasing concentrations of the peptide under test (0-1 μM), and incubated for 4 h at 37 °C. Following incubation, biofilm analysis by crystal violet staining revealed a significant dose-dependent inhibition of biofilm attachment in the case of *E. coli* ATCC 25922 (Figure 5a) and *S. aureus* MRSA WKZ-2 (Figure 5d) strains treated with r(P)ApoBL (continuous line in Figure 5a, d) or r (P)ApoBS (smaller dashed line in Figure 5a, d) peptides. Similar results were obtained on these two strains in the case of peptides CATH-2 (larger dashed line in Figure 5a, d) and LL-37 (dotted line in Figure 5a, d). Strong effects were also displayed by ApoB derived peptides on biofilm attachment in the case of *P. aeruginosa* PAO1 strain (Figure 6d). A less pronounced effect of ApoB derived peptides (about 20% inhibition of biofilm formation) was observed, instead, on *P. aeruginosa* ATCC 27853 biofilm attachment (Figure 6a). Second, we tested the effect of ApoB derived peptides on biofilm formation. To investigate this phenomenon, we followed the experimental procedure described above with the only exception that bacterial cells were incubated with increasing concentrations of peptides for 24 h at 37 °C. Also in this case, we observed a significant dose-dependent inhibition of biofilm formation in the case of *E. coli* ATCC 25922 (Figure 5b) and *S. aureus* MRSA WKZ-2 (Figure 5e) strains treated with r(P)ApoB$_L$ (Figure 5b, e) or r(P)ApoB$_S$ (Figure 5b, e) peptides. Similar effects were elicited by peptides CATH-2 (Figure 5b, e) and LL-37 (Figure 5b, e). ApoB derived peptides strongly affected also *P. aeruginosa* PAO1 biofilm formation (Figure 6e). In the case of *P. aeruginosa* ATCC 27853, instead, a less pronounced effect (about 20% biofilm formation inhibition) was observed for all the peptides under test (Figure 6b). Third, we tested the effect of ApoB derived peptides on pre-formed biofilms. By incubating pre-formed biofilms of *E. coli* ATCC 25922 (Figure 5c) and S. aureus MRSA WKZ-2 (Figure 5f) strains with increasing concentrations of r(P)ApoB$_L$ (Figure 5c, f) or r(P)ApoB$_S$ (Figure 5c, f), we found a significant reduction (about 50%), an effect even stronger than that observed in the case of CATH-2 peptide (Figure 5c, f). Similar results were observed in the case of *P. aeruginosa* PAO1 strain (Figure 6f). On the other hand, when the peptides were tested on *P. aeruginosa* ATCC 27853 pre-formed biofilm, a slight effect (about 20% reduction) was observed for all the peptides except for CATH-2, which was found to have a strong effect (about 50% reduction, Figure 6c).

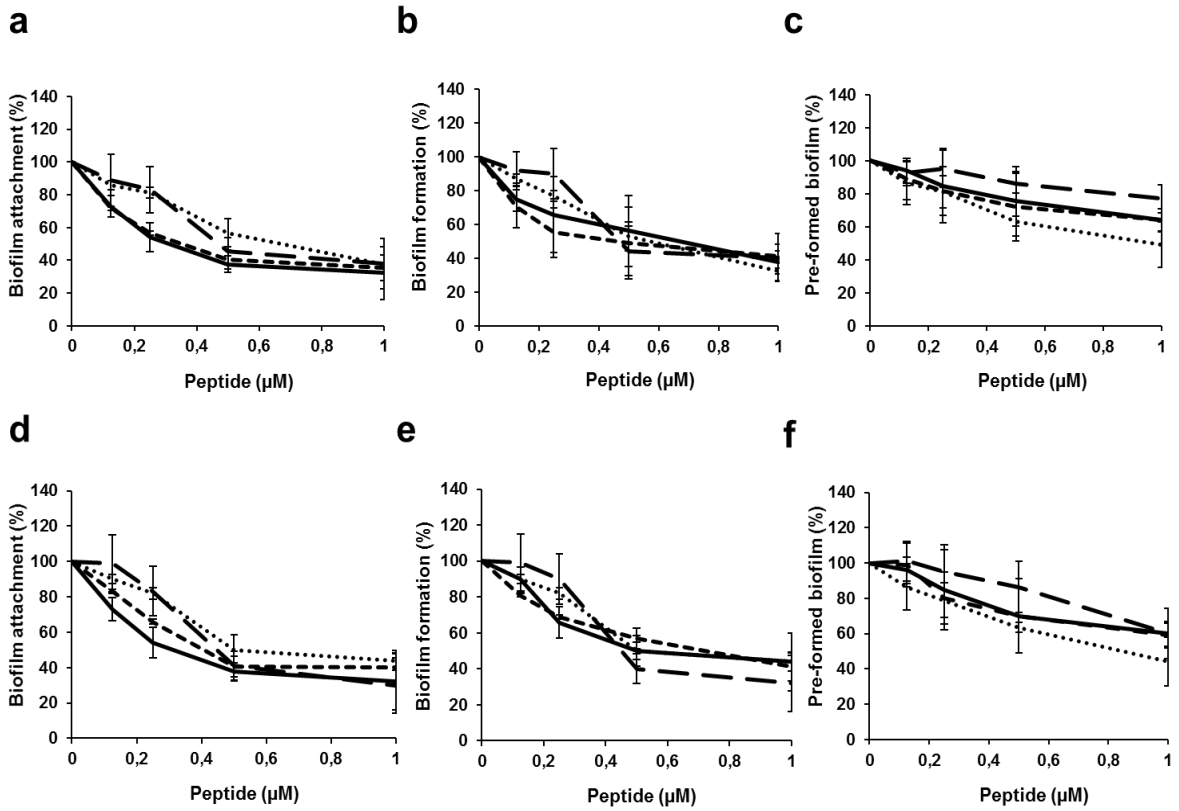

Figure 5. Anti-biofilm activity of r(P)ApoB$_L$ (–), r(P)ApoB$_S$ (- - -), CATH-2 (——), and LL-37 (•••) peptides on *E. coli* ATCC 25922 (a, b, c) and *S. aureus* MRSA WKZ-2 (d, e, f) strains in BM_2 medium. The effects of increasing concentrations of peptides were evaluated either on biofilm attachment (a, d), biofilm formation (b, e), or on pre-formed (c, f) biofilm. Biofilm was stained with crystal violet and measured at 630 nm. Data represent the mean (±standard deviation, SD) of at least three independent experiments, each one carried out with triplicate determinations. For all the experimental points, *P < 0.05, **P < 0.01, or ***P < 0.001 were obtained for control versus treated samples.

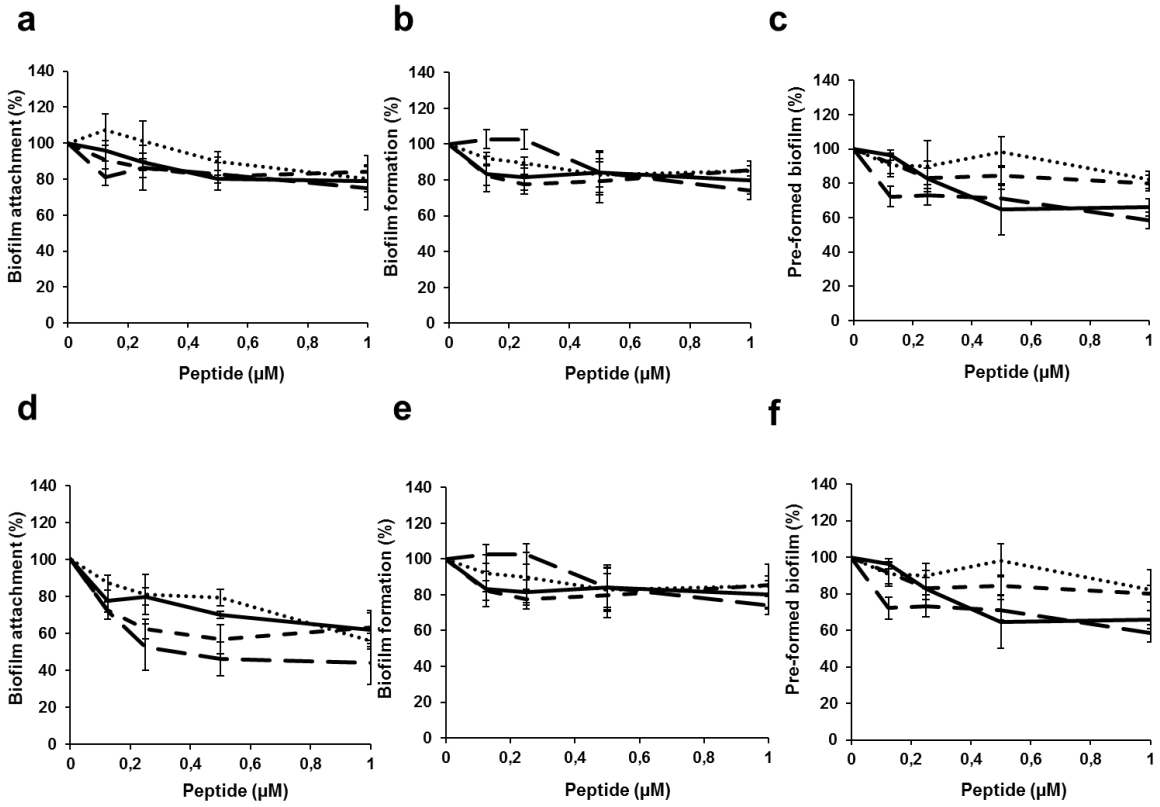

Figure 6. Anti-biofilm activity of r(P)ApoB$_L$ (–), r(P)ApoB$_S$ (- - -), CATH-2 (——), and LL-37 (•••) peptides on *P. aeruginosa* ATCC 27853 (a, b, c) and *P. aeruginosa* PAO1 (d, e, f) strains in BM_2 medium. The effects of increasing concentrations of peptides were evaluated either on biofilm attachment (a, d), biofilm formation (b, e), or on pre-formed (c, f) biofilm. Biofilm was stained with crystal violet and measured at 630 nm. Data represent the mean (± standard deviation, SD) of at least three independent experiments, each one carried out with triplicate determinations. For all the experimental points, *P < 0.05, or **P < 0.01 were obtained for control versus treated samples.

We also evaluated the percentage of viable bacterial cells inside the biofilm structure by colony counting assay. We found that, even at the highest ApoB derived peptides concentrations tested, a significant percentage of bacterial cells appeared to be still alive (Table 5). Similar results were also obtained in the case of LL-37 and CATH-2 control peptides on both *P. aeruginosa* strains (Table 5), even if it has to be noticed that, in the case of biofilm formation, both control peptides affected the viability of *P. aeruginosa* PAO1 cells more than ApoB derived peptides (Table 5). CATH-2 and LL-37 control peptides were also found to strongly impair the viability of *E. coli* ATCC 25922 and *S. aureus* MRSA WKZ-2 cells in the case of biofilm eradication (Table 5).

	BIOFILM											
	Attachment (%)				Formation (%)				Eradication (%)			
	r(P)ApoB$_L$	r(P)ApoB$_S$	CATH-2	LL-37	r(P)ApoB$_L$	r(P)ApoB$_S$	CATH-2	LL-37	r(P)ApoB$_L$	r(P)ApoB$_S$	CATH-2	LL-37
Pseudomonas aeruginosa ATCC 27853	79±9	84±8	75±5	80±7	80±9	86±5	74±5	85±3	75±5	80±6	58±9	82±5
Pseudomonas aeruginosa PAO1	62±14	63±11	44±11	56±4	44±16	53±5	47±8	34±12	49±14	54±17	63±11	54±11
	CELL VIABILITY											
	In biofilm attachment (%)				In biofilm formation (%)				In biofilm eradication (%)			
	r(P)ApoB$_L$	r(P)ApoB$_S$	CATH-2	LL-37	r(P)ApoB$_L$	r(P)ApoB$_S$	CATH-2	LL-37	r(P)ApoB$_L$	r(P)ApoB$_S$	CATH-2	LL-37
Pseudomonas aeruginosa ATCC 27853	76±11	68±10	91±5	60±13	66±13	64±14	96±16	77±15	70±15	59±9	59±12	69±5
Pseudomonas aeruginosa PAO1	52±12	77±15	45±7	47±7	55±14	57±14	35±16	25±14	44±15	86±6	50±10	58±9

Table 5. Effect of r(P)ApoB$_L$, r(P)ApoB$_S$, CATH-2, and LL-37 peptides (1 µM) on biofilm attachment, formation, and eradication. To determine the percentage of viable bacterial cells inside the biofilm structure, biofilm was lysed with Triton X-100 (0,1%), bacterial cells were ten-fold diluted, and colonies were counted after an incubation of 16 h at 37 °C. Data are expressed as percentage with respect to control untreated samples, and represent the mean (± standard deviation, SD) of at least three independent experiments, each one carried out with triplicate determinations.

To deepen on ApoB derived peptides anti-biofilm activity, we also performed studies in continuous-flow chambers. To this purpose, we tested *P. aeruginosa* PAO1 pre-formed biofilm in the absence or in the presence of r(P)ApoB$_L$ (Figure 7 b) or r(P)ApoB$_S$ (Figure 7 c) peptide tested at 1 µM concentration. To do this, biofilm growth was carried out for 48 h at 37 °C. Afterwards, pre-formed biofilm was treated with the peptide under test for 24 h. Analyses revealed that both peptides are able to strongly eradicate pre-formed biofilm, with the strongest effects observed in the presence of r(P)ApoB$_L$ peptide.

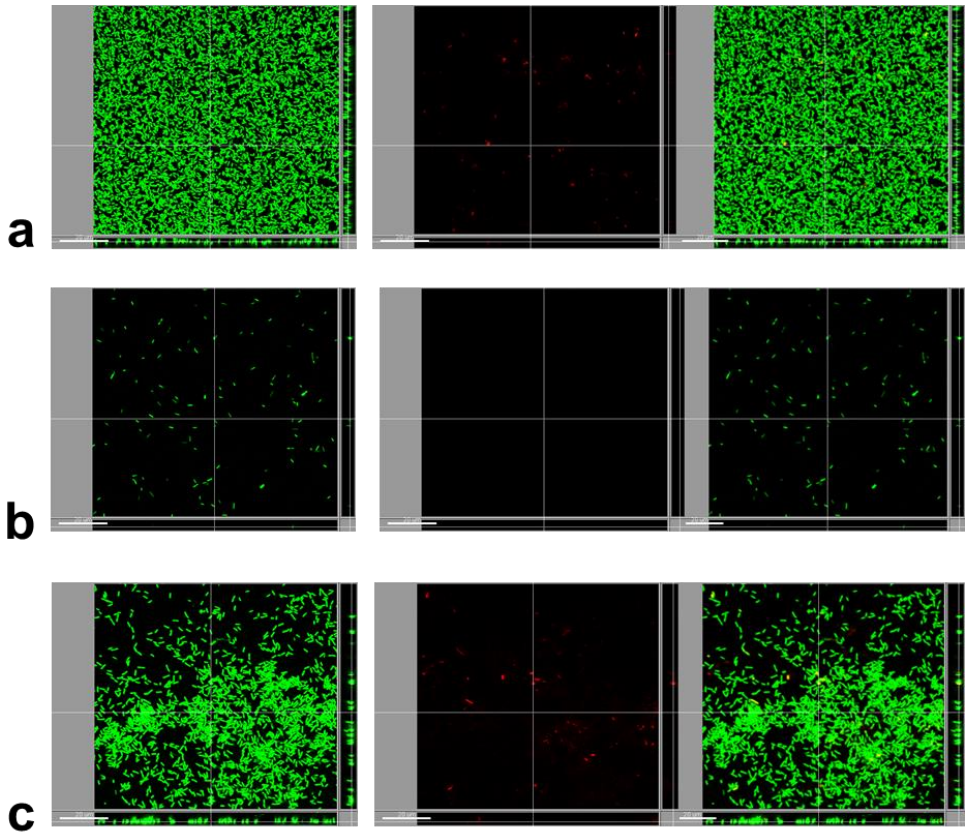

Figure 7. Flow cell analysis of *P. aeruginosa* PAO1 pre-formed biofilm in the absence (a) or in the presence of 1 µM r(P)ApoB$_L$ peptide (b) or of 1 µM r(P)ApoB$_S$ peptide (c). Biofilms have been stained and visualized using SYTO-9 to stain live biofilm cells (green) and propidium iodide, a normally cell-impermeable dye, to stain dead cells (red). Images were acquired by wide-field fluorescence microscopy.
(a) PAO1 biofilm untreated. (b) PAO1 biofilm treated with 1 µM r(P)ApoB$_L$. (c) PAO1 biofilm treated 1 µM with r(P)ApoB$_S$. On the left, images of PAO1 biofilm stained with SYTO-9; in the middle, images of PAO1 biofilm stained with propidium iodide; on the right, merged images are reported. Each panel shows xy, yz, and xz dimensions. Scale bar = 20 µm.

3.7. Biocompatibility of r(P)ApoB$_L$ and r(P)ApoB$_S$ peptides

The development of HDPs as therapeutic agents is strictly related to their selective toxicity towards bacterial cells [33]. The presence of zwitterionic phospholipids and cholesterol on the outer leaflet of eukaryotic cell membranes largely accounts for the preference of HDPs for bacterial membranes over eukaryotic membranes [34, 35]. To deepen on the therapeutic potential of ApoB derived peptides, we analysed their cytotoxic effects towards a panel of mouse and human eukaryotic cells. The addition of increasing concentrations (from 0.625 to 20 µM) of ApoB derived peptides to mouse macrophages Raw 264.7 cells for 24 h did not result in any significant reduction in cell viability (Figure 8a and c). A slight toxicity was detected only at the highest peptide concentrations tested (10 and 20 µM in Figure 8a and c). We also tested ApoB derived peptides on murine embryo fibroblasts BALBc 3T3 and their tumor counterpart, *i.e.* SVT2 simian virus 40-transformed cell line (Figure 8b and d). A slight toxicity (10-20%) was detected only in the case of SVT2 cells at the highest concentration tested (20 µM in Figure 8b and d). Moreover, no significant toxic effects were detected when ApoB derived peptides were assayed on human cervical

cancer HeLa cells (Figure 8b and d), while a slight toxicity (~20%) was observed in the case of human keratinocytes (HaCaT cells) at the highest concentration (20 μM in Figure 8b and d). ApoB derived peptides were also tested on murine red blood cells (RBCs) to exclude hemolytic effects. As shown in Figure 9, both peptides did not exert any lytic effect on mouse RBCs, even at the highest concentration tested (20 μM).

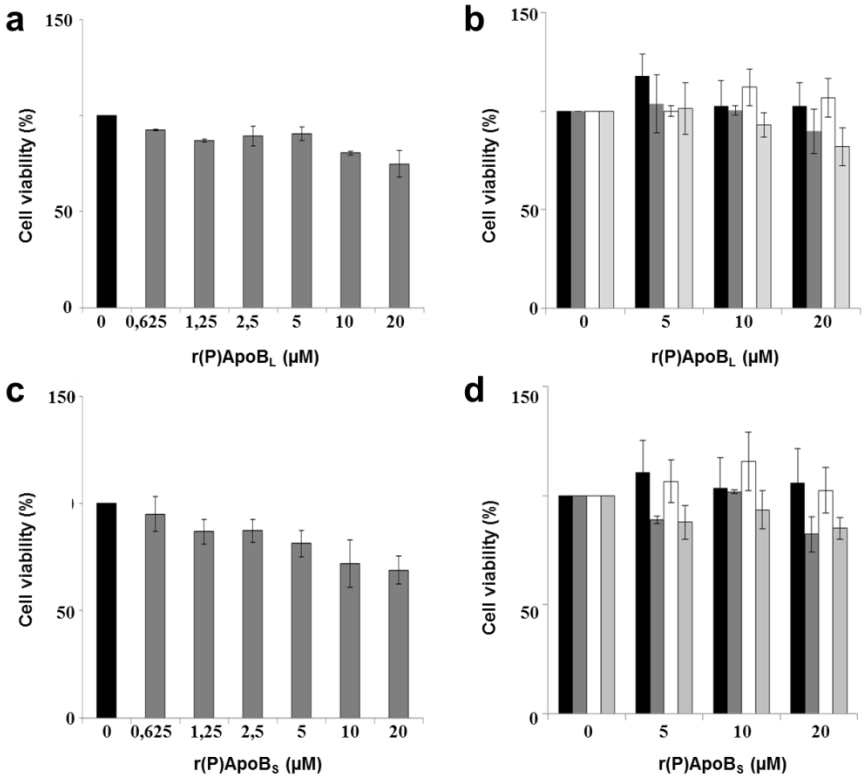

Figure 8. Effects of r(P)ApoB$_L$ (**a, b**) and r(P)ApoB$_S$ (**c, d**) peptides on the viability of RAW 264.7 (**a, c**), BALBc 3T3 (black bars in **b, d**), SVT2 (dark grey bars in **b, d**), Hela (white bars in **b, d**), and HaCaT (light grey bars in **b, d**) cells. Cell viability was assessed by WST-1 (**a, c**) or MTT (**b, d**) assay, and expressed as the percentage of viable cells with respect to controls (untreated cells). Error bars indicate standard deviations obtained from at least three independent experiments, each one carried out with triplicate determinations.

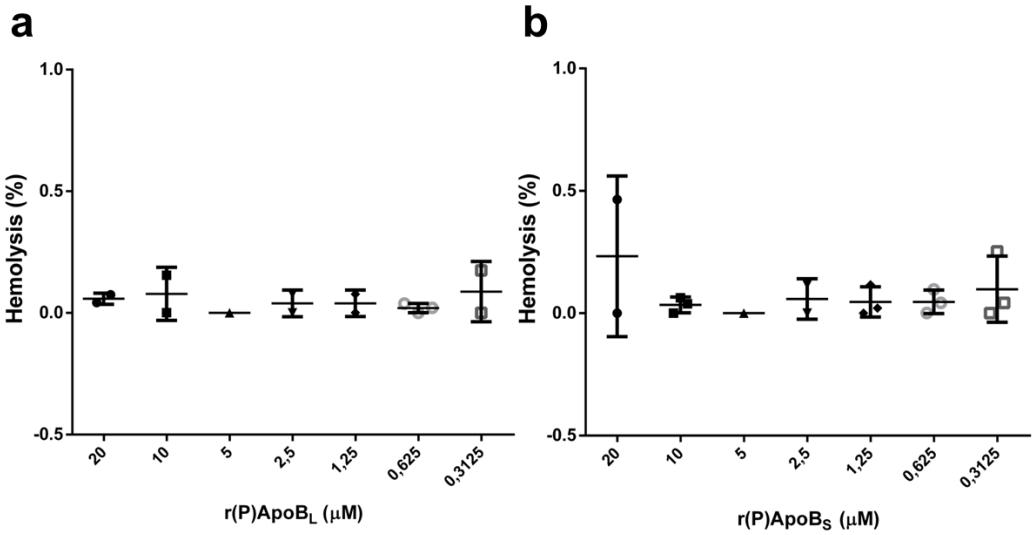

Figure 9. Hemolytic activity of r(P)ApoB$_L$ (a) and r(P)ApoB$_S$ (b) peptides towards murine red blood cells (RBCs) after 1 h incubation at 37 °C. Data represent the mean (± standard deviation, SD) of at least three independent experiments, each one carried out with triplicate determinations.

3.8. Wound healing activity of r(P)ApoB$_L$ peptide

Numerous studies support the hypothesis that human HDPs promote wound healing in skin, by modulating cytokine production, cell migration, proliferation and, in some cases, angiogenesis [36]. Based on this, we performed experiments to test whether r(P)ApoB$_L$ peptide is able to stimulate wound re-epithelialization by human keratinocytes (HaCaT cell line). To this purpose, we performed a classical *in vitro* wound healing assay to evaluate peptide effects on cell migration. HaCaT cell monolayers were pre-treated with 3 μM mitomycin C for 30 min, and then wounded with a pipette tip to remove cells from a specific region of the monolayers.

Cells were then washed with PBS and incubated with r(P)ApoB$_L$ (0, 0.5, 10, and 20 μM). As it is well known that the spreading of cells in the wound area is due to two mechanisms, i.e. cell motility and cell proliferation [16,19,37], a pre-treatment with mitomycin C allowed us to exclude any influence of cell proliferation on the wound healing process. In Figure 10a, we reported the images acquired during a time-lapse wound healing experiment on control cells, and on cells treated with 20 μM r(P)ApoB$_L$ peptide at three time points, i.e. at time 0 and at 3 and 5 h after the lag time (t_L), defined as a transient time period (t_L) before the linear decrease of the wound area (see below). By the comparison of the images of treated and untreated cells at each time point, it emerged that the cells treated with 20 μM peptide were able to close the wound faster than the control cells. In order to quantify the wound closure, we used an automated image analysis software, that allowed us to measure the size of the cell-free area (A) for each time point. The obtained values were normalized with respect to the value measured at time 0 (A_0) for each field of view, and plotted as a function of time (Figure 10b). In Figure 10a, at t = 5 h after t_L, A/A_0 values were found to be 0.20, and 0.07 for the control sample, and for the cells treated with 20 μM peptide, respectively. This evidence suggests that r(P)ApoB$_L$ peptide might be able to stimulate wound re-epithelialization by human keratinocytes. As shown in Figure 10b, where A/A_0 values of control cells are reported as a function of time, after an initial lag phase (t_L), the wound area decreases with a constant

velocity. The initial lag phase, corresponding to a transient time period (t_L) before the linear decrease of the wound area, has been observed for all the analysed samples, and has been found to range between 3 and 5 h independently from peptide concentrations under test (Figure 10c). As the slope (a) of the line represents the measure of the wound closure velocity, each a value calculated in the presence of the peptide was normalized with respect to the value calculated for untreated cells (a_{contr}), and plotted as a function of peptide concentration (Figure 10d). It appeared that the cells treated with the peptide show an increased wound closure velocity with respect to the control cells ($a/a_{contr} > 1$). In particular, in the case of the cells treated with 10 µM peptide, an increment of about 20% in the normalized wound closure velocity ($a/a_{contr} = 1.21$, data statistically significant) was observed. When cells were treated with 20 µM peptide, a slightly higher value of the normalized wound closure velocity was measured ($a/a_{contr} = 1.23$). However, in the latter case, a higher data variability was observed (larger error bar), leading to a limited statistical significance of the result. Overall, our results indicate that r(P)ApoBL peptide is able to promote the migration and the consequent wound healing in HaCaT keratinocyte monolayers when tested at concentration values ranging between 0.5 and 20 µM.

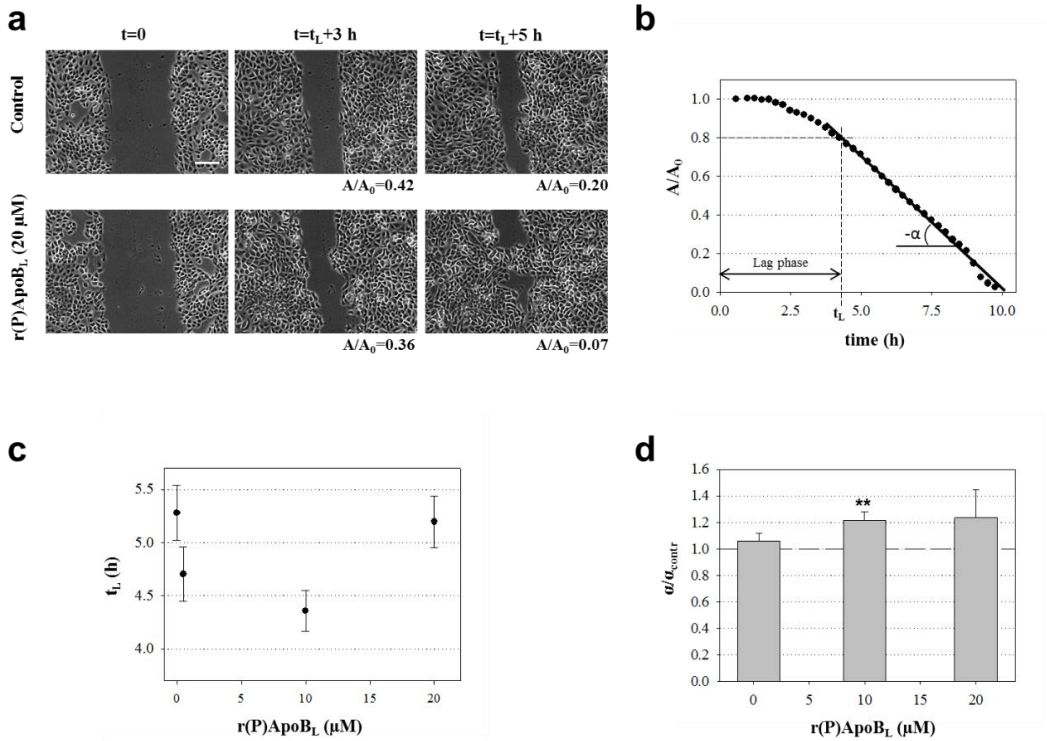

Figure 10. Wound healing activity of r(P)ApoB$_L$ peptide on HaCaT cells monolayer. Cells were pre-treated for 30 min with 3 µM mitomycin C, and then wounded prior to incubation with r(P)ApoB$_L$ peptide (0.5–10–20 µM) for 12 h at 37 °C. Images were acquired for untreated HaCaT cells and for cells treated with 20 µM peptide (a). The lag phase time (t_L) corresponds to the time interval before the linear decrease of the wound area. Images were acquired at time t = 0 (a, on the left), 3 h after t_L (a, in the middle) and 5 h after t_L (a, on the right). For each sample, A/A_0 values are reported, where A is the wound area after a specific incubation time and A_0 is the wound area at time 0. Scale bar = 150 µm. In (b), evolution in time of the wound area (A), normalized with respect to A_0, is reported for a control sample. A homemade automated image analysis software was used to measure the size of the cell-free area (A) for each time point. For A/A_0 values < 0.8, a linear correlation with the incubation time was found. The slope -α of the linear fit, reported as a continuous line, represents a measure of the wound closure velocity. In (c), determined t_L values are reported as a function of peptide concentration (0– 0.5–10–20 µM). In (d), wound closure velocity (a), normalized with respect to control sample (a_{contr}), is reported as a function of peptide concentration (0.5–10–20 µM). The dashed line corresponds to a/a_{contr} = 1. In (c) and (d), each data point represents the mean (±standard error) of three independent experiments. **P < 0.01 was obtained for control versus treated samples.

4. Discussion

Recently, an abundance of multidrug-resistant bacteria has emerged, whereas very few classes of new antibiotics have been discovered. The knowledge that HDPs may prevent infections in many organisms opened interesting perspectives to the applications of these peptides as a new class of antimicrobials. In fact, they initially attracted attention solely for their direct antimicrobial activity, and were studied as promising alternative antibiotic candidates due to their prospective potency, rapid action, and broad spectrum of activity against Gram-negative and Gram-positive bacteria, viruses, fungi and parasites [38, 39]. To date, more than 1,000 natural cationic HDPs with antimicrobial properties have been identified [40]. These peptides constitute a major component of the ancient, nonspecific innate defence system in most multicellular organisms [38, 39]. However, it has to be emphasized that most natural HDPs have, indeed, modest direct antimicrobial activities, and exhibit multiple mechanisms of action, with a consequent low potential to induce *de novo* resistance [38]. This class of peptides includes the bioactive peptides displaying direct antimicrobial activity and those that stimulate the immune system to clear or prevent an infection [38, 40]. In mammals, the expression of mature and biologically active HDPs requires a proteolytic cleavage event determining the release of the “cryptic” bioactive peptide from its precursor protein [41]. In fact, it should be emphasized that a wide variety of human proteins, whose primary functions are not necessarily related to host defense, contain HDPs hidden inside their sequences [42, 43]. Fascinatingly, human proteome could be seen as a yet unexplored source of bioactive peptides with potential pharmacological applications. In this context, apolipoproteins have been identified as a source of bioactive peptides displaying broad anti-infective and antiviral activities [22]. Indeed, the presence of antiviral peptides hidden within apolipoprotein sequences may be related to the fact that lipoproteins and viruses share a similar cell biological niche, having a comparable size and displaying similar interactions with mammalian cells and receptors [1]. ApoB is one of the several apolipoproteins that play key roles in lipoprotein metabolism [44], and represents the ligand for receptor-mediated removal of low density lipoprotein particles from circulation [44]. ApoB contains two LDL (low-density lipoprotein) receptor binding domains, namely region A (ApoB3147-3157) and region B (ApoB3359-3367), which is more uniformly conserved across species and that has been found to be endowed with a significant antiviral activity [1]. Moreover, ApoB derived peptides have been already used in vaccine preparations to treat atherosclerosis [2]. Here, we applied recently developed *in silico* analysis method to a human ApoB isoform [5, 6] and identified a novel “cryptic” HDP (region 887-922). To the best of our knowledge, this ApoB region has never been analysed before, since the biologically active ApoB peptides previously identified are located far from the high scoring region identified in the present work [1, 2]. By *in silico* analysis, we identified an absolute maximum, corresponding to region 887-922 (Figure 1), and a relative maximum, corresponding to residues 887-909 (Figure 1). Here, we focused our attention on these two ApoB sequences by producing in bacterial cells two recombinant HDPs, here named r(P)ApoB$_L$ and (P)ApoB$_S$, 38- and 26-residue long, respectively. Both recombinant peptides were found to exhibit antibacterial activities against both Gram-positive and Gram-negative strains, including the pathogenic strains *P. aeruginosa* PAO1 and *B. globigii* TNO BM013, while having negligible cytotoxic effects on a panel of human

and murine cell lines. Time killing curves also indicated that peptides exert a strong bactericidal activity against susceptible strains. However, it has to be underlined that ApoB derived peptides were found to be ineffective towards *P. aeruginosa* ATCC 27853, methicillin-resistant *S. aureus* (MRSA WKZ-2), and *S. aureus* ATTC 29213 strains, while, in the case of *S. enteriditis* 706 RIVM strain, a significant antibacterial effect was displayed only by r(P)ApoB$_L$ peptide. This observation is in agreement with previous findings indicating that most natural cationic antimicrobial peptides do not appear to be highly optimized for direct antimicrobial activity, since it is likely that multiple modestly active peptides with concomitant immunomodulatory activities work effectively in combination and/or when induced or delivered to sites of infection [45]. Indeed, considering this, we performed combination therapy analyses and found that both ApoB derived peptides are able to act synergistically with commonly used antibiotics or with EDTA, the latter selected for its ability to affect the permeability of bacterial outer membrane, thus sensitizing bacteria to a number of antibiotics [28-30]. Interestingly, synergistic effects were observed towards most of the strains under test, including methicillin-resistant *S. aureus* MRSA WKZ-2, on which the peptides alone were found to be ineffective even at high concentrations (40 µM). Although the use of a single agent to treat pathogens is the most common practice in clinics, combination therapy approaches have several advantages, such as low potential to induce resistant phenotype, efficacy at lower drug doses, with a consequent mitigation of toxic effects, and possibility to target a broad spectrum of pathogens [46]. Interestingly, both r(P)ApoB$_L$ and r(P)ApoB$_S$ peptides showed synergism with systemic antibiotic ciprofloxacin against all the strains under test (FIC indexes ranging from 0.3 to 0.44). This would allow to significantly lower the doses of the antibiotic in the combination therapy approaches, with a consequent decrease of the appearance of resistant clinical isolates, an undesired phenomenon strongly affecting ciprofloxacin efficacy [47]. ApoB derived peptides also showed synergistic effects with colistin and vancomycin against most of the strains under test (FIC indexes ranging from 0.14 to 0.5). Since both colistin and vancomycin are responsible for toxic effects at high concentrations [46,48], a combination therapeutic approach based on a reduced frequency of antibiotic administration and/or exposure to antibiotic may offer several advantages over conventional dosing schemes. However, the most potent synergism was observed for both ApoB derived peptides in combination with EDTA, with FIC indexes ranging from 0.089 to 0.4. In the case of *P. aeruginosa* strains, synergism might be associated to EDTA ability to combine with magnesium ions playing a key role in the self-interaction of LPS molecules, with a consequent LPS release determining an increased permeability of bacterial membrane [29]. This might ultimately facilitate peptide internalization into bacterial cells, thus potentiating the peptide antimicrobial activity. EDTA is also known to determine the release of endogenous phospholipases, with a consequent alteration of Gram-negative bacteria outer membrane [49]. In the case of *S. aureus* strains, the increase of bacterial membrane permeability might be due to the ability of EDTA to solubilize extracellular polymeric substances [50], mainly composed by exopolysaccharides and playing a key role in biofilm establishment.

It should be highlighted that, although in some cases FIC indexes very close to 0.5 make it difficult to discriminate between synergistic and additive effects, no antagonistic interactions were observed between peptides and antimicrobials under

test. Furthermore, combinations of ApoB derived peptides with antibiotics or EDTA were found to have a strong antimicrobial activity also towards strains on which the peptides alone were found to be ineffective, such as both *S. aureus* strains and *P. aeruginosa* ATCC 27853, indicating that in drug combinations a reciprocal facilitation and potentiation of different mechanisms of action is realized.

Interestingly, ApoB derived peptides are also endowed with anti-biofilm activity. Microorganisms growing in a biofilm state are very resilient to the treatment by many antimicrobial agents. Indeed, biofilm infections are a significant problem in chronic and long-term infections, including those colonizing medical devices and implants [31]. Specific cationic HDPs have recently been described to have multispecies anti-biofilm activity, which is independent of their activity against planktonic bacteria. We found that ApoB derived peptides are effective on biofilm formation and biofilm attachment, and, even more interestingly, they strongly affect pre-formed biofilms. Furthermore, ApoB derived peptides display anti-biofilm activity even on bacterial strains not sensitive to the peptide antimicrobial activity, such as *S. aureus* MRSA WKZ-2, and, in the case of sensitive strains, even at peptide concentrations (0.625 – 1 μM) significantly lower than those required to directly kill planktonic cells. This is in agreement with previous reports indicating that LL-37 peptide potently inhibits the formation of bacterial biofilms *in vitro* at the very low and physiologically meaningful concentration of 0.5 μg/mL, significantly lower than that required to kill or inhibit bacterial growth (64 μg/mL) [51]. As a consequence of this, it should be emphasized that even at the highest ApoB derived peptides concentrations tested, a significant percentage of bacterial cells inside the biofilm structure appeared to be still alive. This was observed for both ApoB derived peptides and LL-37 control peptide, while it was less pronounced in the case of CATH-2 peptide. Based on this, it is tempting to speculate that successful therapeutic approaches could be designed by combining anti-biofilm peptides and conventional antibiotics ineffective on biofilm, but effective on bacterial cells entrapped into the biofilm structure.

From a structural point of view, by Far UV-CD analyses, we found that ApoB derived peptides are unstructured in aqueous buffer, and tend to assume a conformation in the presence of membrane mimicking agents. In the presence of increasing concentrations of LPS, r(P)ApoB$_L$ peptide was found to gradually assume a defined structure, what suggests a direct binding of this peptide to LPS. This was not observed, instead, in the case of r(P)ApoB$_S$ peptide. It has also to be highlighted that both r(P)ApoB$_L$ and r(P)ApoB$_S$ peptides are endowed with immunomodulatory activities by significantly decreasing the release of pro-inflammatory IL-6 and NO in LPS induced murine RAW 264.7 macrophages. Both ApoB derived peptides were found to efficiently act either when the cells were co-incubated with the peptide under test in the presence of LPS, or when the cells were pre-treated with the peptide for 2 h and then incubated with LPS for further 24 h, thus indicating that both peptides are able to display a significant protective action. However, it has to be noticed that, differently from r(P)ApoB$_L$ peptide, r(P)ApoB$_S$ was found to play anti-inflammatory activities when co-incubated with LPS, only at the highest peptide concentration tested (20 μM), whereas both r(P)ApoB$_S$ concentrations (5 and 20 μM) were found to efficiently exert a protective effect. This might be due to the fact that ApoB derived peptides probably act through different mechanisms, with r(P)ApoB$_L$ peptide mainly acting by binding to LPS and consequently by interfering with its activity on target cells, and r(P)ApoB$_S$ peptide mainly acting on cell membrane and competing with LPS for the binding to specific cell sites. Therefore, a complex picture emerges, in agreement with the observation that HDPs immunomodulatory activities are

extremely diverse. Further experiments will allow us to elucidate the molecular mechanisms at the basis of ApoB derived peptides anti-inflammatory effects, which might include multiple aspects, such as stimulation of chemotaxis, suppression of bacterial induced pro-inflammatory cytokine production, regulation of neutrophil and epithelial cell apoptosis, modulation of cellular differentiation pathways, and promotion of angiogenesis and wound healing. As for the last aspect, in agreement with previous findings on LL-37 human peptide [53, 54], we found that r(P)ApoB$_L$ peptide is able to stimulate human keratinocytes wound re-epithelialization, an evidence that opens new and interesting perspectives on future topical application of this human HDP.

It has to be underlined that, although there are very few HDPs currently in use in the market, many are progressing through clinical trials that have focused on topic rather than systemic treatment because of peptides potential toxicity. However, it is conceivable that judicious formulations of HDPs for a clinical use, *e.g.* peptide inclusion in liposomal nanoparticles, will avoid undesired toxicity and degradation, thus allowing a sustainable HDPs delivery. Here, we show that both ApoB derived peptides are not toxic for eukaryotic cells and do not determine any hemolytic effect when tested on murine red blood cells. These observations, associated to their multifunctional properties and to their ability to act synergistically in combination with conventional antibiotic drugs, open interesting perspectives to their therapeutic applications.

5. References

1) B.A. Kelly, I. Anti-infective activity of apolipoprotein domain derived peptides in vitro: identification of novel antimicrobial peptides related to apolipoprotein B with anti-HIV activity. BMC Immunol. 11 (2010) 13.

2) C. Pierides, A. Immune responses elicited by apoB-100-derived peptides in mice. Immunol Res. 56 (2013) 96-108.

3) K. Pane, A new cryptic cationic antimicrobial peptide from human apolipoprotein E with antibacterial activity and immunomodulatory effects on human cells. FEBS J. 283 (2016) 2115-2131.

4) E. Notomista, The identification of a novel Sulfolobus islandicus CAMP-like peptide points to archaeal microorganisms as cell factories for the production of antimicrobial molecules. Microb Cell Fact. 14 (2015) 126.

5) S.H. Chen, The complete cDNA and amino acid sequence of human apolipoprotein B-100. J Biol Chem. 261 (1986) 12918-12921.

6) C.Y. Yang, Structure of apolipoprotein B-100 of human low density lipoproteins. Arteriosclerosis. 9 (1989) 96-108.

7) K. Pane, Rational Design of a Carrier Protein for the Production of Recombinant Toxic Peptides in Escherichia coli. PLoS One 11(2016) e0146552.

8) J. Reed, A set of constructed type spectra for the practical estimation of peptide secondary structure from circular dichroism. Anal Biochem. 254 (1997) 36-40.

9) M. A. Amon, Kinetic and conformational properties of a novel T-cell antigen receptor transmembrane peptide in model membranes. Peptide Sci. 14 (2008) 714–724.

10) Wiegand, K. Agar and broth dilution methods to determine the minimal inhibitory concentration (MIC) of antimicrobial substances. Nat Protoc. 3(2008) 163-175.

11) F.C. Odds. Synergy, antagonism, and what the chequerboard puts between them. J Antimicrob Chemother. 52 (2003) 1.

12) J. Li, T. Kleintschek, Hydrophobic liquid-infused porous polymer surfaces for antibacterial applications. ACS Appl Mater Interfaces. 5 (2013) 6704-6711.

13) A. Arciello, Insights into the fate of the N-terminal amyloidogenic polypeptide of ApoA-I in cultured target cells. J Cell Mol Med. 15 (2011) 2652-2663.

14) C.C. Liang, In vitro scratch assay: a convenient and inexpensive method for analysis of cell migration in vitro. Nat Protoc. 2 (2007) 329-333.

15) A. Di Grazia, The Frog Skin-Derived Antimicrobial Peptide Esculentin-1a(1-21)NH2 Promotes the Migration of Human HaCaT Keratinocytes in an EGF Receptor-Dependent Manner: A Novel Promoter of Human Skin Wound Healing? PLoS One. 10 (2015) e0128663.

16) F. Ascione, Wound Healing Revisited: a Transport Phenomena Approach. Chem Eng Sci. DOI: 10.1016/j.ces.2016.11.014, in press.

17) F. Ascione, Comparison between fibroblast wound healing and cell random migration assays in vitro. Exp Cell Res 347 (2016) 123–132.

18) A.Q. Cai, Multi-scale modeling of a wound-healing cell migration assay. J Theor Biol 245 (2007) 576-594.

19) P.K. Maini, Traveling wave model to interpret a wound-healing cell migration assay for human peritoneal mesothelial cells. Tissue Engineering 10 (2004) 475-482.

20) G. Cumming, Error bars in experimental biology. J Cell Biol 177 (2007) 7-11.

21) A.P. Subasinghage, Conformational and membrane interaction studies of the antimicrobial peptide alyteserin-1c and its analogue [E4K] alyteserin-1c. Biochim Biophys Acta 1808 (2011) 1975–1984.

22) R. Gopal, Applications of circular dichroism for structural analysis of gelatin and antimicrobial peptides. Int J Mol Sci 13 (2012) 3229–3244.

23) Y.J. Na, Lactoferrin works as a new LPS-binding protein in inflammatory activation of macrophages. Int Immunopharmacol 4 (2004) 1187-1199.

24) Y.J. Seo, Phorbaketal A, isolated from the marine sponge phorbas sp., exerts its anti-inflammatory effects via NF-kappaB inhibition and heme oxygenase-1 activation in lipopolysaccharide-stimulated macrophages. Mar Drugs 13 (2015) 7005–7019.

25) A. Gosslau, The importance of natural product characterization in studies of their anti-inflammatory activity. Mol Nutr Food Res 55 (2011) 74–82.

26) A. Nathan. Points of control in inflammation. Nature 420 (2002) 846–852.

27) van Dijk M.H., Chicken heterophils are recruited to the site of Salmonella infection and release antibacterial mature Cathelicidin-2 upon stimulation with LPS. Mol Immunol 46 (2009) 1517-1526.

28) M. Vaara. Agents that increase the permeability of the outer membrane. Microbiol Rev. 56 (1992) 395–411.

29) R.E. Hancock. Alterations in outer membrane permeability. Annu Rev Microbiol. 38 (1984) 237–264.

30) A.H. Delcour. Outer membrane permeability and antibiotic resistance. Biochim Biophys Acta. 1794 (2009) 808–816.

31) D. Pletzer, Anti-biofilm peptides as a new weapon in antimicrobial warfare. Curr Opin Microbiol 33 (2016) 35-40.

32) X. Feng, The human antimicrobial peptide LL-37 and its fragments possess both antimicrobial and antibiofilm activities against multidrug-resistant Acinetobacter baumannii. Peptides 49 (2013) 131-137.

33) D. Takahashi, Structural determinants of host defense peptides for antimicrobial activity and target cell selectivity. Biochimie 92 (2010) 1236-1241.

34) K.A. Brogden, Antimicrobial peptides: pore formers or metabolic inhibitors in bacteria? Nat Rev Microbiol 3 (2005) 238–250.

35) D.I. Chan, Tryptophan- and arginine-rich antimicrobial peptides: structures and mechanisms of action. Biochim Biophys Acta 1758 (2006) 1184–1202.

36) M.L. Mangoni, Antimicrobial peptides and wound healing: biological and therapeutic considerations. Exp Dermatol 25 (2016) 167-173.

37) A. Tremel, Cell migration and proliferation during monolayer formation and wound healing. Chemical Engineering Science 64 (2009) 247-25.

38) R.E.W. Hancock, Host defence peptides from invertebrates—emerging antimicrobial strategies. Immunobiology 211 (2006) 315–322.

39) R.E.W. Hancock, The role of cationic anti-microbial peptides in innate host defences. Trends Microbiol 8 (2000) 402–410.

40) A.K. Marr, Antibacterial peptides for therapeutic use: obstacles and realistic outlook. Curr Opin Pharmacol 6 (2006) 468–472.

41) E. Guaní-Guerra, Antimicrobial peptides: general overview and clinical implications in human health and disease. Clin Immunol 135 (2010) 1–11.

42) P. Papareddy, C-terminal peptides of tissue factor pathway inhibitor are novel host defense molecules. J Biol Chem 285 (2010) 28387–28398.

43) E. Andersson, Antimicrobial activities of heparin-binding peptides. Eur J Biochem 271 (2004) 1219–1226.
44) S.G. Young, Recent progress in understanding apolipoprotein B. Circulation 82 (1990) 1574-1594.
45) O.L. Franco, Peptide promiscuity: an evolutionary concept for plant defense. FEBS Lett. 585 (2011) 995–1000.
46) H.M. Nguyen, Limitations of antibiotic options for invasive infections caused by methicillin-resistant *Staphylococcus aureus*: is combination therapy the answer? J Antimicrob Chemother. 65 (2010) 24–36.
47) G.S. Tillotson, Fluoroquinolone resistance: mechanisms and epidemiology. J Med Microbiol. 46 (1997) 457–461.
48) M.E. Evans, Polymyxin B sulfate and colistin: old antibiotics for emerging multiresistant gram-negative bacteria. Ann. Pharmacother. 33 (1999) 960–967.
49) H. Nakaido, Molecular basis of bacterial outer membrane permeability. Microbiol Rev. 49 (1985) 1-32.
50) S.L. Percival, Tetrasodium EDTA as a novel central venous catheter lock solution against biofilm. Infect Control Hosp Epidemiol. 2 (2005) 515–519.
51) J. Overhage, Human Host Defense Peptide LL-37 Prevents Bacterial Biofilm Formation. Infect Immun. 76 (2008) 4176-4182.
52) B.B. Finlay, Can innate immunity be enhanced to treat microbial infections? Nat Rev Microbiol 2 (2004) 497–504.
53) J.D. Heilborn, The cathelicidin anti-microbial peptide LL 37 is involved in re epithelialization of human skin wounds and is lacking in chronic ulcer epithelium. J. Invest. Dermatol. 120 (2003) 379–389.
54) R. Shaykhiev, Human endogenous antibiotic LL-37 stimulates airway epithelial cell proliferation and wound closure. Am. J. Physiol. Lung Cell. Mol. Physiol. 289 (2005) L842–L848.

CHAPTER 4

Structural and functional characterization of novel HDPs identified in the archaeon Sulfolobus islandicus and in human 11-hydroxysteroid dehydrogenase-1 β-like

Rosa Gaglione

Department of Chemical Sciences, PhD in Biotechnology

University of Naples "Federico II", Napoli, Italy

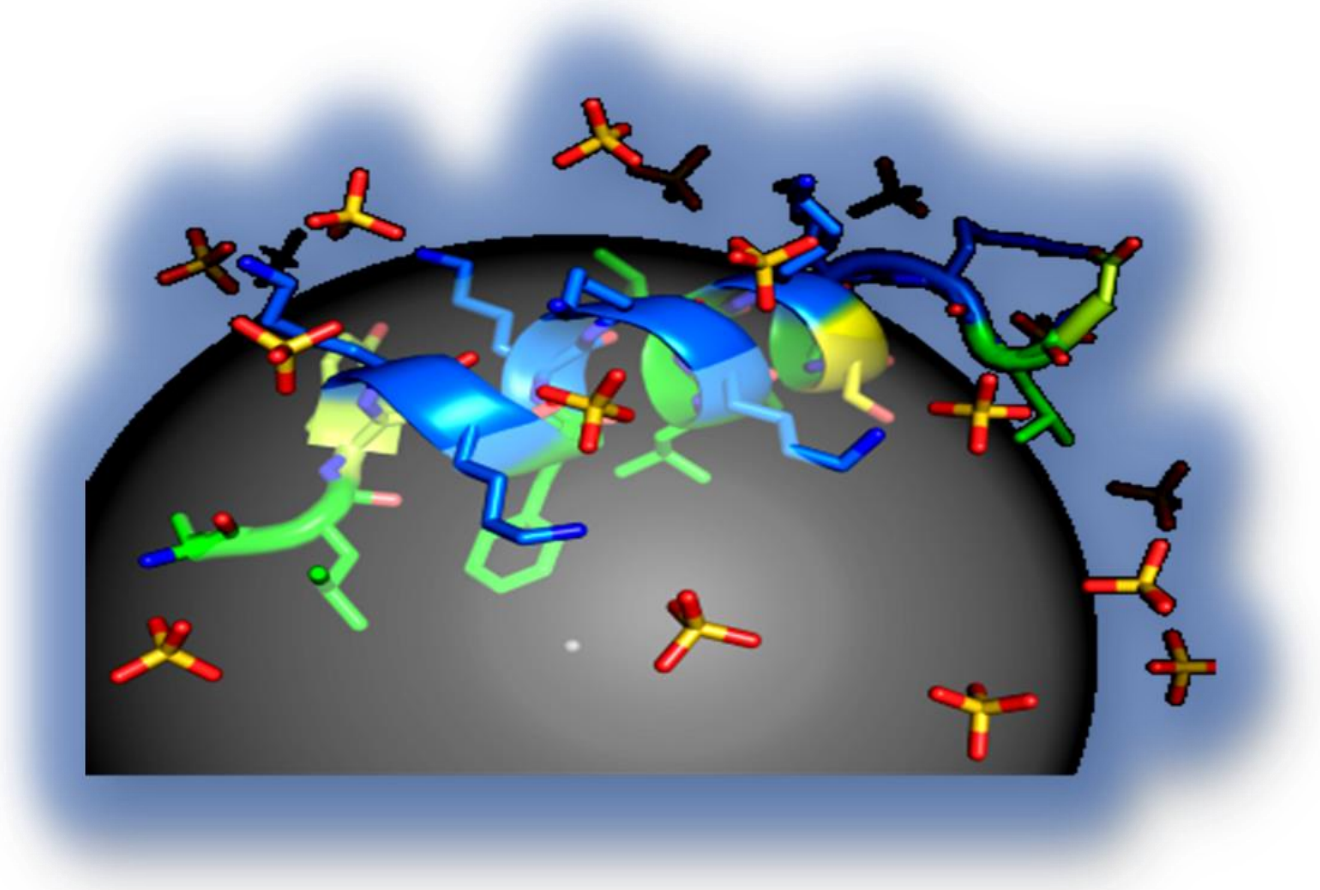

1. Introduction

The development of bioinformatics approaches has greatly improved the identification of putative antimicrobial regions in protein precursors [1]. Along the present Thesis project, by using a recently developed bioinformatics strategy well described in the Chapter 3, we identified a novel HDP at the C-terminus of four isoforms of human 11-hydroxysteroid dehydrogenase-1 β-like and, to the best of our knowledge, the first HDP from an archaeal protein, the transcription factor Stf76 encoded by the hybrid plasmid-virus pSSVx from *Sulfolobus islandicus*.

Human 11β-hydroxysteroid dehydrogenase type 1 (HSD 1) is a known NADP(H)-dependent enzyme that catalyses the conversion of inactive glucocorticoids into active forms. The dysregulation of this enzyme is mainly implicated in the development of metabolic syndromes [2]. On the contrary, human 11-hydroxysteroid dehydrogenase-1 β-like, also known as 11-beta-hydroxysteroid dehydrogenase type 3 (HSD 3), has never been isolated as a protein and its membership to the hydroxysteroid dehydrogenase family has been assigned on the basis of the presence in the gene sequence of a putative dehydrogenase/reductase region partially similar to that extensively studied in HSD 1 [3]. The only type of evidence that supports the existence of HSD 3 as a protein is represented by expression data [4] that indicate the existence of a transcript (Gene ID: 374875) apparently overexpressed in the brain and in lung cancer cells. In the last protein, a high scoring region has been identified by our bioinformatics approach. The selected region includes 26 amino acid residues, and has been obtained as a synthetic peptide, here named GVF27. The HDP was found to exert bactericidal activities against planktonic and sessile bacteria, as well as anti-inflammatory properties on murine cells.

Furthermore, we also demonstrated that DNA binding proteins can be a convenient source of new HDP-like peptides by identifying the first antimicrobial peptide from an archaeal protein, the transcription factor Stf76 encoded by the hybrid plasmid-virus pSSVx from *Sulfolobus islandicus*. This archaeal HDP, named VLL-28, was already shown to possess a broad-spectrum antibacterial activity and to exhibit selective leakage and fusogenic capability on vesicles with a lipid composition similar to that of bacterial membranes [5].

Along this Thesis project, it was characterized for the first time the antitumor activity of VLL-28 peptide. It has been widely reported that several antimicrobial peptides are also able to exert anti-cancer activity [6]. For this reason, they have been named “anti-cancer peptides” (ACPs). Due to the severe side effects of conventional chemotherapeutic agents and to the ability of metastatic tumour cells to develop a “multidrug resistance” phenotype, ACPs have attracted considerable attention; in fact, these peptides could represent a new generation of anti-cancer drugs with a mechanism of action well distinguished from those of conventional chemotherapeutic agents. Most of the ACPs described so far are HDPs able to exert on cancer cells toxic effects higher than those observed on normal cells. [7, 8]. This differential toxicity has been attributed to the fact that cancer cells often show alterations of membrane composition, such as loss of the asymmetric distribution of phospholipids, with the consequent exposure of phosphatidylserine on the outer leaflet, increased production of anionic lipids (*e.g.* sulfated lipids), sialic acid containing glycolipids, glycoproteins and, sometimes, a decreased production of cholesterol. This is responsible for an increased negative charge at the surface of tumor cells, which would favor the binding of ACPs, thus making these cells more susceptible to peptides toxic action. However, in the case of cancer cells, differently from bacterial killing mechanisms, toxicity is not necessarily due to accumulation of the peptide into

the membrane followed by cell lysis. In several cases, it has been demonstrated that ACPs are internalized and that the killing is mainly due to peptide interaction with one or more intracellular targets, such as mitochondria, DNA, cytoplasmic and nuclear proteins (*e.g*. Hsp70 [9] and DNA polymerase β [10], respectively).
By means of a multidisciplinary approach including biochemical, cellular biology and spectroscopic techniques, the mechanisms of action of synthetic VLL-28 and GVF27 peptides have been here analysed and partly elucidated.

2. Materials and Methods

2.1 Peptide Synthesis Reagents

Polypropylene reaction vessels and sintered polyethylene frits were supplied by Alltech Italia. NovaSyn TGR resin, 2-(1H-benzotriazole-1-yl)-1,1,3,3-tetramethyluronium hexafluorophosphate (HBTU), cyano-hydroxyimino-acetic acid ethyl ester (Oxyma) and all amino acids were from Novabiochem-Merck. N,N′-diisopropylethylamine (DIPEA), piperidine, Kaiser test, trifluoroacetic acid (TFA), scavengers, fluorescein isothiocyanate (FITC) and N-methylmorpholine (NMM) were purchased from Sigma-Aldrich. N,N-Dimethylformamide (DMF) was purchased from CARLO ERBA Reagents. Acetonitrile (ACN), dichloromethane (DCM) and diethyl ether were purchased from VWR International. All aqueous solutions were prepared by using water obtained from a Milli-Q gradient A-10 system (Millipore, 18.2 MΩ·cm, organic carbon content ≥ 4 µg/L).

2.2 Peptide Synthesis

The sequence of GVF27 peptide is GVFYPWRFRLLCLLRRWLPRPRAWFI, whereas the sequence of VLL-28 peptide is VLLVTLTRLHQRGVIYRKWRHFSGRKYR.
They were manually synthesized using the fluorenylmethyloxycarbonyl (Fmoc) solid-phase strategy (0.2 mmol). The syntheses were performed on NovaSyn TGR resin (loading 0.24 mmol/g), using all standard amino acids. The Fmoc protecting group was removed by treatment with 30% piperidine in DMF (3 × 10 min). The amino acids in 10-fold excess were pre-activated with HBTU (9.8 equiv)/Oxyma (9.8 equiv)/DIPEA (10 equiv) in DMF for 5 min and then added to the resin suspended in DMF. The reaction was carried out for 1 h and coupling efficiency was assessed by the Kaiser test. The peptides were cleaved off the resin by treatment with a mixture of trifluoroacetic acid (TFA)/water/triisopropylsilane (95:2.5:2.5 v/v/v) for 3 h at room temperature. The resins were filtered, the crude peptides were precipitated with diethyl ether, dissolved in H_2O/ACN solution, and lyophilized. The products were purified by preparative RP-HPLC on a Shimadzu system equipped with a UV−visible detector SPD10A using a Phenomenex Jupiter Proteo column (21.2 × 250 mm; 4 µm; 90 Å) and a linear gradient of H_2O (0.1% TFA)/ACN (0.1% TFA) from 10%–55% of ACN (0.1%TFA) in 15 min at a flow rate of 20 mL/min. The collected fractions containing the peptides were lyophilized giving a final yield of about 35% of each pure product. The identity and purity of the compounds were assessed by the AGILENT Q-TOF LC/MS instrument equipped with a diode array detector combined with a dual ESI source on an Agilent C18 column (2.1 × 50 mm; 1.8 µm; 300 Å) at a flow rate of 200 µL/min and a linear gradient of H_2O (0.01% TFA)/ACN (0.01% TFA) from 5%–70% of ACN (0.01% TFA) in 15 min. Upon mass spectrometry analysis, the purity of the synthesized peptides was found to be ≥ 95%.

2.3 Cell culture

Murine RAW 264.7 cells, malignant SVT2 murine fibroblasts (BALBc 3T3 cells transformed by SV40 virus), parental BALBc 3T3 murine cells, and HEK-293 human embryonic kidney cells were cultured in Dulbecco's Modified Eagle's Medium (Sigma-Aldrich), supplemented with 10% fetal bovine serum (HyClone), 2 mM L-glutamine and antibiotics, in a 5% CO_2 humidified atmosphere at 37 ºC. HRCE (Human Renal Cortical Epithelial) cells (Innoprot) were cultured in basal medium, supplemented with 2% fetal bovine serum, epithelial cell growth supplement and antibiotics, all from Innoprot, in a 5% CO_2 humidified atmosphere at 37 °C.

2.4 Cytotoxicity assays

Cells were seeded in 96-well plates (100 µL per well) at a density of $5x10^3$ per well (SVT2, HEK-293, and HRCE cells) or $2.5x10^3$ per well (BALBc 3T3 cells). VLL-28 peptide was added to the cells 24 h after seeding for time- and dose-dependent cytotoxic assays. At the end of incubation, cell viability was assessed by the MTT assay, as previously described [11]. MTT reagent, dissolved in DMEM without phenol red (Sigma-Aldrich), was added to the cells (100 µL per well) to a final concentration of 0.5 mg/mL. After 4 h incubation at 37 °C, the culture medium was removed and the resulting formazan salts were dissolved by adding isopropanol containing 0.1 N HCl (100 µL per well). Absorbance values of blue formazan were determined at 570 nm using an automatic plate reader (Microbeta Wallac 1420, Perkin Elmer). Cell survival was expressed as percentage of viable cells in the presence of the peptide under test, with respect to control cells grown in the absence of the peptide. In all the experiments described in this paper, controls were performed by supplementing the cell cultures with identical volumes of peptide buffer for the same lengths of time.

2.5 Analysis of cell death

Malignant SVT2 murine fibroblasts and parental BALBc 3T3 murine cells were plated at a density of $2×10^4$ cells/cm^2 in complete medium for 24 h and then exposed to 20 µM VLL-28 peptide for 6, 12 or 24 h. To prepare cell lysates, both untreated and treated cells were scraped off in PBS, centrifuged at 1,000 g for 10 min and solubilised in lysis buffer (1% NP-40 in PBS, pH 7.4) containing protease inhibitors. After 30 min incubation on ice, lysates were centrifuged at 14,000 g for 30 min at 4°C. Upon determination of total protein concentration in the supernatant by the Bradford assay, samples were analyzed by SDS-PAGE followed by Western blotting using specific antibodies directed towards procaspase-3 (Cell Signaling Technology) or p62 (Novus Biologicals) proteins. For normalization to internal standard signals, antibody against β-actin (Sigma-Aldrich) was used. In parallel experiments, cells were treated with puromycin (10 µg/mL) for 12 h or with rapamycin (20 µM) for 24 h, which were used as positive controls for apoptosis and autophagy induction, respectively.

For morphological analyses, cells were seeded on glass coverslips in 24-well plates and grown to semi-confluency. Cells were then incubated for 72 h with 20 µM VLL-28 peptide in complete medium, after which cells were washed with PBS, fixed for 10 min at room temperature (RT) with 4% paraformaldehyde in PBS and mounted in 50% glycerol in PBS. Samples were then examined using a confocal laser-scanner microscope Zeiss LSM 700. All images were taken under identical conditions.

2.6 Membrane preparation

Membranes used to perform NMR experiments were isolated from BALBc 3T3 cells or SVT2 cells and obtained as previously described [12]. In details, cells were detached by using trypsin and washed twice with PBS. Afterwards, the cells were solubilised in PBS and homogenized by means of a pellet pestle (Sigma-Aldrich). Particulate matter was removed by centrifuging at 3,500 rpm for 15 min. The supernatant was then centrifuged at 28,000 rpm for 1 h at 4 °C. The sediment was washed and centrifuged at 28,000 rpm for 30 min at 4 °C. Afterwards, 180 µL of PBS mixed with 20 µL of D_2O were added to the sediment, and the membrane was solubilised by passage through a 25-gauge needle (approximately 20 times).

2.7 Spectroscopic studies

CD spectra of GVF27 and VLL-28 peptides were recorded with a J-810 spectropolarimeter equipped with a Peltier temperature control system (Model PTC-423-S, Jasco Europe). Far-UV measurements (190–260 nm) were carried out at 20 °C by using a 0.1 cm optical path length cell and a peptide concentration of 25 µM in the case of GVF27 and 20 µM in the case of VLL-28. CD spectra were recorded as previously described [13]. Baseline was corrected by subtracting the complete buffer spectrum.

In the case of GVF27 CD spectra, LPS from *Pseudomonas aeruginosa* strain 10 (Sigma-Aldrich) and from *Pseudomonas aeruginosa* clinical strain KK27 [14] were used. Further analyses were carried out in the presence of lipoteichoic acid from *Staphylococcus aureus* (LTA, Sigma-Aldrich). All the measurements were recorded by using different concentrations of each compound (from 0.05 to 1.0 mg/mL). Baseline was corrected by subtracting the spectrum of both LPS and LTA at the same concentrations used for CD spectra in the presence of GVF27 peptide. Additional CD spectra were obtained by using different concentrations of TFE (0-40%). Deconvolutions of CD spectra were obtained by using the web-based program CdPro (http://lamar.colostate.edu/~sreeram/CDPro/). Fluorescence experiments were carried out under the same experimental conditions used for CD analyses. Fluorescence spectra were collected at 20 °C by using a Varian Cary Eclipse spectrophotometer at $\lambda_{excitation}$ of 295 and 280 nm, by using a a 1.0 cm path length cell at 5 ε_{em} and 5 ε_{ex}. Emission spectra (300-400 nm) were collected in the presence of 40% TFE, 5 mg/mL LPS or 10 mg/mL LTA.

In the case of VLL-28 peptide, CD spectra were recorded in the presence of intact cells (800,000 cells) at different incubation times (0-10-30-60 min and 24 h) in PBS buffer. The baseline was corrected by subtracting the spectrum of the cells in the absence of the peptide at the same incubation times.

2.8 Dynamic light scattering (DLS) analysis of LPS micelles

To estimate the size of LPS particles, DLS analyses were performed. By this way, the Hydrodynamic Radii (RH) was measured. DLS analyses were performed by using a Zetasizer Nano ZS (Malvern Instruments) equipped with a 173° backscatter detector, at 25 °C, in disposable sizing cuvettes. DLS measurements were carried out in triplicate on aqueous LPS and LTA samples (0.5 mg/mL). Data were analyzed by using the Software of OMNISIZE (Viscotek). LPS and LTA size measurements were performed before and after peptide addition (0.5 mg/mL).

2.9 LPS binding assay

The ability of GVF27 to neutralize LPS was evaluated by using the commercially available *Limulus amebocyte* lysate (LAL) assay (Pierce® LAL Chromogenic Endotoxin Quantitation Kit, Thermo Scientific) [15]. Briefly, an aliquot (25 µL) of serially diluted peptide (6.25-12.5-25 µM) was added to 25 µL of 0.5 U/mL LPS from *E. coli* O11:B4 for 30 min at 37 °C. The mixture was then incubated with 50 µL of *Limulus amebocyte* lysate reagent for 10 min. Absorbance at 405 nm was measured 10 min after the addition of the chromogenic substrate Ac-Ile-Glu-Ala-Arg-p-nitroanilide (100 µL). The amount of unbound LPS was extrapolated from a standard curve, and the percentage of inhibition was calculated as follows: [(amount of free LPS in control sample) − (amount of free LPS in test sample)] ×100/amount of free LPS in control sample.

2.10 Measurement of nitric oxide production

To determine the levels of NO released by RAW 264.7 cells, a colorimetric assay based on the use of Griess reagent (Sigma Aldrich) was performed. The levels of nitrite (NO^{2-}) in cell supernatants were determined on the basis of a reference curve obtained by testing increasing concentrations (from 1 to 50 µM) of sodium nitrite dissolved in water. Briefly, cell culture supernatants were mixed with equal volumes of 1% sulphanilamide dissolved in 2.5% phosphoric acid, and incubated for 5 min at room temperature. Samples were then diluted 1:1 (v/v) with 0.1% N-(1-naphthyl) ethylenediamine dihydrochloride, and incubated for further 5 min at room temperature. Absorbance values were then determined at 520 nm using an automatic plate reader (FLUOstar Omega, BMG LABTECH).

2.11 Measurement of interleukin-6 production

IL-6 levels were determined by ELISA assay (DuoSet ELISA kits, R&D Systems) following the manufacturer's instructions. Briefly, RAW 264.7 cells (5×10^4) were seeded into 96-well microtiter plates, and grown to semi-confluency. After 24 h, the culture medium was replaced with fresh medium containing the peptides under test (5 or 20 µM) in the presence or in the absence of LPS from *Salmonella Minnesota* (50 ng/mL, Sigma Aldrich) for 24 h at 37 °C. When the protective effect of the peptide was evaluated, cells were pre-incubated with the peptide (5 or 20 µM) for 2 h at 37 °C. Following treatment, cells were washed three times with PBS prior to incubation with LPS (50 ng/mL) for further 24 h at 37 °C. In each case, at the end of incubation, the culture supernatants were collected, and centrifuged at 5,000 rpm for 3 min at room temperature, in order to remove cell debris. Samples were then analysed by reading absorbance values at 450 nm using 550 nm as a reference wavelength at an automatic plate reader (FLUOstar Omega, BMG LABTECH).

2.12 Nuclear magnetic resonance spectroscopy

All NMR experiments were carried out at 298K using an Inova 600 MHz spectrometer (Varian Inova), equipped with a cryogenic probe optimized for ^1H detection. For chemical shift assignment and conformational analysis, 1 mg of VLL-28 peptide was dissolved either in 500 µL of 20 mM sodium phosphate pH 7 containing 10% v/v D_2O or in 500 µL of the same buffer containing 25% (v/v) TFE (2,2,2-trifluoroethanol-D3 99.5% isotopic purity, Sigma-Aldrich). One-dimensional (1D) ^1H spectra were acquired with a spectral width of 7,191.66 Hz, relaxation delay of 1.03 s, 7k data points for acquisition and 16k for transformation. Bi-dimensional (2D) [^1H, ^1H] total correlation spectroscopy (TOCSY) [16, 17], double quantum filtered correlated

spectroscopy (COSY) [18] and nuclear Overhauser effect spectroscopy (NOESY) [19] were performed by acquiring 32 or 64 scans per t1 increment with a spectral width of 7,191.66 Hz along both t1 and t2, 2,048 × 256 data points in t2 and t1, respectively, and recycle delay of 1.0 s. Water suppression was achieved by means of Double Pulsed Field Gradient Spin Echo (DPFGSE) sequence [20, 21]. TOCSY experiments were recorded by using a DIPSI-2 mixing scheme of 70 ms with 7.7 kHz spin-lock field strength. NOESY spectra were carried out with a mixing time of 250 ms. Data were typically apodized with a square cosine window function and zero filled to a matrix of size 4,096 × 1,024 before Fourier transformation and baseline correction.

To analyse VLL-28 interaction with intact cells and isolated cell membranes, sediments corresponding to 18 x 10^6 cells and membranes isolated from 18 x 10^6 cells, obtained as reported above, were solubilized in 150 µL of PBS buffer (pH 7.4) and 10% H_2O, to obtain reference spectra, or in the presence of VLL-28 peptide (430 µM) in PBS buffer. STD spectra were acquired with 10,000 scans with on-resonance irradiation at 5.2 ppm for saturation of membrane lipids resonances and off-resonance irradiation at 30 ppm. A train of 40 Gaussian shaped pulses of 50 ms with 1 ms delay between pulses was used, for a total saturation time of 2 s. STD spectra were obtained by internal subtraction of saturated spectrum from off-resonance spectrum by phase cycling. STD spectra of the peptide alone were also acquired and did not show any signal. 2D [^{1}H, ^{1}H] TOCSY and trNOESY spectra of VLL-28 peptide were acquired in the presence of isolated cell membranes. All NMR data were processed with the software VNMRJ 1.1.D (Varian Inova). 1D spectra were analyzed by using ACD/NMR Processor 12.0 (www.acdlabs.com). 2D TOCSY, COSY and NOESY spectra for proton chemical shift assignment were analyzed by using Homoscope, a tool available in CARA (Computer Aided Resonance Assignment) software [22].

2.13 Statistical analyses

Results are presented as the mean ± standard error of the mean values (SEM) of at least three independent experiments. All samples were compared to negative controls in the absence of the peptide under test. *$p < 0.05$; **$p < 0.01$; ***$p < 0.001$.

3. Results

3.1 STRUCTURAL AND FUNCTIONAL CHARACTERIZATION OF SYNTHETIC GVF27 PEPTIDE

3.1.1 Circular Dichroism and Fluorescence Spectroscopy analyses

Structural analyses by CD spectroscopy provide a qualitative picture of the main structural elements of a given peptide. To elucidate this point, we performed Far-UV CD spectra of synthetic GVF27 peptide both in water and in 10 mM Hepes pH 7.4, and found that the peptide is largely unstructured. On the contrary, it was found to be structured in 40% TFE (Figure 1). This behaviour has been described for several HDPs [23, 24], which have been found prone to assume a specific conformation when interacting with membrane-mimicking agents, such as TFE. Deconvolution data (see Methods), reported in Table 1, indicate that structured GVF27 adopts a predominant α-helical structure, which was found to be ≈ 50%.

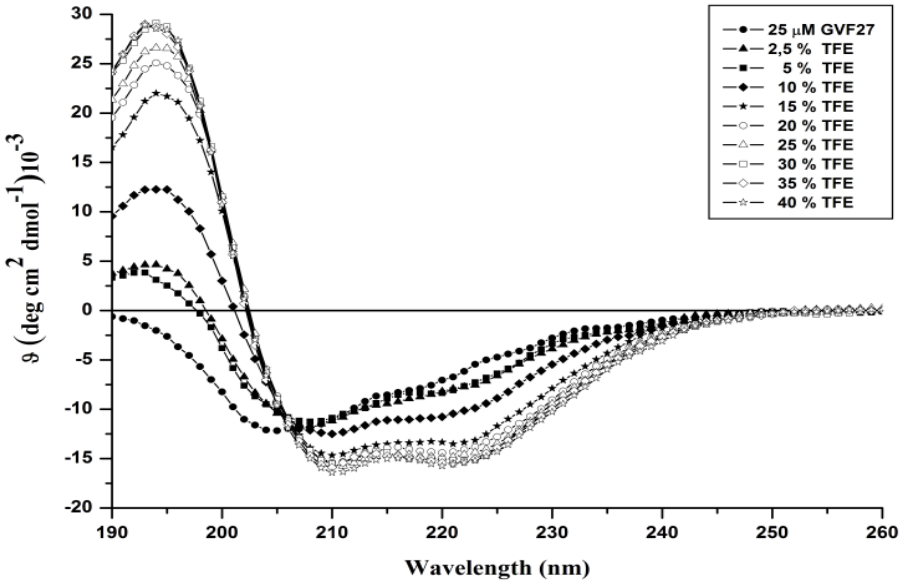

Figure 1. Far-UV CD spectra of GVF27 peptide in the presence of increasing concentrations of TFE.

	α-helix (%)	β-strand (%)	coil (%)
GVF27	**18.2**	**24.0**	**57.8**
GVF27 - 40% TFE	**52.6**	**7.2**	**40.2**
GVF27 - 0,4 mg/mL LPS from *Pseudomonas aeruginosa* strain 10	**30.8**	**18.6**	**50.6**
GVF27 - 0,4 mg/mL LPS from *Pseudomonas aeruginosa* strain KK27	**32.1**	**12.3**	**55.5**
GVF27 - LTA 0,4 mg/mL	**33.0**	**19.5**	**47.5**

Table 1. Secondary structure content of GVF27 peptide, calculated by means of CDPRO program.

To further characterize structural properties of GVF27, we also analysed its interaction with LPS and LTA, the main constituents of the cell wall of Gram-negative and -positive bacteria, respectively. CD spectra in the presence of LPS isolated from two different *P. aeruginosa* strains (strain 10 and clinical isolate KK27 strain) are shown in Figure 2 (panels a and b).
GVF27 CD spectrum in water has a minimum at around 205 nm, indicative of a disordered conformation. In the presence of LPS (Figure 2 a-b), instead, peptide spectra present two minima centred at around 210 and 225 nm, suggesting the ability of the peptide to assume an α-helical conformation upon interaction with LPS. The deconvolution data (Table 1) indicate that the increase in α-helical structure (about 31-32%) is similar in the presence of both types of LPS, whereas amounts of beta and coil structure appear slightly different. When CD spectra were acquired in the presence of LTA (Figure 2c), a relatively flat shape minimum centred at 215 nm was observed. This is indicative of the presence of significant amounts of both α-helical and beta structures, as indicated by deconvolution data (Table 1).

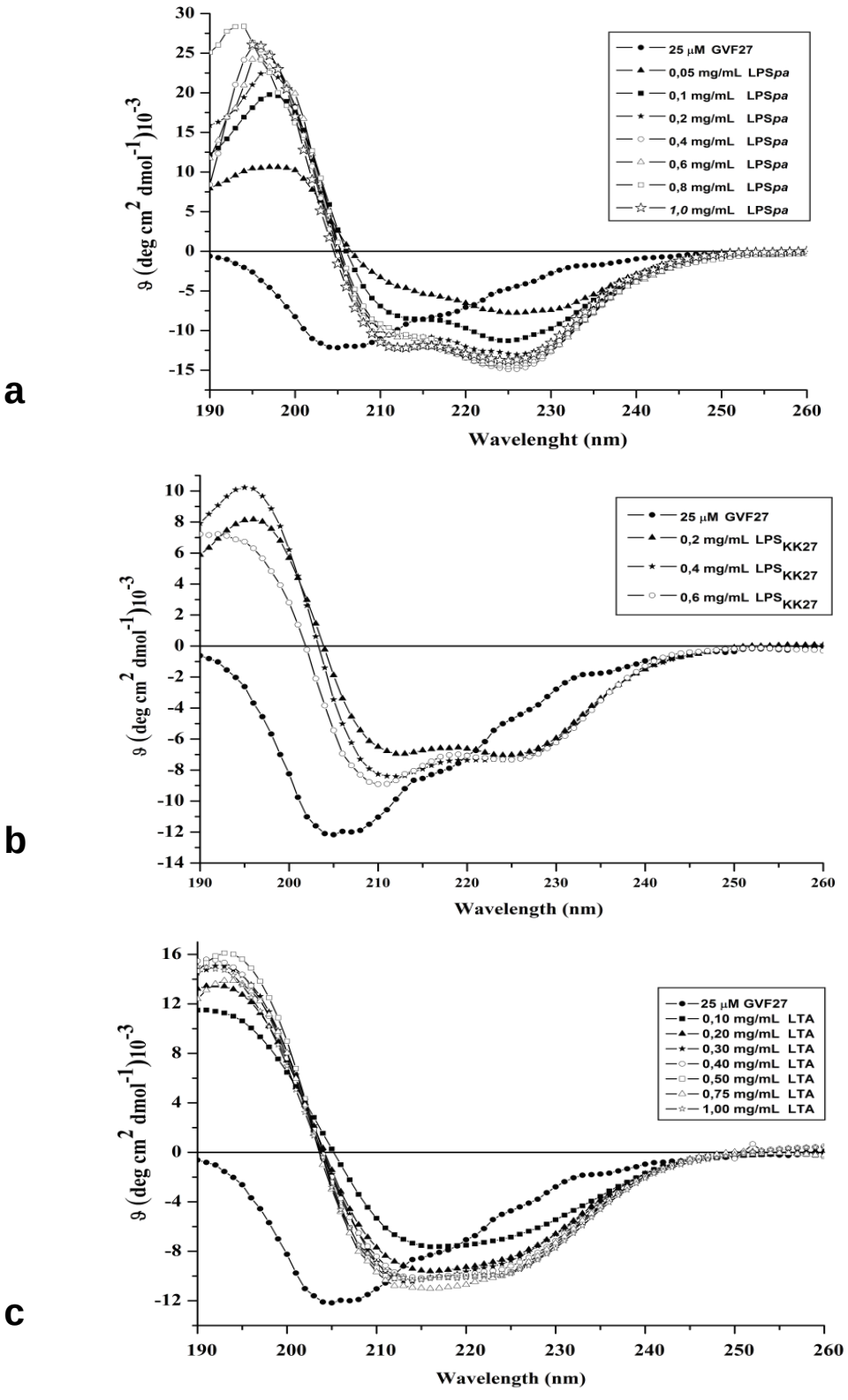

Figure 2. Far-UV CD spectra of GVF27 peptide in the presence of increasing concentrations of LPS from *P. aeruginosa* 10 (a), from *P. aeruginosa* KK27 (b) and of LTA from *Staphylococcus aureus* (c).

Spectrofluorometric data were also collected to analyse the effects of GVF27 interaction with LPS and LTA on peptide tertiary structure (Figure 3). This was performed by taking advantage of the presence of three Trp residues in GVF27 peptide. Fluorescence spectra were recorded upon excitation at 280 nm and 295 nm. Upon peptide interaction with LPS, LTA and TFE, a blue shift of the maximum emission wavelength was observed, indicating that GVF27 becomes structured, in agreement with CD data. In the presence of TFE, instead, a less marked effect was observed (Figure 3).

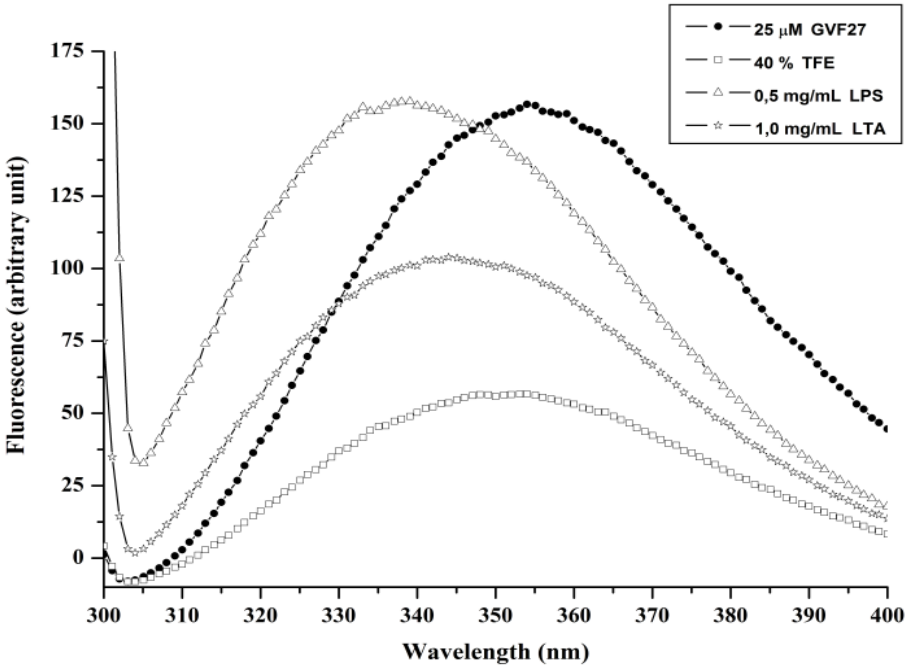

Figure 3. Intrinsic fluorescence spectra of GVF27 peptide in H_2O and in the presence of TFE (40%), LPS (0,5 mg/mL) and LTA (1 mg/mL).

3.1.2 GVF27 peptide assembles LPS aggregates

Dynamic Light Scattering (DLS) is a well-known technique used to measure Brownian motion (diffusion) and size distribution of particles in solution. For this reason, DLS experiments were performed to evaluate whether GVF27 peptide is able to alter the size of LPS and LTA micelles (above their critical micelle concentration). In both cases, GVF27 was found to promote the formation of larger aggregates (Figure 4). In particular, the data indicate that LPS from *Pseudomonas* is poly-dispersed in solution, with major size-populations having a hydrodynamic radius centred at about 40 nm (Figure 4). Incubation of LPS with GVF27 is responsible for a shift of LPS micelles average size to higher values centred at about 260 nm. On the other hand, when the peptide was incubated with LTA, the diameter of the aggregates was found to be about 100 nm (average value), indicating a weaker efficay of GVF27 in determining LTA aggregates association. It can be hypothesized that this aggregation promoting action, already observed for different antimicrobial peptides [25], represents a key element of peptide anti-inflammatory mechanism of action, based on LPS neutralization. In fact, by this way, the peptide might inhibit the interaction of LPS with its cell receptors, with a consequent blocking of cytokine production and release [26].

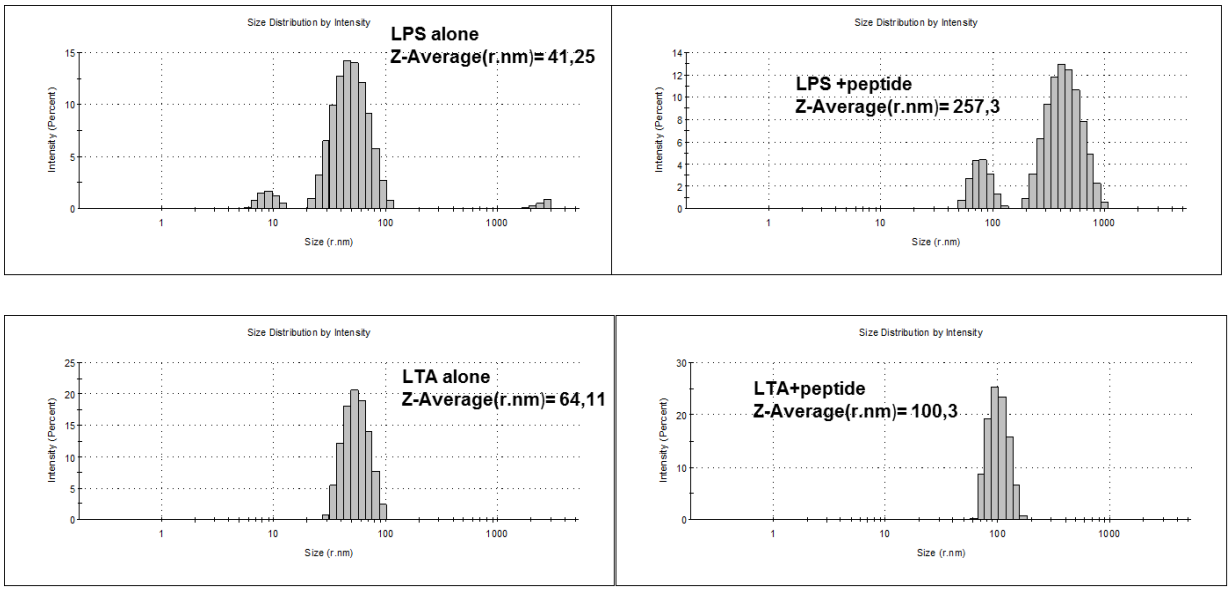

Figure 4. Effect of GVF27 on the structural organization of LPS or LTA micelles. Dynamic light scattering of LPS from *P. aeruginosa* 10 (top) or LTA (bottom) before and after incubation with the peptide.

3.1.3 Anti-inflammatory properties of GVF27 peptide

Data reported above indicate that GVF27 is able to assume specific conformations in the presence of membrane mimicking agents, LPS and LTA, as well as to induce aggregation of LPS, and, to a lesser extent, of LTA. As it has been already reported that several HDPs are able to mitigate up-regulation of LPS-induced pro-inflammatory mediators and cytokines [27], it seemed interesting to verify if GVF27 possesses anti-inflammatory properties. To collect data on potential anti-inflammatory properties of GVF27 peptide, nitric oxide (NO) production and interleukin IL-6 release were analyzed in murine macrophages RAW 264.7 treated with GVF27 and LPS.

NO plays diverse roles in biological systems, since it is a mediator of vasodilatation, platelet aggregation and neurotransmission, and regulates function, death and survival of various cell types including many of those involved in immunity and inflammation [28, 29]. To study the effect of GVF27 on NO production in LPS induced RAW 264.7 cells, we performed three type of treatments: (i) cells were concomitantly treated with peptide (5 or 20 µM) and LPS (50 ng/mL) for 24 h; (ii) cells were treated with the peptide alone (5 or 20 µM) for 2 h and then incubated with LPS from *Salmonella Minnesota* (50 ng/mL) for further 24 h; (iii) cells were first treated for 2 h with LPS (50 ng/mL) and then incubated with the peptide (5 or 20 µM) for further 24 h. As shown in Figure 5A, the co-incubation of cells with GVF27 and LPS determines a strong attenuation of NO production, which was found to be more pronounced in the presence of higher concentrations of the peptide. Conversely, when RAW 264.7 cells were pre-incubated with the peptide and subsequently stimulated with LPS, the effect of GVF27 on NO production was found to be not significant (Figure 5A). Similarly, when RAW 264.7 cells were pre-incubated with LPS and subsequently treated with GVF27 (5 or 20 µM), we revealed a slight dose-dependent reduction of NO production (Figure 5A).

Cytokines are key mediators of inflammatory response. They are small proteins (about 25 kDa) released by many cell types, usually after an activation signal, to

induce a response upon binding to specific receptors. IL-6 is a monomer produced by T cells, macrophages and endothelial cells. It stimulates growth and differentiation of B and T cells, and the production of acute phase proteins, such as C-reactive protein [30]. By ELISA assays we analyzed the effects of GVF27 on IL-6 release in RAW 264.7 cells by following the same experimental scheme described for NO production. The peptide showed a strong inhibitory effect on IL-6 secretion when macrophages were co-incubated with GVF27 (5 or 20 µM) and LPS (50 ng/mL) for 24 h (see Figure 5B). Moreover, we found that GVF27 was able to exert a significant dose-dependent protective effect on RAW 264.7 cells. Indeed, as shown in Figure 5B (on the centre), when RAW 264.7 cells were pre-treated with GVF27 (5 or 20 µM) for 2 h and then incubated with 50 ng/mL LPS for further 24 h, a limited secretion of IL-6 was observed. When cells, instead, were pre-incubated with LPS and then subjected to the action of the peptide (Figure 5B, on the right), a slight secretion of IL-6 was revealed. This suggests that, although cells are incubated with the endotoxin for a very short time, the peptide is indeed still able to attenuate the secretion of the interleukin under test. Collectively, these data clearly indicate that GVF27 peptide is able to exert an intriguing anti-inflammatory action on mouse macrophages under LPS stimulation.

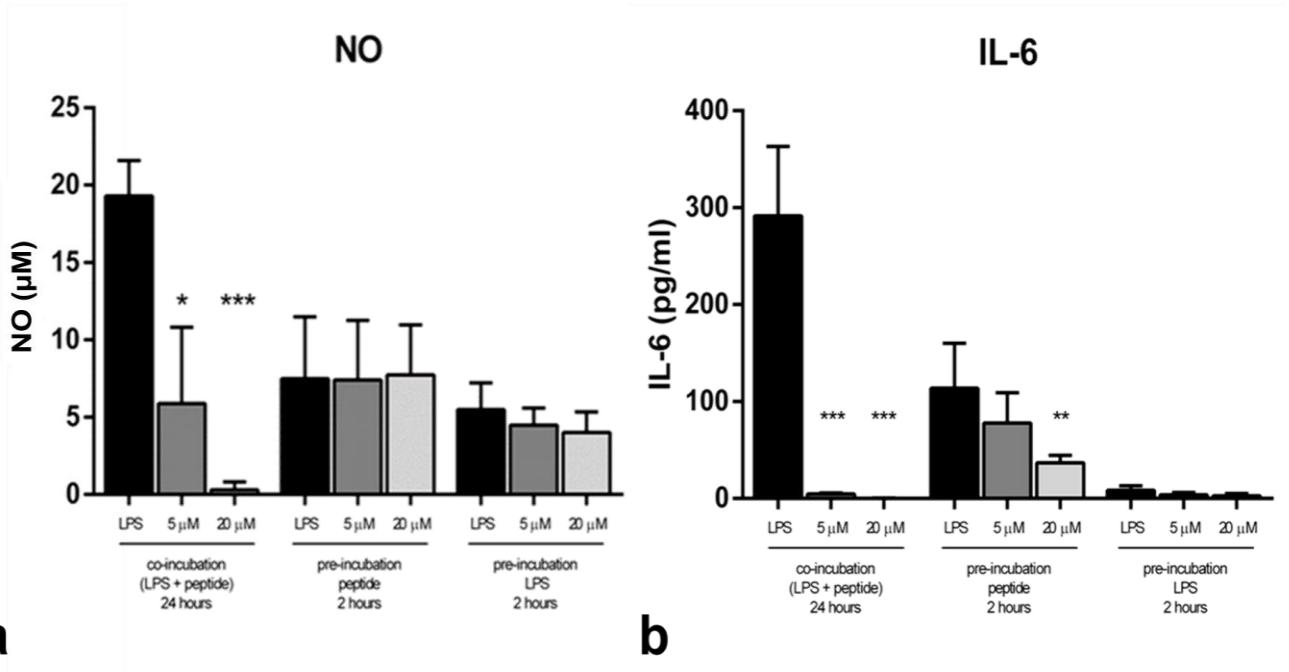

Figure 5. (a) Effect of GVF27 on NO production in LPS induced mouse macrophages RAW 264.7. (b) Effect of GVF27 on IL-6 release in LPS induced mouse macrophages RAW 264.7. All the experiments were carried out for total 24 h. Data represent the mean (± standard deviation, SD) of at least 3 independent experiments, each one carried out with triplicate determinations. *p<0.05, **p<0.01, or ***p<0.001 were obtained for control *versus* treated samples.

Finally, the ability of GVF27 peptide to bind to LPS (Figure 6) was evaluated and further confirmed by using the chromogenic LAL (*Limulus amaebocyte* lysate) assay [31]. To this purpose, the peptide at three different concentrations (6.25 - 12.5 - 25 µM) was incubated with LPS from *Escherichia coli* 011:B4 for 30 minutes at 37 °C,

following the manufacturer instructions. As shown in Figure 6, GVF27 at a concentration of 12.5 μM was found to neutralize about 40% of LPS, whereas GVF27 25 μM completely neutralized LPS, thus supporting the hypothesis that GVF27 might act in a dose-dependent manner as a scavenger of Gram-negative bacteria LPS (Figure 6).

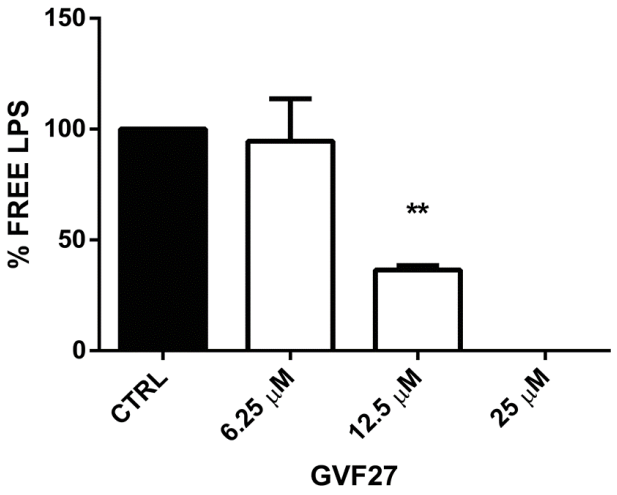

Figure 6. LPS neutralization in the presence of GVF27. Peptide at different concentrations (6.25 – 12.5 – 25 μM) was incubated with the endotoxin (0.25 units/mL) for 30 min at 37 °C and the amount of free endotoxin was quantified by LAL assay. Data represent the mean (± standard deviation, SD) of at least 3 independent experiments, each one carried out with triplicate determinations. *p<0.05, **p<0.01, or ***p< 0.001 were obtained for control *versus* treated samples.

3.2 STRUCTURAL AND FUNCTIONAL CHARACTERIZATION OF VLL-28 PEPTIDE ANTITUMOR ACTION

3.2.1 The selective antitumor action of VLL-28 peptide

The cytotoxicity of VLL-28 peptide was tested on malignant SVT2 murine fibroblasts (BALBc 3T3 cells transformed by SV40 virus). The peptide was found to be a strong inhibitor of malignant fibroblast growth, since a dose- and time-dependent inhibition of cell viability was observed (Figure 7a). Moreover, the peptide was found to be inactive toward the parental non-malignant line of 3T3 fibroblasts tested under the same experimental conditions (Figure 7b), thus indicating that VLL-28 peptide is highly selective for malignant cells. This evidence was also confirmed by morphological analyses through light microscopy of SVT2 (Figure 8a and b) and BALBc 3T3 cells (Figure 8 c and d) untreated (7a, c) or treated (7b, d) with 20 μM VLL-28 peptide. Accordingly, only in the case of SVT2 cancer cells, a severe alteration of cell morphology, together with the massive presence of cell debris, was observed. Remarkably, this peptide was also found to be effective and selective against human tumour cells, as demonstrated by MTT assays performed on transformed HEK-293 cells (Figure 7c). No toxic effects were detected, instead, on primary human renal (HRCE) cells (Figure 7d).

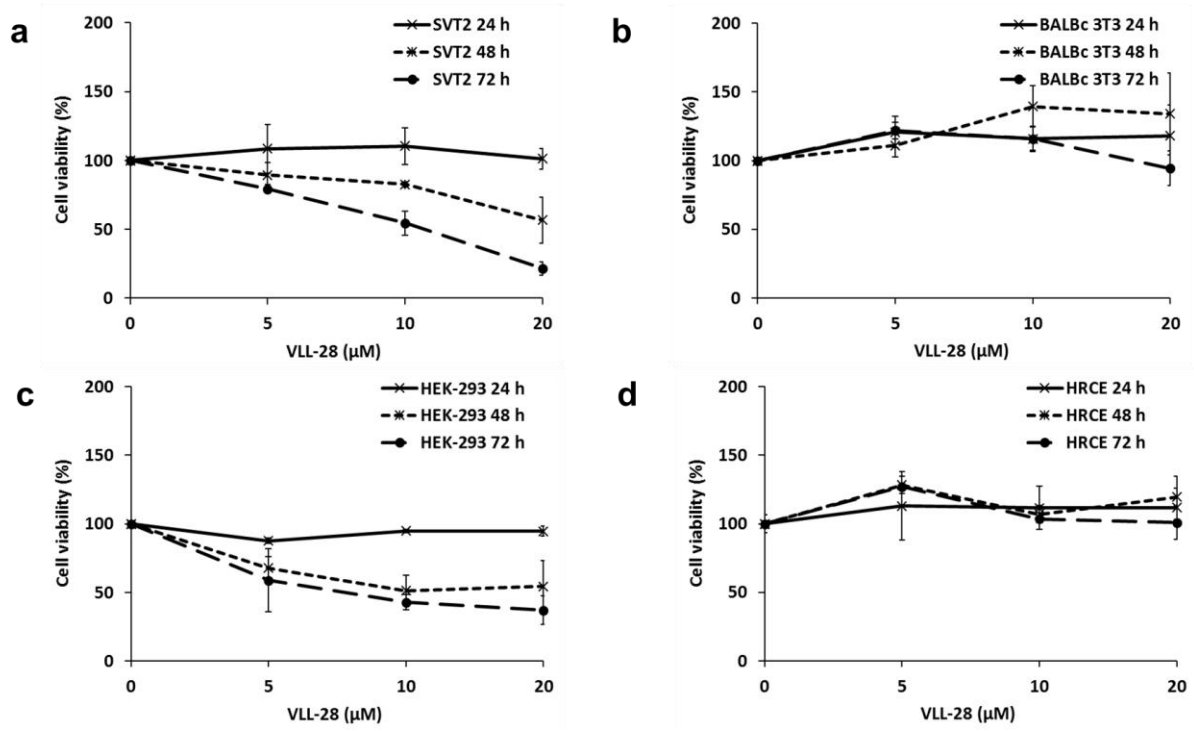

Figure 7. Effects of VLL-28 peptide on the viability of SVT2 (a), BALBc 3T3 (b), HEK-293 (c), or HRCE (d) cells. MTT assays were performed on cells treated with increasing amounts of the peptide (5, 10 and 20 µM) for different lengths of time (24, 48 and 72 h). The viability of cell samples was expressed as the percentage of MTT reduction with respect to control cells, tested under the same conditions but in the absence of the peptide. Data represent the mean (± standard deviation, SD) of at least 4 independent experiments, each one carried out with triplicate determinations. *p<0.05, **p<0.01, or ***p<0.001 were obtained for control *versus* treated samples in the case of SVT2 cells treated with VLL-28 peptide for 48 and 72 h.

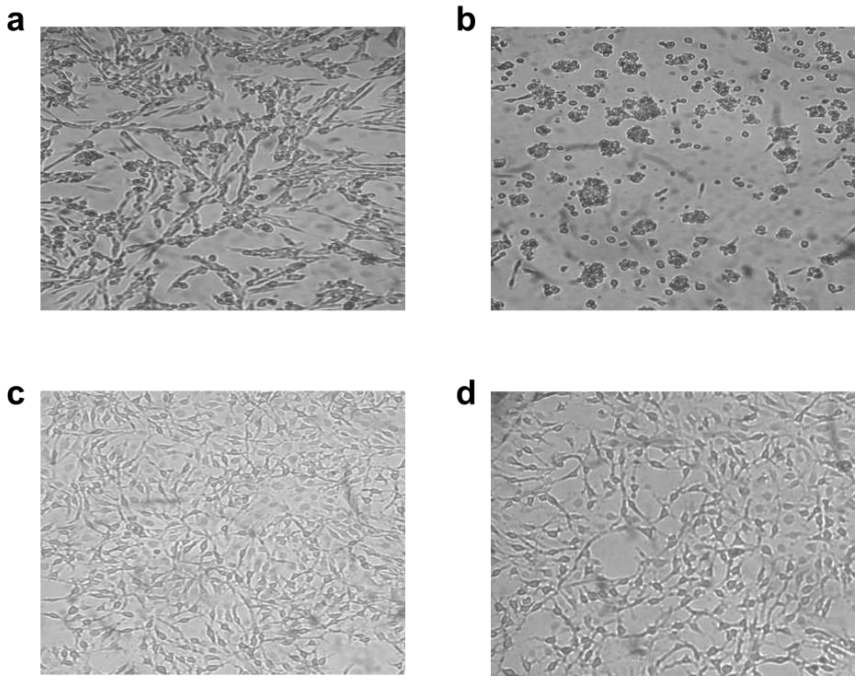

Figure 8. Morphological analyses of SVT2 (a, b) and Balbc 3T3 (c, d) cells untreated (a, c) or treated (b, d) with 20 μM VLL-28 peptide for 72 h. All images were acquired at the same magnification.

3.2.2 Cell death pathway activated by cell treatment with VLL-28 peptide

To elucidate cell death pathways selectively activated by cell treatment with VLL-28 peptide, we performed western blot analyses by using antibodies specifically recognizing pro-caspase 3 and p62 proteins. The activation of procaspase-3 to caspase-3 is a key event in the apoptotic execution phase, since caspase-3 is considered the most important of the executioner caspases and is activated by any of the initiator caspases (caspase-8, caspase-9, or caspase-10) [32]. p62, instead, is generally used as a marker to study autophagic flux, since it accumulates when autophagy is inhibited, whereas p62 decreased levels can be observed when autophagy is induced [33].

To get insight into cell death pathways activated by cell treatment with VLL-28, western blot analyses were performed (Figure 9 a and b). In the case of SVT2 cells, it was observed a significant increase of p62 levels upon 6 h treatment with 20 μM VLL-28 (Figure 9a), indicative of a stress leading to cell death with a consequent block of autophagy flux [34]. Accordingly, procaspase-3 levels were found to be lower than in control cells upon 6 and 12 h treatment with 20 μM VLL-28 (Figure 9a), indicating a significant (about 30%) activation of procaspase-3 to caspase-3 associated to apoptosis induction. This activation appears even stronger (about 50%) upon 24 h treatment (Figure 9a), and is associated to a significant decrease of p62 levels (Figure 9a), in agreement with a time-dependent activation of apoptotic cell pathway.

In the case of non-malignant BALBc 3T3 cells, instead, no significant effects on procaspase-3 and p62 levels were observed upon cell treatment with 20 μM VLL-28 peptide for different time intervals (6, 12 and 24 h) (Figure 9b). In agreement with the results reported above, this indicates that these cells are not susceptible to VLL-28 peptide toxic effects. In conclusion, experimental data indicate that VLL-28 exerts its selective antitumor action through a time-dependent activation of apoptotic cell

pathway, as demonstrated by the progressive maturation of procaspase-3 to the active caspase-3.

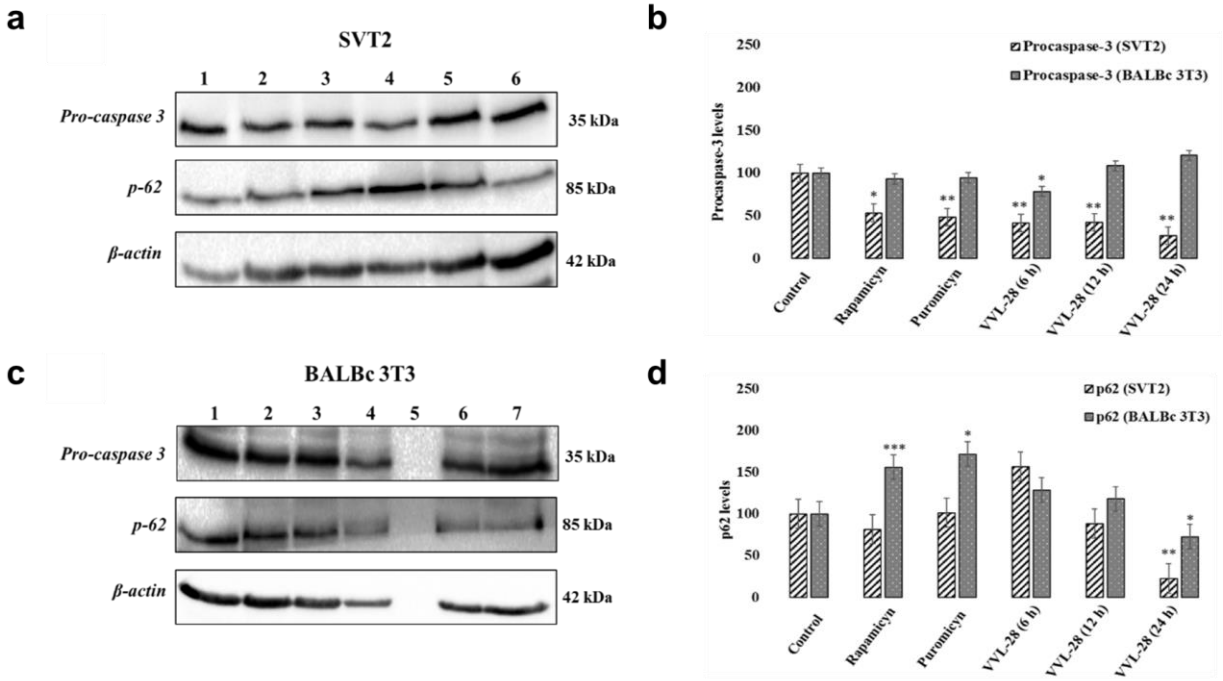

Figure 9. Analysis of cell death pathways activated by the treatment of SVT2 and BALBc 3T3 cells with 20 μM VLL-28 peptide. In a and c, lane 1, total proteins extracted from untreated cells; lane 2, total proteins extracted from cells treated with rapamycin; lane 3, total proteins extracted from cells treated with puromycin; lane 4, total proteins extracted from cells treated with the peptide for 6 h; lane 5, total proteins extracted from cells treated with the peptide for 12 h; lane 6, total proteins extracted from cells treated with the peptide for 24 h. Western blots were performed by using antibodies directed towards procaspase-3, p62, and endogenous β-actin used as an internal standard. The densitometric analyses of protein bands, specifically recognized by anti-procaspase-3 and anti-p62 antibodies, are reported in b and d, respectively, where data represent the mean (± standard deviation, SD) of 3 independent experiments. *$p<0.05$, **$p<0.01$, or ***$p<0.001$ were obtained for control *versus* treated samples.

3.2.3 VLL-28 Far-UV CD analyses in the presence of eukaryotic cells

VLL-28 CD spectra were registered in the presence of either BALBc 3T3 or SVT2 cells (Figure 10). We found that, in the presence of BALBc 3T3 cells, VLL-28 peptide appears structured over time, and a prevalence of α-helical structure is observed upon 1 h incubation (Figure 10a). Indeed, the spectrum shows two minima centred at around 208 and 222 nm, typical of an α-helical structure. Differently, when VLL-28 peptide was analysed in the presence of SVT2 intact cells, a decrease of CD signal was observed, which might be indicative of a fast internalization of VLL-28 peptide into SVT2 target cells, occurring already after 10 min incubation (Figure 10b).

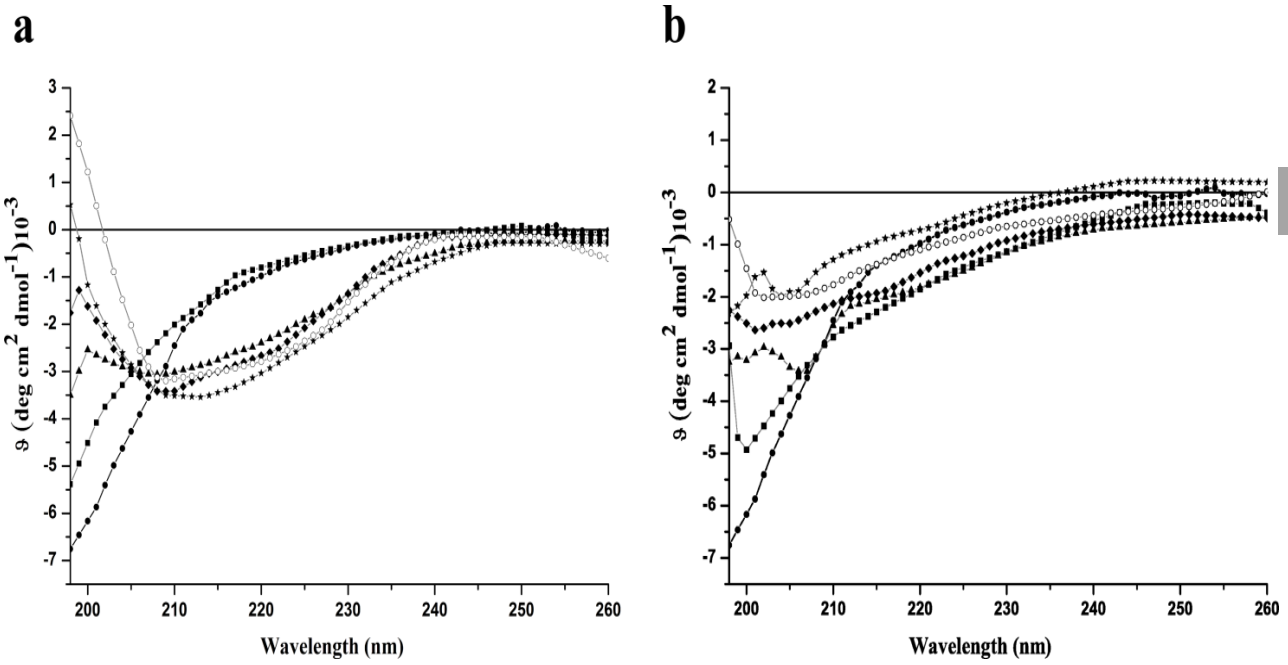

Figure 10. Far UV CD spectra of VLL-28 peptide (●) recorded in the presence of BALBc 3T3 (a) or SVT2 cells (b) after incubation for 0 (■), 10 (▲), 30 (♦), 60 (*) min and 24 h (○).

3.2.4 NMR conformational analysis of VLL-28 peptide

In order to analyse VLL-28 interaction with intact cells and isolated cell membranes, we performed NMR studies. As first, we carried out a conformational analysis of the peptide in the absence and in the presence of TFE (Figure 11 and 12), and found that VLL-28 does not adopt a well-defined conformation in the absence of TFE, as indicated by sharp and low-dispersed resonances in both the amide/aromatic and the aliphatic regions (Figure 12a). On the other hand, in the presence of 25%TFE, resonances of the amide, aromatic and aliphatic protons resulted more dispersed (Figure 11b). In particular, the HN indolic of the tryptophan, clearly distinguishable at 10.14 ppm in the absence of TFE, exhibited up-field shift at 9.94 ppm upon addition of TFE, suggesting a more buried side chain. Moreover, 2D [^{1}H, ^{1}H] NOESY spectrum of VLL-28 peptide was found to contain a significant higher number of cross-peaks with respect to that recorded in the absence of TFE, indicating a more ordered conformation (Figure 12). By using a combination of TOCSY and NOESY spectra, accordingly to the standard procedures, an almost complete assignment of proton resonances of VLL-28 peptide could be achieved in the presence of TFE.

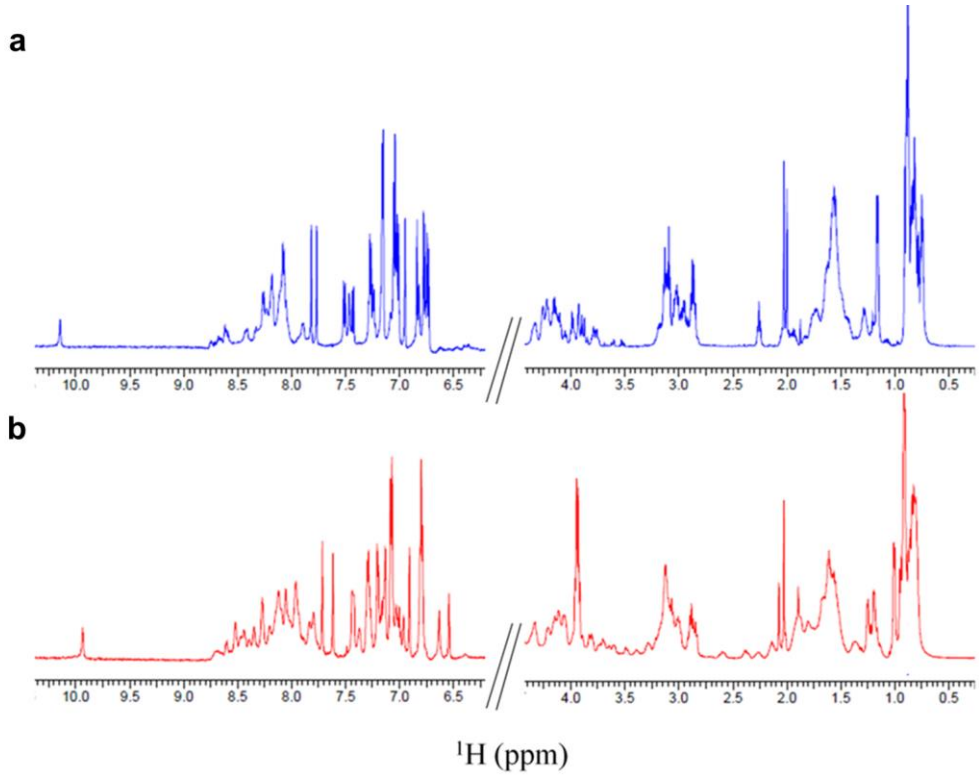

Figure 11. Expansions of the HN/aromatic (left) and the aliphatic (right) regions of the 1D 1H NMR spectrum of VLL-28 in phosphate buffer pH 7 at 298K in the absence (blue, a) and presence (red, b) of 25% TFE. Different vertical scales are used in the HN/aromatic and the aliphatic regions.

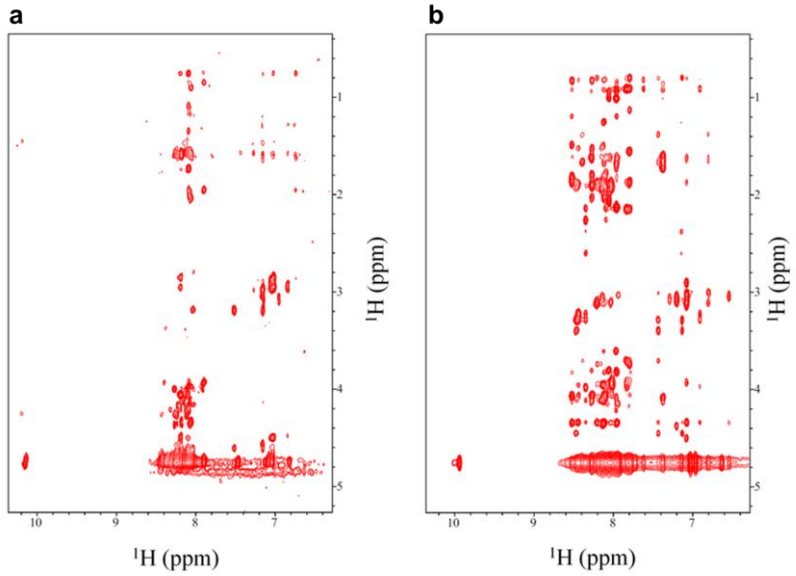

Figure 12. Expansions of the HN-aliphatic and aromatic-aliphatic correlation region of the 2D [1H, 1H] NOESY spectra of VLL-28 peptide in PBS at 298K in the absence (a) and in the presence (b) of 25% TFE.

To assess the secondary structure of VLL-28 peptide in 25% TFE, the Hα chemical shift deviations from random coil values ($\Delta\delta H_\alpha$) and the NOE patterns were analysed.

Interestingly, two regions encompassing residues V^{37}- R^{48} and V^{50}-S^{59} showed the deviations larger than the average $\Delta\delta H_\alpha$ (average= -0.31 ppm), suggesting that the peptide assumes two consecutive helices separated from G^{49} (Figure 13a). Accordingly, H_N-H_N, $H_{\alpha i}$-H_{Ni+3} and $H_{\alpha i}$-$H_{\beta i+3}$ NOEs characteristic of α-helical conformation, not present in the absence of TFE, were observed starting from residues V^{37} to S^{59} (Figure 13b and c).

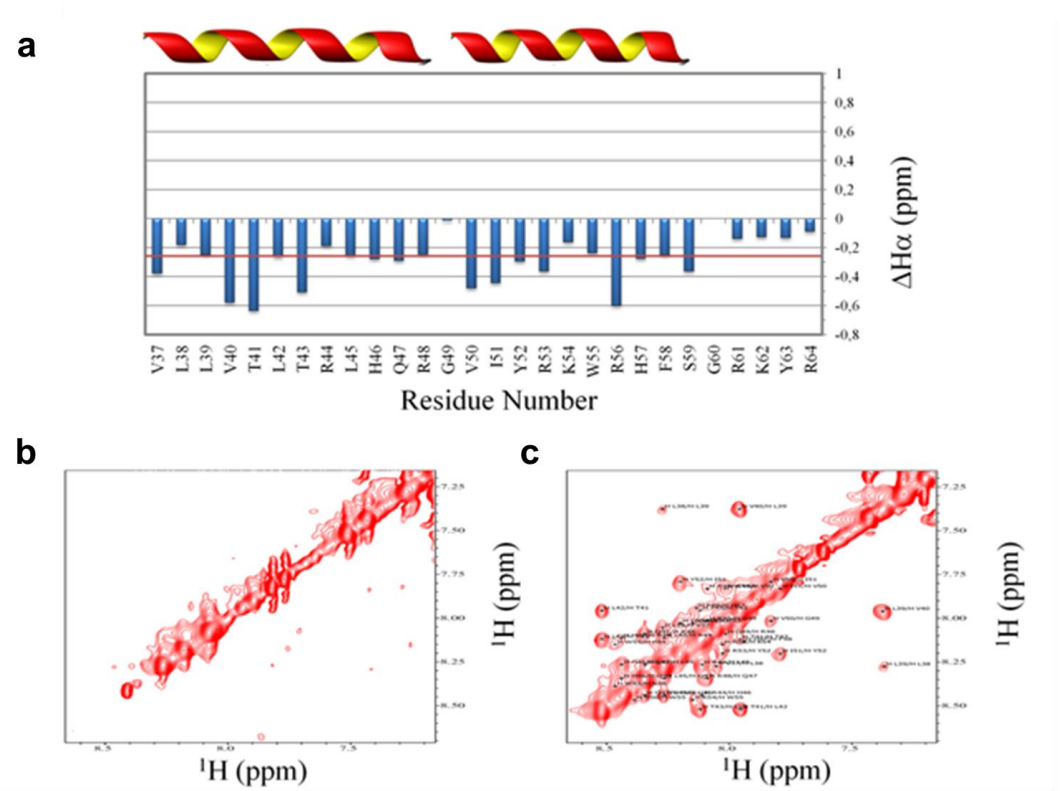

Figure 13. Chemical shift deviation from random coil values of Δα backbone atoms (ΔHα) plotted as a function of residue number (a). Two segments with α-helical conformation, encompassing residues V37-R58 and V50-S59, were suggested from the ΔHαs and are indicated above the plot. In b and c: expansions of the H_N-H_N correlation region of the 2D [^{1}H, ^{1}H] NOESY spectra of VLL-28 peptide in PBS at 298K in the absence and in the presence of 25% TFE, respectively. HN_i-HN_{i+1} cross-peaks, selectively observed in (c), are labeled.

3.2.5 Analysis of VLL-28 binding to tumor and normal cell membranes by NMR studies

In order to gain insight into the mechanism of antitumor action of VLL-28 peptide, we performed NMR saturation transfer difference (STD) binding analyses of the peptide in the presence of intact SVT2 and BALBc 3T3 cells, as well as in the presence of isolated cell membranes. Attempts to study the interaction of the peptide with intact cells failed (data not shown) because the proton resonances in the ^{1}H NMR spectra of VLL-28 peptide vanished in the presence of both cell lines.

Recently, it has been proposed the use of native cell membranes to overcome peptide cell internalization issues in “on-cell” NMR binding experiments [12]. This approach provided several improvements in the quality of the ^{1}H and STD spectra with respect to those acquired in the presence of intact cells. First of all, by using this approach, ^{1}H NMR signals of the peptide appear sharper and better resolved.

Moreover, STD signals are significantly stronger and background signals appear much weaker in both the ^{1}H and the STD spectra. Based on this, we carried out STD NMR experiments of VLL-28 peptide in the presence of isolated cell membranes.
Interestingly, ^{1}H NMR peptide signals resulted well visible in the presence of both SVT2 and BALBc 3T3 cell membranes (Figure 12), what allowed to perform STD NMR binding experiments. In particular, we evaluated the binding capability of VLL-28 peptide to the two main components of cell membranes, *i.e.* proteins and lipids. To do this, we acquired STD spectra at two different saturation frequencies, one to selectively saturate proteins (0.2 ppm) and the other one to saturate lipids (5.2 ppm). Remarkably, ^{1}H STD spectra analyses revealed that VLL-28 peptide receives a detectable saturation transfer in the presence of cell membranes only when lipids are saturated (Figure 14). This effect, found to be negligible in the absence of cell membranes (Figure 14b), indicates the ability of VLL-28 peptide to bind to the lipid component of cell membranes. This finding is in agreement with previous results indicating that the peptide is able to interact with lipids mimicking bacterial membranes [5]. It is worth noting that different patterns of STD signals were obtained in the presence of BALBc 3T3 and SVT2 cell membranes (Figure 14). In particular, a higher number of STD signals, with stronger intensities, were observed in the presence of BALBc 3T3 cell membranes compared to those observed in the presence of SVT2 cell membranes. This might be due to a different mechanism of peptide interaction with membranes isolated from different cell lines. Accordingly, Far-UV CD analyses suggest that the peptide is selectively internalized into SVT2 tumor cells and not into BALBc 3T3 cells.

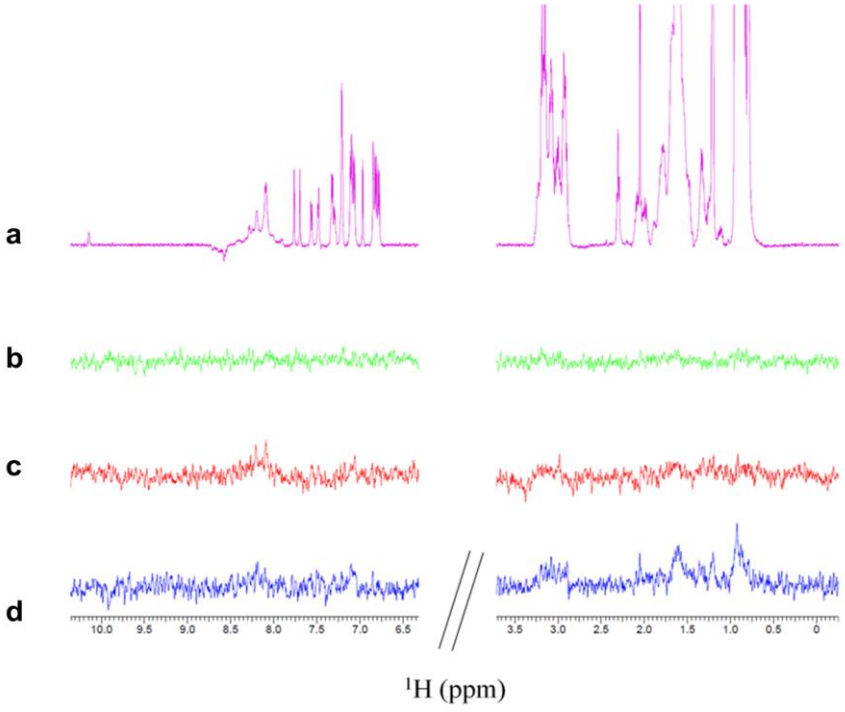

Figure 14. Reference ^{1}H (a) and STD NMR (b) spectra of VLL-28 in the absence and in the presence of SVT2 (c) or BALBc 3T3 (d) cell membranes.

3.8 Definition of membrane interaction sites of VLL-28 peptide

To define membrane interaction sites of VLL-28 peptide, we performed proton assignments in the presence of cell membranes. As a control, data obtained for the

peptide in TFE were used. Because of spectral overlaps, several ambiguities were obtained. Nonetheless, almost all the aromatic protons and some aliphatic protons could be assigned unambiguously. In Table 2, the possible proton assignments of the STD signals plotted in figure 15a are reported. Interestingly, in the HN/aromatic region of the STD spectrum, besides two non-assigned HN signals at 8.19 and 8.10 ppm, several aromatic protons were found to be saturated, especially in the presence of BALBc 3T3 membranes, suggesting that peptide binding to membranes is mediated by hydrophobic interactions. In particular, Y52 and W55 residues seem to be involved in the interaction in the case of both cell lines, whereas F58 is saturated only in the presence of BALBc 3T3 membranes. Moreover, it has to be noticed that the aromatic side chains of Hε1, H46 and H57 at 7.78 and 7.71 ppm are clearly not saturated in the case of both cell membranes, and the STD signal at 7.49 ppm is attributed to the overlapped Hε22 Q47 and Hz2 W55 protons. Based on this, it is very likely that the STD signal at 6.85 ppm, corresponding to the overlapped Hδ2 H57 and HƐ21 Q47, is due to the latter proton. In the aliphatic region, several signals overlap allows the unambiguous identification of only four protons: Hα G49, Hβ3 Y52, Hγ12 I51 and Hγ2 V50. Nonetheless, STD signals from 3.20 to 2.98 ppm show the involvement of the side-chains of Arg and Lys residues in the interaction with membrane. Methyl group of Leu, Val and Thr, localized in the N-terminal region, seem to be involved as well. Overall, these data indicate that the interaction of VLL-28 peptide with cell membranes is mediated by its N-terminal region, as well as by its central region (V37-F58) (Figure 15). It has to be highlighted that both peptide regions assume an α-helical conformation in the presence of TFE. Moreover, as expected, the binding seems to be mainly mediated by aromatic and basic amino acid residues.

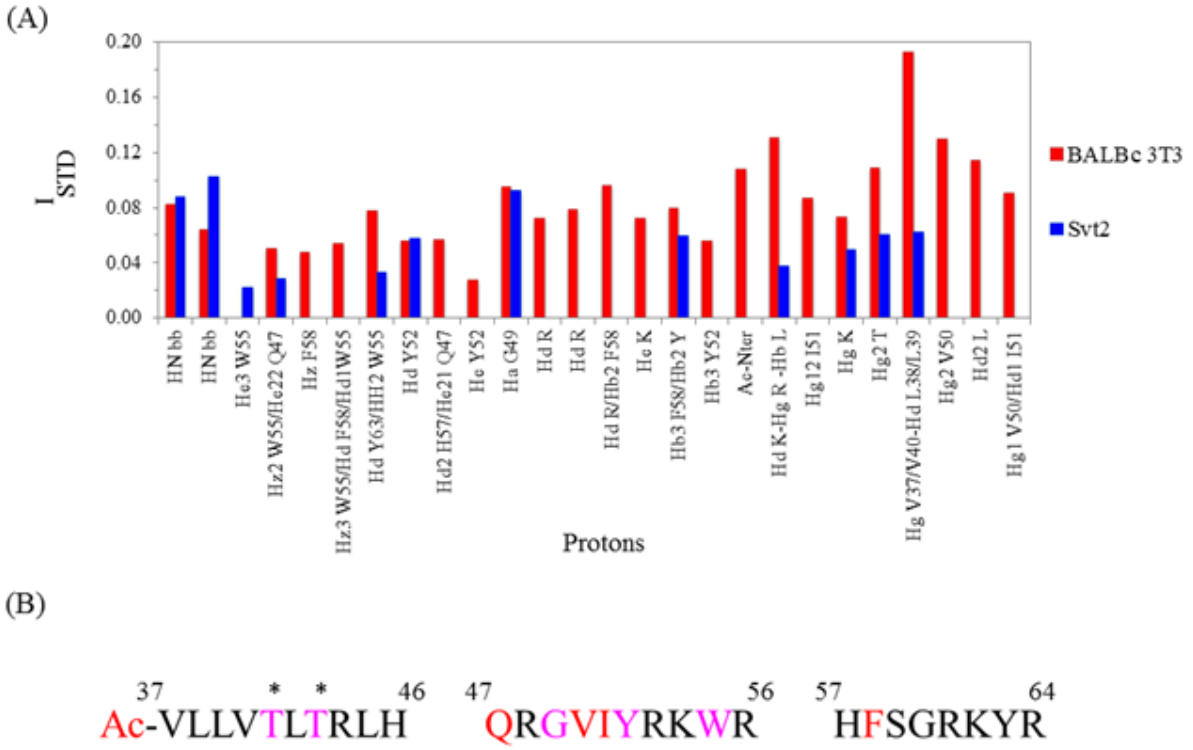

Figure 15. (a) Bar graphs of STD signal intensities (I_{STD}) for the VLL-28 HN/aromatic and aliphatic protons receiving saturation transfer in the presence of BALBc 3T3 (red bars) and SVT2 (blue bars) cells. In the x-axis label, HN_{bb} = not assigned backbone amide protons, R = R44/R48/R53/R61/R64; K = K54/K64; Y = Y52/Y63; L = L38/L39/L45; T = T41/T43. (B) The VLL-28 sequence is reported. VLL-28 residues showing STD effect in the presence of both cell membranes are highlighted in magenta, whereas those affected only in the presence of BALBc 3T3 cells are reported in red. Asterisks indicate that, due to overlapped proton resonances, one or both the threonine residues are possibly involved in the interaction with BALBc 3T3 and SVT2 cell membranes. Residues that are not involved in the binding or that could not be identified unambiguously are indicated in black.

Chemicalshift (ppm)	Assignment	VLL-28 STD signals in cell membranes	
		BALBc 3T3	Svt2
8.19	H^N	++	++
8.10	H^N	++	++
7.56	Hε3 W55	-	+
7.49	Hζ2 W55/Hε22 Q47	++	+
7.31	Hζ F58	+	-
7.21	Hζ3 W55/Hδ F58/Hδ1W55	++	-
7.10	Hδ Y63/HH2 W55	++	+
7.06	Hδ Y52	++	++
6.85	Hδ2 H57/Hε21 Q47	++	-
6.78	Hε Y52	+	-
3.98	Hα G49	++	++
3.20	Hδ Rx	++	-
3.14	Hδ Rx	++	-
3.08	Hδ Rx/Hβ2 F58	++	-
3.05	Hε Kx	++	-
2.98	Hβ3 F58/Hβ2 Yx	++	++
2.90	Hβ3 Y52	++	-
2.05	Ac-Nter	++	-
1.60	Hδ Kx-Hγ Rx -Hβ Lx	++	+
1.36	Hγ12 I51	++	-
1.32	Hγ Kx	++	++
1.20	Hγ2 Tx	++	++
0.93	Hγ V37/V40-Hδ L38/L39	++	++
0.88	Hγ2 V50	++	-
0.86	Hδ2 Lx	++	-
0.79	Hγ1 V50/Hδ1 I51	++	-

Note: Rx= R44/R48/R53/R61/R64; Kx= K54/K64; Yx= Y52/Y63; Lx= L38/L39/L45; Tx= T41/T43

Table 2. VLL-28 residues playing a key role in the binding to BALBc 3T3 and SVT2 cell membranes.

4. Discussion

Host defense peptides (HDPs) are important modulators able to prevent microbial colonization and tissue damage in both mammalian and non-mammalian systems [35]. HDPs beneficial effects may encompass direct antimicrobial activity, binding to and inactivation of endotoxins, such as LPS or LTA, with a consequent reduction of detrimental pro-inflammatory response, as well as direct effects on cell behaviors, such as enhancement of migration and proliferation.

In this Chapter, two novel HDPs identified by using a bioinformatics tool recently developed by our research group have been described. One is the first HDP identified in an archaeal protein, *i.e.* the transcription factor Stf76 encoded by the hybrid plasmid-virus pSSVx from *Sulfolobus islandicus*, here named VLL-28. The

second is a HDP identified in human 11-hydroxysteroid dehydrogenase-1 β-like, here named GVF27.
We demonstrated that GVF27 peptide exhibits very interesting immune-modulating activities. As first, we verified by Far-UV CD analyses that GVF27 is unstructured in aqueous buffer, whereas it assumes an α-helical conformation in the presence of TFE. Further CD analyses together with dynamic light scattering measurements have also highlighted that the peptide is able to interact with both LPS and LTA, thus suggesting that it can bind to microbial surfaces *via* these wall determinants. The ability of GVF27 to interact with LPS has been also confirmed by different experimental approaches, and it has been also demonstrated that the peptide exerts anti-inflammatory activities. Indeed, GVF27 was found to strongly down-regulate NO release and IL-6 production in murine macrophages under LPS stimulation. This effect was obtained by co-incubating the cells with the endotoxin in the presence of the peptide. Moreover, it is worth noting that in murine macrophages pre-treated with GVF27 and then incubated with LPS, a decrease of both NO and IL-6 release was still detectable, thus suggesting the ability of the peptide to exert a protective effect. Based on these observations, at least three different mechanisms might be envisaged to explain GVF27 immune-modulatory properties. Firstly, GVF27 might modulate cell response to pro-inflammatory mediators by acting as an endotoxin scavenger during the initial steps of infection. In this case, the peptide might bind to and neutralize the endotoxin directly. Secondly, GVF27 might mitigate inflammatory dysfunction by interacting with membrane receptors, *i.e.* CD14, with a consequent down-regulation of several pro-inflammatory pathways. Thirdly, endogenous GVF27, upon internalization into paracrine cells, might contribute to the attenuation of the inflammatory response by interacting with intracellular targets. All these observations open an interesting scenario, since GVF27 is a “hidden” peptide in a protein precursor, that has not been yet characterized. Based on our results, it is tempting to speculate that the protein is constitutively present under physiological conditions and able to release, upon a proteolytic event activated by pathogen invasion, a fragment containing GVF27 peptide.
The second part of this Chapter focuses on VLL-28 peptide, which was firstly identified as an antimicrobial peptide. Here, VLL-28 was found to be also endowed with selective antitumor activity. It is well known that the outer surface of cancer cell membranes is generally more negatively charged than that of normal cells, although not as anionic as in bacteria. DLS and NMR data clearly show that VLL-28 interacts with cell membranes of both malignant and not malignant eukaryotic cell lines. The binding has been found to be mainly mediated by aromatic and basic residues in the case of both types of cell membranes, although with slight differences. Nevertheless, CD analyses suggest that VLL-28 peptide might be selectively internalized into tumor cells, a key element to explain peptide selective antitumor activity. Based on this, cell membrane of tumor cells might not be the main target of peptide antitumor action and probably intracellular targets are involved in its mechanism of action. It is also important to highlight that Archaea have been so far considered as source of biotechnologically relevant enzymes, but, to the best of our knowledge, no ACPs have been so far isolated from organisms belonging to this kingdom. Hence, these data represent the first evidence that archaeal microorganisms could bear also an unexplored repertoire of such kind of molecules exerting a trans-kingdom action.

5. References

1) P. Wang, Prediction of antimicrobial peptides based on sequence alignment and feature selection methods, PLoS One. Apr 13;6(4) (2011) e18476.

2) R. Sukhija, Enhanced 11beta-hydroxysteroid dehydrogenase activity, the metabolic syndrome, and systemic hypertension, Am J Cardiol. 98(4) (2016) 544-8.

3) Y. Kallberg, Short-chain dehydrogenases/reductases (SDRs), Eur J Biochem. Sep;269(18) (2002) 4409-17.

4) C. Huang, Isolation and characterization of novel human short-chain dehydrogenase/reductase SCDR10B which is highly expressed in the brain and acts as hydroxysteroid dehydrogenase, Acta Biochim Pol. 56(2) (2009) 279-89.

5) E. Notomista, The identification of a novel Sulfolobus islandicus CAMP-like peptide points to archaeal microorganisms as cell factories for the production of antimicrobial molecules, Microb. Cell Fact. 14 (2015) 126.

6) Diana Gaspar, Castanho.From antimicrobial to anticancer peptides. A review. Frontiers in Microbiology (2013) doi:10.3389/fmicb.2013.00294.

7) Mader, J.S., Cationic antimicrobial peptides as novel cytotoxic agents for cancer treatment. Expert Opin Investig Drugs. Aug; 15(8):933-46.

8) Schweizer, F., Cationic amphiphilic peptides with cancer-selective toxicity. Eur J Pharmacol. (2009) 625(1-3):190-4.

9) Rérole AL, Hsp70: anti-apoptotic and tumorigenic protein. Methods Mol Biol. (2011) 787:205-30.

10) Kuriyama I, Inhibitory effect of novel somatostatin peptide analogues on human cancer cell growth based on the selective inhibition of DNA polymerase β. Bioorg Med Chem. (2013) Jan 15;21(2):403-11.

11) A. Arciello, Insights into the fate of the N-terminal amyloidogenic polypeptide of ApoA-I in cultured target cells, J. Cell Mol. Med. 15 (2011) 2652–2663.

12) Farina B., A Combined NMR and Computational Approach to Determine the RGDechi-hCit-αv β3 Integrin Recognition Mode in Isolated Cell Membranes. Chemistry. (2016) 11;22(2):681-93.

13) S. Correale, A biophysical characterization of the folded domains of KCTD12: insights into interaction with the GABAB2 receptor. J Mol Recognit.;26(10) (2013) 488-95.

14) M. Leone, Solution structure and backbone dynamics of the K18G/R82E Alicyclobacillus acidocaldarius thioredoxin mutant: a molecular analysis of its reduced thermal stability, Biochemistry. 43(20) (2004) 6043-58.

15) K.H. Park, Cell specificity, anti-inflammatory activity, and plausible bactericidal mechanism of designed Trp-rich model antimicrobial peptides, Biochim Biophys Acta. 1788(5) (2009) 1193-203.

16) Braunschweiler L, Applications of 2D NMR Spectroscopy to Carbohydrates, J Magn Reson. (1983) 53:521–528.

17) Bax A., Introduction to Nuclear Magnetic Resonance, J Magn Reson. (1985) 65:355–360.

18) Rance M., Improved spectral resolution in cosy 1H NMR spectra of proteins via double quantum filtering, Biochem Biophys Res Commun. (1983) 117(2):479–485.

19) Kumar A., An NMR Study on the Conformation of Substance P in Acidic Bicelles, Biochemical and Biophysical Research Communications. (1980) 32, Issue 10, 3702-3706.

20) T. L. Hwang, Efficient multiple-solvent suppression for the study of the interactions of organic solvents with biomolecules, J. Magn. Reson. Ser. A (1995), 112, 275–279.

21) C. Dalvit, Efficient multiple-solvent suppression for the study of the interactions of organic solvents with biomolecules, J. Biomol. NMR (1998), 11, 437–444.

22) R. L. J. Keller, The Computer Aided Resonance Assignment Tutorial, Cantina Verlag, Goldau, (2004).

23) D. Pletzer, Hancock, Anti-biofilm peptides as a new weapon in antimicrobial warfare, Curr Opin Microbiol. 33 (2016) 35-40.

24) A.I. Herrera, Membrane Interacting Peptides: A Review, Curr Protein Pept Sci. 17(8) (2016) 827-841.

25) D.S. Wishart, Chemical shifts as a tool for structure determination, Methods Enzymol. 239 (1994) 363-92.

26) P. Güntert, Torsion angle dynamics for NMR structure calculation with the new program DYANA, J. Mol. Biol. 273 (1997) 283–298.

27) M.M. Domingues, Biophysical characterization of polymyxin B interaction with LPS aggregates and membrane model systems, Biopolymers. (2012) 98(4) 338-44.

28) L. Heinbockel, Mechanism of Hbγ-35-induced an increase in the activation of the human immune system by endotoxins, Innate Immun. Apr;21(3) (2015) 305-13.
29) M. Hemshekhar, Functions of Cationic Host Defense Peptides in Immunity, Pharmaceuticals (Basel). Jul 4 (2016) 9(3).
30) T.J. Guzik, Nitric oxide and superoxide in inflammation and immune regulation, J Physiol Pharmacol. 54(4) (2003) 469-87.
31) C.V. Suschek, The role of iNOS in chronic inflammatory processes in vivo: is it damage-promoting, protective, or active at all? Curr Mol Med. (2003) 4(7) 763-75.
32) Elmore S., Apoptosis: a review of programmed cell death. Toxicol Pathol. (2007) 35, 495-516.
33) Bjørkøy, G., Monitoring autophagic degradation of p62/SQSTM1. Methods Enzymol. (2009) 452, 181-197.
34) González-Rodríguez A., Impaired autophagic flux is associated with increased endoplasmic reticulum stress during the development of NAFLD. Cell Death and Disease (2014) 5, e1179.
35) J. Scheller, The pro- and anti-inflammatory properties of the cytokine interleukin-6, Biochim Biophys Acta. (2011) 1813(5) 878-88.

CHAPTER 5

General discussion and concluding remarks

Rosa Gaglione

Department of Chemical Sciences, PhD in Biotechnology

University of Naples "Federico II", Napoli, Italy

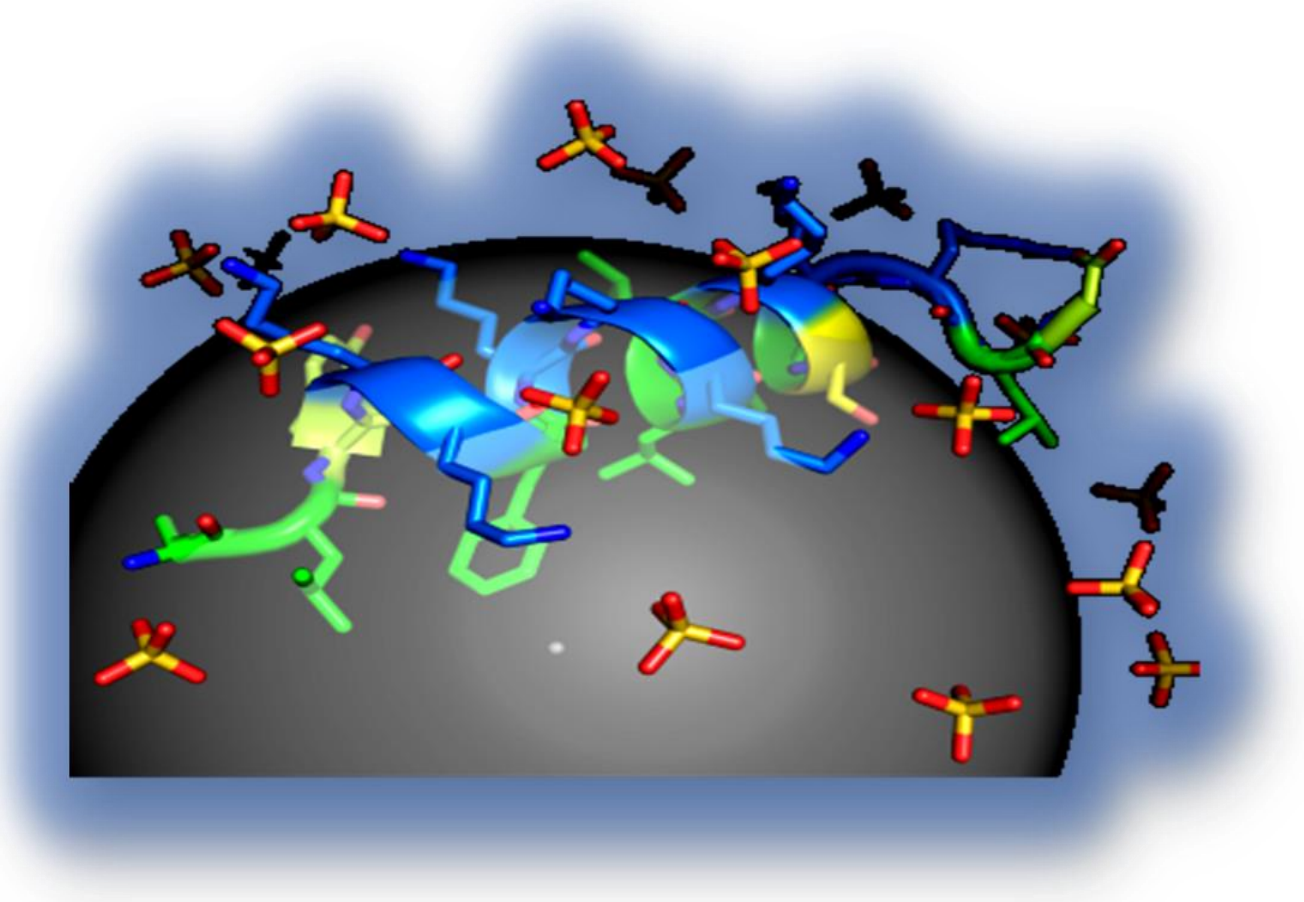

Increasing resistance of bacteria to antibiotics is one of the biggest problems facing healthcare in the 21st century [1, 2]. Important factors behind growing resistance are over-and misuse of antibiotics, including the massive use of antibiotic growth promoters in the livestock industry [3,4]. Therefore, multiple countries have restricted the use of antibiotics for food producing animals [5]. As a consequence, scientists in both the human and veterinary fields are busily investigating alternatives to conventional antibiotics [6, 7].

Host Defense Peptides (HDPs) are believed to be promising alternatives to conventional antibiotics. These highly diverse, short and cationic peptides are an essential part of the innate immune system [8]. In vertebrates, the two main classes of HDPs are cathelicidins and defensins. The broad-spectrum antimicrobial activity, as well as the multiple immunomodulatory functions of HDPs, are important features in their development as anti-infectious [9,10].

It should be emphasized that a wide variety of human proteins, whose primary function is not necessarily related to host defense, contain HDPs hidden inside their sequences [11,12]. Extensive efforts have been paid to the purification of such endogenous bioactive peptides to identify new regulatory mechanisms and the flow of signalling mechanisms, including peptide synthesis, maturation, secretion, and degradation. For instance, mRNAs encoding peptidergic factors are translated into biologically inactive precursor proteins, which are transported into the endoplasmic reticulum and processed by various enzymes, including signal peptidases and prohormone convertases, during the transport from endoplasmic reticulum to secretary vesicles via trans-Golgi networks (Figure 1) [13].

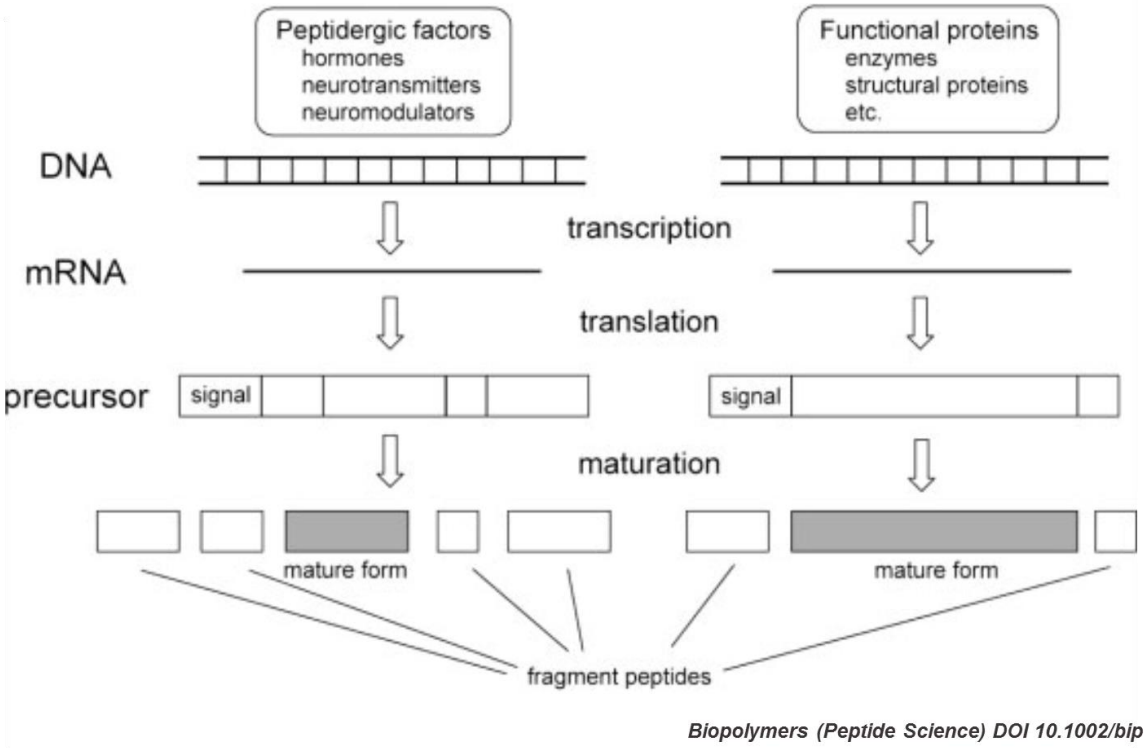

Figure 1. Schematic representation of maturation processes converting inactive precursors of peptidergic factors into functional proteins.

Therefore, it is expected that a large number of unidentified functional peptides can be produced from precursor proteins of peptidergic factors. Furthermore, many fragment peptides may be produced during maturation or degradation processes of functional proteins (such as mitochondrial enzymes and other regulatory proteins). Such peptides might be endowed with several biological activities distinct from those of their parental proteins. These functional cryptic peptides that are hidden in protein precursors are often named ‘‘cryptides’’ [14,15]. Since neutrophils are leukocytes that play central roles in innate defense systems, due to their migration from blood stream to tissue injury sites upon stimulation by various chemo-attractants [16], the presence of unidentified factors that induce immediate migration and activation of neutrophils is expected. Nobuhiko Ueki et al. isolated neutrophil-activating peptidergic factors, such as mitocryptide-1 and -2, that indeed induce immediate migration and activation of neutrophils. Interestingly, during the purification of these two peptides, they isolated further peptide containing fractions able to activate neutrophils [17]. In addition to functional peptides hidden in mammalian proteins, bioactive peptides may be hidden in proteins of many other organisms although they may not be involved in the physiological regulations in mammals. Such peptides are now also actively searched for in proteins of plants and microorganisms to facilitate the developments of drugs and food supplements. These widespread screenings are encouraged by the recent rapid developments in experimental techniques for purification, identification, and synthesis (multiple, simultaneous synthesis, in particular). Smith and his coworkers named ‘‘cryptome’’ the comprehensive screening and identification of hidden peptide sequences with biological activities; they also searched for bioactive peptides produced by enzymatic digestion of various proteins. Yoshikawa and his coworkers isolated ‘‘soymetide’’, a peptide derived from soybean b-conglycinin by tryptic digestion promotingf phagocytosis of neutrophils.

In addition to functional peptides hidden in mammalian proteins, bioactive peptides may be hidden in proteins of many other organisms. Smith and his coworkers named ‘‘cryptome’’ the panel of bioactive peptides hidden in protein precursors and released by maturation processes and hydrolytic events. Recently, the number of databases (genome, cDNA, and protein sequences) collecting cryptic peptides is growing fast and many different species are widely covered. In this scenario, the improvement of prediction technologies is expected to greatly increase the number of identified functional cryptic bioactive peptides, thus greatly contributing to the development of novel drugs and food supplements/nutrients. By using the recently developed in silico method [18] to identify cryptic HDPs in protein precursors and to predict quantitatively their antibacterial activity, novel HDPs were identified within the sequence of known proteins, such as human apolipoprotein E [19], the transcription factor Stf76 from the archaeon *Sulfolobus islandicus* [20], human apolipoprotein B and human 11-hydroxysteroid dehydrogenase-1 β-like. In the latter case, further potential peptides, possibly released by human neutrophil elastase, have been predicted in the C-terminal region of the four isoforms in which GVF27 was identified. Indeed, as shown in Figure 2, these potentially active peptides are virtually superimposable to GVF27 and all have high antimicrobial scores, clearly supporting our idea that it is conceivable to look at human proteins as active reservoirs of HDPs.

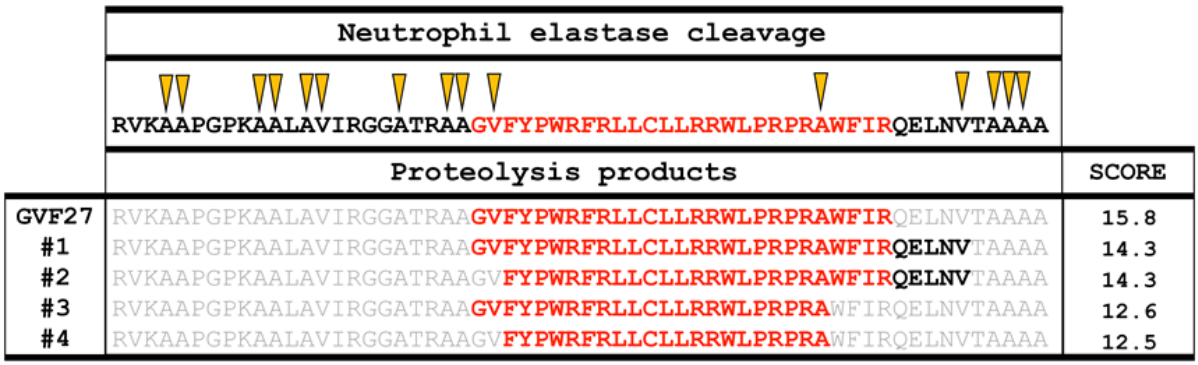

Figure 2. In silico prediction of potential peptides released by human neutrophil elastase from the C-terminal region of the four isoforms containing the GVF27 sequence. For each putative peptide (#1, #2, #3 and #4), the antimicrobial score has been calculated following the bioinformatics procedure.

The main aim of this PhD Thesis was the identification of novel HDPs by using this novel bioinformatics tool, in order to evaluate their potential as antimicrobial, anti-biofilm, anti-inflammatory and anticancer agents.
In general, HDPs isolation from natural sources is a laborious and time-consuming process, not suitable to obtain peptides in large amounts. On the other hand, chemical synthesis, although very efficient, is a complex and costly process [21]. Based on this, a cost-effective and scalable method to produce HDPs is required. Procedures to express HDPs as recombinant peptides have encountered difficulties mainly due to their cytotoxicity to the bacterial host, difficulties to scale up the production protocol and low purification yields [22-24]. To overcome these important issues, we used a novel fusion system based on onconase enzyme used as a carrier [25]. Furthermore, we designed a novel rich and cheap culture medium, and developed an auto-inducing procedure to be applied to a fermentation process. The analysis of the procedure costs highlighted that the unit cost strongly decreased with the production scale at 200, 500 and 1000 mg/batch, thus indicating that the set-up procedure is a cost-effective and competitive strategy to produce the high amounts of peptides required for basic and clinical research (**Chapter 2**).
Once optimized the expression system described in the **Chapter 2**, a broad characterization of the two ApoB derived recombinant peptides was performed (**Chapter 3**). It was observed that both peptides are endowed with a significant antimicrobial activity towards Gram-negative and Gram-positive strains. In most cases, peptide antimicrobial activity was found to be comparable to that of the positive control CATH-2, a well-known antimicrobial peptide [26]. Interestingly, ApoB derived peptides are also endowed with anti-biofilm activity. Microorganisms growing in a biofilm state are very resilient to the treatment with many antimicrobial agents. Indeed, biofilm infections are a significant problem in chronic and long-term infections, including those colonizing medical devices and implants [27]. It was found that ApoB derived peptides exert a strong effect on biofilm formation and biofilm attachment, and, even more interestingly, they strongly affect pre-formed biofilms. Furthermore, ApoB derived peptides display anti-biofilm activity even on bacterial strains not sensitive to the peptide antimicrobial activity, such as S. aureus MRSA WKZ-2, and, in the case of sensitive strains, even at peptide concentrations significantly lower than those required to directly kill planktonic cells. This is in

agreement with previous reports indicating that LL-37 peptide potently inhibits the formation of bacterial biofilms in vitro at the very low and physiologically meaningful concentration of 0.5 μg/mL, significantly lower than that required to kill or inhibit bacterial growth (64 μg/mL) [28]. Moreover, it has been reported that other specific cationic HDPs, such as 1018 peptide, are endowed with multispecies anti-biofilm activity, which has been found to be independent from their activity against planktonic bacteria [29].

It should also be emphasized that even at the highest ApoB derived peptides concentrations tested, a significant percentage of bacterial cells inside the biofilm structure appeared to be still alive. This was observed for both ApoB derived peptides and LL-37 control peptide, while it was less pronounced in the case of CATH-2 peptide. Based on this, it is tempting to speculate that successful therapeutic approaches could be designed by combining anti-biofilm peptides and conventional antibiotics ineffective on biofilm, but effective on bacterial cells entrapped into the biofilm structure.

Moreover, ApoB derived peptides were found to be endowed with anti-inflammatory activity as well as with wound healing promoting properties. We also demonstrated that these two HDPs are able to synergistically act in combination with conventional antibiotics, thus opening interesting perspectives to their future applications in combinatorial therapeutic approaches. Further experiments will allow us to elucidate the molecular mechanisms at the basis of ApoB derived peptides anti-inflammatory effects, which might include multiple aspects, such as stimulation of chemotaxis, suppression of bacterial induced pro-inflammatory cytokine production, regulation of neutrophil and epithelial cell apoptosis, modulation of cellular differentiation pathways, and promotion of angiogenesis and wound healing. As for the last aspect, in agreement with previous findings on LL-37 human peptide [30,31], we found that r(P)ApoBL peptide is able to stimulate human keratinocytes wound re-epithelialization, an evidence that opens new and interesting perspectives on future topical application of this human HDP.

In the Chapter 4, two further cryptic HDPs have been structurally and functionally characterized. The first HDP has been identified in human 11-hydroxysteroid dehydrogenase-1 β-like, while the second represents the first HDP from an archaeal protein, the transcription factor Stf76 encoded by the hybrid plasmid-virus pSSVx from *Sulfolobus islandicus*. By using a multidisciplinary approach including biochemical, cellular biology and spectroscopic techniques, a wide characterization of both peptides was performed revealing very interesting immunomodulatory and anticancer activities.

From a structural point of view, in agreement with the canonical properties of most HDPs, it was verified by CD experiments that GVF27 peptide is unstructured in aqueous buffer, whereas it tends to assume a helical conformation in the presence of TFE. Further tests have also allowed us to highlight peptide binding to both LPS and LTA, albeit in a less effective manner with the latter, thus suggesting that it can bind to the microbial surfaces via these wall determinants. The ability of GVF27 to interact with LPS has been also confirmed by different approaches, thanks to which it has been possible to show that the peptide is able to inhibit the pro-inflammatory response. Indeed, GVF27 strongly down-regulates the release of NO and the production of IL-6 both in LPS pre-treated murine macrophages cells and upon co-administration of the peptide and the endotoxin. Moreover, it is worth noting that in murine macrophages treated with GVF27 and then subjected to LPS stimulation, a decrease of both NO and IL-6 was still detectable, thus indicating tha the peptide is

also able to exert a protective effect. Finally, it seems very interesting the ability of GVF27 to attenuate LPS-induced pro-inflammatory response and its apparent ability to protect the cells by mitigating upstream the effects of infection. In both cases, it seems plausible to hypothesize for GVF27 different targets. In our opinion, at least three mechanisms could be responsible for GVF27 immune-modulatory properties. As first, GVF27 might modulate cellular response to pro-inflammatory mediators by acting as an endotoxin scavenger during initial steps of infection. In this case, the peptide could bind to and neutralize the endotoxin directly. Secondly, GVF27 might reduce inflammatory dysfunction during immune response by interacting with membrane receptors, i.e. CD14, that then would activate down regulation of different pro-inflammatory pathways. Thirdly, endogenous GVF27, or GVF27 internalized by paracrine cells, may contribute to the attenuation of the inflammatory response by interacting with intracellular targets.

VLL-28 peptide, previously identified as an HDP [32], was found to be also endowed with a selective cytotoxic activity towards both murine and human cancer cells. This makes VLL-28 a potential member of anti-cancer peptides (ACPs). In the literature, several have been reported to successfully kill tumor cells both in vitro and in vivo and also to prevent metastases formation [33-35].

However, a clear structure to function relationship analysis of these ACPs is still lacking, although it might greatly contribute to the development of novel and effective drugs. Table1 shows the primary sequence of several ACPs identified in the last years.

Peptide name	Amino acid sequence
D-peptide A	RLYLRIGRR
D-peptide B	RLRLRIGRR
D-peptide C	ALYLAIRRR
D-peptide D	RLLLRIGRR
D-K6L9	LKLLKKLLKKLLKLL
NRC-03	GRRKRKWLRRIGKGVKIIGGAALDHL
NRC-07	RWGKWFKKATHVGKHVGKAALTAYL
Gomesin	ZCRRLCYKQRCVTYCRGR
Hepcidin TH2-3	QSHLSLCRWCCNCCRSNKGC
Dermaseptin B2	GLWSKIKEVGKEAAKAAAKAAGKAALGAVSEAV
PTP7	FLGALFKALSKLL
MGA2	GIGKFLHSAKKFGKAFVGEIMNSGGKKWKMRRNQF–WVKVQRG
HNP-1	ACYCRIPACIAGERRYGTCIYQGRLWAFCC
Tachyplesin	KWCFRVCYRGICYRRCR
Temporin-1CEa	FVDLKKIANIINSIF
NK-2	KILRGVCKKIMRTFLRRISKDILTGKK
Bovine lactoferricin B6 (Lbcin B6)	RRWQWR
Cecropin CB1	KWKVFKKIEKMGRNIRNGIVKAGPKWKVFKKIEK

Table 1. Peptides with anti-cancer activity [36]

ACPs studied can target different solid and hematologic malignancies, and the Table 2 summarizes ACPs able to target solid tumors.

Peptide	Cancer cell	Experimental test	Selectivity	Anticancer activity
D-peptides A, B, C and D	Human cervix, glioma, lung, mouse myeloma, african green monkey kidney	ICL	Yes	Cell membrane disruption
D-K_6L_9	Human prostate	ICL/GEM	Yes	Necrosis via membrane depolarization
NRC-03, NRC-07	Human breast	ICL/GEM	No	Cell membrane lysis with possible pore formation in mitochondria and ROS production
MPI-1	Human cervix, prostate and hepatocellular adenocarcinoma,	GEM	Yes	Necrosis after cell membrane targeting
Polybia-MPI	Human bladder and prostate	ICL	Yes	Cell membrane disruption with probable pore formation

Table 2. Peptides targeting solid tumors [36]

Microorganisms belonging to the archaeal kingdom have been so far considered as a source of biotechnologically relevant enzymes and proteins [37-39]. To the best of our knowledge, potential ACPs have never been identified in this kingdom. Our data represent the first evidence that archaeal microorganisms could bear an unexplored repertoire of such kind of molecules exerting a trans kingdom action. The intrinsic stability to physical and chemical agents of Stf76, the parental source of VLL-28, let us to hypothesize that VLL-28 might be a promising “lead compound” to further develop novel drugs upon chemical modifications, such as introduction of D-amino acids and/or modified amide bounds, which would further increase its stability to proteases [40].
It has to be considered there are very few HDPs currently in use in the market, but many of them are progressing through clinical trials, focused on topic rather than systemic treatment because of peptides potential toxicity or immunogenicity. Here, it was shown that both ApoB derived peptides and GVF27 peptide are not toxic for eukaryotic cells, at least in the experimental conditions tested, and do not determine any hemolytic effect when tested on murine red blood cells. These observations, associated to their multifunctional properties, open interesting perspectives to their therapeutic applications. Moreover, it has to be highlighted that these peptides derive from a human protein and consequently the risk to trigger immune reactions is minimized. On the bases of obtained results, these peptides may be used either alone for topical applications or in combinations with other substances to develop suitable combinatorial therapeutic approaches, and/or in edible films to be used for food packaging and preservation. Suitable delivery systems, such as hydrogels and liposomes, could be also designed to develop novel cosmetic formulations.
In conclusion, the aims of the present PhD Thesis are centred in the main issue of deepening the comprehension of HDPs mechanism of action and structure to

function relationships, a key aspect to further understand the complex role of these intriguing peptides in the defence against infections and to identify novel application fields.

References

1) Arias, C. A. Antibiotic-resistant bugs in the 21st century-a clinical super-challenge. N. Engl. J. Med. 360, 439-443 (2009).

2) World Health Organization. Antibiotic resistance. doi: http://www.who.int/ mediacentre/factsheets/fs194/en/ (2015).

3) Marshall, B. M. Food animals and antimicrobials: impacts on human health. Clin. Microbiol. Rev. 24, 718-733 (2011).

4) Levy, S. B. Antibacterial resistance worldwide: causes, challenges and responses. Nat. Med. 10, S122-9 (2004).

5) Maron, D. F. Restrictions on antimicrobial use in food animal production: an international regulatory and economic survey. Global Health. 9, 48-8603-9-48 (2013).

6) Allen, H. K.Treatment, promotion, commotion: antibiotic alternatives in food-producing animals. Trends Microbiol. 21, 114-119 (2013).

7) Czaplewski, L. Alternatives to antibiotics-a pipeline portfolio review. Lancet Infect. Dis.15, S1473-3099 (2016).

8) Steinstraesser, L. Host defense peptides and their antimicrobial-immunomodulatory duality. Immunobiology 216, 322-333 (2011).

9) Mansour, S. C. Host defense peptides: front-line immunomodulators. Trends Immunol. 35, 443-450 (2014).

10) Narayana, J. L. Antimicrobial peptides: Possible anti-infective agents. Peptides 72, 88-94 (2015).

11) Papareddy P. C-terminal peptides of tissue factor pathway inhibitor are novel host defense molecules. J Biol Chem 285 28387–28398 (2010).

12) E. Andersson. Antimicrobial activities of heparin-binding peptides. Eur J Biochem 271 1219–1226 (2004).

13) Tooze, S. A. Secretory granule biogenesis: rafting to the SNARE. Trends Cell Biol 11, 116–122 (2001).

14) Mukai, H. In Proceedings of the 42nd Japanese Peptide Symposium; pp 207–208 (2006).

15) Rolka, K. European Peptide Society: Gdansk, Poland.

16) Baggiolini, M. Interleukin-8 and related chemotactic cytokines--CXC and CC chemokines. Adv Immunol 55, 97–179 (1994).

17) Mukai, H. In Proceedings of the Second International and the Seventeenth American Peptide Symposium; pp 1014–1015 (2001).

18) Pane K. Antimicrobial potency of cationic antimicrobial peptides can be predicted from their amino acid composition: application to the detection of “cryptic” antimicrobial peptides. Theorical Biologydoi: http://dx.doi.org/10.1016/j.jtbi.2017.02.012 (2017).

19) K. Pane. A new cryptic cationic antimicrobial peptide from human apolipoprotein E with antibacterial activity and immunomodulatory effects on human cells. FEBS J. 283 2115-2131 (2016).

20) E. Notomista. The identification of a novel *Sulfolobus islandicus* CAMP-like peptide points to archaeal microorganisms as cell factories for the production of antimicrobial molecules. Microb Cell Fact. 14 (2015).

21) Andersson L. Large-scale synthesis of peptides. Biopolymers 55:227–250 (2000).

22) Chen Y.Q. Expression of a cytotoxic cationic antibacterial peptide in Escherichia coli using two fusion partners. Protein Expr Purif 57:303– 311 (2008).

23) Piers K.L. Recombinant DNA procedures for producing small antimicrobial cationic peptides in bacteria. Gene 134:7–13 (1993).

24) Zhang L. Determinants of recombinant production of antimicrobial cationic peptides and creation of peptide variants in bacteria. Biochem Biophys Res Commun 247:674–680 (1998).

25) Pane K. Rational Design of a Carrier Protein for the Production of Recombinant Toxic Peptides in Escherichia coli. PLoS One 11e0146552 (2016).

26) Schneider VA, Imaging the antimicrobial mechanism(s) of cathelicidin-2. Sci Rep. 6:32948 (2016).

27) D. Pletzer, Anti-biofilm peptides as a new weapon in antimicrobial warfare. Curr Opin Microbiol 33 35-40 (2016).

28) J. Overhage, Human Host Defense Peptide LL-37 Prevents Bacterial Biofilm Formation. Infect Immun. 76 4176-4182 (2008).
29) C. de la Fuente-Nunez. Broad-spectrum anti-biofilm peptide that targets a cellular stress response. PLoS Pathog. 10 e1004152 (2014).
30) J.D. Heilborn. The cathelicidin anti-microbial peptide LL 37 is involved in re epithelialization of human skin wounds and is lacking in chronic ulcer epithelium. J. Invest. Dermatol. 120 379–389 (2003).
31) R. Shaykhiev. Human endogenous antibiotic LL-37 stimulates airway epithelial cell proliferation and wound closure. Am. J. Physiol. Lung Cell. Mol. Physiol. 289 L842–L848 (2005).
32) Notomista, E. The identification of a novel Sulfolobus islandicus CAMP-like peptide points to archaeal microorganisms as cell factories for the production of antimicrobial molecules, Microb Cell Fact 14 (2015).
33) Cruciani, R.A. Antibioticmagainins exertcytolyticactivityagainst transformed-celllinesthrough channelformation. Proc.Natl.Acad. Sci.U.S.A. (1991).
34) Ellerby, H.M. Anartificially designedpore-formingprotein withanti-tumoreffects. J. Biol. Chem. 278,35311–35316.doi: 10.1074/jbc.M300474200 (2003).
35) Papo, N. Anovellytic peptide composedofDL-amino acids selectivelykillscancercells in cultureandinmice. J. Biol. Chem. 278,21018–21023.doi: 10.1074/jbc.M211204200 (2003).
36) D. Gaspar. From antimicrobial to anticancer peptides. Areview. Frontiers in Micobiology. (2013).
37) Prato, S. Molecular modeling and functional characterization of the monomeric primase-polymerase domain from the Sulfolobus solfataricus plasmid pIT3, Febs J 275, 4389-4402. (2008).
38) Fusco, S. T(lys), a newly identified Sulfolobus spindleshaped virus 1 transcript expressed in the lysogenic state, encodes a DNA-binding protein interacting at the promoters of the early genes, J Virol 87, 5926-5936 (2013).
39) Fusco, S. Unravelling the Role of the F55 Regulator in the Transition from Lysogeny to UV Induction of Sulfolobus Spindle-Shaped Virus 1, J Virol 89, 6453-6461 (2015).
40) De Paola, I. Cullin3-BTB Interface: A Novel Target for Stapled Peptides, PLoS One 10 (2015).

APPENDICES

ABBREVIATIONS

MRSA: methicillin-resistant Staphylococcus aureus; **VRE**: vancomycin-resistant enterococci; **HDPs**: host defence peptides; **AMPs**: antimicrobial peptides; **LPS**: lipopolysaccharide; **ApoE**: Apolipoprotein E; **ApoB**: Apolipoprotein B; **LDL**: low-density lipoprotein; **IL-10**: interleukin-10; **MIC**: minimal inhibitory concentration; **TSA**: Tryptic Soy Agar; **AS**: absolute score; **MHB**: Muller Hinton Broth; **NB**: Nutrient Broth; **LB**: Luria-Bertani; **IPTG**: isopropyl-β-D-thiogalactopyranoside; **TFE**: trifluoroethanol; **TFA**: trifluoroacetic acid; **SDS**: sodium dodecyl sulfate; **FIC**: fractional inhibitory concentration; **EDTA**: ethylenediaminetetraacetic acid; **IL-6**: interleukin-6; **NO**: nitric oxide; **CATH-2**: cathelicidin-2; **ONC**: onconase; **PBS**: phosphate-buffered saline; **CD:** circular dichroism; **DLS**: dynamic light scattering; **MTT**: 3-(4,5-dimethylthiazol-2-yl)-2,5-diphenyltetrazolium bromide; **MALDI-MS**: matrix assisted laser desorption ionisation mass spectrometry; **RBCs**: red blood cells; **WH**: wound healing; **LTA**: lipoteichoic acid; **LAL**: limulus amaebocyte lysate; **SD**: standard deviation; **CFU**: colony forming unit; **HBTU**: 2-(1H-benzotriazole-1-yl)-1,1,3,3-tetramethyluronium hexafluorophosphate; **OXYMA**: cyano-hydroxyimino-acetic acid ethyl ester; **DIPEA**: N,N′-diisopropylethylamine; **MeIm**: 4-methylimidazole; **MSNT**: 1-(Mesitylene-2-sulfonyl)-3-nitro-1,2,4-triazole; **DMF**: N,N-Dimethylformamide; **ACN**: Acetonitrile; **DCM**: dichloromethane; **Fmoc**: fluorenylmethyloxycarbonyl; **TOCSY**: total correlated spectroscopy; **NOESY**: nuclear overhauser effect spectroscopy; **OPEX**: operating expenditure; **CAPEX**: capital expenditure.

LIST OF PUBLICATIONS

- Rusciano G., Pesce G., Zito G., Sasso A., **Gaglione R.**, Del Giudice R., Piccoli R., Monti DM., Arciello A. *Insights into the interaction of the N-terminal amyloidogenic polypeptide of ApoA-I with model cellular membranes.* (2016, Biochimica and Biophysica Acta. doi: 10.1016/j.bbagen.2016.01.010.)

- **Gaglione R.**, Dell'Olmo E., Bosso A., Chino M., Pane K., Ascione., Itri F., Caserta S., Amoresano A., Lombardi A., Haagsman H. P., Piccoli R., Pizzo E., Veldhuizen J. A. E., Notomista E., Arciello A. *Novel human bioactive peptides identified in apolipoprotein B: evaluation of their therapeutic potential.* (2017, Biochemical Pharmacology. http://dx.doi.org/10.1016/j.bcp.2017.01.009)

- Bosso A., Pirone L., **Gaglione R.**, Pane K., Del Gatto A., Zaccaro L., Di Gaetano S., Diana D., Fattorusso R., Pedone E., Cafaro V., Haagsman H.P., van Dijk A., Zanfardino A., Crescenzi O., Arciello A., Varcamonti M., Veldhuizen E.J.A., Di Donato A., Notomista E., Pizzo E. *A new cryptic host defense peptide identified in human 11-hydroxysteroid dehydrogenase-1 β-like: from in silico identification to experimental evidence.* (2017, BBA – General Subjects, submitted manuscript)

- **Gaglione R.**, Pirone L., Farina B., Fusco S., Smaldone G., Aulitto M., Dell'Olmo E., Roscetto E., Del Gatto A., Fattorusso R., Notomista E., Zaccaro L.

Arciello A., Pedone E and Contursi P. *Insights into the anticancer properties of the first antimicrobial peptide from Archaea*. (2017, ACS Chemical Biology, submitted manuscript)

- **Gaglione R.**, Pane K., Dell'Olmo E., Pizzo E., Olivieri G., Notomista E., Arciello A. *Cost-effective production of host defence peptides in Escherichia coli*. (Manuscript in preparation)

LIST OF COMMUNICATIONS

- **Gaglione R.**, Itri F., Pane K., Cafaro V., Piccoli R., Notomista E., Arciello A. *Identification and characterization of novel cryptic cationic antimicrobial peptides from human ApoB*. (58th National Meeting of the Italian Society of Biochemistry and Molecular Biology. Urbino, September 14-16, 2015)

- S. Fusco, E. Notomista, A. Arciello, A. Falanga, **R. Gaglione**, S. Galdiero, E. Pedone, L. Pirone, M. Varcamonti, A. Zanfardino, P. Contursi. *A powerful in silico approach allowed the identification of a new antimicrobial peptide from the third domain of life.* (Dissecting Biological Complexity at the Molecular Level. University of Bologna, Bologna, Italy, 30/03-01/04/2016)

- **Gaglione R.**, Pane K., Itri F., Bosso A., Cafaro V., Pizzo E., Piccoli R., Notomista E., Arciello A. *Novel cryptic cationic antimicrobial peptides from human ApoB.* (ALTANT Conference 2016: Innate Host Defence and Infections. From basic science to applications. 18-20 May 2016, Utrecht, Netherlands)

- Pane K., Bosso A., **Gaglione R.**, Arciello A., Cafaro V., Pizzo E., Notomista E., Di Donato A. *Novel antimicrobial weapons hidden in human secretoma.* (ALTANT Conference 2016: Innate Host Defence and Infections. From basic science to applications. 18-20 May 2016, Utrecht, Netherlands)

- **R. Gaglione**, K. Pane, F. Itri, A. Bosso, E. Dell'Olmo, V. Cafaro, E. Pizzo, E. J. A. Veldhuizen, R. Piccoli, E. Notomista, A. Arciello. *Novel cryptic cationic antimicrobial peptides from human ApoB.* (15th Naples Workshop on bioactive peptides. Peptides: recent developments and future directions. 23-25 June 2016, Naples, Italy)

- **R. Gaglione**, M. Aulitto, A. Del Gatto, B. Farina, S. Fusco, L. Pirone, G. Smaldone, A. Arciello, P. Contursi, R. Fattorusso, E. Notomista, L. Zaccaro, E. Pedone. *Insight into structure and function of an emerging anti-tumor peptide VLL-28.* (15th Naples Workshop on bioactive peptides. Peptides: recent developments and future directions. 23-25 June 2016, Naples, Italy)

- **R. Gaglione**, K. Pane, E. Dell'Olmo, A. Bosso, M. Chino, F. Itri, V. Cafaro, E. Pizzo, E.J. A. Veldhuizen, A. Lombardi, R. Piccoli, E. Notomista, A. Arciello. *Novel human antimicrobial peptides from ApoB are endowed with promising anti-inflammatory properties.* (XIV Congress of the Italian Federation of Life Sciences (FISV), 20-23 September 2016, University of Rome, Sapienza)

EXPERIENCE IN FOREIGN LABORATORIES

Visiting period at the Department of Infectious Diseases and Immunology, Division Molecular Host Defence, Faculty of Veterinary Medicine, Utrecht University, The Netherlands, from 09th May 2016 to 27th October 2016.
The work was carried out in the lab of Professor Henk P. Haagsman and supervised by assistant Professor Edwin J. A. Veldhuizen.

ACKNOWLEDGMENTS

This is my favorite moment: the moment in which I can look over the last years of my life and understand how many people have contributed making this journey possible and very special.
I would like to start by thanking those who believed in me; those who gave me the chance to join a PhD project, which has always been my dream. A huge “Thank You” to my tutor, Professor Renata Piccoli, and my Co-Tutor, Dr. Angela Arciello. During these years, your experience has made my PhD less arduous and I’ve always known that I was able to count on you both. You were my valid testimonials and orientation points during the difficult moments. Professor Piccoli has always been very helpful in correcting my mistakes and at the same time very passionate by participating in the design of the new experiments.
A special “Thank You” to Angela, who prior to being my PhD tutor, was my supervisor for both the bachelor and master’s degree, so… they are six years she has had me around her! Jokes aside, it is great to see how our working and personal relationships have grown and fortified over the years despite the diversities in character or misunderstandings. “Thank You” Angela, because you allowed me to taking the first steps into the science world and you are the reason why I am here today!
Thanks to everyone who has been part of my so called “scientific life”, leaving here a bit of themselves and taking a bit of me: the magnificent FIB group! Those who made the history of this group are: Daria, Rita, Francesco and Anna. The moments we have spent together allowed our group to become wonderful and pleasant, renewing year after year also thanks to the “newcomers” Eliana and Paola. Thanks to all the students who have been part of my studies: Carla, Luca, Emma, Angelica, Roberta ... and many more; you have all been the soul of our lab. Special thanks to D.O.C student and incomparable friend, Simona Allocca. You have been my support and encouragement during the difficult times, a friend with that special smile during our playful moments, and the best student I could have wished to have during the beginning of my PhD. Thank you to two exceptional colleagues in the field of antimicrobial peptides: Katia and Andrea! I remember the moments when I had to leave for my visiting trip to Holland and your encouraging words: “Don’t worry, you’ll be fine in Holland; everyone will love you”! Needless to talk about the support given day by day until I had to substitute you with my Dutch friends!!! Obviously, I'm just kidding! As I always say, God gave me a huge heart big enough to contain all the angels He donated to me.
How could I forget my Dutch experience??? Edwin ... there are no words to express my feelings by saying to you how much your role has been very significant during my period there with you. You had to be only my Dutch scientific supervisor, but you were so much more ... I will never forget your knowledge and experience; your advice and your happiness!!! “Thank you” from the bottom of my heart! “Thanks” to each member of the MHD group. A special “Thank You” to Professor Henk Haagsman who will always remain one of my most valuable examples of scientists!

“Thanks” to two competent and gifted researchers: Albert and Martin. “Thanks” to one of the most unselfish woman I've ever met, Hanne, and thanks to Maaike, Trynsje, Marina, Jiye, Hongwei and Manpreet; you all made my experience, a unique experience with your friendly presence. A special thanks to Heleen, you opened the doors of your home to me, as well as those of your heart. I will be forever grateful! At last, an extraordinary “thanks” to my Italian friends, who shared the special moments through volunteer activities, at my so called “second home”, the Missionary Community of Villaregia. Among the profound and fun meetings; watching a movie or simply eating a pizza ...made me think: “where would I be without you all?” It is impossible to mention the names of all of you, being that I have a page limit for my thesis! Although, this does not take away the friendship given and from which I could not live without.
And *dulcis in fundo* ... a huge “Thank You” to my family, the most precious gift given to me! Without the support of my parents, I would not have been able to accomplish any of this. Without the confidence of my sister and brother, my PhD would not been the same... as it would not be the same without the person who shared everything with me during these years: joy, sorrow, success and failure, Gaetano. He is the half who perfectly complete me.
It is said that the most important people are to be mentioned at the very end, because the last shall be first. Therefore, my biggest gratefulness goes to “God” because without Him this page would remain blank. He gave me gift of life which allowed me to accomplish this amazing journey (and much more) with all the above-mentioned people.

“*It is clear that all mankind has to devote himself to science. Indeed, God created the “man”, so that he knew and understood, and knowing it he loved it, and loving it, he enjoyed it; for this reason, the man has been created to be rational and equipped with senses. Instead for the man, if it is true that the reason has been created for science, if he didn’t use this gift of God according to the divine plan, he would be acting against the natural order of God, simply as the expression “walking without the use of the feet...”*

(*Tommaso Campanella*)

ITALIAN ACKNOWLEDGMENTS

Questo è il mio momento preferito: il momento nel quale posso guardare agli ultimi anni della mia vita e capire quante persone hanno contribuito a rendere speciale questo percorso e soprattutto quanti lo hanno reso possibile.
Devo innanzitutto ringraziare chi ha creduto in me, offrendomi la possibilità di aderire ad un progetto di Dottorato, quello che era sempre stato il mio sogno nel cassetto. Quindi devo dire un immenso grazie al mio Tutor, Professoressa Renata Piccoli e al mio Co-Tutor, la Dottoressa Angela Arciello. Durante questi anni, la vostra esperienza ha reso il mio percorso meno faticoso e ho sempre saputo di avere un valido punto di riferimento a cui potermi rivolgere nei momenti di difficoltà. La Professoressa Piccoli si è sempre dimostrata disponibile nel correggere i miei errori e appassionata nel partecipare alla progettazione di nuovi esperimenti. Devo però un grazie particolare ad Angela, perché prima che Tutor di Dottorato, è stata mio relatore sia per la laurea triennale, che per la laurea magistrale, quindi sommando … sono circa sei anni che le sono tra i piedi! Ma a parte gli scherzi, è stato bello vedere come il nostro rapporto lavorativo (ma anche e soprattutto quello personale), è

cresciuto negli anni e si è fortificato, andando al di là di ogni diversità caratteriale o incomprensione. Grazie Angela, ho mosso il mio primo passo nel mondo della scienza per merito tuo, e per merito tuo oggi sono qui!
Grazie a tutti coloro che passando nella mia vita di laboratorio, hanno lasciato un po' di sé e preso un po' di me: il magnifico gruppo FIB! C'è chi ha fatto la storia di questo gruppo, come Daria, Rita, Francesco e Anna, voi solo sapete quante ne abbiamo passate insieme… ma è anche grazie ai "nuovi" arrivati, come Eliana e Paola, che il nostro gruppo è diventato più bello e si è rinnovato anno dopo anno. Grazie a tutti gli studenti passati di qui, Carla, Luca, Emma, Angelica, Roberta… e tanti tanti ancora …siete stati voi l'anima di questo posto. Un ringraziamento particolare alla studentessa D.O.C e amica insuperabile, Simona Allocca. Sei stato faro nella notte nei momenti difficili, amica sorridente nei momenti scherzosi e la migliore studentessa che potessi desiderare al mio fianco per l'inizio del mio Dottorato.
E grazie a due colleghi eccezionali, validi punti di riferimento nel campo dei peptidi antimicrobici: Katia e Andrea! Ricordo ancora le vostre parole prima che partissi per il periodo all'estero: "stai tranquilla, ti troverai bene in Olanda, tutti ti vorranno bene" e telematicamente mi avete sostenuto giorno dopo giorno… fin quando vi ho sostituiti con i miei nuovi amici olandesi!!! Ovviamente sto scherzando, come dico sempre, Dio mi ha donato un cuore così grande in modo da poter contenere tutti gli angeli che mi ha donato.
E potrei mai dimenticare la mia esperienza olandese??? Edwin … non ci sono parole adatte per dirti quanto sei stato rilevante nella mia esperienza lì con voi. Dovevi essere solo il mio tutor scientifico, ma sei stato molto di più… non dimenticherò mai i tuoi insegnamenti, i tuoi consigli e la tua allegria!!! Grazie di vero cuore! E grazie a ciascun membro del gruppo MHD: grazie a colui che resterà per sempre uno dei miei più validi esempi di scienziato, il Professore Henk Haagsman, grazie a due fantastici e validi ricercatori, Albert e Martin, grazie alla donna più disponibile che io abbia mai incontrato, Hanne e grazie a coloro che hanno reso la mia esperienza unica con la loro accoglienza: Maaike, Trynsje, Marina, Jiye, Hongwei e Manpreet. Un grazie particolare va soprattutto ad Heleen! Grazia amica mia, perché mi hai aperto le porte di casa tua, oltre che quelle del tuo cuore. Ti sarò riconoscente per sempre!
E grazie a tutti i miei amici italiani! Con voi condivido la vita *in toto*: attraverso il volontariato presso la mia seconda casa, la Comunità Missionaria di Villaregia, attraverso incontri profondi o scherzosi, guardando un film o semplicemente mangiando una pizza … dove sarei senza di voi…? È impossibile riportare i nomi di tutti voi, ho un limite stabilito di pagine per la mia tesi! Ma come più volte vi ho detto, l'amicizia che mi donate è linfa vitale per me, non potrei viverne senza.
E *dulcis in fundo* … un GRAZIE grande quanto l'Universo al dono più prezioso che la vita mi ha fatto: la mia famiglia! Grazie a TUTTA la mia famiglia! Senza il sostegno dei miei genitori, non avrei fatto niente di tutto questo, senza la fiducia di mia sorella e di mio fratello, il mio percorso non sarebbe stato lo stesso… come non sarebbe stato lo stesso senza colui che ha condiviso tutto con me in questi anni: gioie, dolori, successi ed insuccessi, la metà con la quale perfettamente mi completo, Gaetano.
Si dice che le persone più importanti vanno menzionate alla fine, perché gli ultimi saranno i primi. E allora la mia riconoscenza più grande va a Colui senza il quale questa pagina sarebbe rimasta bianca... Grazie a Dio, perché donandomi la vita ha consentito tutto questo (e molto altro) e attraverso ognuna delle persone menzionate fin qui (e non), si è reso onnipresente in ogni passo di questo incredibile viaggio.

“È chiaro che tutto il genere umano è tenuto a dedicarsi alle scienze. Infatti Dio creò l’uomo, affinché lo conoscesse, e conoscendolo lo amasse, e amandolo ne godesse; per questa ragione l’uomo è stato creato razionale e dotato di sensi. Invece l’uomo, se è vero che la ragione è fatta per le scienze, qualora non utilizzasse questo dono di Dio secondo il progetto divino, agirebbe contro l’ordine naturale di Dio, quasi non volesse usare i piedi per camminare”

(Tommaso Campanella)

Biochimica et Biophysica Acta 1860 (2016) 795–801

Contents lists available at ScienceDirect

Biochimica et Biophysica Acta

journal homepage: www.elsevier.com/locate/bbagen

Insights into the interaction of the N-terminal amyloidogenic polypeptide of ApoA-I with model cellular membranes

Giulia Rusciano [a,*], Giuseppe Pesce [a], Gianluigi Zito [a], Antonio Sasso [a], Rosa Gaglione [b], Rita Del Giudice [b], Renata Piccoli [b,c], Daria Maria Monti [b,c], Angela Arciello [b,c]

[a] Department of Physics E. Pancini, University of Naples Federico II, via Cintia, 80126-I, Naples, Italy
[b] Department of Chemical Sciences, University of Naples Federico II, via Cintia, 80126-I, Naples, Italy
[c] INBB, Istituto Nazionale di Biostrutture e Biosistemi, Italy

ARTICLE INFO

Article history:
Received 4 September 2015
Received in revised form 27 December 2015
Accepted 6 January 2016
Available online 25 January 2016

Keywords:
Amyloidosis
Raman tweezers
ApoA-I
Model membranes
Lipid phases

ABSTRACT

Background: About twenty variants of apolipoprotein A-I (ApoA-I) are associated to hereditary systemic amyloidoses. Although the molecular bases of this disease are still largely unknown, it has been hypothesized that ApoA-I proteolysis is a key event in pathogenesis, since it triggers the release of an N-terminal fragment (80–100 residue long) that misfolds to form amyloid deposits in peripheral organs and tissues. It is also known that cell membrane lipids play a key role in the fibrillogenic pathway. In the case of ApoA-I related amyloidosis caused by L174S mutation, the 93-residue N-terminal fragment of ApoA-I ([1-93]ApoA-I) was found to be the major constituent of *ex vivo* fibrils.
Methods: With the main goal to investigate the interaction of either [1-93]ApoA-I and ApoA-I with biomimetic membranes, we set-up an experimental system based on the Raman Tweezers methodology. We tested GUVs composed by two types of zwitterionic lipids with a different fluidity degree, *i.e.* dioleoylphosphatidylcholine (DOPC) and dipalmitoylphosphatidylcholine (DPPC).
Results: We found that [1-93]ApoA-I induces conformational disorder in an ordered lipid bilayer. When interacting with fluid phases, instead, the fragment was found to be able to penetrate the membrane bilayer inducing an alignment of lipid chains.
Conclusions: The interaction features of [1-93]ApoA-I with biomimetic membranes strongly depend on the lipid phase. Full-length ApoA-I was found to have similar effects, even if significantly less pronounced.
General significance: Our observations shed light on still largely unknown molecular bases of ApoA-I fibrillogenic domain interaction with membranes.

1. Introduction

It is known that the interaction of proteins with chemical groups exposed on a membrane surface is able to modify their conformational states [1–3]. On the other hand, it has also been reported that proteins can alter membrane fluidity, and/or permeate the membrane bilayer, eventually extracting membrane lipids [4]. In the case of natively unfolded polypeptides, it has been demonstrated that, upon interaction with surfaces, they readily adopt helical structures that represent key intermediates in the amyloid formation process [5]. In particular, anionic surfaces and anionic phospholipid-rich membranes can play key roles either in triggering protein–protein aggregation (fibrillogenesis) by acting as conformational catalysts for amyloid fibril deposition [1], or as inhibitors of fibrillogenesis [6].

Membranes also play a key role in amyloidoses associated with specific variants of apolipoprotein A-I (ApoA-I), the major structural component of high density lipoproteins (HDL). Specific ApoA-I mutations are responsible for well-known familial systemic amyloidosis [7], characterized by amyloid deposition in peripheral organs, such as heart, liver or kidneys. In rarer cases, amyloid is also found in the testes and adrenal glands [7–9]. Notably, the molecular bases of the onset and development of this pathology are still largely unknown.

The prevailing concept in this field is that ApoA-I proteolysis is a key event in the development of the disease, since it triggers the release of the N-terminal fragment (80–100 residue long) that misfolds to form amyloid deposits [10]. In both lipid-bound and lipid-free ApoA-I, this region 80–100 forms well-ordered helical structures [11–13] and is expected to be protected from proteolysis. Nevertheless, it is emerging that a single point amyloidogenic mutation is able to profoundly alter the protein 3D structure, thus presumably exposing protein regions to proteolytic attack. In ApoA-I amyloidosis caused by the presence of L174S mutation, the 93-residue N-terminal polypeptide of ApoA-I (henceforth denoted as [1-93]ApoA-I) was found to be the major constituent of *ex vivo* fibrils [14]. Recently, we produced a recombinant

* Corresponding author.
E-mail address: giulia.rusciano@unina.it (G. Rusciano).

http://dx.doi.org/10.1016/j.bbagen.2016.01.010
0304-4165/

version of this polypeptide, which was found to be natively unfolded in aqueous solutions at pH 7.0 [15]. Upon acidification to pH 4.0, we observed a conformational transition towards a helical state, which we have proposed to be a key intermediate in the fibrillogenic pathway, leading to the formation of a β-sheet-based polymeric structure that evolves into typical amyloid fibrils [15]. Moreover, we also demonstrated that a lipid environment induces and stabilizes helical intermediates of [1-93]ApoA-I, thus affecting its aggregation pathway [16]. This is noteworthy considering that ApoA-I functional role is strictly related to its interactions with lipids and that the N-terminal region of ApoA-I contributes to the binding of the native protein to lipids [17–18]. In particular, cholesterol, a natural ApoA-I ligand, is able to induce a transition towards a helical conformation and to inhibit protein aggregation in a concentration- and time-dependent manner [16]. Similar to cholesterol, zwitterionic, negatively and positively charged liposomes were found to be able to increase the helical content, with negatively charged liposomes showing the greatest effect in inducing helical species [16].

The work presented herein is committed to shed light on the interaction of the fibrillogenic polypeptide [1-93]ApoA-I with cellular membranes. It has to be noticed that interaction of unaggregated [1-93]ApoA-I with cell membranes represents a key event in the development of ApoA-I associated amyloidoses, but molecular details and consequences of this interaction are still largely unknown. We investigated the role of membrane fluidity by taking advantage of the use of Giant Unilamellar Vesicles (GUVs) as synthetic biomimetic systems. GUVs are spherical phospholipid bilayers entrapping a closed water-filled compartment [19], typically used to gain insight into membrane organization and response to external agents. Plasma membrane of eukaryotic cells may be considered as composed of small fluid domains, in which lipids are arranged in a liquid–crystalline phase nucleated within a continuous, more ordered gel phase [20]. Hence, in order to properly simulate these membrane phases, we used GUVs composed of two kinds of zwitterionic lipids endowed with different fluidity properties, such as dioleoylphosphatidylcholine (DOPC) and dipalmitoylphosphatidylcholine (DPPC). Since DOPC and DPPC melting temperatures are −16.5 °C and 41.3 °C, respectively, they are representative of the fluid-like state L_α (DOPC) and of the gel state L_β (DPPC) at room temperature (T = 24 °C) [21]. Analyses were performed by taking advantage of *Raman Tweezers* (RT) methodology, *i.e.* the combination of a Raman spectrometer and an Optical Tweezers (OT) [22]system [23]. This approach presents specific benefits with respect to well-consolidated techniques used to investigate membrane properties, such as Differential Scanning Calorimetry (DSC) [24], and fluorescence-based techniques [25,26]. As a matter of fact, RT can be used to trap and interrogate single objects, in order to provide information on their chemical components, without the need of sample labeling. Moreover, the analysis of Raman spectra is able to reveal molecular details of protein species/lipid interaction features. In particular, on the bases of selected Raman band changes, it is possible to identify the specific lipid moieties involved into the interaction with proteins. Furthermore, the use of OT allows the investigation of GUVs in the absence of any surface-induced spurious effect. Furthermore, RT allows the acquisition of the signal from a single GUV, thus giving the possibility to explore the heterogeneity of the system under investigation. In the present study, GUV manipulation by OT, combined with the non-destructive nature of Raman spectroscopy, gave us the opportunity to follow over time the interaction of single GUVs with the proteins under test. Being Raman spectra sensitive to molecular conformations, we were able to observe the reorganization of GUV phospholipid bilayer upon interaction with ApoA-I or with [1-93]ApoA-I. Interestingly, our results, besides revealing that [1-93]ApoA-I plays a key role in ruling ApoA-I interaction with membranes, indicate that the interaction of the fibrillogenic polypeptide with DPPC–GUVs has effects that resemble lipid phase transition induced by melting. Instead, the interaction with DOPC-based bilayers induces an alignment of membrane lipid chains, similar to that induced by cholesterol [27]. The same phenomena, even if significantly less pronounced, were observed for full-length ApoA-I.

2. Material and methods

2.1. Proteins under test

ApoA-I was purchased from Sigma-Aldrich (St Louis, MO, USA). [1-93]ApoA-I polypeptide was expressed and purified as previously described [16], omitting the neutralization step with ammonium hydroxide. The final yield of the procedure was estimated to be 2.5 mg/L of bacterial culture. Pure [1-93]ApoA-I was lyophilized and stored at −70 °C until use. For experimental purposes, the polypeptide was dissolved in the appropriate buffer and centrifuged before use.

2.2. Experimental set-up

The Raman analysis presented in this work was performed by using a combined Optical Tweezers and micro-Raman system. The set-up has been described in detail elsewhere [23,28]. Briefly, it consisted essentially in a home-made inverted microscope, endowed with a trapping beam (Nd:YAG, 1064 nm, Ventus 1064) and a Raman probe at 532 nm (Spectra Physics Millennia Xs). The microscope was equipped with a 100× objective lens (Olympus oil-immersion infinity corrected objective, 1.4 N.A.), in which both lasers were injected through a dichroic mirror, reflecting near-IR radiation and being transparent to visible radiation. The back-scattered photons followed back along the same optical pathway, reaching finally a holographic notch filter where the elastically scattered photons were suppressed. The resulting radiation was focused through a 50 μm aperture pinhole for confocal detection geometry and subsequently sent to a spectrometer (TRIAX 180, Jobin-Yvon) for the spectral analysis. The Raman radiation was detected by using a thermoelectrically cooled charge-coupled device (Pixis 100, Princeton Instruments), at the spectrometer exit. Raman spectra were acquired in the 900–1800 cm^{-1} spectral range. It should be noticed that the CH_2/CH_3 stretching bands in the 2800–3000 cm^{-1} region also provide information about the order of lipid architecture. However, in our case, the analysis of Raman bands in this region is complicated by the presence of the broad Raman bands in the 3000 cm^{-1} region due to H_2O. In fact, even if H_2O is a weak scatterer, Raman spectra of GUVs in aqueous solution present a significant contribution from water, due to the reduced scattering volume from the very thin (~5 nm) GUV membrane. The sample under investigation was placed in a chamber consisting of two 150 μm glass coverslips (Knittel Glasser, thickness no.1), sealed with parafilm stripes, which also act as an ~100 μm spacer. In order to maximize the GUV signal, the membrane was placed in the Raman confocal scattering volume by acting on the galvo-mirrors controlling the trapping laser beam position.

2.3. Data analysis

Principal Component Analysis (PCA) is a statistical tool that allows the decomposition of a multidimensional data set, in order to reduce its dimensionality while retaining the relevant characteristics contributing to most of its variance [29]. From a mathematical point of view, PCA is an orthogonal linear transformation that converts the original data (variables) into a new basis of uncorrelated coordinates (Principal Components, PCs), which are a linear combination of the original variables. PCs are ordered on the basis of their contribution to variation, with the first PC exhibiting the greatest contribution. The results of a PCA are given in terms of component scores and loadings. Loadings are the coefficients of the linear combination defining the PCs, in that they express the contribution of each original variable to the global variance of data set. Scores, instead, are the coordinates of the original data in the PC space. When PCA is applied to Raman spectra, the loadings enable the identification of the more relevant variables (*i.e.* wavenumbers), providing information on how they are correlated. Each score represents a whole spectrum plotted in a three dimensional space (score space), with points corresponding to similar spectra clustered together [30].

2.4. Preparation of DPPC– and DOPC–GUVs

GUVs were prepared following a procedure similar to that previously described [19]. Briefly, 3 mg of lipids (DOPC or DPPC) by Avanti were dissolved in 500 μL of chloroform (0.1 M). An aliquot (20 μL) of this solution was added to 200 μL of methanol and 980 μL of chloroform in a 50 mL round-bottom flask. Water (2.8 mL) was then slowly added alongside the flask walls. Finally, this solution was rotoevaporated for 3 min at a pressure of 10 mbar and a temperature of ~40 °C. This procedure provides vesicles whose diameter is in the range between 1 and 30 μm, as observed by bright field microscopy [31]. Vesicles with a diameter in the 4–8 μm range were selected for the experiments.

3. Results and discussion

As first, we acquired the Raman spectra of [1-93]ApoA-I and full-length ApoA-I in aqueous buffer. Fig. 1 shows the spectrum of a 0.76 μM [1-93]ApoA-I (*a*) and a 7.6 μM ApoA-I (*b*) aqueous solution in the spectral range between 900 and 1800 cm^{-1}.

Spectra were acquired by using a Raman probe power of 3 mW and an integration time $\tau = 30$ s. Under these experimental conditions, both signals exhibit only broad features due to the weak Raman bending mode around 1640 cm^{-1}, while no significant contribution from proteinaceous bands was detected, as a consequence of the low protein concentration. Trace *c* and *d* in Fig. 1 show, instead, the Raman spectra of an optically trapped DPPC– or DOPC–GUV, respectively, acquired under the same experimental conditions of traces *a* and *b* (no proteins added). The obtained Raman spectra present spectral features mainly arising from vibrations of the hydrocarbon chains, with minor contribution of polar groups. The assignment of the prominent peaks, reported in Table 1, has been performed on the basis of the criteria reported in [32–36].

According to these papers, the low-wavelength region is dominated by skeletal optical modes (SOM). These modes, being mainly C—C stretching vibrations delocalized along the entire acyl chain, provide information on the *intrachain* conformation. In particular, the relative intensity of trans/gauche peaks can be used to monitor the transition of a lipid to an ordered/disordered phase [37]. On the other hand, CH modes are essentially not coupled to the chain and are sensitive to lateral interactions inside the bilayer, so that the strength of these vibrations provides information on the *interchain* order. In particular, according to ref. [32], the decrease of the CH bending mode in CH_2 with respect to that in CH_3 is indicative of a reduced interchain order. In the case of DOPC–GUV spectrum, a strong feature at 1655 cm^{-1} takes into account the presence of the C═C bond. Obviously, the ratio of trans-to-gauche band intensity is larger for DPPC– than for DOPC–GUV, indicating that there is a higher degree of conformational order in the fully saturated lipid. After this preliminary step, we proceeded to investigate the interaction of [1-93]ApoA-I and ApoA-I with DPPC– and DOPC–GUVs. To this purpose, polypeptide and full-length protein were incubated with preformed GUVs at a protein:lipid molar ratio of ~1:100, up to 2 h (τ_{fin}). It should be noticed that, even at a lipid-to-protein molar ratio of 100:1, the lipid architecture can be significantly perturbed by proteins. As a matter of fact, due to the different sizes of proteins and lipids, protein–lipid interaction is not a one-to-one interaction. In particular, assuming for ApoA-I an effective diameter of 4.5 nm (estimated from its molecular weight, 28 kDa) and taking into account that head group area of one lipid molecule is ~0.71 nm^2, it is possible to estimate that ~25 lipid molecules directly interact with a single full-length protein. Moreover, it should be also noticed that both full-length protein and polypeptide can oligomerize in aqueous solution. In particular, ApoA-I exhibits an apparent hydrodynamic diameter of 11 nm in aqueous solution, which is consistent with the size of a protein dimer [38] This means that each dimer potentially interacts with ~130 lipid molecules. For this study, we acquired the Raman spectrum of 40 single, optically trapped GUVs at the initial state (τ_0) and at the end of incubation (τ_{fin}). Moreover, to follow the kinetics of lipid/protein

Table 1
Assignment of the prominent Raman features observed in DPPC– and DOPC–GUVs [32–34,36].

Wavenumber (cm^{-1})	Assignment
1063	SOM (trans)
1080	SOM (gauche)
1098	SOM (trans)
1128	SOM (trans)
1240	PO_2^- antisym stretch
1264	═C—H bend
1296	CH_2 twist
1440	CH bend in CH_2
1460	CH bend in CH_3
1655	C═C stretch
1735	C═O stretch

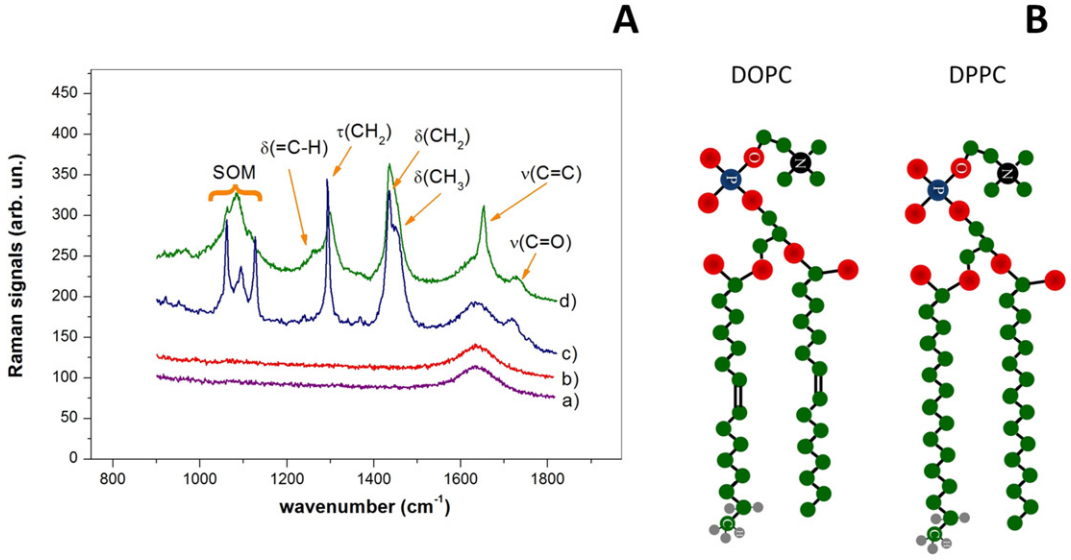

Fig. 1. Representative Raman spectra of proteins and lipids (DPPC and DOPC) under investigation. (A) Raman spectra of a 0.76 μM [1–93]ApoA-I (a) and a 7.6 μM full-length ApoA-I (b) aqueous solution in the spectral range between 900 and 1800 cm^{-1}. Spectra were obtained with an integration time of 30 s and a power of ~3 mW on the sample. c, d: single DPPC– (c) and DOPC–GUV (d) Raman spectra, acquired under the same experimental conditions in the absence of proteins. (B) Sketch of the chemical structure of DOPC and DPPC.

interaction, for 5 GUVs we performed a spectral interrogation every 2 min for the first 30 min, and then every 10 min up to 2 h. As a *control*, these analyses were performed on simple GUVs (no proteins added).

3.1. Interaction of [1-93]ApoA-I with DPPC–GUVs (gel phase)

Fig. 2A reports typical spectra of DPPC–GUVs analyzed upon incubation with the polypeptide (trace *a*) or the full-length protein (trace *b*), acquired at τ_{fin}.

Remarkably, quite relevant changes with respect to τ_0 were observed in both cases, even if more pronounced in the case of [1-93]ApoA-I. The main spectral changes involve the region 1170–1270 cm $^{-1}$, associated with interactions of the PO_2^- groups of the phospholipid polar head moiety, as well as regions 950–1100 cm $^{-1}$ and 1400–1480 cm $^{-1}$, which are sensitive to variations in the acyl chain order. The most striking differences specifically associated with the interaction of [1-93]ApoA-I with DPPC–GUVs lie in region 1170–1270 cm $^{-1}$. Actually, two additional bands are present around 1218 and 1240 cm $^{-1}$ and appear to be notably pronounced in the case of Raman spectra of DPPC–GUVs recorded in the presence of the fibrillogenic polypeptide. These bands are much less pronounced in the presence of ApoA-I and appear to be hardly visible in the absence of proteins (Fig. 1)[35]. According to literature [36], the aforementioned bands are associated with the asymmetric stretching vibrations of the PO_2^- groups. In particular, it has been previously reported that the antisymmetric stretching band lies around 1240 cm $^{-1}$ in dry DPPC–GUV and shifts to ~1220 cm $^{-1}$ in fully hydrated DPPC [36]. From Fig. 2, it is possible to note that lipid–protein interaction is responsible for a strong decrease of the *all-trans* band at 1128 cm $^{-1}$, as well as of the band at 1063 cm $^{-1}$ [37]. On the contrary, the *gauche* marker around 1080 cm $^{-1}$, generally associated with the presence of gauche chain segments [37], is significantly more pronounced upon DPPC–GUV interaction with the fibrillogenic polypeptide. This kind of spectral changes has been observed at a temperature almost corresponding to the lipid phase transition [32]. Under these conditions, lipid physical state passes from the ordered gel phase I_{β} (below T_c), where the hydrocarbon chains are fully extended and closely packed, to the more disordered I_{α} phase (above T_c), where the hydrocarbon chains are randomly oriented and fluid. In agreement with this, the band around 1440 cm $^{-1}$ appears to be weakened with respect to that around 1460 cm $^{-1}$, which is indicative of a reduced lateral packing, and a consequent more disordered lipid chain architecture [32,34]. To better assess the differences between the three analyzed samples, we evaluated the intensity of the most prominent peaks involved in spectral changes by performing a fitting with a multi peak Gaussian function in all the aforementioned regions. In particular, to properly take into account the presence of all spectral features, we used a 4 Gaussian convolution for 950–1100 cm $^{-1}$ region, a 2 Gaussian convolution for 1170–1270 cm $^{-1}$ region and a 2 Gaussian convolution for 1400–1480 cm $^{-1}$ region. In all the cases, a fourth order polynomial curve was added in order to take into account a residual background not completely removed by the subtraction of the background signal. In Fig. 2B, we show a typical result of the fitting procedure for one of the spectra acquired for the polypeptide in the 950–1100 cm $^{-1}$ region, at $\tau = 0$ and $\tau = \tau_{fin}$. The same procedure was used for all the GUV spectra acquired for the three investigated samples. Some significant outcomes of this procedure are reported in Fig. 2C.

In more detail, panel *i*) reports the mean values of $\alpha = (I_{1218} + I_{1240})$, *i.e.* the integrated area under the two aforementioned PO_2^- stretching bands, along with the standard deviations over the 40 GUV spectra. As mentioned above, this parameter fully differentiates the analyzed samples, highlighting the ability of the polypeptide to interact with the

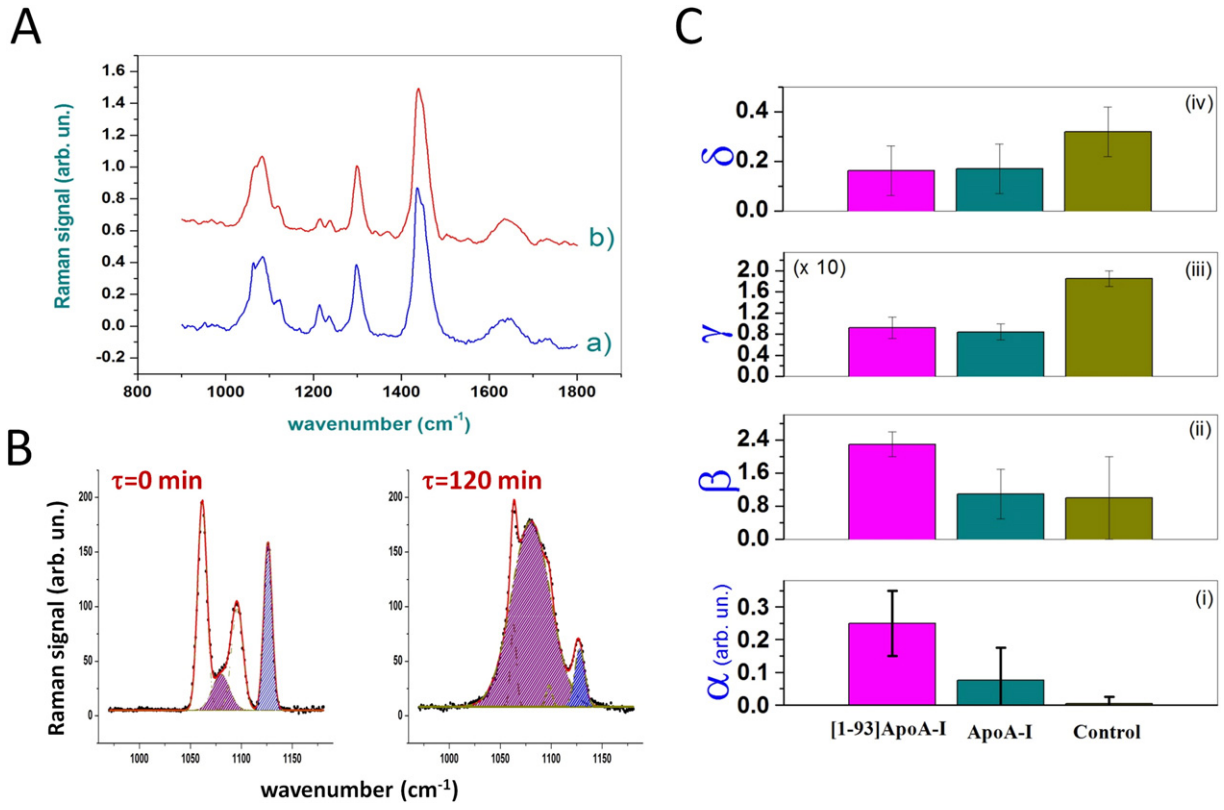

Fig. 2. Analysis of the interaction of ApoA-I and [1-93]ApoA-I with DPPC GUVs. (A) Typical normalized Raman signals of DPPC GUVs upon incubation with [1-93]ApoA-I (trace *a*) or full-length protein (trace *b*), acquired at τ_{fin} (120 min). (B) Representative fitting curves for a spectrum of the polypeptide in the region 950–1100 cm^{-1}. The dotted lines represent the separate contributions of the four Gaussian curves used as fit functions. Moreover, hatched areas correspond to the integrated area under the peaks used for evaluation of γ. (C) α (*i*), β (*ii*), γ (*iii*) and δ (*iv*) mean values obtained by the fitting procedure are exemplified in panel B. The error bars correspond to the standard deviations over the 40 spectra analyzed for each sample.

polar heads of DPPC. A similar behavior, although at a much lesser extent, was recorded for the full-length protein. As a matter of fact, it is reasonable to think that the polypeptide interacts with the PO $\bar{2}$ bond in a manner that induces some modifications of the PO $\bar{2}$ bond polarizability, responsible for the enhanced Raman activity. It should be also pointed out that, differently from the polypeptide sample, the spectra corresponding to the ApoA-I–GUV complex present a consistent fluctuation of the ratio $\beta = I_{1218}/I_{1240}$, as reported in Fig. 2C, panel *ii*. This is clearly suggestive of a random protein positioning in the lipid head region, which gives rise to a different environment for the PO $\bar{2}$ bond. Intriguingly, in this frame, the lower β value for ApoA-I with respect to [193]ApoA-I could be ascribed to a lower exposure to solvent of the PO $\bar{2}$ bond in the case of full-length protein with respect to its fragment. The two additional parameters reported in Fig. 2C, namely the ratios $\gamma = I_{1128}/I_{1080}$ (panel *iii*) and $\delta = I_{1440}/I_{1460}$ (panel *iv*), are indicative of the protein/polypeptide interaction with the lipid acyl chains. As discussed above, their decrease with respect to the pure lipid case is indicative of a reduced order for the acyl chain assembly. In particular, the similar γ and δ values obtained in our analysis clearly prove that the polypeptide shares with the full-length ApoA-I protein the ability to interact with the lipid membrane bilayer. This, in turn, is likely due to the presence, in both protein and fragment helices, of a non-polar side, clearly prone to be buried into the hydrophobic region of the bilayer. Notably, our observations are in agreement with recently published data indicating that 1-83 ApoA-I peptide, which is part of [1-93]ApoA-I analyzed herein, contains four most probable membrane-binding regions [39]. Globally, these observations let us hypothesize that the ApoA-I N-terminal fibrillogenic domain is responsible for protein/fibril attachment to the surface of lipid vesicles.

Interestingly, all the spectral modifications induced by both polypeptide and full-length protein are detected very early (within ~5 min), reaching a steady state within 20 min. Fig. 3A reports the time evolution of γ obtained for a single optically trapped DPPC–GUV interacting with [1-93]ApoA-I. A similar evolution has been observed also for the other parameters evaluated herein, as well as for GUVs upon interaction with ApoA-I. In both cases, their behavior resembles a sigmoidal curve, with a transition in the 10–30 min region. This indicates that the interaction of both the fibrillogenic polypeptide and the full-length protein with DPPC–GUVs have effects that resemble the lipid phase transition induced by melting, which are much more pronounced in the case of the fibrillogenic polypeptide [32]. This observation could be also verified by using DSC on a statistically significant number of GUVs. However, it has to be noticed that, in the case of the approach herein proposed, sample heterogeneity is completely masked.

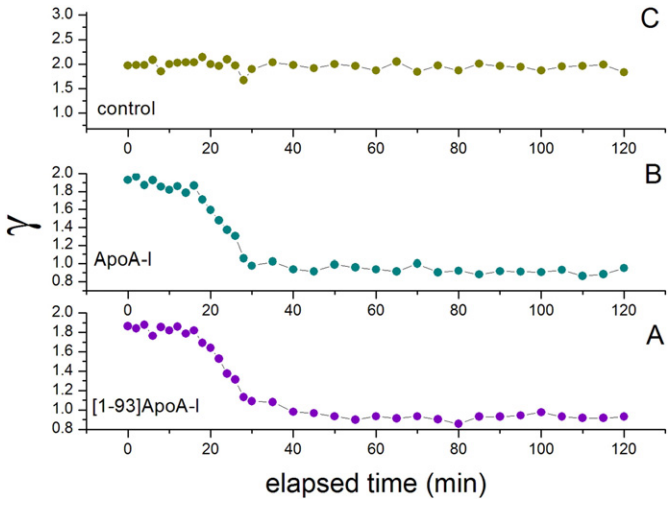

Fig. 3. Kinetic analysis of protein–DPPC GUV interaction. Time evolution of observed gamma for a single, optically trapped DPPC–GUV interacting with the polypeptide (A), the full-length protein (B) and in the absence of proteins (C).

3.2. Interaction of [1-93]ApoA-I with DOPC–GUVs (liquid phase)

As mentioned above, the effect of ApoA-I fibrillogenic fragment on the fluid membrane phase was explored by analyzing its interaction with DOPC–GUVs at room temperature (~24 °C). However, different from the DPPC–GUVs case, the spectroscopic effect of this interaction was not immediately detectable. Although, in principle, this could be ascribed to a weak lipid–protein interaction, we argued that this could be likely due to the obvious difficulty in identifying protein effects in a relatively disordered structure. Therefore, in order to appreciate the fine tuning of DOPC–GUV spectra upon interaction with proteins, we choose to analyze our set of data by Principal Component Analysis (PCA). PCA was performed by using a home-made *MATLAB*, *MathWorks* software, based on the use of the *princomp* routine. Before analysis, Raman spectra were pre-processed by removing a fourth-order polynomial curve and eliminating spurious signals deriving from cosmic ray contributions. Spectra were also normalized and mean centered before the decomposition in PCs.

Fig. 4 shows the three-dimensional score plot obtained by analyzing the 120 spectra for the first 3 PCs, which globally take into account almost 92% of the total spectra variability (see Fig. 4B) In the score plot, the symbols corresponding to [1-93]ApoA-I–GUV and ApoA-I–GUV complexes are triangles and squares, respectively, while spectra corresponding to GUVs are represented by dots. Interestingly, points corresponding to the spectra of each sample tend to be clustered together, with some overlapping between the two protein-containing systems. Most of data variability (~75%) is taken into account by PC1. Notably, PC1 scores of the samples containing the polypeptides and the full-length protein are quite apart from the pure GUV sample, which, instead, occupy a score plot region of relatively low PC1 score values. The reason of this differentiation can be figured out by PC1 loading inspection (Fig. 5A) This loading exhibits main features at around 1655 cm^{-1}, associated with olefinic vibrations of unsaturated chain segments.

In particular, they appear as negative peaks, with some overlapping with dispersive-like features, indicative of a shift to lower wavenumbers of the corresponding Raman peaks. According to literature [40], a shift of olefinic vibration to lower wavenumbers can be indicative of an elongation of the C═C bond. Therefore, positive PC1 scores correspond to spectra of lipid structures where C═C bond is weakened (negative load features) and/or elongated (dispersive load features). As PC1, also PC2 component provides differentiation between the two protein-containing systems and the pure DOPC–GUVs, although points corresponding to the first two samples occupy the same score plot region. As a matter of fact, the main features of PC2 loading lie in the region around 1450 cm^{-1}, including the two CH modes around 1440 cm^{-1} and 1460 cm^{-1}. Clearly, the simultaneous presence of a positive feature around 1440 cm^{-1} and a negative feature around 1460 cm^{-1} suggests that higher PC2 score values correspond to more ordered lipid structures. Interestingly, the improved acyl chain order seems to be somewhat related to the shift of olefinic band highlighted by PC1 loading. In particular, a more ordered acyl chains configuration could result from a higher interchain pressure, giving rise to a repulsion between chains lying at opposite sides of the C═C bonds and, as a consequence, to a C═C bonding elongation. The last PC herein analyzed, PC3, takes into account about 10% of the total data variability. As for PC2, this component highlights differences between spectra of pure DOPC with respect to the two protein-containing systems, with the latter exhibiting PC3 scores spread out through PC3 score axis. However, the mean PC3 score is higher for [1-93]ApoA-I (triangles) than for full-length ApoA-I (squares), therefore suggesting a more pronounced effect of [1-93] ApoA-I with respect to the full-length protein on the lipid membrane (Fig. 4A). PC3 loading is quite complex, presenting both positive and

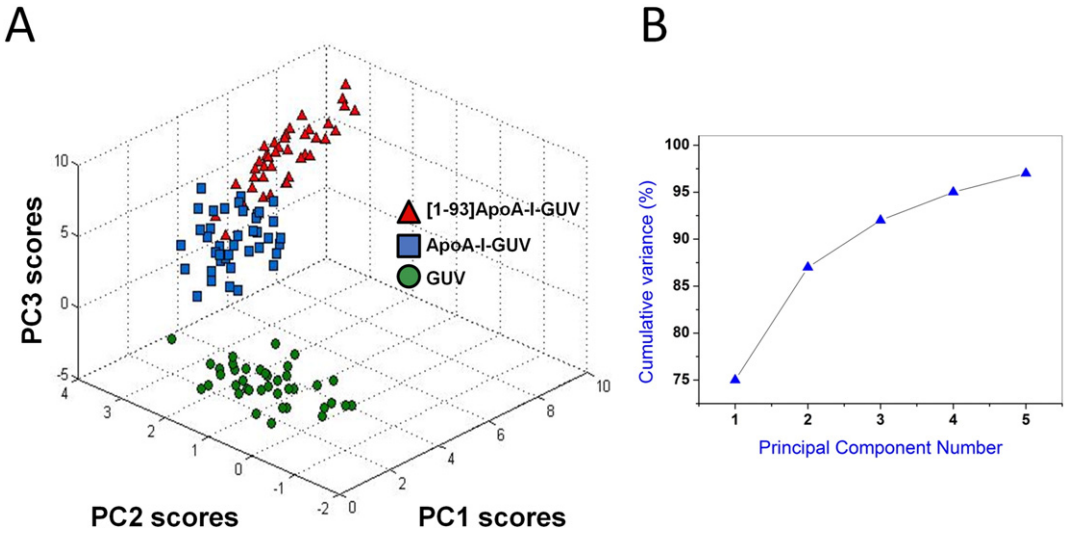

Fig. 4. PC analysis of DOPC–GUVs upon interaction with ApoA-I fibrillogenic polypeptide or the full-length protein. (A) Score plot relative to the PC analysis of DOPC–GUV spectra acquired at τ_0. Points corresponding to [1-93]ApoA-I–GUV complexes and ApoA-I–GUV spectra are represented by triangles and squares, respectively, while spectra corresponding to GUVs in the absence of proteins are represented by dots. (B) Cumulative variance for the first 5 PCs.

negative features. The prominent positive peak is around 1440 cm $^{-1}$, in close proximity with a negative feature at 1460 cm $^{-1}$, and this, as for PC2, can be read in terms of a higher interchain order. Notably, PC3 loading also exhibits relatively sharp bands at 1063 and 1128 cm $^{-1}$, which are all correlated to C—C vibrations of *trans* isomers, indicating that the increase in PC3 scores implies an increased number of trans isomers. The corresponding decrease of gauche isomers is, instead, pointed out by the negative load peak at ~1080 cm $^{-1}$. Therefore, PC3 highlights the presence of lipid structures characterized by a higher order in both intermolecular and intramolecular acyl chains.

As for the DPPC case, we also analyzed the time evolution of single, optically trapped GUVs. However, in this case, the time evolution was followed by PC analysis of single GUVs spectrally interrogated while interacting with polypeptides/proteins (no meaningful data can be extracted for DOPC-–GUVs in aqueous buffer) Fig. 6 reports the PC1 score evolution for the two protein-containing samples. Interestingly, both sets of data suggest a faster interaction with respect to DPPC–GUVs, with a *steady state* reached upon 10 min incubation. This outcome could be due to the higher fluidity of DOPC bilayer.

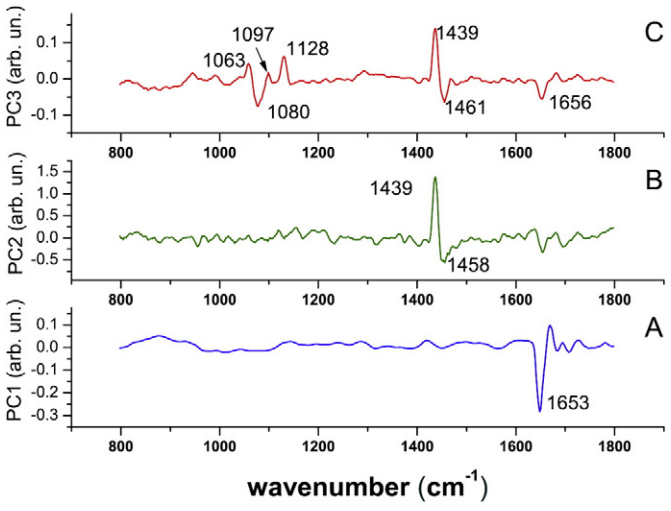

Fig. 5. Analysis of the interaction of ApoA-I and [1-93]ApoA-I with DOPC–GUVs by PCA. PC1-, PC2- and PC3-loading plot (curves A, B and C, respectively) resulting from the analysis of all the 120 GUV spectra.

4. Conclusions

Globally, our results indicate that the interaction features of [1-93]ApoA-I with eukaryotic membranes strongly depend on the lipid phase. In particular, ApoA-I N-terminal fibrillogenic polypeptide was found to induce a conformational disorder in ordered gel lipid bilayers. In addition, the fibrillogenic polypeptide was also found to induce changes in vibrations close to the polar part of phospholipids, in particular in PO_2^- stretching band. On the basis of this observation, we conjecture that a significant portion of [1-93]ApoA-I molecules is not deeply buried inside the bilayer, but remains in close proximity to the membrane–water interface. Similar effects, even if significantly less pronounced, were observed when DPPC–GUVs were incubated with full-length ApoA-I.

We also provide evidence that [1-93]ApoA-I is able to interact with liquid-like lipid bilayers, simulated by DOPC–GUVs. In this case, we analyzed our data set by PCA and demonstrated that [193]ApoA-I polypeptide can reside within the lipid bilayer, inducing an additional pressure between adjacent lipid chains. This limits chain movements and favors the more *ordered* CH bending mode in CH_2 with respect to that in CH_3. We also observed a reduction of C═C band, probably ascribed to

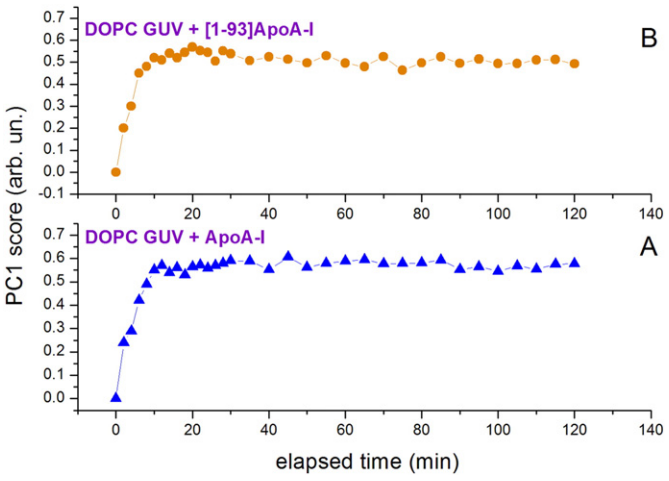

Fig. 6. Kinetic analysis of protein–DOPC–GUV interaction. PC1-score time evolution for a single optically trapped GUV interacting with [1-93]ApoA-I (A) and ApoA-I (B) molecules.

reduced mobility of C═C bonds due to the peptide residence in the *kink* region of lipid chains. Interestingly, our analyses on DOPC-–GUVs suggest the absence of a significant interaction of either [1-93]ApoA-I or ApoA-I with lipid polar heads. This could indicate that, in the fluid (L_α) phase, protein species tend to penetrate the membrane bilayer, instead of remaining in proximity to the lipid–water interface. This observation is also in agreement with the reported existence of plasma membrane areas endowed with high affinity for full-length ApoA-I [41], as well as with our previous results indicating that [1-93]ApoA-I polypeptide is efficiently internalized and subsequently degraded in target cells [42]. To our knowledge, the ability of the polypeptide to penetrate membrane fluid phases inducing an alignment of lipid chains has not been previously described. This indicates that the polypeptide may alter the bilayer mechanical stability, with effects similar to those induced by cholesterol [43–45], an event that might play an important role in the development of the pathology.

Globally, our observations, revealing the specific ability of a natively unfolded pathogenic polypeptide to insert in, and possibly to cross cell membranes, provide a contribute to shed light on the intriguing and still largely unknown molecular level details of its interaction with biological membranes.

References

[1] J. Fantini, N. Yahi, Expert Rev. Mol. Med. 12 (2010) e27.
[2] G. Shanmugam, R. Jayakumar, Biopolymers 76 (2004) 421–434.
[3] A. Kakio, Y. Yano, D. Takai, Y. Kuroda, O. Matsumoto, Y. Kozutsumi, K. Matsuzaki, J. Pept. Sci. 10 (2004) 612–621.
[4] X. Hou, S.J. Richardson, M.I. Aguilar, D.H. Small, Biochemistry 44 (2005) 11618–11627.
[5] A. Abedini, D.P. Raleigh, Protein Eng. Des. Sel. 22 (2009) 453–459.
[6] M. Zhu, A.L. Fink, J. Biol. Chem. 278 (2003) 16873–16877.
[7] L. Obici, G. Franceschini, L. Calabresi, S. Giorgetti, M. Stoppini, G. Merlini, V. Bellotti, Amyloid 13 (2006) 191–205.
[8] L. Obici, V. Bellotti, P. Mangione, M. Stoppini, E. Arbustini, L. Verga, I. Zorzoli, E. Anesi, G. Zanotti, C. Campana, M. Vigan, G. Merlini, Am. J. Pathol. 155 (1999) 695–702.
[9] M. Eriksson, S. Schönland, S. Yumlu, U. Hegenbart, H. von Hutten, Z. Gioeva, P. Lohse, J. Buttner, H. Schmidt, Röcken C., J. Mol. Diagn. 11 (2009) 257–262.
[10] E. Adachi, A. Kosaka, K. Tsuji, C. Mizuguchi, H. Kawashima, A. Shigenaga, K. Nagao, K. Akaji, A. Otaka, H. Saito, FEBS Lett. 588 (2014) 389–394.
[11] X. Mei, D. Atkinson, J. Biol. Chem. 286 (2011) 38570–38582.
[12] D.W. Borhani, D.P. Rogers, J.A. Engler, C.G. Brouillette, Proc. Natl. Acad. Sci. U. S. A. 94 (1997) 12291–12296.
[13] P.S. Chetty, L. Mayne, S. Lund-Katz, D. Stranz, S.W. Englander, M.C. Phillips, Proc. Natl. Acad. Sci. U. S. A. 106 (2009) 19005–19010.
[14] P. Mangione, M. Sunde, S. Giorgetti, M. Stoppini, G. Esposito, L. Gianelli, L. Obici, Protein Sci. 10 (2001) 187–199.
[15] S. Di Gaetano, F. Guglielmi, A. Arciello, P. Mangione, M. Monti, D. Pagnozzi, S. Raimondi, S. Giorgetti, S. Orrú, C. Canale, P. Pucci, C.M. Dobson, V. Bellotti, R. Piccoli, Biochem. Biophys. Res. Commun. 351 (2006) 223–228.
[16] D.M. Monti, F. Guglielmi, M. Monti, F. Cozzolino, S. Torrassa, A. Relini, P. Pucci, A. Arciello, R. Piccoli, Eur. Biophys. J. 39 (2010) 1289–1299.
[17] P.G. Frank, Y.L. Marcel, J. Lipid Res. 41 (2000) 853–872.
[18] M. Tanaka, P. Dhanasekaran, D. Nguyen, S. Ohta, S. Lund-Katz, M.C. Phillips, H. Saito, Biochemistry 45 (2006) 10351–10358.
[19] A. Moscho, O. Orwar, D.T. Chiu, B.P. Modi, R.N. Zare, Proc. Natl. Acad. Sci. U. S. A. 93 (1996) 11443–11447.
[20] Y. Sun, M. Hao, C.P. Liang, D.L. Silver, C. Cheng, F.R. Maxfield, A.R. Tall, J. Biol. Chem. 278 (2003) 5813–5820.
[21] Z.V. Leonenko, E. Finot, H. Ma, T.E.S. Dahms, D.T. Cramb, Biophys. J. 86 (2004) 3783–3793.
[22] N. Malagnino, G. Pesce, A. Sasso, E. Arimondo, Opt. Commun. 214 (2002) 15–24.
[23] G. Rusciano, A.C. De Luca, G. Pesce, A. Sasso, Anal. Chem. 79 (2007) 3708–3715.
[24] R.N. McElhaney, Biochim. Biophys. 864 (1986) 361–421.
[25] W. Hohlweg, S. Kosol, K. Zangger, Curr. Protein Pept. Sci. 13 (2012) 267–279.
[26] T. Parasassi, E.K. Krasnowska, L. Bagatolli, E. Gratton, J. Fluoresc. 8 (1988) 365–373.
[27] T.M. Ferreira, F. Coreta-Gomes, O.H. Samuli Ollila, M.J. Moreno, W.L.C. Vaz, D. Topgaarda, Phys. Chem. Chem. Phys. 15 (2013) 1976–1989.
[28] G. Rusciano, A.C. De Luca, G. Pesce, A. Sasso, Carbon 47 (2009) 2950–2957.
[29] I.T. Jolliffe, Principal Component Analysis, Springer Verlag, Berlin, 2002.
[30] G. Rusciano, Phys. Med. 26 (2010) 233–239.
[31] A.G. Lee, Lipid-protein interactions in biological membranes: a structural perspective, Biochim. Biophys. Acta 1612 (2003) 1–40.
[32] B.P. Gaber, P. Yanger, W.L. Peticolas, Biophys. J. 21 (1978) 161–176.
[33] B.P. Gaber, W.L. Peticolas, Biochim. Biophys. Acta 465 (1977) 260–274.
[34] Z.D. Schultz, I.W. Levin, Annu. Rev. Anal. Chem. 4 (2011) 343–366.
[35] Parker, F.S. Applications of Infrared, Raman and Resonance Raman Spectroscopy in Biochemistry, Plenum Press, New York and London.
[36] J.L.R. Arrondo, F.M. Goñi, Chem. Phys. Lipids 96 (1998) 53–68.
[37] T. Gilman, Kauffman J.W., H.J. Pownall, Biochemistry 20 (1981) 656–661.
[38] R. Del Giudice, A. Arciello, F. Itri, A. Merlino, M. Monti, M. Buonanno, A. Penco, D. Canetti, G. Petruka, S.M. Monti, A. Relini, P. Pucci, R. Piccoli, D.M. Monti, Biochim. Biophys. Acta 1860 (2016) 434–444.
[39] V. Trusova, G. Gorbenko, M. Girych, E. Adachi, C. Mizuguchi, R. Sood, P. Kinnunen, H. Saito, J. Fluoresc. 25 (2015) 253–261.
[40] P.T.T. Wong, H.H. Mantsch, Biophys. J. 54 (1988) 781–790.
[41] S.A. Sánchez, M.A. Tricerri, G. Ossato, Gratton. E., Biochim. Biophys. Acta 1798 (2010) 1399–1408.
[42] A. Arciello, N. De Marco, R. Del Giudice, F. Guglielmi, P. Pucci, A. Relini, D.M. Monti, R. Piccoli, J. Cell. Mol. Med. 15 (2011) 2652–2663.
[43] D.A. Pink, T.J. Green, D. Chapman, Biochemistry 19 (1980) 349–356.
[44] P.F. Almeida, Biophys. J. 100 (2011) 420–429.
[45] M.J.L. de Lange, M. Bonn, M. Muller, Chem. Phys. Lipids 146 (2007) 76–84.

Biochemical Pharmacology xxx (2017) xxx–xxx

Contents lists available at ScienceDirect

Biochemical Pharmacology

journal homepage: www.elsevier.com/locate/biochempharm

Novel human bioactive peptides identified in Apolipoprotein B: Evaluation of their therapeutic potential

Rosa Gaglione [a,b], Eliana Dell'Olmo [a], Andrea Bosso [b,c], Marco Chino [a], Katia Pane [c], Flora Ascione [d], Francesco Itri [a], Sergio Caserta [d,e,f], Angela Amoresano [a], Angelina Lombardi [a], Henk P. Haagsman [b], Renata Piccoli [a,g], Elio Pizzo [c], Edwin J.A. Veldhuizen [b], Eugenio Notomista [c], Angela Arciello [a,g,*]

[a] Department of Chemical Sciences, University of Naples Federico II, 80126 Naples, Italy
[b] Department of Infectious Diseases and Immunology, Division Molecular Host Defence, Faculty of Veterinary Medicine, Utrecht University, Utrecht, The Netherlands
[c] Department of Biology, University of Naples Federico II, 80126 Naples, Italy
[d] Department of Chemical, Materials and Production Engineering, University of Naples Federico II, 80125 Naples, Italy
[e] CEINGE Biotecnologie Avanzate, Via Sergio Pansini, 5, 80131 Naples, Italy
[f] Consorzio Interuniversitario Nazionale per la Scienza e Tecnologia dei Materiali (INSTM), UdR INSTM Napoli Federico II, P.le Tecchio, 80, 80125 Naples, Italy
[g] Istituto Nazionale di Biostrutture e Biosistemi (INBB), Italy

ARTICLE INFO

Article history:
Received 2 December 2016
Accepted 23 January 2017
Available online xxxx

Keywords:
Host defence peptides
Apolipoprotein B
Immunomodulation
Lipopolysaccharide
Bacterial biofilm
Combination therapy
Wound healing
Biocompatibility

ABSTRACT

Host defence peptides (HDPs) are short, cationic amphipathic peptides that play a key role in the response to infection and inflammation in all complex life forms. It is increasingly emerging that HDPs generally have a modest direct activity against a broad range of microorganisms, and that their anti-infective properties are mainly due to their ability to modulate the immune response. Here, we report the recombinant production and characterization of two novel HDPs identified in human Apolipoprotein B (residues 887–922) by using a bioinformatics method recently developed by our group. We focused our attention on two variants of the identified HDP, here named r(P)ApoB$_L$ and r(P)ApoB$_S$, 38- and 26-residue long, respectively. Both HDPs were found to be endowed with a broad-spectrum antimicrobial activity while they show neither toxic nor haemolytic effects towards eukaryotic cells. Interestingly, both HDPs were found to display a significant anti-biofilm activity, and to act in synergy with either commonly used antibiotics or EDTA. The latter was selected for its ability to affect bacterial outer membrane permeability, and to sensitize bacteria to several antibiotics. Circular dichroism analyses showed that SDS, TFE, and LPS significantly alter r(P)ApoB$_L$ conformation, whereas slighter or no significant effects were detected in the case of r(P)ApoB$_S$ peptide. Interestingly, both ApoB derived peptides were found to elicit anti-inflammatory effects, being able to mitigate the production of pro-inflammatory interleukin-6 and nitric oxide in LPS induced murine macrophages. It should also be emphasized that r(P)ApoB$_L$ peptide was found to play a role in human keratinocytes wound closure *in vitro*. Altogether, these findings open interesting perspectives on the therapeutic use of the herein identified HDPs.

1. Introduction

The excessive and sometimes improper use of antibiotics has been responsible for the development of resistant bacterial isolates, the so-called 'superbugs', such as methicillin-resistant *Staphylococcus aureus* (MRSA) [1], vancomycin-resistant enterococci (VRE), and multidrug-resistant *Pseudomonas*, *Klebsiella*, and *Acinetobacter* [2]. This made the search for novel antimicrobial therapies and approaches imperative. In this scenario, the broad immunomodulatory properties of naturally occurring host defence peptides (HDPs) have attracted considerable attention. HDPs, also known as antimicrobial peptides (AMPs), are evolutionarily conserved molecules of the innate immune system. They are a

Abbreviations: MRSA, methicillin-resistant *Staphylococcus aureus*; VRE, vancomycin-resistant enterococci; HDPs, host defence peptides; AMPs, antimicrobial peptides; LPS, lipopolysaccharide; ApoE, Apolipoprotein E; ApoB, Apolipoprotein B; LDL, low-density lipoprotein; IL-10, interleukin-10; MIC, minimal inhibitory concentration; TSA, Tryptic Soy Agar; AS, absolute score; MHB, Muller Hinton Broth; NB, Nutrient Broth; IPTG, isopropyl-β-D-thiogalactopyranoside; TFE, trifluoroethanol; SDS, sodium dodecyl sulfate; FIC, fractional inhibitory concentration; EDTA, ethylenediaminetetraacetic acid; IL-6, interleukin-6; NO, nitric oxide; CATH-2, cathelicidin-2; ONC, onconase; PBS, phosphate-buffered saline; CD, circular dichroism; MTT, 3-(4,5-dimethylthiazol-2-yl)-2,5-diphenyltetrazolium bromide; MALDI-MS, matrix assisted laser desorption ionisation mass spectrometry; RBCs, red blood cells; WH, wound healing.

* Corresponding author at: Department of Chemical Sciences, University of Naples Federico II, 80126 Naples, Italy
E-mail address: anarciel@unina.it (A. Arciello).

http://dx.doi.org/10.1016/j.bcp.2017.01.009
0006-2952/

key element of the ancient, nonspecific innate defence system in most multicellular organisms, representing the first line of defence against invading microbes [3,4]. Found in all complex living organisms, HDPs have first attracted considerable attention for their modest antimicrobial activity directed towards a broad spectrum of pathogens including bacteria, viruses, fungi, and protozoa [3,4]. Natural HDPs have a size ranging from 12 to 50 amino acids, are mostly cationic owing to the presence of high levels of lysine and arginine residues, and contain over 50% hydrophobic amino acids [3,5]. These properties are at the basis of HDPs' ability to interact with membranes, and, in some cases, to penetrate cell membranes. In model systems, HDPs associate preferentially with negatively charged membranes of bacteria-like composition, but many peptides are also able to translocate into host cells. To date, the molecular bases of their selectivity towards bacterial membranes are still poorly understood [6]. It has been suggested that HDPs tend to translocate into bacterial cells owing to the presence of a large electrical potential gradient [7]. However, although HDPs' direct antimicrobial mechanism of action against bacteria mainly involves interaction with the bacterial membrane, multiple targets have been identified, such as cell wall peptidoglycans, cytosolic RNA, proteins, or cytosolic enzymes/chaperones [6,8]. Hence, the selection of resistance mechanisms in bacteria is improbable, since the removal of a single target, *e.g.* by mutation, would still allow other targets to mediate HDPs direct killing activity [8]. However, it is becoming increasingly evident that these peptides are endowed with a wide range of biological activities, such as multispecies anti-biofilm properties, modulation of innate immune response, and anticancer, analgesic, antioxidant and anti-inflammatory activities [3,9–13]. Therefore, although these bioactive peptides were often named AMPs, more recently they have been termed as HDPs to describe more appropriately the breadth of their activities [14]. Due to HDPs' multifunctional properties, as well as to the increased bacterial resistance to conventional antibiotics, these peptides have great chance to be used as anti-infective and immunomodulatory therapeutics. Although very few HDPs are currently in use in the market, many of them are progressing through clinical trials for the treatment of diseases including microbial infections, organ failure, immune disorders, wound healing, diabetes and cancer [15,16]. Currently, most of the therapies based on HDPs that have entered clinical trials were designed for topical applications [17], presumably due to issues concerning their stability and toxicity [18].

Natural cationic HDPs are encoded by genes from many organisms. In mammals, HDPs are expressed in a variety of cell types including monocytes/macrophages, neutrophils, epithelial cells, keratinocytes, and mast cells [19–21]. They are usually synthesized as pro-peptides from which mature and biologically active HDPs are released by bacterial and/or host proteases [20]. Apolipoproteins are a source of bioactive peptides. Previous reports have shown that peptides derived from the cationic receptor binding region of Apolipoprotein E (ApoE141-149) are endowed with broad anti-infective activity [22]. Apolipoprotein B (ApoB) also contains two LDL (low-density lipoprotein) receptor binding domains, namely region A (ApoB3147-3157) and region B (ApoB3359-3367). Region B, more uniformly conserved across species and primarily involved in receptor binding, has been found to be endowed with a significant antiviral activity [22]. Moreover, peptides derived from ApoB have been already used in vaccine preparations to treat atherosclerosis [23]. When ApoE deficient mice have been immunized with ApoB661–680 and ApoB3136–3155 peptides, a significant increase of the levels of peptide-specific immunoglobulins was detected accompanied by a concomitant increase of secreted interleukin-10 (IL-10) levels, with no effect on IFN-γ expression levels, thus indicating that ApoB derived peptides are able to modulate the immune response [23].

Recently, our group developed an *in silico* method [K. Pane et al. submitted, 24] to identify HDPs in protein precursors and to predict quantitatively their antibacterial activity. This method assigns to any given peptide an antimicrobial score, called "absolute score" (AS), on the basis of net charge, hydrophobicity and length of the peptide and of two bacterial strain-dependent weight factors defining the contribution of charge and hydrophobicity to the antimicrobial activity. We demonstrated that AS is directly proportional to the antimicrobial activity of HDPs expressed as Log(1000/MIC), where MIC is the minimal inhibitory concentration of the peptide. Score values lower than 6.5 are considered not significant as they correspond to predicted MIC values higher than 200 μM, while for score values higher than about 10 the linear relationship is no longer valid, and an increase in the score does not necessarily correspond to a concomitant increase in the antimicrobial activity. In order to analyse a protein potentially bearing hidden antimicrobial regions, the AS values of all the peptides of the desired length contained in a precursor protein can be plotted as a function of peptide sequence and length, thus obtaining an accurate map of the antimicrobial activity determinants. This method allows the identification of novel HDPs within the sequence of known proteins ("cryptic" HDPs), as demonstrated by the identification of a novel cationic HDP endowed with antibacterial and immunomodulatory activities in human ApoE [24], and in the transcription factor Stf76 from the archaeon *Sulfolobus islandicus*. In the last case, peptide VVL-28 represents the first antimicrobial peptide derived from an archaeal protein [25].

On the basis of the interesting results obtained in the case of human ApoE, we applied our *in silico* analysis method to a human Apolipoprotein B (ApoB) isoform [26,27]. In Fig. 1, the isometric plot of region 882–929 of this ApoB variant is shown. An absolute maximum, corresponding to region 887–922 (AS = 12.0), and a relative maximum, corresponding to residues 887–909 (AS = 10.6), are shown (Fig. 1). Even if several ApoB functional regions have already been analysed, and in some cases biologically active peptides were obtained [22,23], to the best of our knowledge, this is the first report identifying ApoB region 887–922 as a source of HDPs.

Here, we report the recombinant production and characterization of two variants of the putative HDP identified by our bioinformatics method in human ApoB, *i.e.* peptides ApoB887-923 and ApoB887-911. Both peptides include at the C-terminal side one (as in the case of ApoB887-923), or two (as in the case of ApoB887-911) small uncharged residues (serine, glycine or threonine), which are not present in the regions highlighted in the AS plot (Fig. 1). These residues have been arbitrarily included to avoid that the negatively charged C-terminus of the peptide is adjacent to the antimicrobial region.

To evaluate the therapeutic potential of these peptides, we analysed their structure, antimicrobial and anti-biofilm activities, the ability to act in synergy with conventional antibiotics, their anti-inflammatory and wound healing properties, and their possible toxic effects on eukaryotic cells.

2. Materials and methods

2.1. Bacterial strains and growth conditions

Eight bacterial strains were used in the present study, *i.e. E. coli* ATCC 25922, methicillin-resistant *Staphylococcus aureus* (MRSA WKZ-2), *Salmonella enteriditis* 706 RIVM, *Bacillus globigii* TNO BM013, *Bacillus licheniformis* ATTC 21424, *Staphylococcus aureus* ATTC 29213, *Pseudomonas aeruginosa* ATCC 27853, and *Pseudomonas aeruginosa* PAO1. All bacterial strains were grown in Muller Hinton Broth (MHB, Becton Dickinson Difco, Franklin Lakes, NJ)

Please cite this article in press as: R. Gaglione et al., Novel human bioactive peptides identified in Apolipoprotein B: Evaluation of their therapeutic potential, Biochem. Pharmacol. (2017), http://dx.doi.org/10.1016/j.bcp.2017.01.009

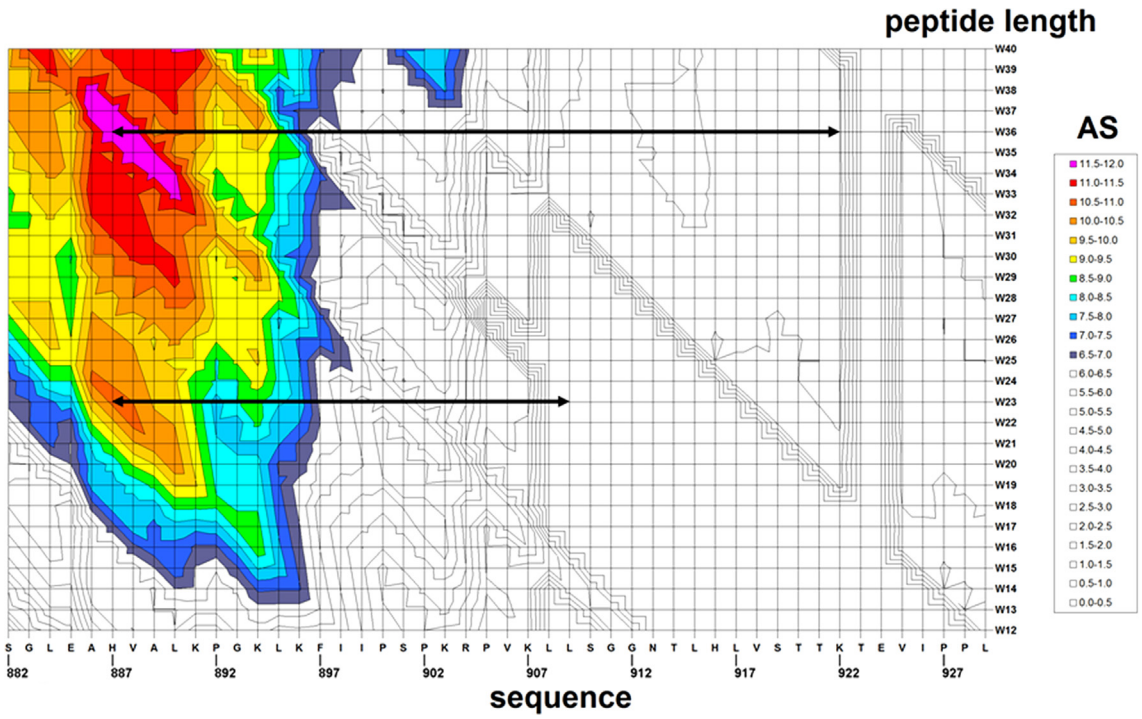

Fig. 1. Isometric plot showing the absolute score values (AS) of peptides with a length ranging from 12 to 40 residues (W12-W40) in the region 882–929 of ApoB. Colors were used to highlight AS values higher than 6.5, and corresponding to predicted MIC values on *S. aureus* lower than 200 μM.

and on Tryptic Soy Agar (TSA; Oxoid Ltd., Hampshire, UK). In all the experiments, bacteria were inoculated and grown overnight in MHB at 37 °C. The next day, bacteria were transferred to a fresh MHB tube and grown to mid-logarithmic phase.

2.2. Cell culture

Murine RAW 264.7 cells, malignant SVT2 murine fibroblasts (BALBc 3T3 cells transformed by SV40 virus), parental murine BALBc 3T3 cells, and human HeLa and HaCaT cells were from ATCC, Manassas, VA. Cells were cultured in Dulbecco's modified Eagle's medium (Sigma Aldrich, Milan, Italy), supplemented with 10% foetal bovine serum (HyClone, GE Healthcare Lifescience, Chicago, IL) and antibiotics, in a 5% CO_2 humidified atmosphere at 37 °C.

2.3. Synthetic peptides

CATH-2 peptide was obtained from CPC Scientific Inc. (Sunnyvale, USA), and LL-37 peptide was from Sigma Aldrich, Milan, Italy.

2.4. Expression ad isolation of recombinant ApoB derived peptides

Expression and isolation of recombinant peptides was carried out as previously described [24,28]. Briefly, *E. coli* BL21(DE3) cells were transformed with pET recombinant plasmids, and grown in 10 mL of Terrific Broth medium (TB) containing 100 μg/mL of ampicillin, at 37 °C up to OD_{600nm} of 2. These cultures were used to inoculate 1 L of TB/ampicillin medium. Glucose at final concentration of 4 g/L was added to cultures to limit protein expression before induction with IPTG. Cultures were incubated at 37 °C up to OD_{600nm} of 3.5–4. Expression of recombinant proteins was induced by addition of IPTG (isopropyl-β-D-thiogalactopyranoside) at final concentration of 0.7 mM. Cells were harvested after overnight induction by centrifugation at 8,000*g* for 15 min at 4 °C and washed with 50 mM Tris–HCl buffer pH 7.4. The bacterial pellet was suspended in 50 mM Tris-HCl buffer pH 7.4 containing 10 mM ethylenediaminetetraacetic acid (EDTA), and sonicated in a cell disruptor (10 x 1 min cycle, on ice). The suspension was then centrifuged at 18,000*g* for 60 min at 4 °C. The insoluble fractions were washed three times in 0.1 M Tris–HCl buffer pH 7.4 containing 10 mM EDTA, 2% Triton X-100, and 2 M urea, followed by repeated washes in 0.1 M Tris–HCl buffer pH 7.4. Following washing steps, 100 mg of fusion proteins were dissolved in 10 mL of denaturing buffer (6 M guanidine/HCl in 50 mM Tris–HCl, pH 7.4) containing 10 mM β-mercaptoethanol. Mixtures were incubated at 37 °C for 3 h under nitrogen atmosphere on a rotary shaker, and then centrifuged at 18,000*g* for 60 min at 4 °C. Soluble fractions were then collected and purified by affinity chromatography on Ni Sepharose™ 6 Fast Flow resin (GE Healthcare Lifescience, Chicago, IL). The chromatographic fractions were analysed by 15% SDS/PAGE, pooled, and extensively dialyzed against 0.1 M acetic acid pH 3 at 4 °C. Any insoluble material was removed by centrifugation and filtration. The sample containing the fusion construct was then acidified to pH 2.0 by the addition of 0.6 M HCl to allow the cleavage of Asp-Pro linker peptide, purged with N_2, and incubated at 60 °C for 24 h in a water bath. The pH was then increased to 7–7.2 by the addition of 1 M NH_3, and incubated overnight at 28 °C to selectively precipitate the carrier ONC-DCless-H6, that is insoluble at neutral or alkaline pH values. The peptides were isolated from insoluble components by repeated cycles of centrifugation, and finally lyophilized. Their purity was checked by SDS/PAGE and mass spectrometry analyses. Lyophilized peptides were then dissolved in pure water, unless differently specified, and quantified by BCA assay (ThermoFisher Scientific, Waltham, MA).

2.5. Mass spectrometry analyses

Matrix-assisted laser desorption/ionisation mass spectrometry (MALDI-MS) was carried out on a 4800 Plus MALDI TOF/TOF mass spectrometer (Applied Biosystems, Framingham, MA) equipped with a nitrogen laser (337 nm). The peptide samples (1 mL) were mixed (1:1, v/v) with a 10 mg/mL solution of a-cyano-4-

Please cite this article in press as: R. Gaglione et al., Novel human bioactive peptides identified in Apolipoprotein B: Evaluation of their therapeutic potential, Biochem. Pharmacol. (2017), http://dx.doi.org/10.1016/j.bcp.2017.01.009

hydroxycinnamic acid in acetonitrile/50 mM citrate buffer (70:30 v/v). Mass calibration was performed using external peptide standards purchased from Applied Biosystems, Framingham, MA. Spectra were acquired using 5,000 shots/spectrum in a mass (m/z) range of 1,000–5,000 amu and raw data were analysed using Data Explorer Software provided by the manufacturer.

2.6. Circular dichroism spectroscopy

CD experiments were performed on a Jasco J-815 circular dichroism spectropolarimeter, calibrated for intensity with ammonium [D10] camphorsulfonate ($[\theta_{290.5}] = 7{,}910$ deg cm^2 dmol^{-1}). The cell path length was 0.01 cm. CD spectra were collected at 25 °C in the 190–260 nm (far-UV) at 0.2 nm intervals, with a 20 nm/min scan rate, 2.5 nm bandwidth and a 16 s response. Spectra are reported in terms of mean residue ellipticity, calculated by dividing the total molar ellipticity by the number of amino acids in the molecule. Each spectrum was corrected by subtracting the background, and reported without further signal processing. Lyophilized peptides were dissolved in ultra-pure water (Romil, Waterbeach, Cambridge, GB) at a concentration of 100 μM, determined on the basis of peptide dry weight and BCA assay (ThermoFisher Scientific, Waltham, MA). CD spectra of the peptides were collected in the absence or in the presence of increasing concentrations of trifluoroethanol (TFE, Sigma Aldrich, Milan, Italy), SDS (Sigma Aldrich, Milan, Italy) or lipopolysaccharide (LPS) from *E.coli* 0111:B4 strain (Sigma Aldrich, Milan, Italy). CD spectra were corrected by subtracting every time the contribution of the compound under test at any given concentration. CD spectra deconvolution was performed by using the program PEPFIT, that is based on peptide-derived reference spectra [29], in order to estimate secondary structure contents. A Microsoft Excel-ported version of PEPFIT was used for convenience [30].

2.7. Measurement of IL-6 release

IL-6 levels were determined by ELISA assay (DuoSet ELISA kits, R&D Systems, Minneapolis, MN) following the manufacturer's instructions. Briefly, RAW 264.7 cells (5×10^4) were seeded into 96-well microtiter plates, and grown to semi-confluency. After 24 h, the culture medium was replaced with fresh medium containing the peptide under test (5 or 20 μM) in the presence or in the absence of LPS from *Salmonella Minnesota* (50 ng/mL, Sigma Aldrich, Milan, Italy) for 24 h at 37 °C. When the protective effect of peptides was evaluated, cells were pre-incubated with the peptide under test (5 or 20 μM) for 2 h at 37 °C. Following treatment, cells were washed three times with PBS prior to incubation with LPS (50 ng/mL) for further 24 h at 37 °C. In each case, at the end of incubation, the culture supernatants were collected, and centrifuged at 5,000 rpm for 3 min at room temperature, in order to remove cell debris. Samples were then analysed by reading absorbance values at 450 nm using 550 nm as a reference wavelength at an automatic plate reader (FLUOstar Omega, BMG LABTECH, Ortenberg, Germany).

2.8. Determination of NO production

To determine the levels of NO released by RAW 264.7 cells, a colorimetric assay based on the use of Griess reagent (Sigma Aldrich, Milan, Italy) was performed. The levels of nitrite (NO^{2-}) in cell supernatants were determined on the basis of a reference curve obtained by testing increasing concentrations (from 1 to 50 μM) of sodium nitrite dissolved in water. Briefly, cell culture supernatants were mixed with equal volumes of 1% sulphanilamide dissolved in 2.5% phosphoric acid, and incubated for 5 min at room temperature. Samples were then diluted 1:1 (v/v) with 0.1% N-(1-naphthyl) ethylenediamine dihydrochloride, and incubated for further 5 min at room temperature. Absorbance values were then determined at 520 nm using an automatic plate reader (FLUOstar Omega, BMG LABTECH, Ortenberg, Germany).

2.9. Antimicrobial activity assay

The antimicrobial activity of ApoB derived peptides was tested towards eight bacterial strains, *i.e. E. coli* ATCC 25922, methicillin-resistant *Staphylococcus aureus* (MRSA WKZ-2), *Salmonella enteriditis* 706 RIVM, *Bacillus globigii* TNO BM013, *Bacillus licheniformis* ATCC 21424, *Staphylococcus aureus* ATCC 29213, *Pseudomonas aeruginosa* ATCC 27853, and *Pseudomonas aeruginosa* PAO1. In each case, bacteria were grown to mid-logarithmic phase in MHB at 37 °C. Cells were then diluted to 2×10^6 CFU/mL in Nutrient Broth (Difco, Becton Dickinson, Franklin Lakes, NJ) containing increasing amounts of either r(P)ApoB$_L$ or r(P)ApoB$_S$ peptide (0,625–40 μM). In each case, starting from a peptide stock solution, twofold serial dilutions were sequentially carried out, accordingly to broth microdilution method [31]. Following overnight incubation, MIC_{100} values were determined as the lowest peptide concentration responsible for no visible bacterial growth.

2.10. Killing kinetics studies

To kinetically analyse bacterial killing by ApoB derived peptides, experiments were performed on *E. coli* ATTC 25922 and *Bacillus licheniformis* ATTC 21424 strains. To this purpose, bacteria were grown overnight in MHB medium, then diluted in fresh MHB, and incubated at 37 °C until logarithmic phase of growth was reached. Bacteria were then diluted to 4×10^6 CFU/mL in a final volume of 150 μL of Nutrient Broth 0.5X (Difco, Becton Dickinson, Franklin Lakes, NJ), and mixed with the peptide under test (1:1 v/v). For each strain, increasing concentrations of peptide were analysed (ranging from 0 to 20 μM or from 0 to 10 μM in the case of *E. coli* ATTC 25922 and *Bacillus licheniformis* ATTC 21424 strains, respectively). At defined time intervals, samples (20 μL) were serially diluted (from 10- to 10,000-fold), and 100 μL of each dilution was plated on TSA. Following an incubation of 16 h at 37 °C, bacterial colonies were counted.

2.11. Synergy evaluation

Synergism between ApoB derived peptides and antimicrobial agents was assessed by the so called "checkerboard" assay against *S. aureus* MRSA WKZ-2, *E. coli* ATCC 25922, *P. aeruginosa* ATCC 27853, *P. aeruginosa* PAO1, and *S. aureus* ATCC 29213 strains. To this purpose, ApoB derived peptides were tested in combination with EDTA or antibiotics, such as ciprofloxacin, colistin, erythromycin, kanamycin sulfate, and vancomycin. All these antimicrobial agents were from Sigma Aldrich, Milan, Italy. Twofold serial dilutions of each ApoB derived peptide and each antimicrobial agent were tested in combination on each strain tested. To do this, we tested peptide concentrations ranging from 0 to 20 μM. Compound concentrations tested on each strain are reported in Table 1. The fractional inhibitory concentration (FIC) index was calculated as follows: $FIC_A + FIC_B$, where FIC_A = MIC of drug A in combination/MIC of drug A alone, and FIC_B = MIC of drug B in combination/MIC of drug B alone. FIC indexes $\leqslant 0.5$ were classified as synergism, whereas FIC indexes between 0.5 and 4 were associated to additive or "no interaction" effects [32]. Antagonism is usually associated to a FIC index > 4.

Please cite this article in press as: R. Gaglione et al., Novel human bioactive peptides identified in Apolipoprotein B: Evaluation of their therapeutic potential, Biochem. Pharmacol. (2017), http://dx.doi.org/10.1016/j.bcp.2017.01.009

Table 1
Range of antimicrobial agent concentrations tested on each strain for combination therapy analyses.

	S. aureus ATCC 29213	*S. aureus* MRSA WKZ-2	*P. aeruginosa* ATCC 27853	*P. aeruginosa* PAO1	*E. coli* ATCC 25922
Ciprofloxacin	0–0,5 μg/mL	0–1 μg/mL	0–2 μg/mL	0–1 μg/mL	0–0,03 μg/mL
Colistin	0–8 μg/mL	0–8 μg/mL	0–4 μg/mL	0–4 μg/mL	0–8 μg/mL
Erythromycin	0–4 μg/mL	0–4 μg/mL	0–16 μg/mL	0–128 μg/mL	0–128 μg/mL
Vancomycin	0–0,25 μg/mL	0–0,5 μg/mL	0–32 μg/mL	0–4 μg/mL	0–0,25 μg/mL
Kanamycin	0–0,5 μg/mL	0–0,125 μg/mL	0–64 μg/mL	0–8 μg/mL	0–0,125 μg/mL
EDTA	0–24,53 μg/mL	0–49,07 μg/mL	0–392,5 μg/mL	0–196,2 μg/mL	0–98,14 μg/mL

Each antimicrobial agent was tested for synergistic effects with ApoB derived peptides (0–20 μM) within the concentration range listed in the table, depending from the sensitivity of the specific bacterial strain.

2.12. Anti-biofilm activity

Anti-biofilm activity of ApoB derived peptides was tested on *S. aureus* MRSA WKZ-2, *E. coli* ATCC 25922, *P. aeruginosa* ATCC 27853, and *P. aeruginosa* PAO1 strains. Bacteria were grown overnight in MHB (Becton Dickinson Difco, Franklin Lakes, NJ), and then diluted to 1×10^8 CFU/mL in BM2 medium [33] containing increasing peptide concentrations (0–1 μM). Incubations with the peptides were carried out either for 4 h, in order to test peptide effects on biofilm attachment, or for 24 h, in order to test peptide effects on biofilm formation. When peptide effects on preformed biofilm were evaluated, bacterial biofilms were formed for 24 h at 37 °C, and then treated with increasing concentrations (0–1 μM) of the peptide under test. In all the cases, at the end of the incubation, the crystal violet assay was performed. To do this, the planktonic culture was removed from the wells, which were washed three times with sterile PBS prior to staining with 0.04% crystal violet (Sigma Aldrich, Milan, Italy) for 20 min. The colorant excess was eliminated by three successive washes with sterile PBS. Finally, the crystal violet was solubilised with 33% acetic acid and samples optical absorbance values were determined at 630 nm by using a microtiter plate reader (FLUOstar Omega, BMG LABTECH, Germany). To determine the percentage of viable bacterial cells inside the biofilm structure, upon biofilm disruption with 0,1% Triton X-100 (Sigma Aldrich, Milan, Italy), bacterial cells were ten-fold diluted on solid TSA and incubated for 16 h at 37 °C. Once evaluated the number of colony forming units, bacterial cell survival was calculated as follows: $(CFU_{\text{in treated sample}}/CFU_{\text{in untreated sample}}) \times 100$.

2.13. Cytotoxicity assays

Cytotoxic effects of ApoB derived peptides on RAW 264.7 cells were determined by using the cell proliferator reagent WST-1 (Roche Applied Science, Mannheim, Germany). To this purpose, RAW 264.7 cells were plated into 96-well plates at a density of 5×10^4 cells in 100 μL medium per well, and incubated overnight at 37 °C. Afterwards, cells were treated with increasing concentrations (0–20 μM) of the peptide under test for 24 h at 37 °C. Following incubation, peptide-containing medium was removed, and 100 μL of fresh medium containing 10% WST-1 reagent was added to each well. Following an incubation of 30 min at 37 °C in the dark, sample absorbance values were measured at 450 nm using 650 nm as a reference wavelength at a microtiter plate reader (FLUOstar Omega, BMG LABTECH, Germany).

Cytotoxic effects of peptides on the viability of malignant SVT2 murine fibroblasts, parental murine BALBc 3T3 fibroblasts, human HeLa cells, and human HaCaT keratinocytes were determined by using the 3-(4,5-dimethylthiazol-2-yl)-2,5-diphenyltetrazolium bromide (MTT) assay (Sigma Aldrich, Milan, Italy), as previously described [34]. Briefly, cells were seeded into 96-well plates at a density of 5×10^3/well in 100 μL medium per well, and incubated overnight at 37 °C. Afterwards, cells were treated with increasing concentrations (0–20 μM) of the peptide under test for 24 h at 37 °C. Following incubation, the peptide-containing medium was removed, and 100 μL of MTT reagent, dissolved in DMEM without phenol red (Sigma Aldrich, Milan, Italy), were added to the cells (100 μL/well) at a final concentration of 0.5 mg/mL. After 4 h at 37 °C, the culture medium was removed and the resulting formazan salts were dissolved by the addition of isopropanol containing 0.1 N HCl (100 μL/well). Absorbance values of blue formazan were determined at 570 nm using an automatic plate reader (Microbeta Wallac 1420, Perkin Elmer).

In all the cases, cell survival was expressed as the percentage of viable cells in the presence of the peptide under test, with respect to control cells grown in the absence of the peptide.

2.14. Haemolytic activity

The release of haemoglobin from mouse erythrocytes was used as a measure for the haemolytic activity of ApoB derived peptides. To do this, EDTA anti-coagulated mouse blood was centrifuged for 10 min at 800*g* at 20 °C, in order to obtain red blood cells (RBCs), which were washed three times, and 200-fold diluted in PBS. Subsequently, 75 μL aliquots of RBCs were added to 75 μL peptide solutions (final concentration ranging from 0 to 20 μM) in 96-well microtiter plates, and the mixture was incubated for 1 h at 37 °C. Following the incubation, the plate was centrifuged for 10 min at 1,300*g* at 20 °C, and 100 μL supernatant of each well were transferred to a new 96-well plate. Absorbance values were determined at 405 nm by using an automatic plate reader (FLUOstar Omega, BMG LABTECH, Germany), and the percentage of haemolysis was calculated by comparison with the control samples containing no peptide (negative control) or 0.2% (v/v) Triton X-100 (positive control, complete lysis). Haemolysis (%) = $[(Abs_{405\ nm}\ \text{peptide} - Abs_{405\ nm}\ \text{negative control})/(Abs_{405\ nm}\ 0.2\%\ \text{Triton} - Abs_{405\ nm}\ \text{negative control})] \times 100$.

2.15. Wound healing assay

Wound healing activity of r(P)ApoB$_L$ peptide was evaluated *in vitro* as previously described [35]. Human HaCaT keratinocytes were seeded into 12-well plates at a density of 6.3×10^5 cells/well in 1 mL medium per well. Following an incubation of 24 h at 37 °C, cells were pre-treated with 3 μM mitomycin C for 30 min, in order to inhibit cell proliferation [36]. Cell monolayers were then wounded with a pipette tip to remove cells from a specific region of the monolayer. The culture medium was then removed and the cells were washed twice with PBS. Cells were then incubated with fresh culture medium containing increasing concentrations of r(P)ApoB$_L$ peptide (0–0.5–10–20 μM). Wound closure was then followed by multiple field time-lapse microscopy (TLM) experiments, using an inverted microscope (Zeiss Axiovert 200, Carl Zeiss, Germany) equipped with an incubator to control temperature, humidity and CO_2 percentage [37,38]. Images were iteratively acquired in phase contrast with a CCD video camera (Hamamatsu

Orca AG, Japan) by using a 5× objective. The microscope was also equipped with a motorized stage and focus control (Marzhauser, Germany) enabling automated positioning of the acquired samples. The workstation was controlled through a homemade software in Labview. Each cell sample was analysed in duplicate, and in any case at least two fields of view were selected. Since three independents experiments were carried out, from 8 to 12 independent fields of view were analysed for each sample. The delay between consecutive imaging of the same field of view was set to 15 min. The wound closure dynamics were quantified by using a homemade automated image analysis software, that allowed to measure the size of the wound area for each time point (A). For each field of view, determined values were normalized with respect to the value of the wound area at time 0 (A_0), and plotted as function of time. After an initial lag phase, the wound area was found to decrease with a constant velocity [39,40]. By reporting A/A_0 values as a function of time, a linear decrease was observed for A/A_0 values lower than 0.8 (Fig. 9b). For each sample, the lag time t_L was calculated as the time required to obtain an initial wound closure corresponding to $A/A_0 = 0.8$. Being R^2 typically higher than 0.98, the linear range of the curve was fitted, and the slope ($-\alpha$) was considered a measure of the wound closure velocity. The values of wound closure velocity obtained for each field of view from three independent experiments were averaged (α), and normalized with respect to the value of the corresponding control sample (α_{contr}). For each peptide concentration tested, α/α_{contr} values obtained from three independent experiments were averaged and the standard error of the mean was calculated to account for reproducibility [41].

2.16. Statistical analysis

Statistical analysis was performed using a Student's *t*-Test. Significant differences wereindicated as $^{*}(P < 0.05)$, $^{**}(P < 0.01)$ or $^{***}(P < 0.001)$.

3. Results

3.1. Recombinant production of ApoB derived peptides

Expression of HDPs in bacterial cells can be deleterious to the host due to their toxicity. For this reason, we used a procedure to produce HDPs as fusion proteins with onconase (ONC), a frog ribonuclease that mediates the delivery to inclusion bodies very efficiently, as previously described [24,27], thus avoiding toxicity problems. DNA sequences encoding peptide ApoB887-923 or

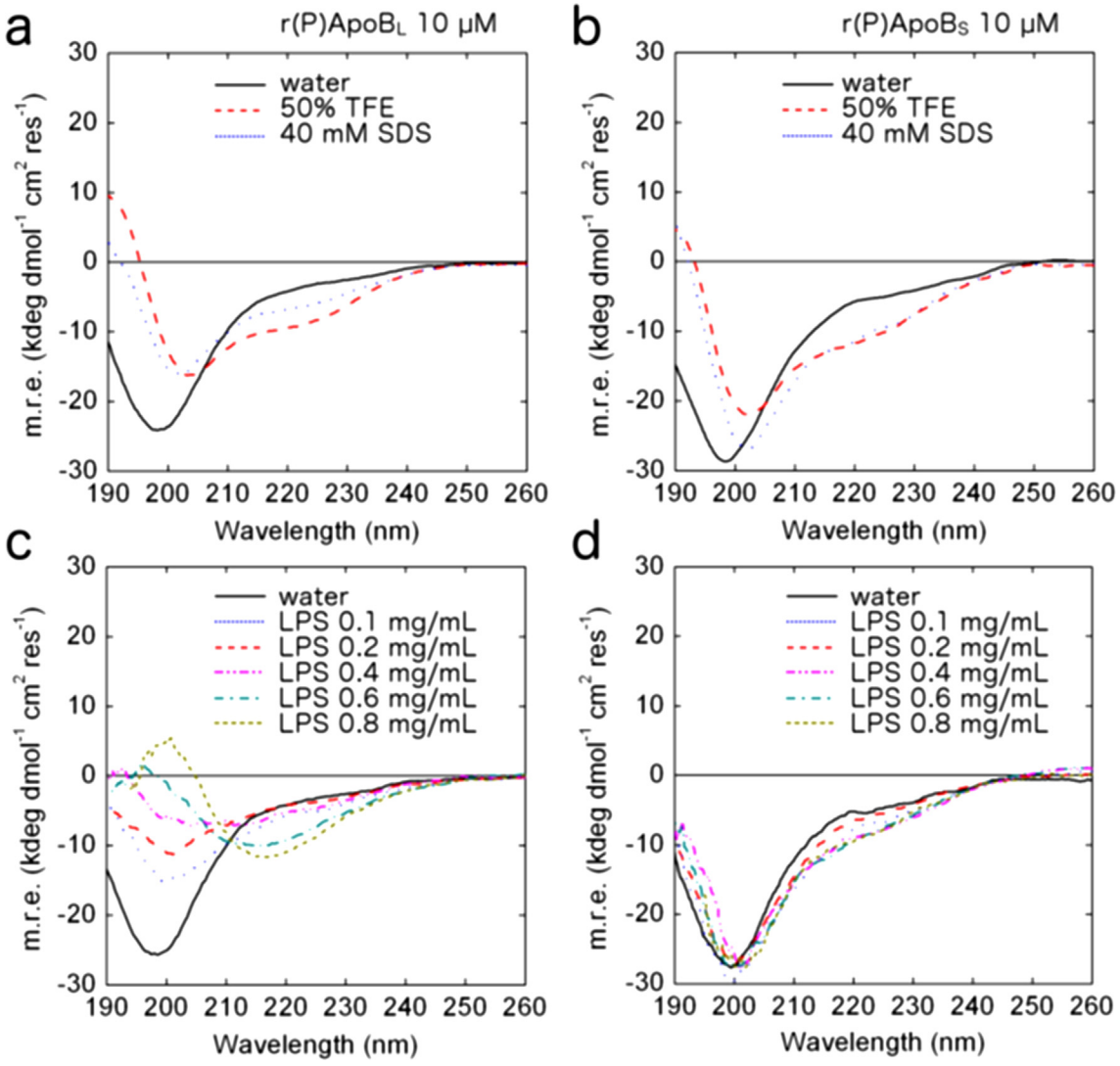

Fig. 2. Far-UV CD spectra of recombinant peptides r(P)ApoB$_L$ (a, c) and r(P)ApoB$_S$ (b, d) at a concentration of 10 μM in the presence of increasing concentrations of membrane-mimicking agents TFE or SDS at micellar concentrations (a, b) or of LPS (c, d).

Please cite this article in press as: R. Gaglione et al., Novel human bioactive peptides identified in Apolipoprotein B: Evaluation of their therapeutic potential, Biochem. Pharmacol. (2017), http://dx.doi.org/10.1016/j.bcp.2017.01.009

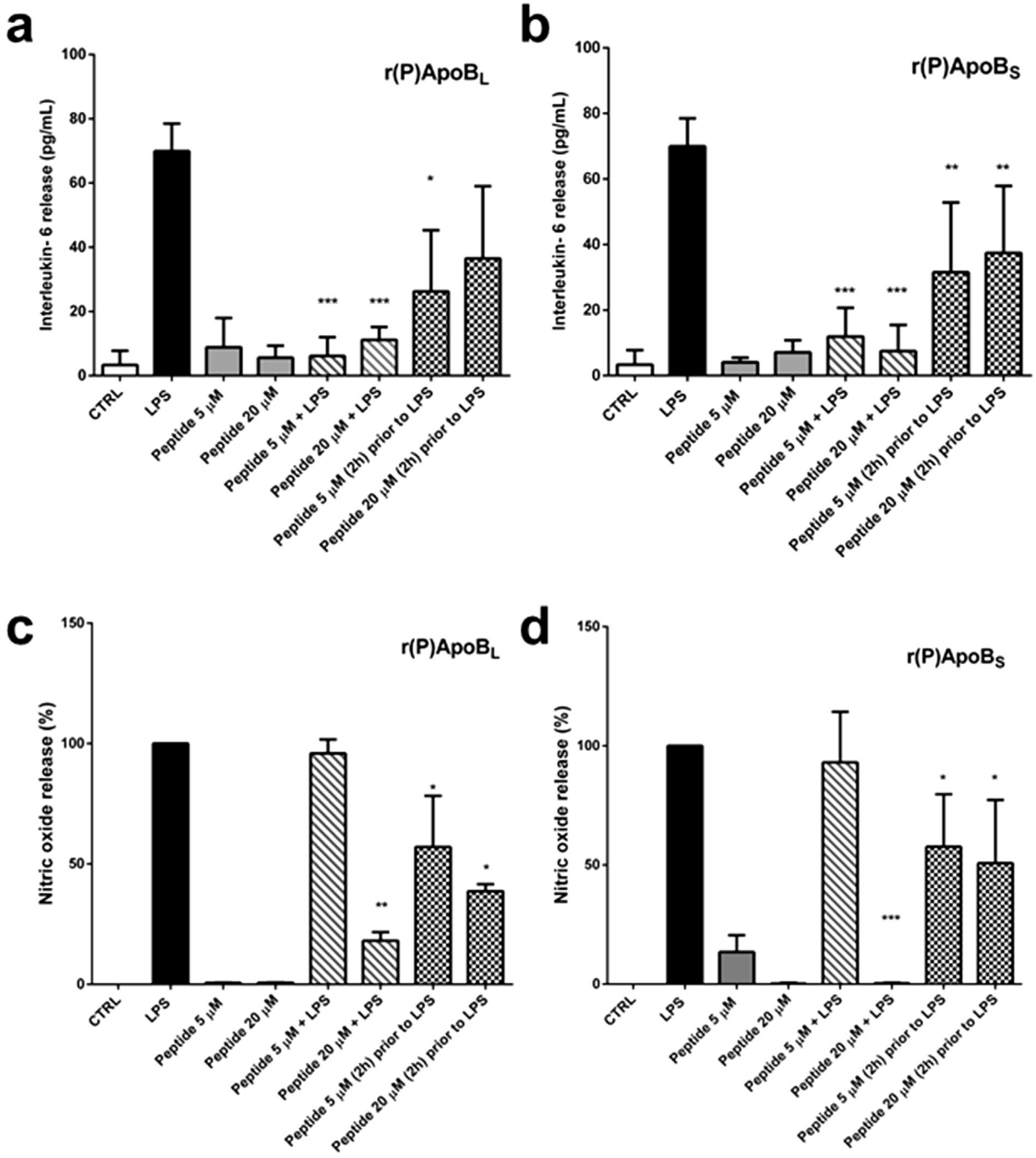

Fig. 3. Effects of ApoB derived peptides on the release of IL-6 (a, b) and NO (c, d) in mouse macrophages RAW 264.7 stimulated with LPS (50 ng/mL) from *Salmonella Minnesota*. The effects of r(P)ApoB$_L$ (a, c) and r(P)ApoB$_S$ (b, d) peptides were evaluated either co-incubating cells with the peptide under test (5 or 20 μM) and LPS (oblique grey lanes) or by treating cells with the peptide under test (5 or 20 μM) for 2 h at 37 °C prior to incubation with LPS (chessboard bars). Results were compared to those obtained in the case of control untreated cells (white bars), cells stimulated with the LPS alone (black bars), or cells incubated with two different concentrations (5 or 20 μM) of peptide (grey bars). Data represent the mean (±standard deviation, SD) of at least three independent experiments, each one carried out with triplicate determinations. $^{*}P < 0.05$, $^{**}P < 0.01$, or $^{***}P < 0.001$ were obtained for control *versus* treated samples.

peptide ApoB887-911, synthesized by MWG Biotech in conformity with the *E. coli* codon usage, were cloned into the expression vector pET22b(+), downstream to a sequence encoding a mutated form of ONC. The resulting fusion proteins contain a His tag sequence, positioned between the ONC and the peptide moieties, suitable for an easy purification of the fusion protein, a flexible linker (Gly-Thr-Gly), and a dipeptide (Asp-Pro), which is cleaved in mild acidic conditions thus allowing the release of the peptide from the carrier. Since the carrier is insoluble at neutral or alkaline pH, ApoB derived peptides were isolated from insoluble components by repeated cycles of centrifugation, and finally lyophilized. Peptides' purity was checked by SDS/PAGE and matrix assisted laser desorption ionisation (MALDI) mass spectrometry analyses. Recombinant peptides were found to be 99% pure. Molecular mass values of ApoB887-923 and ApoB887-911 were found to be 4,072.3 Da (Theoretical MH^+ 4072.7) and 2,820.9 Da (Theoretical MH^+ 2820.2), respectively, values which are in agreement with the expected molecular weights of the peptides with the addition of a Pro

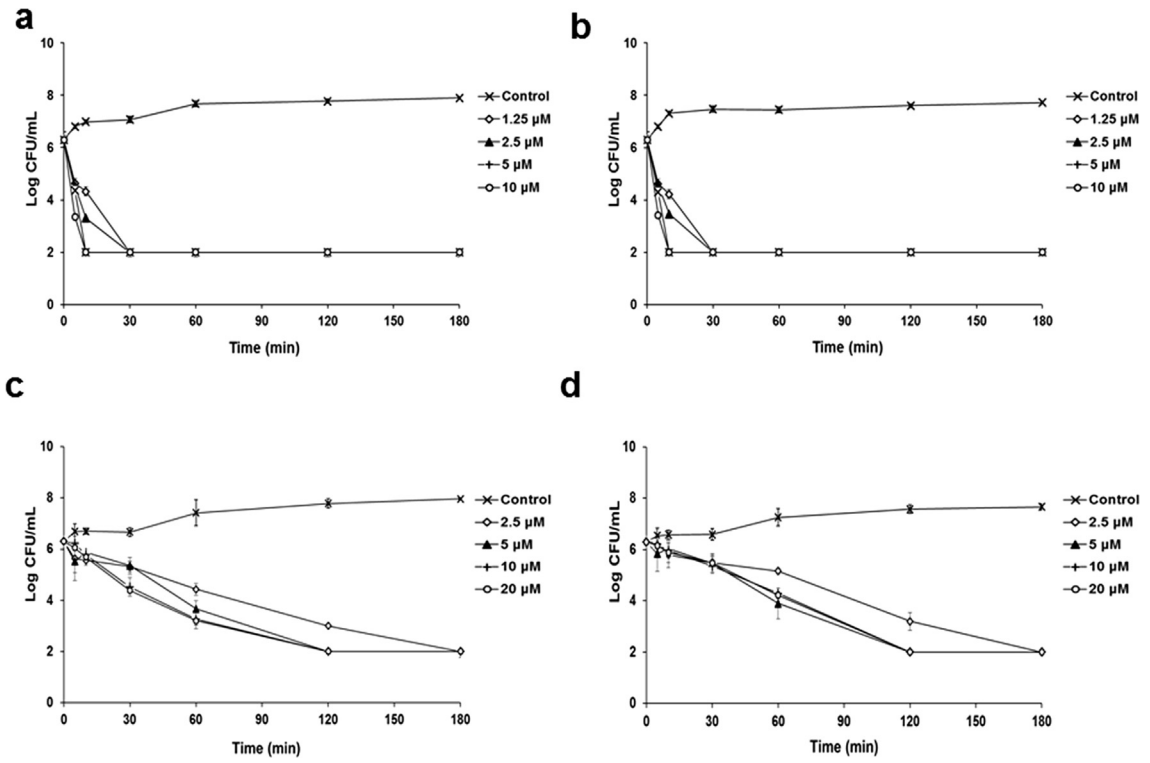

Fig. 4. Time killing curves obtained by incubating *Bacillus licheniformis* ATTC 21424 (a, b) and *E. coli* ATTC 25922 (c, d) strains with increasing concentrations of r(P)ApoB$_L$ (a, c) or r(P)ApoB$_S$ (b, d) peptides for different lengths of time. Data represent the mean (±standard deviation, SD) of at least three independent experiments, each one carried out with triplicate determinations.

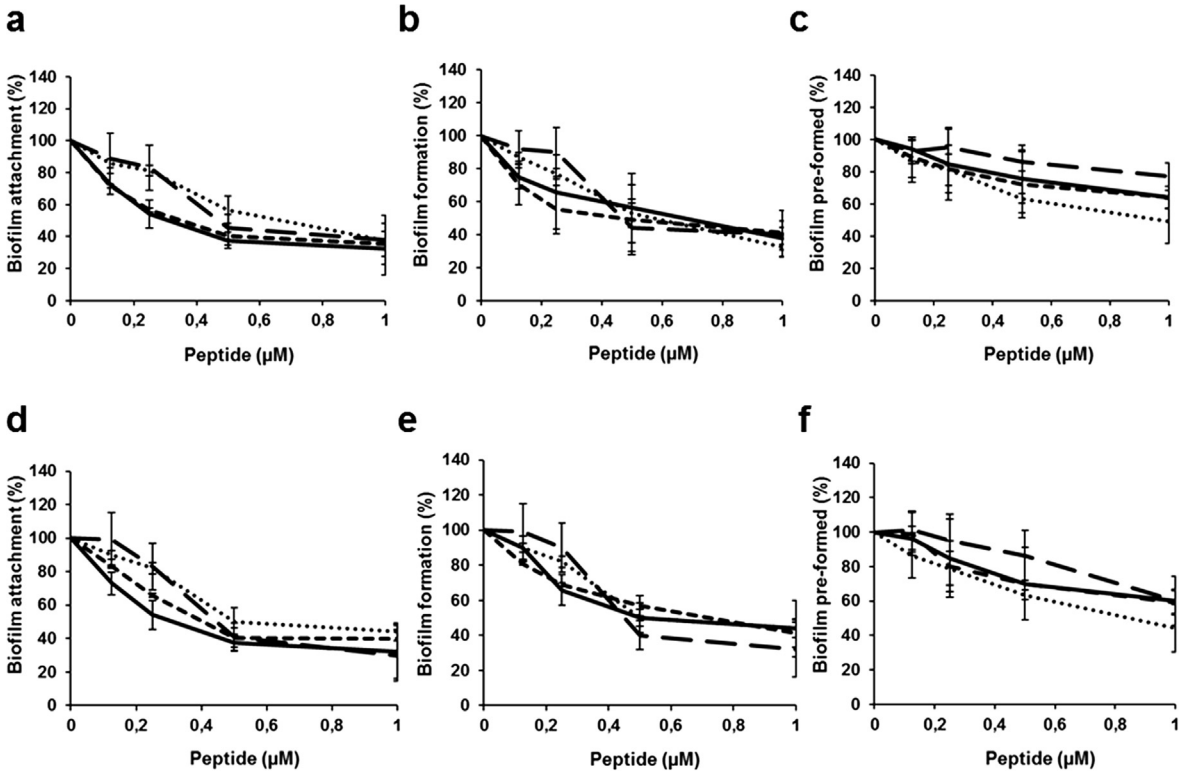

Fig. 5. Anti-biofilm activity of r(P)ApoB$_L$ (–), r(P)ApoB$_S$ (---), CATH-2 (– – –), and LL-37 (●●●) peptides on *E. coli* ATCC 25922 (a, b, c) and *S. aureus* MRSA WKZ-2 (d, e, f) strains in BM2 medium. The effects of increasing concentrations of peptides were evaluated either on biofilm attachment (a, d), biofilm formation (b, e), or on pre-formed (c, f) biofilm. Biofilm was stained with crystal violet and measured at 630 nm. Data represent the mean (±standard deviation, SD) of at least three independent experiments, each one carried out with triplicate determinations. For all the experimental points, $^{*}P < 0.05$, $^{**}P < 0.01$, or $^{***}P < 0.001$ were obtained for control *versus* treated samples.

Please cite this article in press as: R. Gaglione et al., Novel human bioactive peptides identified in Apolipoprotein B: Evaluation of their therapeutic potential, Biochem. Pharmacol. (2017), http://dx.doi.org/10.1016/j.bcp.2017.01.009

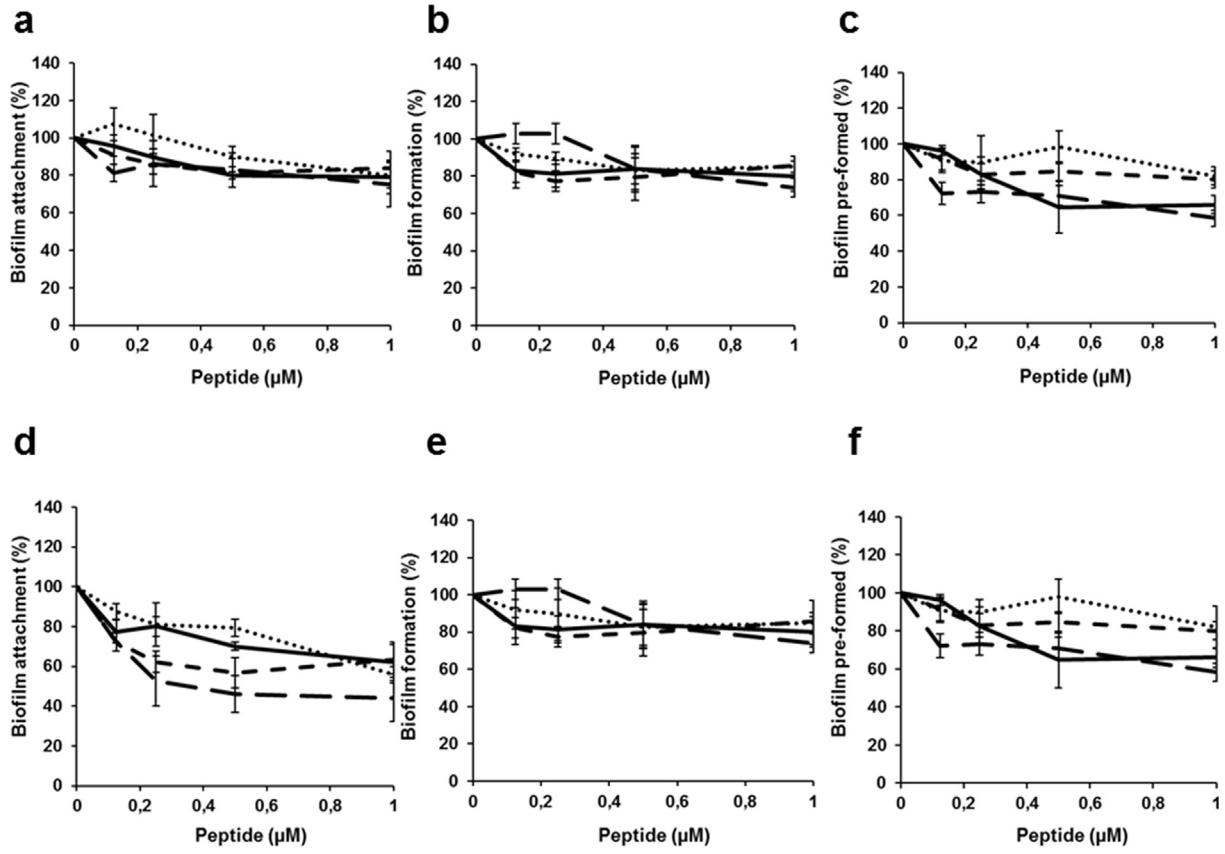

Fig. 6. Anti-biofilm activity of r(P)ApoB$_L$ (–), r(P)ApoB$_S$ (---), CATH-2 (– – –), and LL-37 (•••) peptides on *P. aeruginosa* ATCC 27853 (a, b, c) and *P. aeruginosa* PAO1 (d, e, f) strains in BM2 medium. The effects of increasing concentrations of peptides were evaluated either on biofilm attachment (a, d), biofilm formation (b, e), or on pre-formed (c, f) biofilm. Biofilm was stained with crystal violet and measured at 630 nm. Data represent the mean (±standard deviation, SD) of at least three independent experiments, each one carried out with triplicate determinations. For all the experimental points, $^{*}P < 0.05$, or $^{**}P < 0.01$ were obtained for control *versus* treated samples.

residue deriving from the cleavage of the Asp-Pro bond. The final yield of peptides ApoB887-923 and ApoB887-911, here named r(P)ApoB$_L$ and r(P)ApoB$_S$, was about 7 and 4 mg/L of bacterial culture, respectively.

3.2. Conformational analyses of r(P)ApoB$_L$ and r(P)ApoB$_S$ peptides by Far-UV circular dichroism

To analyse the secondary structure of recombinant ApoB derived peptides, we performed Far-UV CD spectra, and found that both peptides are largely unstructured in pure water (Fig. 2a and b). We also evaluated the effects of membrane-mimicking agents, such as TFE and SDS at micellar concentrations, on peptide conformation. We found that r(P)ApoB$_L$ secondary structure shifts mainly towards an α-helical conformation in presence of both membrane-mimicking agents, and only a partial (<10%) increase in β-strand content is observed (Table 2). This is clearly evidenced by the presence of two broad minima at around 208 and 222 nm, and a maximum at <200 nm (Fig. 2a). A similar behavior has been described for different HDPs [24,42,43], and suggests that r(P)ApoB$_L$ peptide is prone to assume a specific ordered conformation when interacting with membrane-mimicking agents. Similar effects, even if significantly less pronounced, were observed in the case of r(P)ApoB$_S$ peptide (Fig. 2b and Table 2). No appreciable β-strand formation was observed for this peptide, probably indicating that, in the r(P)ApoB$_L$ peptide, β-strand propensity is mainly localized in the C-terminus region.

We also analysed by CD spectroscopy the effects of the endotoxin LPS (lipopolysaccharide), the predominant glycolipid in the outer membrane of Gram-negative bacteria [44], on the peptide conformations (Fig. 2c and d and Table 2). When r(P)ApoB$_L$ secondary structure was analysed in the presence of increasing concentrations (from 0.1 to 0.8 mg/mL) of *E. coli* LPS, the progressive appearance of a maximum at approximately 200 nm and of a minimum at approximately 218 nm suggested that the peptide tends to assume a prevalently β-strand conformation, probably induced by its interaction with LPS (Fig. 2c and Table 2). As expected on the basis of previous analyses, in which r(P)ApoB$_S$ does not show any β-strand content, no significant effects were observed in the case of r(P)ApoB$_S$ (Fig. 2d and Table 2) under the experimental conditions tested.

3.3. Analysis of the immunomodulatory activity of r(P)ApoB$_L$ and r(P)ApoB$_S$ peptides

Based on CD analyses, we hypothesized that an interaction between r(P)ApoB$_L$ peptide and LPS occurs. Since it is widely reported that HDPs are able to mitigate the pro-inflammatory effects induced by endotoxins [45], we tested the anti-inflammatory properties of ApoB derived peptides by monitoring their effects on LPS induced interleukin-6 (IL-6) release, as well as on nitric oxide (NO) release in murine macrophages (RAW 264.7 cell line). In fact, it is known that, upon activation by internal and external stimuli, macrophages produce and secrete various endogenous inflammatory mediators, such as nitric oxide (NO) and pro-inflammatory cytokines, including interleukin-6 [46,47].

To test the effects of ApoB derived peptides on the release of IL-6, ELISA assays were performed on LPS stimulated RAW 264.7 cells. As shown in Fig. 3a and b, a significant release of IL-6 was observed in control cells incubated with LPS from *Salmonella*

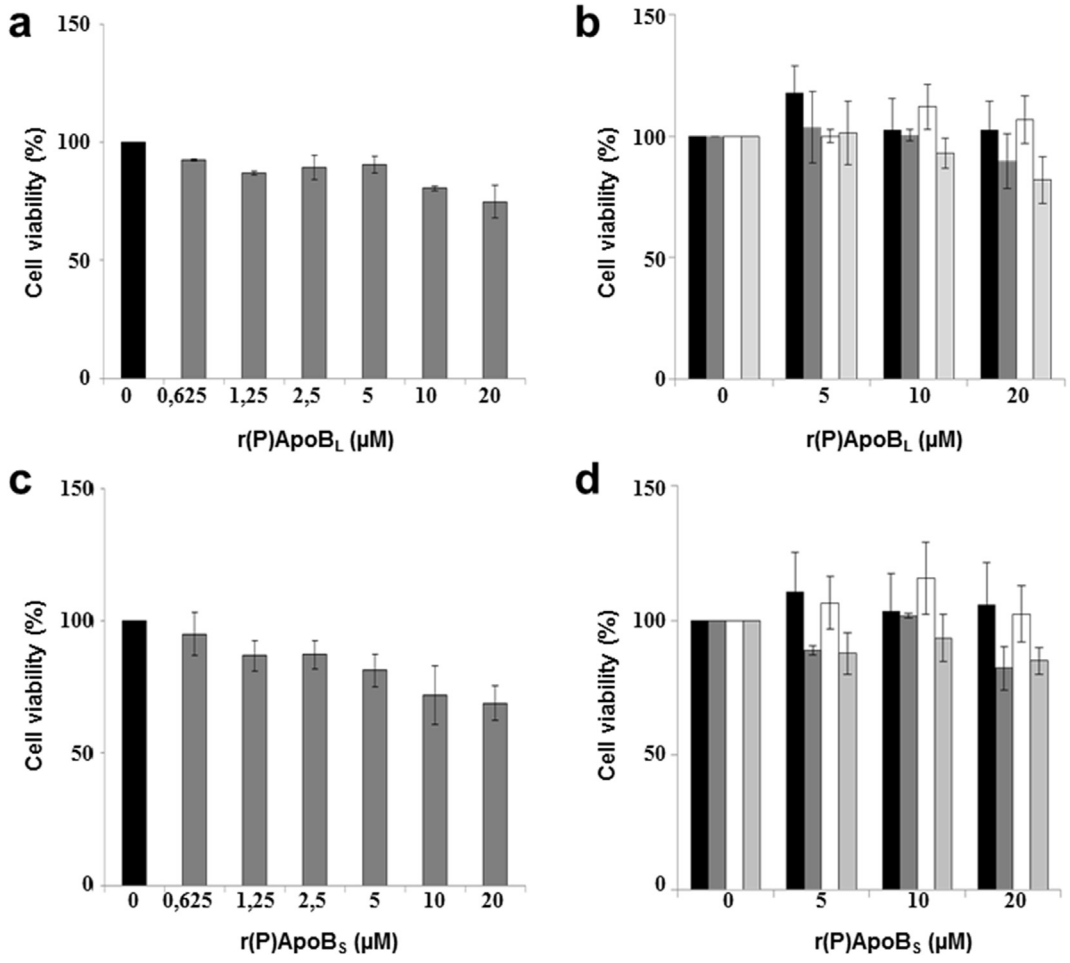

Fig. 7. Effects of r(P)ApoB$_L$ (a, b) and r(P)ApoB$_S$ (c, d) peptides on the viability of RAW 264.7 (a, c), BALBc3T3 (black bars in b, d), SVT2 (dark grey bars in b, d), Hela (white bars in b, d), and HaCaT (light grey bars in b, d) cells. Cell viability was assessed by WST-1 (a, c) or MTT (b, d) assay, and expressed as the percentage of viable cells with respect to controls (untreated cells). Error bars indicate standard deviations obtained from at least three independent experiments, each one carried out with triplicate determinations.

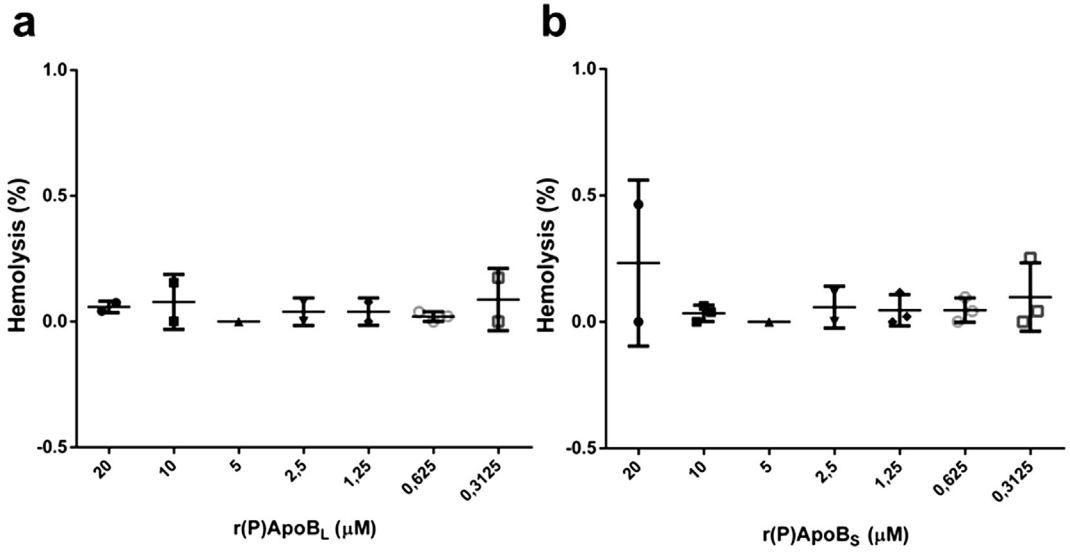

Fig. 8. Haemolytic activity of r(P)ApoB$_L$ (a) and r(P)ApoB$_S$ (b) peptides towards murine red blood cells (RBCs) after 1 h of incubation at 37 °C. Data represent the mean (±standard deviation, SD) of at least three independent experiments, each one carried out with triplicate determinations.

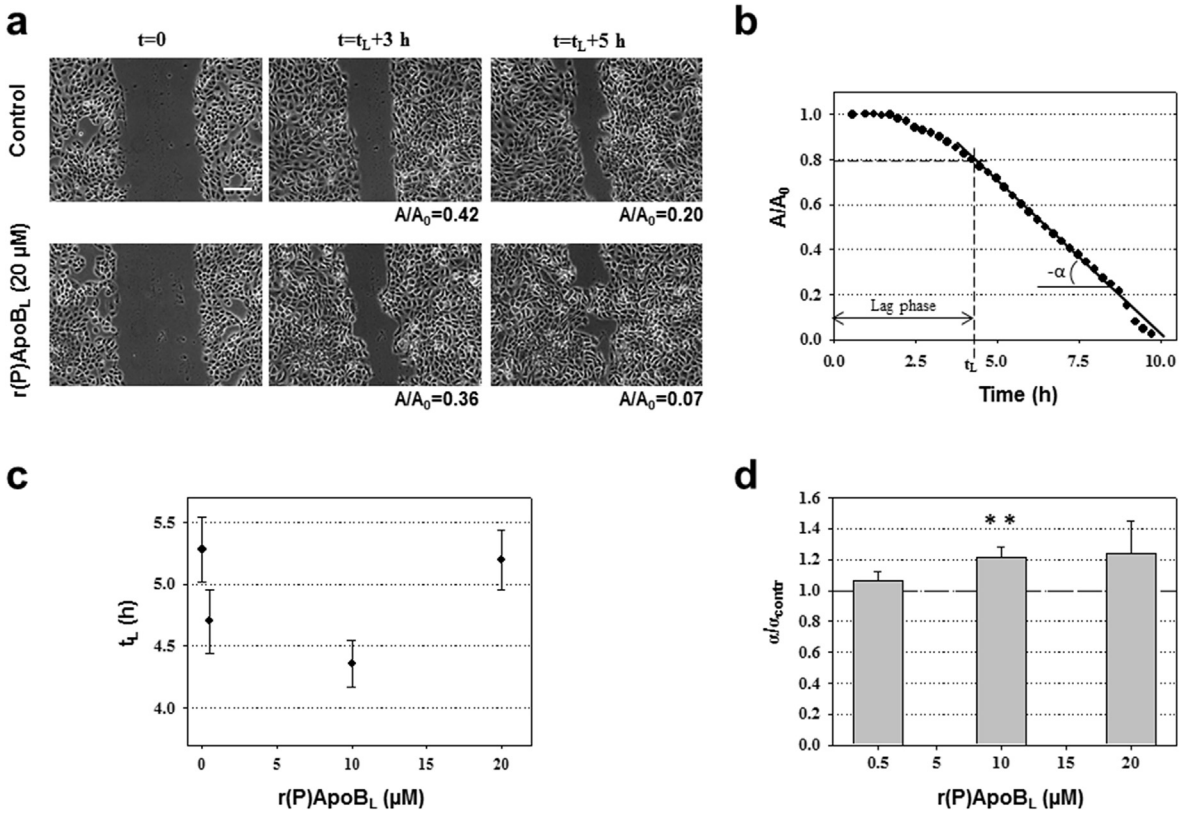

Fig. 9. Wound healing activity of r(P)ApoB$_L$ peptide on HaCaT cells monolayer. Cells were pre-treated for 30 min with 3 μM mitomycin C, and then wounded prior to incubation with r(P)ApoB$_L$ peptide (0.5–10–20 μM) for 12 h at 37 °C. Images were acquired for untreated HaCaT cells and for cells treated with 20 μM peptide (a). The lag phase time (t_L) corresponds to the time interval before the linear decrease of the wound area. Images were acquired at time t = 0 (a, on the left), 3 h after t_L (a, in the middle) and 5 h after t_L (a, on the right). For each sample, A/A_0 values are reported, where A is the wound area after a specific incubation time and A_0 is the wound area at time 0. Scale bar = 150 μm. In (b), evolution in time of the wound area (A), normalized with respect to A_0, is reported for a control sample. A homemade automated image analysis software was used to measure the size of the cell-free area (A) for each time point. For A/A_0 values < 0.8, a linear correlation with the incubation time was found. The slope $-\alpha$ of the linear fit, reported as a continuous line, represents a measure of the wound closure velocity. In (c), determined t_L values are reported as a function of peptide concentration (0–0.5–10–20 μM). In (d), wound closure velocity (α), normalized with respect to control sample (α_{contr}), is reported as a function of peptide concentration (0.5–10–20 μM). The dashed line corresponds to $\alpha/\alpha_{contr} = 1$. In (c) and (d), each data point represents the mean (±standard error) of three independent experiments. $^{**}P < 0.01$ was obtained for control *versus* treated samples.

Table 2
Analysis of r(P)ApoB$_L$ and r(P)ApoB$_S$ peptides secondary structure.

	H_2O			TFE		
	α-Helix (%)	β-Strand (%)	Random coil (%)	α-Helix (%)	β-Strand (%)	Random coil (%)
r(P)ApoB$_L$	5	12	83	26	18	56
r(P)ApoB$_S$	7	3	90	26	0	74
	SDS			LPS		
	α-Helix (%)	β-Strand (%)	Random coil (%)	α-Helix (%)	β-Strand (%)	Random coil (%)
r(P)ApoB$_L$	17	21	62	11	64	25
r(P)ApoB$_S$	29	3	68	18	2	80

Secondary structure content of ApoB derived peptides in water and in the presence of trifluoroethanol (TFE), sodium dodecyl sulfate (SDS), and lipopolysaccharide (LPS), calculated by means of PEPFIT program.

Minnesota (50 ng/mL). When murine macrophages were incubated with LPS (50 ng/mL) in the presence of either r(P)ApoB$_L$ (Fig. 3a) or r(P)ApoB$_S$ (Fig. 3b) peptide (two different peptide concentrations), a strong decrease of IL-6 release was observed with respect to LPS induced control cells. Moreover, we found that both peptides have a significant protective effect on LPS stimulated RAW 264.7 cells. In fact, when macrophages were pre-treated for 2 h with either r(P)ApoB$_L$ or r(P)ApoB$_S$ peptide and then incubated for further 24 h with LPS, a significant decrease of IL-6 release was observed (Fig. 3a and b).

Similar results were observed when the effects of ApoB derived peptides were tested on NO release (Fig. 3c and d). Also in this case, following co-incubation of cells with LPS from *Salmonella Minnesota* and either r(P)ApoB$_L$ or r(P)ApoB$_S$ peptide, a significant attenuation of NO release with respect to control cells was detected (Fig. 3c and d). However, in this case, it has to be noticed that a significant effect of peptides on NO release was observed only at the highest peptide concentration tested (20 μM), while at 5 μM concentration both peptides were found to be almost ineffective (Fig. 3c and d). However, when RAW 264.7 cells were

pre-treated for 2 h with 5 or 20 μM of either r(P)ApoB$_L$ or r(P)ApoB$_S$ peptide and subsequently stimulated for 24 h with LPS (50 ng/mL), a significant reduction of NO release was observed even at 5 μM peptide concentration (Fig. 3c and d), thus confirming the protective effect of both peptides on LPS stimulated RAW 264.7 cells.

3.4. Antimicrobial activity of r(P)ApoB$_L$ and r(P)ApoB$_S$ peptides

The antibacterial activity of recombinant ApoB derived peptides was determined by measuring their MIC$_{100}$ values on a panel of Gram-negative and Gram-positive bacterial strains (Table 3). A significant antimicrobial activity of r(P)ApoB$_L$ and r(P)ApoB$_S$ peptides was detected towards four out of eight strains tested, *i.e. E. coli* ATCC 25922, *P. aeruginosa* PAO1, *B. globigii* TNO BM013, and *B. licheniformis* 21424, for which almost identical MIC$_{100}$ values were calculated for both ApoB derived peptides. Notably, MIC$_{100}$ values were found to be comparable or even significantly lower than those determined when control cathelicidin-2 (CATH-2), a known HDP from chicken [48], was tested (Table 3). These data indicate that r(P)ApoB$_L$ and r(P)ApoB$_S$ peptides are endowed with a broad-range antimicrobial activity, being effective on both Gram-negative and Gram-positive bacterial strains. On the other hand, ApoB derived peptides were found to be ineffective towards *P. aeruginosa* ATCC 27853, methicillin-resistant *S. aureus* (MRSA WKZ-2), and *S. aureus* 29213 (Table 3), while, in the case of *S. enteriditis* 706 RIVM, a significant antibacterial effect was elicited only by r(P)ApoB$_L$ peptide.

To analyse the kinetic of peptides bactericidal activity, kinetic killing curves were obtained by treating *E. coli* ATTC 25922 and *B. licheniformis* ATTC 21424 strains, highly susceptible to both peptides (Table 3), with increasing concentrations of either r(P)ApoB$_L$ or r(P)ApoB$_S$ for different times (0–180 min). We found that, at the highest peptide concentrations tested (5–10 μM), *B. licheniformis* cells were killed within 10 min, while at the lowest peptide concentrations (1.25–2.5 μM) the same effect was obtained within 30 min (Fig. 4a and b). When peptides were tested on *E. coli* ATTC 25922 at high concentrations (5–10-20 μM), bacterial cells were killed within 120 min, while at the lowest peptide concentration (2.5 μM) the same effect was obtained within 180 min (Fig. 4c and d).

3.5. Combination therapy analyses

To potentiate the antimicrobial efficacy of recombinant ApoB derived peptides for therapeutic purposes, especially against *P. aeruginosa* and *S. aureus* strains, we carried out combination therapy analyses by concomitantly administrating peptides and antibiotics in various combinations to bacteria. One of the best known tests to evaluate synergism between two compounds is the so called "chequerboard" experiment, in which a two-dimensional array of serial concentrations of test compounds is used as the basis for calculation of a fractional inhibitory concentration (FIC) index to demonstrate that paired combinations of agents can exert inhibitory effects that are more than the sum of their effects alone [32]. It is generally accepted that FIC indexes $\leqslant$0.5 are indicative of "synergy"; FIC indexes comprised between >0.5 and 4.0 are, instead, associated to "additive" or "no interaction" effects, whereas FIC indexes >4.0 are indicative of "antagonism" [32].

As reported in Table 4, all the combinations tested were found to be effective, either with additive or synergistic effects between peptides and antibiotics. Notably, no FIC indexes higher than 2 were measured.

The most potent combinations were obtained in the presence of EDTA, which was selected for its ability to affect bacterial outer membrane permeability, thus sensitizing bacteria to a number of antibiotics [49–51]. Very pronounced synergistic effects were observed for both ApoB derived peptides in combination with EDTA on *S. aureus* MRSA WKZ-2 and both *P. aeuroginosa* strains.

Both peptides were found to act synergistically with (i) ciprofloxacin on all the strains tested (Table 4); (ii) colistin on all the strains tested, except for *S. aureus* ATTC 29213 (Table 4); (iii) vancomycin on *S. aureus* MRSA WKZ-2, *P. aeruginosa* strains and *E. coli* ATTC 25922 (Table 4); (iv) erythromycin on *P. aeruginosa* ATCC

Table 3
Antibacterial activity of ApoB derived peptides.

	MIC$_{100}$ (μM) r(P)ApoB$_L$	r(P)ApoB$_S$	CATH-2
Gram-negative strains			
Escherichia coli ATCC 25922	10	10	10
Pseudomonas aeruginosa ATCC 27853	>40	>40	10
Pseudomonas aeruginosa PAO1	20	20	20
Salmonella enteriditis 706 RIVM	10	>40	10
Gram-positive strains			
Staphilococcus aureus MRSA WKZ-2	>40	>40	10
Bacillus globigii TNO BMO13	5	2.5	5
Bacillus licheniformis ATCC 21424	1.25	1.25	20
Staphylococcus aureus ATCC 29213	>40	>40	10

Minimum Inhibitory Concentration (MIC, μM) values determined for r(P)ApoB$_L$ and r(P)ApoB$_S$ peptides tested on a panel of Gram-positive and Gram-negative bacterial strains. Chicken CATH-2 peptide was used as a positive control. Values were obtained from a minimum of three independent experiments.

Table 4
Combination therapy analyses.

Bacterial strains	Antibiotic	ΣFICI[a] r(P) ApoB$_L$	r(P) ApoB$_S$
Methicillin resistant *S. aureus MRSA WKZ-2*	Ciprofloxacin	0,328	0,365
	Colistin	0,340	0,350
	Erythromycin	1,094	1,375
	Vancomycin	0,425	0,316
	Kanamycin	2,000	0,387
	EDTA	0,278	0,360
S. aureus ATTC 29213	Ciprofloxacin	0,340	0,413
	Colistin	1,049	1,024
	Erythromycin	1,049	1,146
	Vancomycin	1,049	1,097
	Kanamycin	1,049	0,352
	EDTA	1,049	0,351
P. aeruginosa ATCC 27853	Ciprofloxacin	0,347	0,328
	Colistin	0,267	0,255
	Erythromycin	0,389	0,170
	Vancomycin	0,379	0,306
	Kanamycin	0,479	1,030
	EDTA	0,333	0,089
P. aeruginosa PAO1	Ciprofloxacin	0,396	0,444
	Colistin	0,144	0,266
	Erythromycin	0,569	0,556
	Vancomycin	0,500	0,486
	Kanamycin	0,507	0,389
	EDTA	0,396	0,438
E. coli ATCC 25922	Ciprofloxacin	0,363	0,442
	Colistin	0,438	0,292
	Erythromycin	1,243	1,292
	Vancomycin	0,428	0,426
	Kanamycin	0,603	0,572
	EDTA	0,729	0,750

Fractional inhibitory concentration (FIC) indexes determined for r(P)ApoB$_L$ and r(P)ApoB$_S$ peptides tested in combination with antibiotics or EDTA on Gram-positive and Gram-negative bacterial strains. Indexes were obtained from a minimum of three independent experiments, each one carried out with triplicate determinations.

27853 (Table 4). In the latter case, a FIC index of 0.38 and 0.17 for r(P)ApoB$_L$ and r(P)ApoB$_S$ peptides, respectively, was obtained. In the case of kanamycin, the response varied depending on the peptide and the specific bacterial strain. In fact, r(P)ApoB$_L$ was found to act synergistically with this antibiotic prevalently on Gram-negative bacteria, particularly on the *P. aeruginosa* strains, whereas r(P)ApoB$_S$ peptide was found to be very active in the presence of kanamycin against both *S. aureus* strains as well as against *P. aeruginosa* PAO1 strain (FIC indexes < 0.4).

It should be emphasized that combinations of ApoB derived peptides with antibiotics or EDTA were found to have a strong antimicrobial activity also towards strains on which the peptides alone were found to be ineffective, such as both *S. aureus* strains and *P. aeruginosa* ATCC 27853 (Table 3). Notably, we did not observe any antagonistic interactions between the peptides and the antimicrobials under test.

3.6. Anti-biofilm activity of r(P)ApoB$_L$ and r(P)ApoB$_S$ peptides

Anti-biofilm peptides represent a very promising approach to treat biofilm-related infections and have an extraordinary ability to interfere with various stages of the biofilm growth mode [52]. To test whether recombinant ApoB derived peptides are endowed with anti-biofilm activity, we performed experiments on different bacterial strains, such as *E. coli* ATCC 25922, *Pseudomonas aeruginosa* PAO1, *Pseudomonas aeruginosa* ATCC 27853, and methicillin-resistant *Staphylococcus aureus* MRSA WKZ-2 in BM2 medium. The same experiments were also performed using LL-37 control peptide, that is a human antimicrobial peptide known to have a significant anti-biofilm activity against multidrug-resistant bacterial strains [53]. We also tested for the first time CATH-2 anti-biofilm activity. Three different approaches were followed. At first, we tested the peptide effects on biofilm attachment. To do this, the bacterial culture, following overnight growth, was diluted in BM2 medium containing increasing concentrations of the peptide under test (0–1 μM), and incubated for 4 h at 37 °C. Following incubation, biofilm analysis by crystal violet staining revealed a significant dose-dependent inhibition of biofilm attachment in the case of *E. coli* ATCC 25922 (Fig. 5a) and *S. aureus* MRSA WKZ-2 (Fig. 5d) strains treated with r(P)ApoB$_L$ (continuous line in Fig. 5a, d) or r(P)ApoB$_S$ (smaller dashed line in Fig. 5a, d) peptides. Similar results were obtained on these two strains in the case of peptides CATH-2 (larger dashed line in Fig. 5a, d) and LL-37 (dotted line in Fig. 5a, d). Strong effects were also displayed by ApoB derived peptides on biofilm attachment in the case of *P. aeruginosa* PAO1 strain (Fig. 6d). A less pronounced effect of ApoB derived peptides (about 20% inhibition of biofilm formation) was observed, instead, on *P. aeruginosa* ATCC 27853 biofilm attachment (Fig. 6a).

Second, we tested the effect of ApoB derived peptides on biofilm formation. To investigate this phenomenon, we followed the experimental procedure described above with the only exception that bacterial cells were incubated with increasing concentrations of peptides for 24 h at 37 °C. Also in this case, we observed a significant dose-dependent inhibition of biofilm formation in the case of *E. coli* ATCC 25922 (Fig. 5b) and *S. aureus* MRSA WKZ-2 (Fig. 5e) strains treated with r(P)ApoB$_L$ (Fig. 5b, e) or r(P)ApoB$_S$ (Fig. 5b, e) peptides. Similar effects were elicited by peptides CATH-2 (Fig. 5b, e) and LL-37 (Fig. 5b, e). ApoB derived peptides strongly affected also *P. aeruginosa* PAO1biofilm formation (Fig. 6e). In the case of *P. aeruginosa* ATCC 27853, instead, a less pronounced effect (about 20% biofilm formation inhibition) was observed for all the peptides under test (Fig. 6b).

Third, we tested the effect of ApoB derived peptides on preformed biofilms. By incubating preformed biofilms of *E. coli* ATCC 25922 (Fig. 5c) and *S. aureus* MRSA WKZ-2 (Fig. 5f) strains with increasing concentrations of r(P)ApoB$_L$ (Fig. 5c, f) or r(P)ApoB$_S$ (Fig. 5c, f), we found a significant reduction (about 50%), an effect even stronger than that observed in the case of CATH-2 peptide (Fig. 5c, f). Similar results were observed in the case of *P. aeruginosa* PAO1 strain (Fig. 6f). On the other hand, when the peptides were tested on *P. aeruginosa* ATCC 27853 preformed biofilm, a slight effect (about 20% reduction) was observed for all the peptides except for CATH-2, which was found to have a strong effect (about 50% reduction, Fig. 6c).

We also evaluated the percentage of viable bacterial cells inside the biofilm structure by colony counting assay. We found that, even at the highest ApoB derived peptides concentrations tested, a significant percentage of bacterial cells appeared to be still alive (Table 5). Similar results were also obtained in the case of LL-37 and CATH-2 control peptides on both *P. aeruginosa* strains (Table 5), even if it has to be noticed that, in the case of biofilm formation, both control peptides affected the viability of *P. aeruginosa* PAO1 cells more than ApoB derived peptides (Table 5). CATH-2 and LL-37 control peptides were also found to strongly impair the viability of *E. coli* ATCC 25922 and *S. aureus* MRSA WKZ-2 cells in the case of biofilm eradication (Table 5).

3.7. Biocompatibility of r(P)ApoB$_L$ and r(P)ApoB$_S$ peptides

The development of HDPs as therapeutic agents is strictly related to their selective toxicity towards bacterial cells [54]. The presence of zwitterionic phospholipids and cholesterol on the

Table 5
Effects of peptides on the viability of bacterial cells inside the biofilm structure.

	In biofilm attachment (%)				In biofilm formation (%)				In biofilm eradication (%)			
	r(P)ApoB$_L$	r(P)ApoB$_S$	CATH-2	LL-37	r(P)ApoB$_L$	r(P)ApoB$_S$	CATH-2	LL-37	r(P)ApoB$_L$	r(P)ApoB$_S$	CATH-2	LL-37
***E. coli* ATCC 25922**	105±7	101±9	15±5	97±8	79±7	79±9	40±3	73±12	83±14	80±5	15±2	37±6
MRSA WKZ-2	90±7	102±9	35±5	70±4	66±7	60±8	23±3	69±12	66±11	70±3	10±2	17±6
***P. aeruginosa* ATCC 27853**	76±11	68±10	91±5	60±13	66±13	64±14	96±16	77±15	70±15	59±9	59±12	69±5
P. aeruginosa PAO1	52±12	77±15	45±7	47±7	55±14	57±14	35±16	25±14	44±15	86±6	50±10	58±9

Effects of r(P)ApoB$_L$, r(P)ApoB$_S$, CATH-2, and LL-37 peptides (1 μM) on the viability of bacterial cells inside the biofilm structure. To determine the percentage of viable bacterial cells, biofilm was lysed with Triton X-100 (0,1%), bacterial cells were ten-fold diluted, and colonies were counted after an incubation of 16 h at 37 °C. Data are expressed as percentage with respect to control untreated samples, and represent the mean (±standard deviation, SD) of at least three independent experiments, each one carried out with triplicate determinations. For all the experimental points, $^{*}P < 0.05$, or $^{**}P < 0.01$ were obtained for control *versus* treated samples.

Please cite this article in press as: R. Gaglione et al., Novel human bioactive peptides identified in Apolipoprotein B: Evaluation of their therapeutic potential, Biochem. Pharmacol. (2017), http://dx.doi.org/10.1016/j.bcp.2017.01.009

outer leaflet of eukaryotic cell membranes largely accounts for the preference of HDPs for bacterial membranes over eukaryotic membranes [55,56]. To deepen on the therapeutic potential of ApoB derived peptides, we analysed their cytotoxic effects towards a panel of mouse and human eukaryotic cells. The addition of increasing concentrations (from 0.625 to 20 μM) of ApoB derived peptides to mouse macrophages Raw 264.7 cells for 24 h did not result in any significant reduction in cell viability (Fig. 7a and c). A slight toxicity was detected only at the highest peptide concentrations tested (10 and 20 μM in Fig. 7a and c). We also tested ApoB derived peptides on murine embryo fibroblasts BALBc 3T3 and their tumor counterpart, *i.e.* SVT2 simian virus 40-transformed cell line (Fig. 7b and d). A slight toxicity (10–20%) was detected only in the case of SVT2 cells at the highest concentration tested (20 μM in Fig. 7b and d). Moreover, no significant toxic effects were detected when ApoB derived peptides were assayed on human cervical cancer HeLa cells (Fig. 7b and d), while a slight toxicity (~20%) was observed in the case of human keratinocytes (HaCaT cells) at the highest concentration (20 μM in Fig. 7b and d). ApoB derived peptides were also tested on murine red blood cells (RBCs) to exclude haemolytic effects. As shown in Fig. 8, both peptides did not exert any lytic effect on mouse RBCs, even at the highest concentration tested (20 μM).

3.8. Wound healing activity of r(P)ApoB$_L$ peptide

Numerous studies support the hypothesis that human HDPs promote wound healing in skin, by modulating cytokine production, cell migration, proliferation and, in some cases, angiogenesis [57]. Based on this, we performed experiments to test whether r(P)ApoB$_L$ peptide is able to stimulate wound re-epithelialization by human keratinocytes (HaCaT cell line). To this purpose, we performed a classical *in vitro* wound healing assay to evaluate peptide effects on cell migration. HaCaT cell monolayers were pre-treated with 3 μM mitomycin C for 30 min, and then wounded with a pipette tip to remove cells from a specific region of the monolayers. Cells were then washed with PBS and incubated with r(P)ApoB$_L$ (0, 0.5, 10, and 20 μM). As it is well known that the spreading of cells in the wound area is due to two mechanisms, *i.e.* cell motility and cell proliferation [37,40,58], a pre-treatment with mitomycin C allowed us to exclude any influence of cell proliferation on the wound healing process.

In Fig. 9a, we reported the images acquired during a time-lapse wound healing experiment on control cells, and on cells treated with 20 μM r(P)ApoB$_L$ peptide at three time points, *i.e.* at time 0 and at 3 and 5 h after the lag time (t_L), defined as a transient time period (t_L) before the linear decrease of the wound area (see below). By the comparison of the images of treated and untreated cells at each time point, it emerged that the cells treated with 20 μM peptide were able to close the wound faster than the control cells. In order to quantify the wound closure, we used an automated image analysis software, that allowed us to measure the size of the cell-free area (A) for each time point. The obtained values were normalized with respect to the value measured at time 0 (A_0) for each field of view, and plotted as a function of time (Fig. 9b). In Fig. 9a, at t = 5 h after t_L, A/A_0 values were found to be 0.20, and 0.07 for the control sample, and for the cells treated with 20 μM peptide, respectively. This evidence suggests that r(P)ApoB$_L$ peptide might be able to stimulate wound re-epithelialization by human keratinocytes. As shown in Fig. 9b, where A/A_0 values of control cells are reported as a function of time, after an initial lag phase (t_L), the wound area decreases with a constant velocity. The initial lag phase, corresponding to a transient time period (t_L) before the linear decrease of the wound area, has been observed for all the analysed samples, and has been found to range between 3 and 5 h independently from peptide concentrations under test (Fig. 9c).

As the slope (α) of the line represents the measure of the wound closure velocity, each α value calculated in the presence of the peptide was normalized with respect to the value calculated for untreated cells (α_{contr}), and plotted as a function of peptide concentration (Fig. 9d). It appeared that the cells treated with the peptide show an increased wound closure velocity with respect to the control cells ($\alpha/\alpha_{contr} > 1$). In particular, in the case of the cells treated with 10 μM peptide, an increment of about 20% in the normalized wound closure velocity ($\alpha/\alpha_{contr} = 1.21$, data statistically significant) was observed. When cells were treated with 20 μM peptide, a slightly higher value of the normalized wound closure velocity was measured ($\alpha/\alpha_{contr} = 1.23$). However, in the latter case, a higher data variability was observed (larger error bar), leading to a limited statistical significance of the result.

Overall, our results indicate that r(P)ApoB$_L$ peptide is able to promote the migration and the consequent wound healing in HaCaT keratinocyte monolayers when tested at concentration values ranging between 0.5 and 20 μM.

4. Discussion

Recently, an abundance of multidrug-resistant bacteria has emerged, whereas very few classes of new antibiotics have been discovered. The knowledge that HDPs may prevent infections in many organisms opened interesting perspectives to the applications of these peptides as a new class of antimicrobials. In fact, they initially attracted attention solely for their direct antimicrobial activity, and were studied as promising alternative antibiotic candidates due to their prospective potency, rapid action, and broad spectrum of activity against Gram-negative and Gram-positive bacteria, viruses, fungi and parasites [59,60]. To date, more than 1,000 natural cationic HDPs with antimicrobial properties have been identified [61]. These peptides constitute a major component of the ancient, nonspecific innate defence system in most multicellular organisms [3,19,59,60]. However, it has to be emphasized that most natural HDPs have, indeed, modest direct antimicrobial activities, and exhibit multiple mechanisms of action, with a consequent low potential to induce *de novo* resistance [59]. This class of peptides includes both the bioactive peptides displaying direct antimicrobial activity and those that stimulate the immune system to clear or prevent an infection [59,61]. In mammals, the expression of mature and biologically active HDPs requires a proteolytic cleavage event determining the release of the "cryptic" bioactive peptide from its precursor protein [62]. In fact, it should be emphasized that a wide variety of human proteins, whose primary functions are not necessarily related to host defence, contain HDPs hidden inside their sequences [63,64]. Fascinatingly, human proteome could be seen as a yet unexplored source of bioactive peptides with potential pharmacological applications. In this context, apolipoproteins have been identified as a source of bioactive peptides displaying broad anti-infective and antiviral activities [22]. Indeed, the presence of antiviral peptides hidden within apolipoprotein sequences may be related to the fact that lipoproteins and viruses share a similar cell biological niche, having a comparable size and displaying similar interactions with mammalian cells and receptors [22]. ApoB is one of the several apolipoproteins that play key roles in lipoprotein metabolism [65], and represents the ligand for receptor-mediated removal of low density lipoprotein particles from circulation [65]. ApoB contains two LDL (low-density lipoprotein) receptor binding domains, namely region A (ApoB3147-3157) and region B (ApoB3359-3367), which is more uniformly conserved across species and that has been found to be endowed with a significant antiviral activity

Please cite this article in press as: R. Gaglione et al., Novel human bioactive peptides identified in Apolipoprotein B: Evaluation of their therapeutic potential, Biochem. Pharmacol. (2017), http://dx.doi.org/10.1016/j.bcp.2017.01.009

[22]. Moreover, ApoB derived peptides have been already used in vaccine preparations to treat atherosclerosis [23]. Here, we applied our *in silico* analysis method to a human ApoB isoform [26,27] and identified a novel "cryptic" HDP (region 887–922). To the best of our knowledge, this ApoB region has never been analysed before, since all the previously identified biologically active ApoB peptides are far from the high scoring region identified in the present work [22,23]. By applying our *in silico* analysis, we identified an absolute maximum score, corresponding to region 887–922 (Fig. 1), and a relative maximum score, corresponding to residues 887–909 (Fig. 1). Here, we focused our attention on these two ApoB sequences by producing in bacterial cells two recombinant HDPs, here named r(P)ApoB$_L$ and (P)ApoB$_S$, 38- and 26-residue long, respectively. Both recombinant peptides were found to exhibit antibacterial activities against both Gram-positive and Gram-negative strains, including the pathogenic strains *P. aeruginosa* PAO1 and *B. globigii* TNO BM013, while having negligible cytotoxic effects on a panel of human and murine cell lines. Time killing curves also indicated that peptides exert a strong bactericidal activity against susceptible strains. However, it has to be underlined that ApoB derived peptides were found to be ineffective towards *P. aeruginosa* ATCC 27853, methicillin-resistant *S. aureus* (MRSA WKZ-2), and *S. aureus* ATTC 29213 strains, while, in the case of *S. enteriditis* 706 RIVM strain, a significant antibacterial effect was displayed only by r(P)ApoB$_L$ peptide. This observation is in agreement with previous findings indicating that most natural cationic antimicrobial peptides do not appear to be highly optimized for direct antimicrobial activity, since it is likely that multiple modestly active peptides with concomitant immunomodulatory activities work effectively in combination and/or when induced or delivered to sites of infection [66]. Indeed, considering this, we performed combination therapy analyses and found that both ApoB derived peptides are able to synergistically act with either commonly used antibiotics or EDTA, the latter selected for its ability to affect bacterial outer membrane permeability, thus sensitizing bacteria to a number of antibiotics [49–51]. Interestingly, synergistic effects were observed towards most of the strains under test, including methicillin-resistant *S. aureus* MRSA WKZ-2, on which peptides alone were found to be ineffective even at high concentrations (40 μM). Although the use of a single agent to treat pathogens is the most common practice in clinics, combination therapy approaches have several advantages, such as low potential to induce resistant phenotype, efficacy at lower drug doses, with a consequent mitigation of toxic effects, and possibility to target a broad spectrum of pathogens [67]. Interestingly, both r(P)ApoB$_L$ and r(P)ApoB$_S$ peptides showed synergism with systemic antibiotic ciprofloxacin against all the strains under test (FIC indexes ranging from 0.3 to 0.44). This would allow to significantly lower the doses of the antibiotic in the combination therapy approaches, with a consequent decrease of the appearance of resistant clinical isolates, an undesired phenomenon strongly affecting ciprofloxacin efficacy [68]. ApoB derived peptides also showed synergistic effects with colistin and vancomycin against most of the strains under test (FIC indexes ranging from 0.14 to 0.5). Since both colistin and vancomycin are responsible for toxic effects at high concentrations [67,69], a combination therapeutic approach based on a reduced frequency of antibiotic administration and/or exposure to antibiotic may offer several advantages over conventional dosing schemes. However, the most potent synergism was observed for both ApoB derived peptides in combination with EDTA, with FIC indexes ranging from 0.089 to 0.4. In the case of *P. aeruginosa* strains, synergism might be associated to EDTA ability to combine with magnesium ions playing a key role in the self-interaction of LPS molecules, with a consequent LPS release determining an increased permeability of bacterial membrane [50]. This might ultimately facilitate peptide internalization into bacterial cells, thus potentiating the peptide antimicrobial activity. EDTA is also known to determine the release of endogenous phospholipases, with a consequent alteration of Gram-negative bacteria outer membrane [70]. In the case of *S. aureus* strains, the increase of bacterial membrane permeability might be due to the ability of EDTA to solubilize extracellular polymeric substances [71], mainly composed by exopolysaccharides and playing a key role in biofilm establishment.

It should be highlighted that, although in some cases FIC indexes very close to 0.5 make it difficult to discriminate between synergistic and additive effects, no antagonistic interactions were observed between peptides and antimicrobials. Furthermore, combinations of ApoB derived peptides with antibiotics and EDTA were found to have a strong antimicrobial activity also towards strains on which the peptides alone were found to be ineffective, such as both *S. aureus* strains and *P. aeruginosa* ATCC 27853, indicating that in drug combinations a reciprocal facilitation and potentiation of different mechanisms of action is realized.

Interestingly, ApoB derived peptides are also endowed with anti-biofilm activity. Microorganisms growing in a biofilm state are very resilient to the treatment by many antimicrobial agents. Indeed, biofilm infections are a significant problem in chronic and long-term infections, including those colonizing medical devices and implants [52]. Specific cationic HDPs have recently been described to have multispecies anti-biofilm activity, which is independent of their activity against planktonic bacteria [9]. We found that ApoB derived peptides are effective on biofilm formation and biofilm attachment, and, even more interestingly, they strongly affect pre-formed biofilms. Furthermore, ApoB derived peptides display anti-biofilm activity even on bacterial strains not sensitive to the peptide antimicrobial activity, such as *S. aureus* MRSA WKZ-2, and, in the case of sensitive strains, even at peptide concentrations (0.625–1 μM) significantly lower than those required to directly kill planktonic cells. This is in agreement with previous reports indicating that LL-37 peptide potently inhibits the formation of bacterial biofilms *in vitro* at the very low and physiologically meaningful concentration of 0.5 μg/mL, significantly lower than that required to kill or inhibit bacterial growth (64 μg/mL) [72]. As a consequence of this, it should be emphasized that even at the highest ApoB derived peptides concentrations tested, a significant percentage of bacterial cells inside the biofilm structure appeared to be still alive. This was observed for both ApoB derived peptides and LL-37 control peptide, while it was less pronounced in the case of CATH-2 peptide. Based on this, it is tempting to speculate that successful therapeutic approaches could be designed by combining anti-biofilm peptides and conventional antibiotics ineffective on biofilm, but effective on bacterial cells entrapped into the biofilm structure.

From a structural point of view, by Far UV-CD analyses, we found that ApoB derived peptides are unstructured in aqueous buffer, and tend to assume a conformation in the presence of membrane mimicking agents. In the presence of increasing concentrations of LPS, r(P)ApoB$_L$ peptide was found to gradually assume a defined structure, what suggests a direct binding of this peptide to LPS. This was not observed, instead, in the case of r(P)ApoB$_S$ peptide. It has also to be highlighted that both r(P)ApoB$_L$ and r(P)ApoB$_S$ peptides are endowed with immunomodulatory activities by significantly decreasing the release of pro-inflammatory IL-6 and NO in LPS induced murine RAW 264.7 macrophages. Both ApoB derived peptides were found to efficiently act either when the cells were co-incubated with the peptide under test in the presence of LPS or when the cells were pre-treated with the peptide for 2 h and then incubated with LPS for further 24 h, thus indicating that both peptides are able to display a significant protective action. However, it has to be noticed that, differently from r(P)ApoB$_L$ peptide, r(P)ApoB$_S$ was found to play anti-

Please cite this article in press as: R. Gaglione et al., Novel human bioactive peptides identified in Apolipoprotein B: Evaluation of their therapeutic potential, Biochem. Pharmacol. (2017), http://dx.doi.org/10.1016/j.bcp.2017.01.009

inflammatory activities, when co-incubated with LPS, only at the highest peptide concentration tested (20 μM), whereas both r(P)ApoB$_S$ concentrations (5 and 20 μM) were found to efficiently exert a protective effect. This might be due to the fact that ApoB derived peptides probably act through different mechanisms, with r(P)ApoB$_L$ peptide mainly acting by binding to LPS and consequently interfering with its activity on target cells, and r(P)ApoB$_S$ peptide mainly acting on cell membrane and competing with LPS for the binding to specific cell sites. Therefore, a complex picture emerges, in agreement with the observation that HDPs immunomodulatory activities are extremely diverse [14]. Further experiments will allow us to elucidate the molecular mechanisms at the basis of ApoB derived peptides anti-inflammatory effects, which might include multiple aspects, such as stimulation of chemotaxis, suppression of bacterial induced pro-inflammatory cytokine production, regulation of neutrophil and epithelial cell apoptosis, modulation of cellular differentiation pathways, and promotion of angiogenesis and wound healing. As for the last aspect, in agreement with previous findings on LL-37 human peptide [73,74], we found that r(P)ApoB$_L$ peptide is able to stimulate human keratinocytes wound re-epithelialization *in vitro*, an evidence that opens new and interesting perspectives on future topical applications of this human HDP.

It has to be underlined that, although there are very few HDPs currently in use in the market, many are progressing through clinical trials that have focused on topic rather than systemic treatment because of peptides potential toxicity. However, it is conceivable that judicious formulations of HDPs for a clinical use, *e.g.* peptide inclusion in liposomal nanoparticles, will avoid undesired toxicity and degradation, thus allowing a sustainable HDPs delivery [18]. Here, we show that both ApoB derived peptides are not toxic for eukaryotic cells and do not determine any haemolytic effect when tested on murine red blood cells. These observations associated to their multifunctional properties and to their ability to synergistically act in combination with conventional antibiotic drugs open interesting perspectives to their therapeutic applications.

Conflict of interest statement

None declared.

Acknowledgements

We acknowledge “Programma di scambi internazionali con Università ed Istituti di ricerca stranieri per la mobilità di breve durata di docenti, ricercatori e studiosi” of the University of Naples Federico II, that financially supported scientific exchanges between Universities of Naples and Utrecht. The technical expert assistance by Dr. Johanna L. M. Tjeerdsma-van Bokhoven is acknowledged.

References

[1] M.T. Parker, J.H. Hewitt, Methicillin resistance in Staphylococcus aureus, Lancet 1 (1970) 800–804.
[2] J.N. Pendleton, S.P. Gorman, B.F. Gilmore, Clinical relevance of the ESKAPE pathogens, Exp. Rev. Anti Infect. Ther. 11 (2013) 297–308.
[3] M. Zasloff, Antimicrobial peptides of multicellular organisms, Nature 415 (2002) 389–395.
[4] D.A. Phoenix, S.R. Dennison, F. Harris, Antimicrobial Peptides: Their History, Evolution, and Functional Promiscuity, Wiley, 2013.
[5] R.E. Hancock, R. Lehrer, Cationic peptides: a new source of antibiotics, Trends Biotechnol. 16 (1998) 82–88.
[6] J.D. Hale, R.E. Hancock, Alternative mechanisms of action of cationic antimicrobial peptides on bacteria, Exp. Rev. Anti Infect. Ther. 5 (2007) 951–959.
[7] E.C. Spindler, J.D. Hale, T.H. Jr Giddings, R.E. Hancock, R.T. Gill. Deciphering the mode of action of the synthetic antimicrobial peptide Bac8c, Antimicrob. Agents Chemother. 55 (2012) 1706–1716.
[8] C.D. Fjell, J.A. Hiss, R.E. Hancock, G. Schneider, Designing antimicrobial peptides: form follows function, Nat. Rev. Drug Discov. 11 (2012) 37–51.
[9] C. de la Fuente-Nunez, F. Reffuveille, E.F. Haney, S.K. Straus, R.E. Hancock, Broad-spectrum anti-biofilm peptide that targets a cellular stress response, PLoS Pathog. 10 (2014) e1004152.
[10] A.F.G. Cicero, F. Fogacci, A. Colletti, Potential role of bioactive peptides in prevention and treatment of chronic diseases: a narrative review, Br. J. Pharmacol. (2016), http://dx.doi.org/10.1111/bph.13608.
[11] R.E.W. Hancock, M.G. Scott, The role of antimicrobial peptides in animal defences, Proc. Natl. Acad. Sci. U.S.A. 97 (2000) 8856–8861.
[12] D. Yang, A. Biragyn, D.M. Hoover, J. Lubkowski, J.J. Oppenheim, Multiple roles of antimicrobial defensins, cathelicidins, and eosinophil-derived neurotoxin in host defense, Annu. Rev. Immunol. 22 (2004) 181–215.
[13] D. Yang, A. Biragyn, L.W. Kwak, J.J. Oppenheim, Mammalian defensins in immunity: more than just microbicidal, Trends Immunol. 23 (2002) 291–296.
[14] A.T.Y. Yeung, S.L. Gellatly, R.E.W. Hancock, Multifunctional cationic host defence peptides and their clinical applications, Cell. Mol. Life Sci. 68 (2011) 2161–2176.
[15] D.M. Easton, A. Nijnik, M.L. Mayer, R.E.W. Hancock, Potential of immunomodulatory host defense peptides as novel anti-infectives, Trends Biotechnol. 27 (2009) 582–590.
[16] T.A. Waldmann, Immunotherapy: past, present and future, Nat. Med. 9 (2003) 269–277.
[17] J. Kindrachuk, E. Scruten, S. Attah-Poku, K. Bell, A. Potter, L.A. Babiuk, P.J. Griebel, S. Napper, Stability, toxicity, and biological activity of host defense peptide BMAP28 and its inversed and retro-inversed isomers, Biopolymers 96 (2011) 14–24.
[18] M. Sobczak, C. Dębek, E. Olędzka, R. Kozłowski, Polymeric systems of antimicrobial peptides – strategies and potential applications, Molecules 18 (2013) 14122–14137.
[19] K.L. Brown, R.E.W. Hancock, Cationic host defense (anti-microbial) peptides, Curr. Opin. Immunol. 18 (2006) 24–30.
[20] E. Guaní-Guerra, T. Santos-Mendoza, S.O. Lugo-Reyes, L.M. Terán, Antimicrobial peptides: general overview and clinical implications in human health and disease, Clin. Immunol. 135 (2010) 1–11.
[21] N. Mookherjee, R.E.W. Hancock, Cationic host defence peptides: innate immune regulatory peptides as a novel approach for treating infections, Cell. Mol. Life Sci. 64 (2007) 922–933.
[22] B.A. Kelly, I. Harrison, Á. McKnight, C.B.B. Dobson, Anti-infective activity of apolipoprotein domain derived peptides in vitro: identification of novel antimicrobial peptides related to apolipoprotein B with anti-HIV activity, BMC Immunol. 11 (2010) 13.
[23] C. Pierides, A. Bermudez-Fajardo, G.N. Fredrikson, J. Nilsson, E. Oviedo-Orta, Immune responses elicited by apoB-100-derived peptides in mice, Immunol. Res. 56 (2013) 96–108.
[24] K. Pane, V. Sgambati, A. Zanfardino, G. Smaldone, V. Cafaro, T. Angrisano, E. Pedone, S. Di Gaetano, D. Capasso, E.F. Haney, V. Izzo, M. Varcamonti, E. Notomista, R.E. Hancock, A. Di Donato, E. Pizzo, A new cryptic cationic antimicrobial peptide from human apolipoprotein E with antibacterial activity and immunomodulatory effects on human cells, FEBS J. 283 (2016) 2115–2131.
[25] E. Notomista, A. Falanga, S. Fusco, L. Pirone, A. Zanfardino, S. Galdiero, M. Varcamonti, E. Pedone, P. Contursi, The identification of a novel Sulfolobus islandicus CAMP-like peptide points to archaeal microorganisms as cell factories for the production of antimicrobial molecules, Microb. Cell Fact. 14 (2015) 126.
[26] S.H. Chen, C.Y. Yang, P.F. Chen, D. Setzer, M. Tanimura, W.H. Li, A.M. Gotto, L. Chan, The complete cDNA and amino acid sequence of human apolipoprotein B-100, J. Biol. Chem. 261 (1986) 12918–12921.
[27] C.Y. Yang, Z.W. Gu, S.A. Weng, T.W. Kim, S.H. Chen, H.J. Pownall, P.M. Sharp, S. W. Liu, W.H. Li, A.M. Jr, Gotto. Structure of apolipoprotein B-100 of human low density lipoproteins, Arteriosclerosis 9 (1989) 96–108.
[28] K. Pane, L. Durante, E. Pizzo, M. Varcamonti, A. Zanfardino, V. Sgambati, A. Di Maro, A. Carpentieri, V. Izzo, A. Di Donato, V. Cafaro, E. Notomista, Rational design of a carrier protein for the production of recombinant toxic peptides in Escherichia coli, PLoS ONE 11 (2016) e0146552.
[29] J. Reed, T.A. Reed, A set of constructed type spectra for the practical estimation of peptide secondary structure from circular dichroism, Anal. Biochem. 254 (1997) 36–40.
[30] M.A. Amon, M. Ali, V. Bender, K. Hall, M.-I. Aguilar, J. Aldrich-Wright, N. Manolios, Kinetic and conformational properties of a novel T-cell antigen receptor transmembrane peptide in model membranes, Peptide Sci. 14 (2008) 714–724.
[31] I. Wiegand, K. Hilpert, R.E. Hancock, Agar and broth dilution methods to determine the minimal inhibitory concentration (MIC) of antimicrobial substances, Nat. Protoc. 3 (2008) 163–175.
[32] F.C. Odds, Synergy, antagonism, and what the chequerboard puts between them, J. Antimicrob. Chemother. 52 (2003) 1.
[33] J. Li, T. Kleintschek, A. Rieder, Y. Cheng, T. Baumbach, U. Obst, T. Schwartz, P.A. Levkin, Hydrophobic liquid-infused porous polymer surfaces for antibacterial applications, ACS Appl. Mater Interfaces 5 (2013) 6704–6711.
[34] A. Arciello, N. De Marco, R. Del Giudice, F. Guglielmi, P. Pucci, A. Relini, D.M. Monti, R. Piccoli, Insights into the fate of the N-terminal amyloidogenic polypeptide of ApoA-I in cultured target cells, J. Cell Mol. Med. 15 (2011) 2652–2663.

[35] C.C. Liang, A.Y. Park, J.L. Guan, In vitro scratch assay: a convenient and inexpensive method for analysis of cell migration in vitro, Nat. Protoc. 2 (2007) 329–333.
[36] A. Di Grazia, F. Cappiello, A. Imanishi, A. Mastrofrancesco, M. Picardo, R. Paus, M.L. Mangoni, The frog skin-derived antimicrobial peptide esculentin-1a(1–21)NH2 promotes the migration of human HaCaT keratinocytes in an EGF receptor-dependent manner: a novel promoter of human skin wound healing? PLoS ONE 10 (2015) e0128663.
[37] F. Ascione, S. Caserta, S. Guido, Wound healing revisited: a transport phenomena approach, Chem. Eng. Sci. 160 (2017) 200–209.
[38] F. Ascione, A. Vasaturo, S. Caserta, V. D'Esposito, P. Formisano, S. Guido, Comparison between fibroblast wound healing and cell random migration assays in vitro, Exp. Cell Res. 347 (2016) 123–132.
[39] A.Q. Cai, K.A. Landman, B.D. Hughes, Multi-scale modeling of a wound-healing cell migration assay, J. Theor. Biol. 245 (2007) 576–594.
[40] P.K. Maini, D.L.S. McElwain, D.I. Leavesley, Traveling wave model to interpret a wound-healing cell migration assay for human peritoneal mesothelial cells, Tissue Eng. 10 (2004) 475–482.
[41] G. Cumming, F. Fidler, D.L. Vaux, Error bars in experimental biology, J. Cell Biol. 177 (2007) 7–11.
[42] A.P. Subasinghage, D. O'Flynn, J.M. Conlon, C.M. Hewage, Conformational and membrane interaction studies of the antimicrobial peptide alyteserin-1c and its analogue [E4K]alyteserin-1c, Biochim. Biophys. Acta 2011 (1808) 1975–1984.
[43] R. Gopal, J.S. Park, C.H. Seo, Y. Park, Applications of circular dichroism for structural analysis of gelatin and antimicrobial peptides, Int. J. Mol. Sci. 13 (2012) 3229–3244.
[44] Y.J. Na, S.B. Han, J.S. Kang, Y.D. Yoon, S.K. Park, H.M. Kim, K.H. Yang, C.O. Joe, Lactoferrin works as a new LPS-binding protein in inflammatory activation of macrophages, Int. Immunopharmacol. 4 (2004) 1187–1199.
[45] Y.J. Seo, K.T. Lee, J.R. Rho, J.H. Choi, Phorbaketal A, isolated from the marine sponge phorbas sp., exerts its anti-inflammatory effects via NF-kappaB inhibition and heme oxygenase-1 activation in lipopolysaccharide-stimulated macrophages, Mar. Drugs 13 (2015) 7005–7019.
[46] A. Gosslau, S. Li, C.T. Ho, K.Y. Chen, N.E. Rawson, The importance of natural product characterization in studies of their anti-inflammatory activity, Mol. Nutr. Food Res. 55 (2011) 74–82.
[47] C. Nathan, Points of control in inflammation, Nature 420 (2002) 846–852.
[48] A. van Dijk, M.H. Tersteeg-Zijderveld, J.L. Tjeerdsma-van Bokhoven, A.J. Jansman, E.J. Veldhuizen, H.P. Haagsman, Chicken heterophils are recruited to the site of Salmonella infection and release antibacterial mature Cathelicidin-2 upon stimulation with LPS, Mol. Immunol. 46 (2009) 1517–1526.
[49] M. Vaara, Agents that increase the permeability of the outer membrane, Microbiol. Rev. 56 (1992) 395–411.
[50] R.E. Hancock, Alterations in outer membrane permeability, Annu. Rev. Microbiol. 38 (1984) 237–264.
[51] A.H. Delcour, Outer membrane permeability and antibiotic resistance, Biochim. Biophys. Acta 1794 (2009) 808–816.
[52] D. Pletzer, S.R. Coleman, R.E.W. Hancock, Anti-biofilm peptides as a new weapon in antimicrobial warfare, Curr. Opin. Microbiol. 33 (2016) 35–40.
[53] X. Feng, K. Sambanthamoorthy, T. Palys, C. Paranavitana, The human antimicrobial peptide LL-37 and its fragments possess both antimicrobial and antibiofilm activities against multidrug-resistant Acinetobacter baumannii, Peptides 49 (2013) 131–137.
[54] D. Takahashi, S.K. Shukla, O. Prakash, G. Zhang, Structural determinants of host defense peptides for antimicrobial activity and target cell selectivity, Biochimie 92 (2010) 1236–1241.
[55] K.A. Brogden, Antimicrobial peptides: pore formers or metabolic inhibitors in bacteria? Nat. Rev. Microbiol. 3 (2005) 238–250.
[56] D.I. Chan, E.J. Prenner, H.J. Vogel, Tryptophan- and arginine-rich antimicrobial peptides: structures and mechanisms of action, Biochim. Biophys. Acta 1758 (2006) 1184–1202.
[57] M.L. Mangoni, A.M. McDermott, M. Zasloff, Antimicrobial peptides and wound healing: biological and therapeutic considerations, Exp. Dermatol. 25 (2016) 167–173.
[58] A. Tremel, A. Cai, N. Tirtaatmadja, B.D. Hughes, G.W. Stevens, K.A. Landman, A. J. O'Connor, Cell migration and proliferation during monolayer formation and wound healing, Chem. Eng. Sci. 64 (2009) 247.
[59] R.E.W. Hancock, K.L. Brown, N. Mookherjee, Host defence peptides from invertebrates—emerging antimicrobial strategies, Immunobiology 211 (2006) 315–322.
[60] R.E.W. Hancock, G. Diamond, The role of cationic anti-microbial peptides in innate host defences, Trends Microbiol. 8 (2000) 402–410.
[61] A.K. Marr, W.J. Gooderham, R.E.W. Hancock, Antibacterial peptides for therapeutic use: obstacles and realistic outlook, Curr. Opin. Pharmacol. 6 (2006) 468–472.
[62] E. Guaní-Guerra, T. Santos-Mendoza, S.O. Lugo-Reyes, L.M. Terán, Antimicrobial peptides: general overview and clinical implications in human health and disease, Clin. Immunol. 135 (2010) 1–11.
[63] P. Papareddy, M. Kalle, G. Kasetty, M. Mörgelin, V. Rydengård, B. Albiger, K. Lundqvist, M. Malmsten, A. Schmidtchen, C-terminal peptides of tissue factor pathway inhibitor are novel host defense molecules, J. Biol. Chem. 285 (2010) 28387–28398.
[64] E. Andersson, V. Rydengard, A. Sonesson, M. Morgelin, L. Bjorck, A. Schmidtchen, Antimicrobial activities of heparin-binding peptides, Eur. J. Biochem. 271 (2004) 1219–1226.
[65] S.G. Young, Recent progress in understanding apolipoprotein B, Circulation 82 (1990) 1574–1594.
[66] O.L. Franco, Peptide promiscuity: an evolutionary concept for plant defense, FEBS Lett. 585 (2011) 995–1000.
[67] H.M. Nguyen, C.J. Graber, Limitations of antibiotic options for invasive infections caused by methicillin-resistant *Staphylococcus aureus*: is combination therapy the answer? J. Antimicrob. Chemother. 65 (2010) 24–36.
[68] G.S. Tillotson, I. Dorrian, J. Blondeau, Fluoroquinolone resistance: mechanisms and epidemiology, J. Med. Microbiol. 46 (1997) 457–461.
[69] M.E. Evans, D.J. Feola, R.P. Rapp, Polymyxin B sulfate and colistin: old antibiotics for emerging multiresistant gram-negative bacteria, Ann. Pharmacother. 33 (1999) 960–967.
[70] H. Nakaido, M. Vaara, Molecular basis of bacterial outer membrane permeability, Microbiol. Rev. 49 (1985) 1–32.
[71] S.L. Percival, P. Kite, K. Eastwood, R. Murga, J. Carr, M.J. Arduino, Tetrasodium EDTA as a novel central venous catheter lock solution against biofilm, Infect. Control Hosp. Epidemiol. 2 (2005) 515–519.
[72] J. Overhage, A. Campisano, M. Bains, E.C. Torfs, B.H. Rehm, R.E.W. Hancock, Human host defense peptide LL-37 prevents bacterial biofilm formation, Infect. Immun. 76 (2008) 4176–4182.
[73] J.D. Heilborn, M.F. Nilsson, G. Kratz, G. Weber, O. Sørensen, N. Borregaard, M. Ståhle-Bäckdahl, The cathelicidin anti-microbial peptide LL 37 is involved in re epithelialization of human skin wounds and is lacking in chronic ulcer epithelium, J. Invest. Dermatol. 120 (2003) 379–389.
[74] R. Shaykhiev, C. Beisswenger, K. Kändler, J. Senske, A. Püchner, T. Damm, J. Behr, R. Bals, Human endogenous antibiotic LL-37 stimulates airway epithelial cell proliferation and wound closure, Am. J. Physiol. Lung Cell. Mol. Physiol. 289 (2005) L842–L848.

Please cite this article in press as: R. Gaglione et al., Novel human bioactive peptides identified in Apolipoprotein B: Evaluation of their therapeutic potential, Biochem. Pharmacol. (2017), http://dx.doi.org/10.1016/j.bcp.2017.01.009

A new cryptic host defense peptide identified in human 11-hydroxysteroid dehydrogenase-1 β-like: from in *silico* identification to experimental evidence

A. Bosso[1,4*], L. Pirone[2*], R. Gaglione[3,4], K. Pane[1], A. Del Gatto[2], L. Zaccaro[2], S. Di Gaetano[2], D. Diana[2], R. Fattorusso[5], E. Pedone[2], V. Cafaro[1], H.P. Haagsman[4], A. van Dijk[4], M.R. Scheenstra[4], A. Zanfardino[1], O. Crescenzi[3], A. Arciello[3], M. Varcamonti[1], E.J.A. Veldhuizen[4], A. Di Donato[1], E. Notomista[1], E. Pizzo[1]

[1] Department of Biology, University of Naples Federico II, 80126, Naples, Italy;
[2] IBB, CNR, 80134, Naples, Italy;
[3] Department of Chemical Sciences, University of Naples Federico II, 80126, Naples, Italy
[4] Department of Infectious Diseases and Immunology, Utrecht University, 3584 CS Utrecht, Holland
[5] Department of Environmental, Biological and Pharmaceutical Sciences and Technologies, University of Campania "Luigi Vanvitelli", I-81100 Caserta, Italy;

*** Contributed equally**

Corresponding author

Elio Pizzo
Department of Biology, University of Naples Federico II, 80126, Naples, Italy
elipizzo@unina.it; +39-081679151

Abbreviations

HDP: host defence peptides; **LPS**: lipopolysaccharide; **LTA**: lipoteichoic acid; **MIC**: Minimum inhibitory concentration; **SD**: standard deviation; **CD**: circular dichroism; **TFE**: trifluoroethanol; **IL-6**: interleukin 6; **NO**: nitric oxide; **CFU**: colony forming unit; **RBC**: Red blood cell; **HBTU**: 2-(1H-benzotriazole-1-yl)-1,1,3,3-tetramethyluronium hexafluorophosphate; **Oxyma**: cyano-hydroxyimino-acetic acid ethyl ester; **DIPEA**: N,N′-diisopropylethylamine; **TFA**: trifluoroacetic acid; **MeIm**: 4-methylimidazole; **MSNT** : 1-(Mesitylene-2-sulfonyl)-3-nitro-1,2,4-triazole; **DMF**: N,N-Dimethylformamide; **ACN**: Acetonitrile; **DCM**: dichloromethane; **Fmoc**: fluorenylmethyloxycarbonyl; **CATH-2**: cathelicidin-2; **TSA**: Tryptic Soy Agar; **AS**: absolute score; **MHB**: Muller Hinton broth; **NB**: Nutrient Broth

Abstract

Background
Host Defence Peptides (HDPs) are evolutionarily conserved components of innate immunity. Human HDPs, produced by a variety of immune cells of hematopoietic and epithelial origin, are generally grouped into two families: beta structured defensins and variably-structured cathelicidins. We report the characterization of a very promising cryptic human HDP, here called GVF27, identified in 11-hydroxysteroid dehydrogenase-1 β-like protein.

Methods
Conformational analysis of GVF27 and its propensity to bind endotoxins were performed by NMR, Circular Dichroism, Fluorescence and Dynamic Light Scattering experiments. Crystal violet and WST-1 assays, ATP leakage measurement and colony counting procedures were used to investigate antimicrobial, anti-biofilm, cytotoxicity and hemolytic activities. Anti-inflammatory properties were evaluated by ELISA.

Results
GVF27 possesses significant antibacterial properties on planktonic cells and sessile bacteria forming biofilm, as well as promising dose dependent abilities to inhibit attachment or eradicate existing mature biofilm. It is unstructured in aqueous buffer, whereas it tends to assume a helical conformation in mimic membrane environments as well as it is able to bind lipopolysaccharide (LPS) and lipoteichoic acid (LTA). Notably it is

not toxic towards human and murine cell lines and triggers a significant innate immune response by attenuating expression levels of pro-inflammatory interleukins and release of nitric oxide in LPS induced macrophages

Conclusion
Human GVF27 may offer significant advantages as leads for the design of human-specific therapeutics.

General significance
Human cryptic host defence peptides are naturally no immunogenic and for this they are a real alternative for solving the lack of effective antibiotics to control bacterial infections.

Highlights

A new human cryptic peptide, named GVF27, has been identified in 11-hydroxysteroid dehydrogenase-1 β-like

GVF27 is unstructured in aqueous buffer but assumes a well defined conformation in mimic membrane environments

GVF27 exerts anti-biofilm actions and broad spectrum antimicrobial activities

GVF27 binds bacterial endotoxins as LPS and LTA

GVF27 induces mitigation of pro-inflammatory mediators production in LPS induced murine macrophages

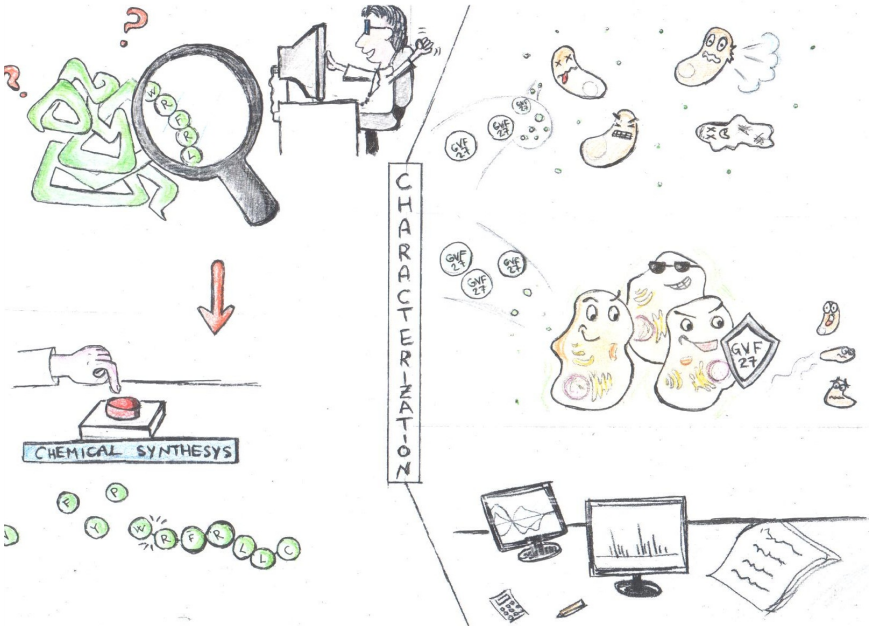

1. Introduction

Antimicrobial peptides are natural multifunctional molecules produced by various organisms such as mammals, arthropods, plants and bacteria [1,2]. The largest group of antimicrobial peptides includes cationic antimicrobial peptides, also called host defense peptides (HDPs), effectors of the innate immune system that contribute to the rapid clearance of adverse biological agents [3]. In contrast to conventional antibiotics, HDP-mediated killing of microorganisms occurs via multiple mechanisms attacking both the cell membrane and/or intracellular targets [4]. Cationic HDPs have been proved to be active against virtually all types of existing pathogens which have shown none or poor ability to develop resistance to their antimicrobial activity [4,5]. In fact, it has been proposed that the resistance mechanisms would have high impacts on fitness and virulence of the mutants, since the pathogens need to acquire mutations on membrane and wall composition [6]. For this reason, current reports point out to the great potential of this class of innate immune molecules to constitute a novel group of wide spectrum therapeutic effectors.

Cationic HDPs are divided into subgroups on the basis of their amino acid composition and structure [7]: α-helical peptides, linear peptides enriched for specific amino acids (e.g. proline and arginine), and peptides containing cysteine residues and prone to form stable β-sheets. Cationic HDPs generally contain 12–50 amino acids, with 2-9 positively charged lysine or arginine residues, and up to 50% hydrophobic amino acids. They are able to interact with and insert into biomembranes on the basis of their hydrophobicity and net positive charge, conformational flexibility and secondary structure [8]. Additionally, many cationic HDPs can potentially prevent septic shock via their anti-endotoxic activity through electrostatic interactions with lipopolysaccharides (LPS) and lipoteichoic acid (LTA) in the bacterial membrane [9,10].

In addition to their antimicrobial activity, HDPs are able to modulate immune response, including the boosting of innate immunity and the suppression of inflammatory responses/endotoxaemia [11,12]. It has been noted indeed that some HDPs regulate LPS-induced gene transcription and cytokine production by several mechanisms as inhibition of LPS-induced translocation of the NF-kB subunits p50 and p65 [13], selective inhibition of gene transcription (e.g. p50, TNFAIP2) [13], reduction of the expression of others (TNF-α) [13], triggering of MAPK pathways that can impact on pro-inflammatory pathways [14], direct interaction with LPS to reduce its binding to LBP, MD2, or another component of the TLR4 receptor complex, thus reducing activation of the downstream pathway [15], and protection against the development of endotoxin shock *in vivo* [16]. Cationic HDPs may act either directly or indirectly, by selectively inducing chemokine production in immune cells and recruitment of other immune cells to the site of infection [17,18]. At the same time, HDPs may enhance antigen uptake and presentation and inhibit apoptosis of neutrophils and macrophages [17,18].

Cationic HDPs are expressed in different cell types, including monocyte/macrophages, neutrophils, epithelial cells, keratinocytes and mast cells. Some HDPs are constitutively expressed, whereas others are inducible by pathogen signature molecules, inflammatory conditions or tissue injury [19]. They are generally expressed as pro-peptides that undergo subsequent proteolytic processing to release the biologically active, mature host defense peptide [20].

It has been widely reported that in multicellular eukaryotes several proteins, with properties not necessarily associated to immunity, are sources of "cryptic" cationic host defense peptides [21]. These HDP releasing proteins release biologically active peptides only after their proteolytic processing by bacterial and/or host proteases.

The use of bioinformatic approaches has increased the possibility to highlight the presence of putative antimicrobial regions in proteins, thus representing an extremely useful tool for the discovery of new cryptic host defense peptides [22]. The bioinformatic strategy we recently developed [23] for the identification of potential HDP releasing proteins and the accurate localization of the fragment(s) hidden in their amino acidic sequences, is an example of such a procedure. The procedure we have developed is based on the finding that the antimicrobial potency (AP) of an HDP [defined as AP = Log(1000/MIC)] is linearly

correlated to an “absolute score” (AS) which depends on charge, hydrophobicity and length of the peptide, and on two bacterial strain specific coefficients which determine the contribution of charge and hydrophobicity to the antimicrobial potency. Calculation of AS by a sliding window analysis provides a simple and effective method to localize HDPs (“cryptic” HDPs) contained within the structure of proteins, but also to analyze the internal structure of long HDPs, thus providing a very valuable tool for HDP identification and analysis.

Analyzing a pool of human secreted proteins using this approach, we identified a region rich in very high scoring peptides (see Figure S1A and B) at the C-terminus of four isoforms of human 11-hydroxysteroid dehydrogenase-1 β-like (accession number UniProtKB: Q7Z5J1). It should be noted that human 11β-hydroxysteroid dehydrogenase type 1 (HSD 1) is a known NADP(H)-dependent enzyme that catalyzes the conversion of inactive glucocorticoids into active forms and its dysregulation is mainly implicated in the development of metabolic syndromes [24]. On the contrary, human 11-hydroxysteroid dehydrogenase-1 β-like, also known as 11-beta-hydroxysteroid dehydrogenase type 3 (HSD 3), the sequence in which the high scoring region has been found, has never been isolated as a protein and its membership to the hydroxysteroid dehydrogenase family has been assigned on the basis of the presence in the gene sequence of a putative dehydrogenase/reductase region partially similar to that extensively studied in HSD 1 [25]. The only type of evidence that supports the existence of HSD 3 as a protein is represented by expression data [26] that indicate the existence of a transcript (Gene ID: 374875) apparently overexpressed in the brain and in lung cancer cells.

The isometric plot of the C-terminal region shows an absolute maximum (AS = 18.7 using the parameters determined for *S. aureus* C623) corresponding to a 39 residue long peptide (the longer arrow in Figure S1A) and a local maximum (AS = 16.1) corresponding to a 26 residue long peptide (the shorter arrow in Figure S1A). The region selected for the characterization (Figure S1A and C), herein called GVF27, corresponds to this local maximum plus the glycine residue located upstream the 26 residues. The glycine residue was included in the peptide as, according to [27], a glycine at the N-terminus of an antimicrobial peptide is favorable for the activity.

In this work, we fully characterize peptide GVF27 describing its bactericidal properties against planktonic and sessile bacteria, its cytotoxic and anti-inflammatory effects on murine cells and its structural properties in the presence of mimic membrane agents and wall bacterial determinants, such as LPS and LTA.

A

```
SP|Q7Z5J1-2|DHI1L_HUMAN      MKVLLLTGLGALFFAYYWDDNFDPASLQGARVLLTGANAGVGEELAYHYARLGSHLVLTA 60
SP|Q7Z5J1-5|DHI1L_HUMAN      ------------------------------------------------------------
SP|Q7Z5J1-6|DHI1L_HUMAN      MKVLLLTGLGALFFAYYWDDNFDP---------------------------------- 24
SP|Q7Z5J1-7|DHI1L_HUMAN      ------------------------------------------------------------

SP|Q7Z5J1-2|DHI1L_HUMAN      HTEALLQKVVGNCRKLGAPKVFYIAADMASPEAPESVVQFALDKLGGLDYLVLNHIGGAP 120
SP|Q7Z5J1-5|DHI1L_HUMAN      -------------------------MASPEAPESVVQFALDKLGGLDYLVLNHIGGAP 33
SP|Q7Z5J1-6|DHI1L_HUMAN      ---------------------------------------GGLDYLVLNHIGGAP 39
SP|Q7Z5J1-7|DHI1L_HUMAN      ------------------------------------------------------------

SP|Q7Z5J1-2|DHI1L_HUMAN      AGTRARSPQATRWLMQVNFVSYVQLTSRALPSLTDSKGSLVVVSSLLGRVPTSFSTPYSA 180
SP|Q7Z5J1-5|DHI1L_HUMAN      AGTRARSPQATRWLMQVNFVSYVQLTSRALPSLTDSKGSLVVVSSLLGRVPTSFSTPYSA 93
SP|Q7Z5J1-6|DHI1L_HUMAN      AGTRARSPQATRWLMQVNFVSYVQLTSRALPSLTDSKGSLVVVSSLLGRVPTSFSTPYSA 99
SP|Q7Z5J1-7|DHI1L_HUMAN      -------------MQVNFVSYVQLTSRALPSLTDSKGSLVVVSSLLGRVPTSFSTPYSA 46

SP|Q7Z5J1-2|DHI1L_HUMAN      AKFALDGFFGSLRRELDVQDVNVAITMCVLGLRDRASAAEAVRGVTRVKAAPGPKAALAV 240
SP|Q7Z5J1-5|DHI1L_HUMAN      AKFALDGFFGSLRRELDVQDVNVAITMCVLGLRDRASAAEAVRGVTRVKAAPGPKAALAV 153
SP|Q7Z5J1-6|DHI1L_HUMAN      AKFALDGFFGSLRRELDVQDVNVAITMCVLGLRDRASAAEAVRGVTRVKAAPGPKAALAV 159
SP|Q7Z5J1-7|DHI1L_HUMAN      AKFALDGFFGSLRRELDVQDVNVAITMCVLGLRDRASAAEAVRGVTRVKAAPGPKAALAV 106

SP|Q7Z5J1-2|DHI1L_HUMAN      IRGGATRAAGVFYPWRFRLLCLLRRWLPRPRAWFIRQELNVTAAAA 286
SP|Q7Z5J1-5|DHI1L_HUMAN      IRGGATRAAGVFYPWRFRLLCLLRRWLPRPRAWFIRQELNVTAAAA 199
SP|Q7Z5J1-6|DHI1L_HUMAN      IRGGATRAAGVFYPWRFRLLCLLRRWLPRPRAWFIRQELNVTAAAA 205
SP|Q7Z5J1-7|DHI1L_HUMAN      IRGGATRAAGVFYPWRFRLLCLLRRWLPRPRAWFIRQELNVTAAAA 152
```

B

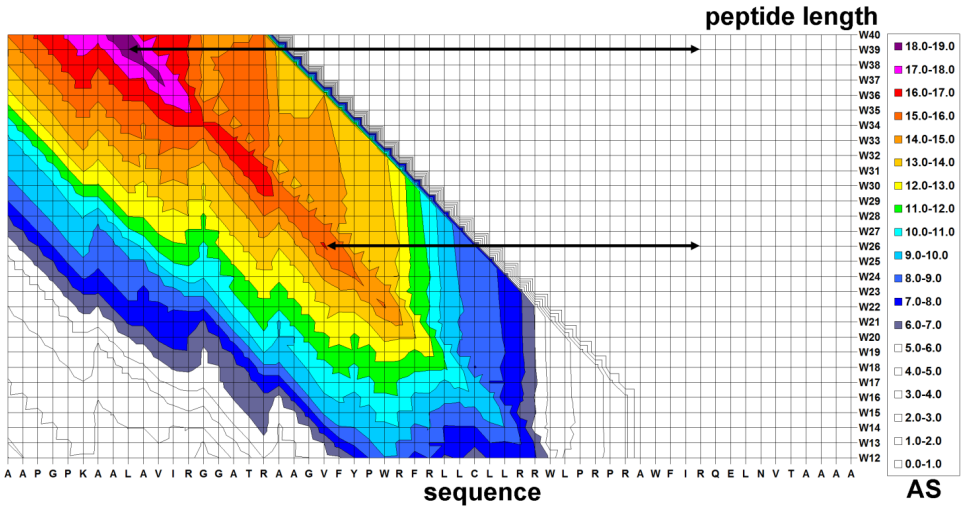

C

```
1                                   27
GVFYPW F LLCLL  WLP P AWFI
```

Figure S1 Analysis of the hypothetical antimicrobial region at the C-terminus of isoforms 2, 5, 6 and 7 of human 11-hydroxysteroid dehydrogenase-1 like. Panel A shows a multiple alignment of isoforms 2, 5, 6 and 7 of human 11-hydroxysteroid dehydrogenase 1 β-like. The region highlighted in yellow has been selected for the analysis shown in panel B. Peptide GVF27 is shown in red. **Panel B** shows an isometric plot of the absolute antimicrobial scores (AS) of all the peptides of length between 12 and 40 residues (W12-W40 on the ordinate) in the C-terminus of human 11-hydroxysteroid dehydrogenase 1 β-like. AS values were calculated using the parameters determined for strain *S. aureus* C623. Colors have been used to highlight scores corresponding to significant hypothetical MIC values, in particular an AS > 7 corresponds to a hypothetical MIC lower than 65 μM. **Panel C** shows the sequence of GVF27 colored according to the properties of amino acids (blue, positively charged; green, hydrophobic; grey, glycine and proline).

2. Materials and methods

2.1 Peptide synthesis

Peptide GVF27 was manually synthesized using the fluorenylmethyloxycarbonyl (Fmoc) solid-phase strategy (0.1 mmol). Synthesis was performed on NovaSyn TGA resin (loading 0.25 mmol/g), using all standard amino acids. The first amino acid was bound to the resin by treatment with Fmoc-Thr(tBu)-OH (5equiv)/MSNT (5 equiv)/MeIm (3.75 equiv) in DCM for 3 h. Fmoc protecting group was removed by reaction with 30% piperidine in DMF (3 × 10 min). The amino acids in 10-fold excess were pre-activated with HBTU (9.8 equiv)/HOBT (9.8 equiv)/DIPEA (10 equiv) in DMF for 5 min and then added to the resin suspended in DMF. The reaction was carried out for 1 h and coupling efficiency was assessed by the Kaiser test. The peptide was cleaved off the resin by treatment with a mixture of trifluoroacetic acid (TFA)/water/triisopropylsilane (95:2.5:2.5 v/v/v) for 3 h at room temperature. Resin was filtered, and crude peptide was precipitated with diethyl ether, dissolved in H_2O/ACN solution, and lyophilized. The product was purified by preparative RP-HPLC on a Shimadzu system equipped with a UV−visible detector SPD10A using a Phenomenex Jupiter Proteo column (21.2 × 250 mm; 4 μm; 90 Å) and a linear gradient of H_2O (0.1% TFA)/ACN (0.1% TFA) from 20%–80% of ACN (0.1%TFA) in 20 min at a flow rate of 20 mL/min. Identity and purity of the compound were assessed by LC/MS using an AGILENT Q-TOF LC/MS instrument equipped with a diode array detector combined with a dual ESI source and an Agilent C18 column (2.1 × 50 mm; 1.8 μm; 300 Å) at a flow rate of 200 μL/min and a linear gradient of H_2O (0.01% TFA)/ACN (0.01% TFA) from 5%–70% of ACN (0.01% TFA) in 15 min.

2.2 Antimicrobial activity assays

Antimicrobial activity of GVF27 peptide was tested against *Escherichia coli* ATCC 25922, MRSA WKZ-2 (methicillin-resistant *Staphylococcus aureus*), *Salmonella enteriditis* 706 RIVM, *Bacillus globigii* TNO BM013, *Bacillus licheniformis* ATCC 21424, *Staphylococcus aureus* ATCC 29213, *Pseudomonas aeruginosa* PAO1, and *Pseudomonas aeruginosa* ATCC 27853. Bacteria were grown to mid-logarithmic phase in Muller Hinton broth (MHB) at 37°C. Cells were then diluted to 2 x 10^6 CFU/mL in Difco 0.5X Nutrient Broth (Becton-Dickenson, Franklin Lakes, NJ) containing increasing amounts of GVF27 (0,6-40 μM). Starting from a peptide stock solution, two-fold serial dilutions were sequentially carried out, accordingly to broth microdilution method [28]. Following over-night incubation, MIC_{100} values were determined as the lowest peptide concentration responsible for no visible bacterial growth. Similar antimicrobial assays to test salt resistant properties of GVF27 have been carried out following the same procedure described above and using 0.5X Nutrient Broth medium containing physiological concentrations of divalent cations as $CaCl_2$ and $MgSO_4$ (0.265 g/L and 0.097 g/L respectively).

2.3 Killing kinetics

To assess the time point of bacterial growth inhibition, killing kinetics with GVF27 were performed. Two different peptide concentrations (1 or 10 μM GVF27) were incubated with mid-logarithmic (2×10^6 CFU/mL) *E. coli* ATCC 25922 or MRSA WKZ-2. At 1, 5, 10, 20, 30, 60 and 120 min, 100 μL aliquots were taken and immediately plated on TSA. Additionally, 20 μL aliquots were diluted 10- to 1,000-fold and again 100 μL was plated. After 16 h incubation at 37 °C the surviving bacteria were counted.

2.4 ATP leakage measurements

MRSA WKZ-2 and *Escherichia coli* ATCC 25922 were grown in Muller Hinton broth (MHB) at 37°C to mid-logarithmic phase. Bacteria were centrifuged, resuspended in 10 mM phosphate buffer pH 7.0 + 1:100 MHB and diluted to 2×10^7 CFU/mL. From each diluted sample, 60 μL of bacterial suspension were

incubated with 60 µL peptide solution (0.5 or 2 µM) for 5 min at 37°C. Samples were then centrifuged, the supernatant was stored at 4°C until further use, and the bacterial pellet was suspended in lysis buffer and further incubated at 100°C. Cell lysates were centrifuged and supernatants were kept on ice. Subsequently, both intra- and extracellular ATP levels were determined using the Roche ATP bioluminescence kit HS II (Roche Diagnostics Nederland B.V., Almere, the Netherlands), according to the manufacturer's protocols.

2.5 Serum Stability Assays

The proteolytic susceptibility of GVF27 peptide was determined in 50% (v:v) human serum (Lonza, Basel, Switzerland). Human serum was previously activated by cooling at 4°C, centrifugation at 13,000 x g for 5 min and incubation at 37°C for 10 min in order to eliminate the lipid fraction. Then, 250 μL of serum was added to a 250 μL of an aqueous solution of GVF27 at a concentration of 1 mg/mL. The mixture was incubated at 37°C and, after 1, 2, 3 and 24 h, samples (25 µL) were centrifuged at 13,000 x g for 5 min and the supernatant was added to 75 µL of H_2O containing 0.1% TFA and further centrifuged. Supernatants were finally analyzed by the analytical Agilent 1200 Series Liquid Chromatograph, equipped with a binary pump delivery system, robotic autosampler, column thermostat and multi-wavelength detector. An ET 250/8/4 Nucleosil 5-C18 column Machery-Nagel column (300 x 4 mm, 5 μm) and a linear gradient of H_2O (0.1%TFA)/CH_3CN (0.1%TFA) from 5 to 70% of CH_3CN (0.1%TFA) in 30 min at flow rate of 1 mL/min were employed. The experiment was run in duplicate.

2.6 Anti-biofilm activity assays

Escherichia coli strain ATCC 25922 was grown over-night in Muller Hinton broth (MHB) and then diluted to 1×10^8 CFU/mL in BM2 medium containing increasing peptide concentrations (0.125-32 μM). Incubation with the peptide was carried out either for 4 h, in order to test peptide effects on biofilm attachment, or for 24 h, in order to test peptide effects on biofilm formation. When peptide effects on preformed biofilm were evaluated, bacterial biofilms were formed for 24 h at 37 °C, and then treated with increasing concentrations of the peptide (0.125-32 μM). In all the cases, at the end of the incubation, the crystal violet assay [29] was performed. To do this, the planktonic culture was removed from the wells, which were washed three times with sterile PBS prior to staining with 0.04% crystal violet for 20 min. The colorant excess was eliminated by three successive washes with sterile PBS. Finally, the crystal violet was solubilized with 33% acetic acid and samples optical absorbance values were determined at 630 nm by using a microtiter plate reader (FLUOstar Omega, BMG LABTECH, Germany). To determine the percentage of viable bacterial cells inside the biofilm structure, upon biofilm disruption with 0,1% Triton X-100, bacterial cells were ten-fold diluted on solid TSA and incubated for 16 h at 37 °C. Once evaluated the number of colony forming units, bacterial cell survival was calculated as follows: $(_{CFU\text{in treated sample}}/CFU_{\text{in untreated sample}})$ x 100.

2.7 Cytotoxicity Assay

Cytotoxic effects of peptide on RAW 264.7 cells were determined using the cell proliferation reagent WST-1 (Roche Applied Science, Mannheim, Germany), designed to be used for the spectrophotometric quantification of cell proliferation. Briefly 5×10^4 cells were seeded into a 96-well plate and incubated at 37°C with 5% CO_2. Medium was then replaced with 100 µL of fresh media containing peptide solution to a final concentration ranging from 0–40 µM/well. After 24 h of incubation at 37°C, the peptide-containing medium was removed, and 100 µL of fresh medium containing 10% WST-1 reagent was added to each well and

incubated for 30 min at 37°C in the dark. Subsequently, the absorbance was measured in a microtiter plate reader (FLUOstar Omega, BMG labtech) at 450 nm, using 650 nm as the reference wavelength.

2.8 Hemolytic Assay

EDTA anti-coagulated mouse blood was centrifuged for 10 min at 800 × g (20°C) to sediment the red blood cells. Pelleted RBCs were washed three times and diluted 200-fold in PBS. In 96-well polypropylene plates, 75 µL of serial peptide dilutions (0–80 µM) were mixed with an equal volume of RBC suspension and incubated for 1 h at 37 °C. PBS served as baseline and a 0.2% (v/v) Triton X-100 solution served as a control for complete lysis. Supernatants, collected after 10 min centrifugation at 1300 × g (20°C), were transferred into polystyrene 96-wells plates and absorbance was measured at 405 nm. Hemolysis (%) was calculated as follows: ((APeptide –ABlank)/(ATriton – ABlank)) × 100.

2.9 Measurement of nitric oxide production

Nitric oxide production was assessed as the accumulation of nitrite (NO_2^-) in cell supernatants as a result of 24 h incubation period. Nitrite concentrations were determined by a colorimetric reaction using the Griess reagent. Briefly, cell culture supernatants were mixed with an equal volume of 1% sulfanilamide (dissolved in 2.5% phosphoric acid) and incubated for 5 min. The same volume of 0.1% N-(1-naphthyl) ethylenediamine dihydrochloride was added and incubated for 5 min. The absorbance was measured at 520 nm using a 96-well microplate reader (FLUOstar Omega, BMG labtech).

2.10 Inhibition of IL-6 production mediated by GVF27

The ability of the peptide to modulate cytokine production in RAW 264.7 cells was measured by ELISA (enzyme-linked immunosorbent assay). Cells (5×10^4 cells/well) were seeded into 96-wells microtiter plates. The next day, culture medium was discarded and replaced with fresh medium either containing 1) a mixture of peptide (5 or 20 µM) and 50 ng/mL LPS (co-incubation) or 2) peptide alone (5 or 20 µM) for an initial incubation of 2 h followed by addition of 50 ng/mL LPS from *Salmonella* Minnesota (pre-incubation) or, 3) 50 ng/mL LPS for an initial incubation of 2 h followed by addition of peptide (5 or 20 µM, post-incubation). In all the cases, culture supernatants were collected after a total of 24 h incubation time. After each initial incubation with either LPS or peptide, the cells were washed three times with PBS prior to the subsequent addition of peptide or LPS to remove any residual traces of agents used during the pre-incubation. Expression levels of mouse IL-6 were measured using the commercial available DuoSet ELISA kits (R&D Systems), following the protocols provided by the manufacturer. All samples were centrifuged briefly at 5,000 rpm for 3 min at room temperature to remove cell debris prior to use. Microtiter plates were read at 450 nm using 550 nm as a reference wavelength to correct optical imperfections of the microtiter plate.

2.11 LPS binding assay

The ability of GVF27 to neutralize LPS was determined using the commercially available Limulus amebocyte lysate (LAL) assay (Pierce® LAL Chromogenic Endotoxin Quantitation Kit, Thermo Scientific, USA) [30]. Briefly, 25 µL of serially diluted peptide (25,12.5, 6.25 µM) was added to 25 µL of 0.5 U/ml *E. coli* O11:B4 LPS for 30 min at 37 °C, followed by incubation with 50 µL of amoebocyte lysate reagent for 10 min. Absorbance at 405 nm was measured 10 min after the addition of 100 µL of the chromogenic

substrate, Ac-Ile-Glu-Ala-Arg-p-nitroanilide. The amount of non-bound LPS was extrapolated from a standard curve, and percentage inhibition calculated as: [(amount of free LPS in control samples) − (amount of free LPS in test samples)] × 100/amount of free LPS in control samples.

2.12 Spectroscopic studies

CD spectra of GVF27 were recorded with a J-810 spectropolarimeter equipped with a Peltier temperature control system (Model PTC- 423-S, Jasco Europe, Cremella, LC, Italy). Far-UV measurements (190–260 nm) were carried out at 20° C using a 0.1 cm optical path length cell and a peptide concentration of 25 μM. CD spectra were recorded as described elsewhere [31,32]. Baseline was corrected by subtracting the complete buffer spectrum. CD spectra were carried out in the presence of LPS from *Pseudomonas aeruginosa* strain 10 (Sigma, purified by phenol extraction) and from *P. aeruginosa* clinical strain KK27 (kindly provided by Prof. De Castro). Further analyses were carried out in the presence of lipotechoic acid from *Staphylococcus aureus* (LTA, Product Number L 2515, Sigma). All measurements were recorded using different concentration of each compound (from 0.05 to 1.0 mg/mL). Baseline was corrected by subtracting the spectrum of both LPS and LTA alone at the same concentration. Additional CD spectra were performed using different concentrations of trifluoroethanol (TFE) (0-40%). Deconvolutions of CD spectra were obtained using the web-based program CdPro (http://lamar.colostate.edu/~sreeram/CDPro/).

Fluorescence experiments were carried out under the same conditions used for CD analyses. Fluorescence spectra were collected at 20°C using a Varian Cary Eclipse spectrophotometer at λ excitation of 295 and 280 nm, a 1.0 cm path length cell at 5 ε_{em} and 5 ε_{ex}. Emission spectra (300-400 nm) were collected in the presence of 40% TFE, 5 mg/mL LPS or 10 mg/mL LTA.

2.13 LPS micelles measurements by using dynamic light scattering (DLS)

To estimate the average size of the LPS particles, the Hydrodynamic Radii (RH) was measured by Dynamic Light Scattering technique (DLS). DLS measurements were carried out using a Zetasizer Nano ZS (Malvern Instruments, Westborough, MA) equipped with a 173° backscatter detector, at 25 °C, using a disposable sizing cuvette. DLS measurements in triplicate were carried out on aqueous LPS and LTA samples at 0.5 mg/mL. Data were analyzed using the Software of OMNISIZE (Viscotek). LPS and LTA size measurements were performed before and after peptide addition (0.5 mg/mL).

2.14 Nuclear magnetic resonance spectroscopy

NMR experiments were recorded at 25 °C on a Varian Unity INOVA 600 MHz NMR spectrometer equipped with a cold probe. Two-dimensional (2D) nuclear Overhauser effect spectroscopy (NOESY), total correlation spectroscopy (TOCSY) and 2D double-quantum-filtered correlated spectroscopy (DQFCOSY) experiments were recorded [33]. NOESY mixing times were 200 ms and TOCSY mixing times were 70 ms. These experiments were collected with 512 and 1024 complex points with acquisition times of 64 and 128 ms in the indirectly and directly acquired 1H dimensions, respectively. The DQFCOSY experiment was collected with 1024 and 2048 complex points and acquisition times of 128 and 256 ms in the indirectly and directly acquired 1H dimensions, respectively. In all experiments water suppression was obtained using pre-saturation in order to simultaneously suppress the hydroxyl protons from TFE that are in fast exchange with protons from water. Hydroxyl protons from TFE were seen to attenuate signals in both 1D and 2D datasets in WATERGATE based suppression. 1D spectra were analyzed using ACD/NMR Processor 12.0 (ACD/NMR

Processor Freeware, Version 12.01 Advanced Chemistry Development, Inc., Toronto, ON, Canada (2012), www.acdlabs.com). 2D TOCSY and NOESY spectra for 1H chemical shift assignment were analyzed using Neasy, a tool available in CARA (Computer Aided Resonance Assignment) software (Keller, R. L. J. The Computer Aided Resonance Assignment Tutorial. CANTINA Verlag, 2004, downloaded from cara.nmr.ch). Structure calculation was performed with the program CYANA version 2.1 [34]. The NOE cross peak intensities were used to obtain distance constraints. The angle restraints were derived from 3JHNHα coupling constants. Structure calculations were initiated from 100 random conformers; the 20 structures with the lowest CYANA target function ns were analyzed with the programs MOLMOL [35] and PyMOL Molecular Graphics System, Version 1.8 Schrödinger, LLC. (http://www.pymol.org/).

2.15 Statistics

Results are presented as the mean ± standard error of the mean (SEM) of at least three independent experiments. Statistical significance was assessed using one-way ANOVA in Prism software, version 6.02 (GraphPad Prism, La Jolla, CA, USA). All samples were compared to the negative control. *$p < 0.05$; **$p < 0.01$; ***$p < 0.001$.

3. Results

3.1 Antibacterial activity

The antibacterial effectiveness of synthetic GVF27 (see Methods) was determined by measuring its MIC values on a panel of Gram-negative and Gram-positive strains (**Table 1**). All GVF27 MIC values are comparable to those observed for control peptide CATH-2 [36,37] both on Gram-negative and Gram-positive strains (**Table 1**). In order to verify salt resistant properties of GVF27, MIC values were determined also in the presence of physiological amounts of divalent cations (see Methods). As shown in **Table S1,** MIC values determined in the presence of divalent cations were practically identical to those obtained in NB (see **Table 1 and S1**), thus indicating that antimicrobial properties of GVF27 are not affected by the different experimental conditions tested. When the killing rate of GVF27 was measured, none of the strains analyzed (MRSA WKZ-2 and *E.coli* ATCC 25922) survived after 2 h at 10 μM peptide doses (see **Figure S2**).

GRAM POSITIVE STRAINS	**GVF27**	**CATH-2**	**GRAM NEGATIVE STRAINS**	**GVF27**	**CATH-2**
	MIC values (μM)			**MIC values (μM)**	
MRSA WKZ-2	5	10	***E. coli*** **ATCC 25922**	10	10
B. globigii **TNO BMO13**	5	5	***P. aeruginosa*** **ATCC 27853**	10	10
B. licheniformis **ATCC 21424**	5	20	***P. aeruginosa*** **PAO1**	20	20
S. aureus **ATCC 29213**	5	10	***S. enteriditis*** **706 RIVM**	10	10

Table 1 Minimum Inhibitory Concentration (MIC, μM) values of GVF27 peptide, compared to those obtained for chicken cathelicidin-2 (CATH-2), against a panel of Gram-positive and Gram-negative bacteria. Values were obtained from a minimum of three independent trials.

GRAM POSITIVE STRAINS	0.5X NB	0.5X NB + cations	GRAM NEGATIVE STRAINS	0.5X NB	0.5X NB + cations
	MIC values (μM)			MIC values (μM)	
MRSA WKZ-2	5	10	***E. coli* ATCC 25922**	10	10
***B. globigii* TNO BMO13**	5	5	***S. enteriditis* 706 RIVM**	10	40

Table S1 Minimum Inhibitory Concentration (MIC, μM) values of GVF27 peptide, tested in different media, against a panel of two Gram-positive and two Gram-negative bacteria. Values were obtained from a minimum of three independent trials.

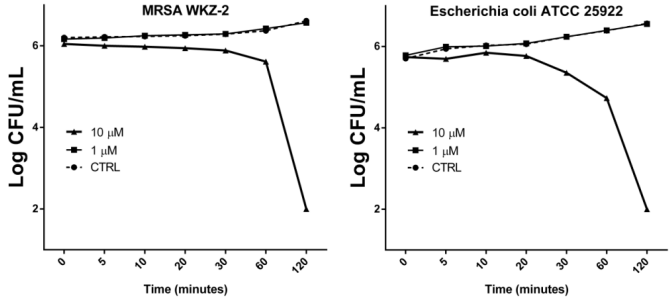

Figure S2 Antibacterial activity rate of GVF27, evaluated by colony count assay, against MRSA WKZ-2 and *Escherichia coli* ATCC 25922.

One of the mechanisms through which HDPs kill bacterial cells is by forming pores into biological membranes, resulting in the leakage of small molecules [38, 39]. We tried to collect data on the mechanism of the antibacterial activity of GVF27 by measuring ATP levels in the media in which bacterial cells are grown in the presence of the peptide. In fact, in bacterial cells intracellular ATP concentration is maintained constant and the release of ATP into the environment can be detected by chemiluminescence, which indicates the disruption of the cell membrane. Thus, we performed an assay to detect ATP leakage using two bacterial strains, *E. coli* and MRSA, treated with two different doses of GVF27 for 20 min (see Methods). As shown in **Figure 1** (panels A and B), the presence of ATP in the culture media is evident. Thus, we can confidently conclude that GVF27 has a lytic effect both on MRSA WKZ-2 and on *E.coli* cells, with MRSA WKZ-2 cells being particularly sensitive to the peptide. As it is shown in **Figure 1**, GVF27 induced in MRSA WKZ-2 cells a release of 70% ATP at a concentration of 0.5 μM. To obtain the same degree of ATP leakage in *E. coli* cells it was necessary a higher concentration of GVF27.

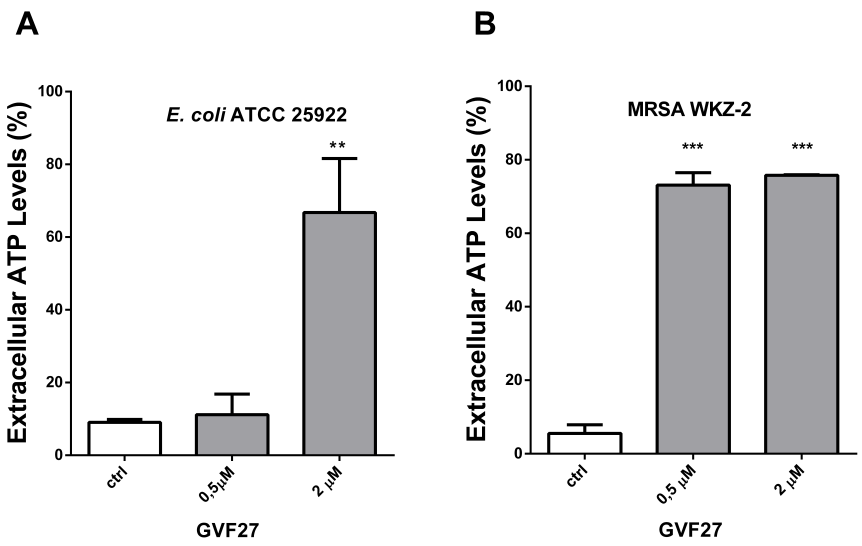

Figure 1. GVF27-induced ATP leakage in *Escherichia coli* ATCC 25922 (A) and MRSA WKZ-2 (B) after treatment with 0.5 or 2 µM GVF27. The assays were performed in three independent experiments.

Bacteria mainly exist as multicellular aggregates embedded within a self-produced extracellular polymeric matrix. In this condition, known as biofilm, growing microbial cells are physiologically distinct from planktonic cells. As natural HDPs have emerged as promising anti biofilm candidates to be used as an alternative to conventional antibiotics, we evaluated if GVF27 is endowed with anti-biofilm activity by performing experiments on *E. coli* ATCC 25922 in BM2 medium. *E. coli* was grown over-night, diluted in BM2 medium containing increasing concentrations of the peptide (from 0,125 to 32 µM), and then incubated for 24 h, at 37˚C. Following incubation, the analysis of biofilm production by crystal violet staining revealed a dose-dependent inhibition of biofilm formation, with about 90% inhibition at the highest concentration of peptide tested (**Figure 2A**). We also collected data that would indicate that GVF27 peptide exerts a significant effect on biofilm attachment. To investigate this, we followed the experimental procedure described above with the only exception that bacterial cells were incubated with increasing concentrations of peptide for 4 h, at 37°C. Also in this case, we observed a dose-dependent inhibition of biofilm attachment, with almost total inhibition at 32 µM peptide concentration (**Figure 2A**). Interestingly, GVF27 was found to exert significant effects also on preformed biofilms. This was evaluated by incubating preformed biofilm (see Methods) with increasing concentrations of the peptide for 24 h, at 37°C. At the highest peptide concentration tested, we observed a significant (~20%) reduction of the preformed biofilm (**Figure 2A**).

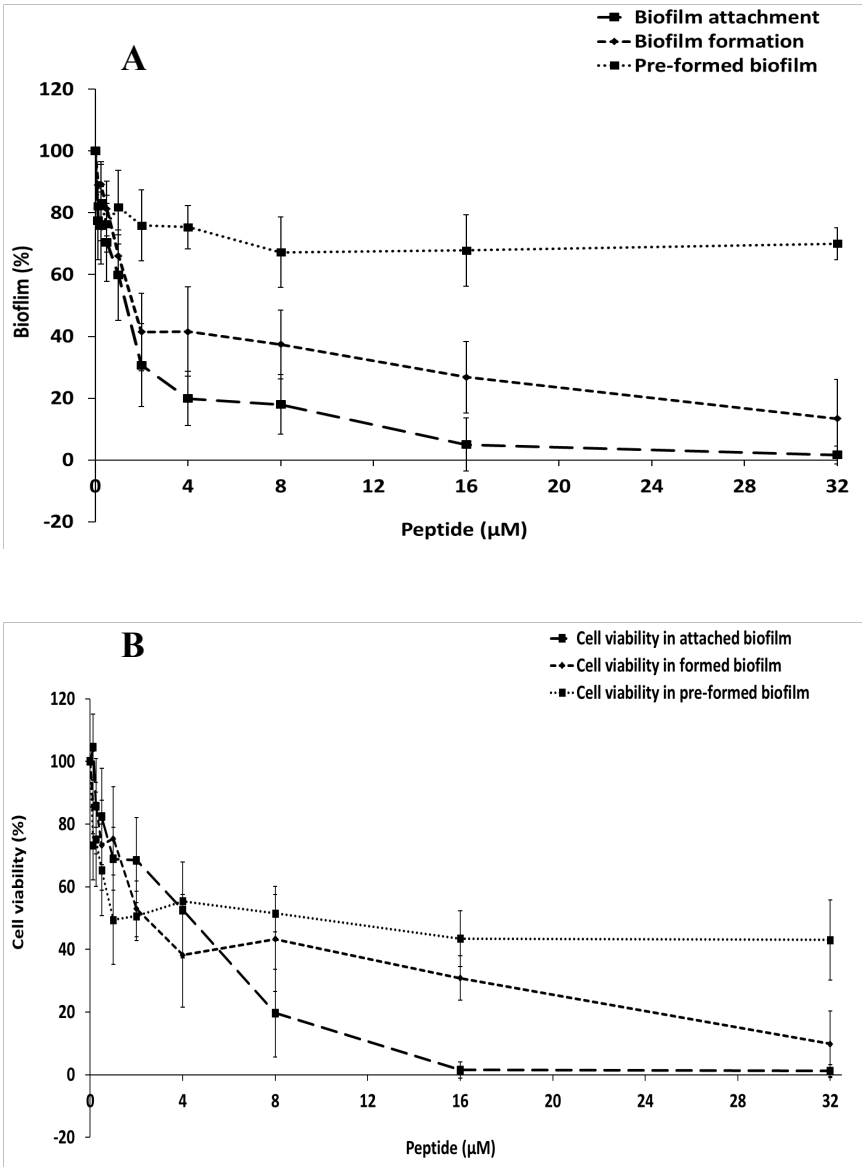

Figure 2. A. Biofilm inhibitory activity of GVF27 against *E. coli* strain in BM2 medium. The effects of increasing concentrations of GVF27 peptide were evaluated either on biofilm formation, biofilm attachment, or on pre-formed biofilm. Biofilm was stained with crystal violet and measured at 630 nm. Shown are mean + SD values of three independent experiments. **B. Effects of increasing concentrations of GVF27 peptide on the viability of *E. coli* ATCC 25922 bacterial cells inside the biofilm structure.** Cell viability was assessed by colony counting assay and expressed as the percentage of viable bacterial cells in treated samples with respect to the control untreated sample. Shown are mean + SD values of three independent experiments.

Experiments					
Biofilm formation		Biofilm attachment		Pre-formed biofilm	
Peptide [μM]	p-value	Peptide [μM]	p-value	Peptide [μM]	p-value
0,125	0,476	0,125	0,449	0,125	0,189
0,25	0,349	0,25	0,160	0,25	0,137
0,5	0,662	0,5	0,424	0,5	0,144
1	0,137	1	0,463	1	0,085
2	0,647	2	0,509	2	0,102
4	0,249	4	0,383	4	0,128
8	0,059	8	0,087	8	0,105
16	0,027	16	0,023	16	0,082
32	0,016	32	0,025	32	0,027

Table S3 P-values obtained for the experiments showed in Figure 2A

In all cases, we also evaluated the percentage of viable bacterial cells inside the biofilm by colony counting assay. We found (**Figure 2B**) an almost total reduction of bacterial viability when 32 μM GVF27 was added prior to biofilm attachment, a significant reduction (90%) when it was added prior to biofilm formation and a reduction of about 50% when the peptide was tested on pre-formed biofilm.

3.2 Cytotoxicity assays of GVF27 on eukaryotic cells

As already reported [38, 39], the promising interest in the use of HDPs stems from their selective action on bacterial cells. We thus studied the cytotoxic effect of GVF27 towards mouse macrophages and erythrocytes. The addition of increasing concentrations (from 0.6 to 40 μM) of GVF27 to mouse macrophages RAW 264.7 cells for 24 h did not result, in any significant reduction in cell viability (**Figure S3A**). The same peptide concentrations were tested also on mouse erythrocytes to detect any hemolytic activity of GVF27. As shown in **Figure S3B** , the peptide did not exert any lytic effect on mouse red blood cells, even at the highest concentration tested. The cytotoxicity of GVF27 was also measured against human keratinocytes (HaCat) and on human cervical cancer cells (HeLa). In all cases, no significant cytotoxicity was ever observed (data not shown). It should be underlined that GVF27 is toxic to bacterial cells (**Table 1, figures S2, 1 and 2**) at concentrations similar to that used in the cytotoxicity assays described above. Moreover, it should be noted that all the experiments mentioned above were carried out after an incubation time of 24 h, since the analysis of GVF27 stability in serum (see Methods) indicated that peptide degradation was almost complete after 24h (see **Table S2**).

Time (hour)	Area %
0	100
1	63
2	41
3	30
24	6

Table S2 Analysis of serum stability of GVF27 by RP-HPLC (see Methods)

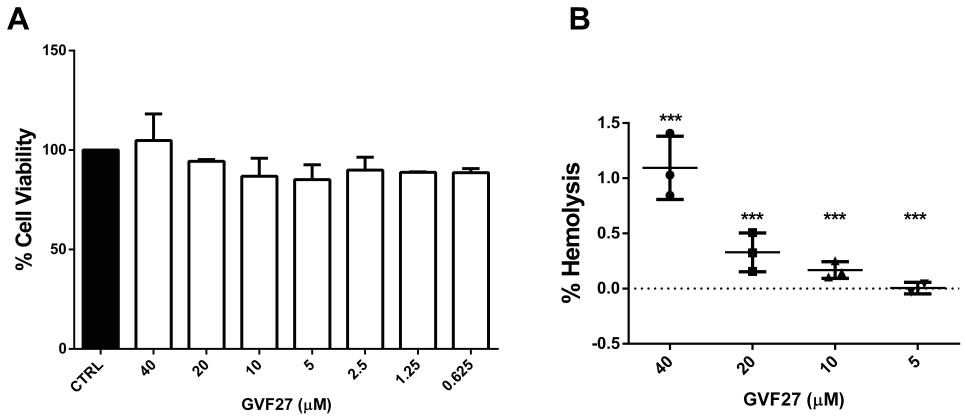

Figure S3 Cytotoxicity of GVF27 on eukaryotic cells. A) Effect of GVF27 on the viability of mouse macrophages RAW 264.7. B) Hemolytic activity of GVF27 on mouse erythrocytes. In both experiments the mean values ± SD from three independent experiments run in triplicate are shown.

3.3 Conformational studies of GVF27

3.3.1 Circular Dichroism and Fluorescence

Structural analysis by CD spectroscopy provides a qualitative picture of the structural elements that are present in a given peptide. Far-UV CD spectra indicate that GVF27 is largely unstructured both in water and in 10 mM Hepes pH 7.4. On the contrary, it is structured in 40% TFE (**Figure 3**). This behavior can be observed also for other HDPs [40, 41], all prone to assume a specific conformation when interacting with membrane-mimicking agents like TFE. Moreover, deconvolution data (see Methods) reported in **Table 2**, indicate that structured GVF27 adopts a predominant helical structure (approximately of ≈ 50%).

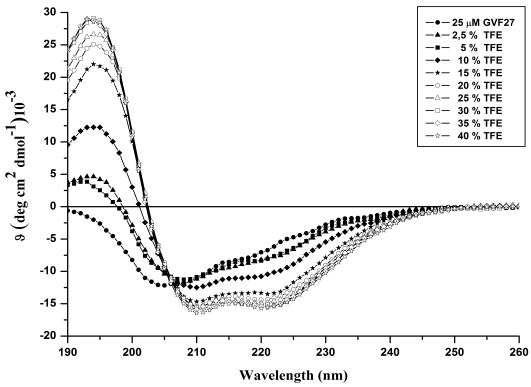

Figure 3: Far UV CD of GVF27 in the presence of increasing concentrations of TFE

	% α-helical	% β-strand	% coil
GVF27	18.2	24.0	57.8
GVF27 - 40 %TFE	52.6	7.2	40.2
GVF27 - 0,4 mg/mL LPS from *Pseudomonas aeruginosa* strain 10	30.8	18.6	50.6
GVF27 - 0,4 mg/mL LPS from *Pseudomonas aeruginosa* strain KK27	32.1	12.3	55.5
GVF27 - LTA 0,4 mg/mL	33.0	19.5	47.5

Table 2: Secondary structure content of GVF27, calculated by means of CDPRO program.

To further characterize structural properties of GVF27, the interaction with LPS and LTA, the main constituents of the cell wall of Gram negative and positive bacteria, respectively, was analyzed. CD spectra in the presence of LPS isolated from two different *P. aeruginosa* strains (strain 10 and clinical isolate KK27 strain) are shown in **Figure 4** (panels A and B).

GVF27 spectrum in water has a minimum at around 205 nm, indicating that the peptide is in a disordered conformation. Instead, in the presence of LPS (**Fig. 4A-B**), the peptide spectra present two minima centered around 210 and 225 nm, suggesting that in both cases it is able to assume a helical conformation upon interaction. The deconvolution data (Table 2) confirm that both LPSs induce a similar increase in the amount of helical structure (about 31-32%) but with slightly different amounts of beta and coil structure.

CD spectra, acquired in the presence of LTA, (**Figure 4C**), showed a relatively flat shape minimum centered at 215 nm, due to the presence of significant amounts both of alpha and beta structures as shown by deconvolution data (Table 2).

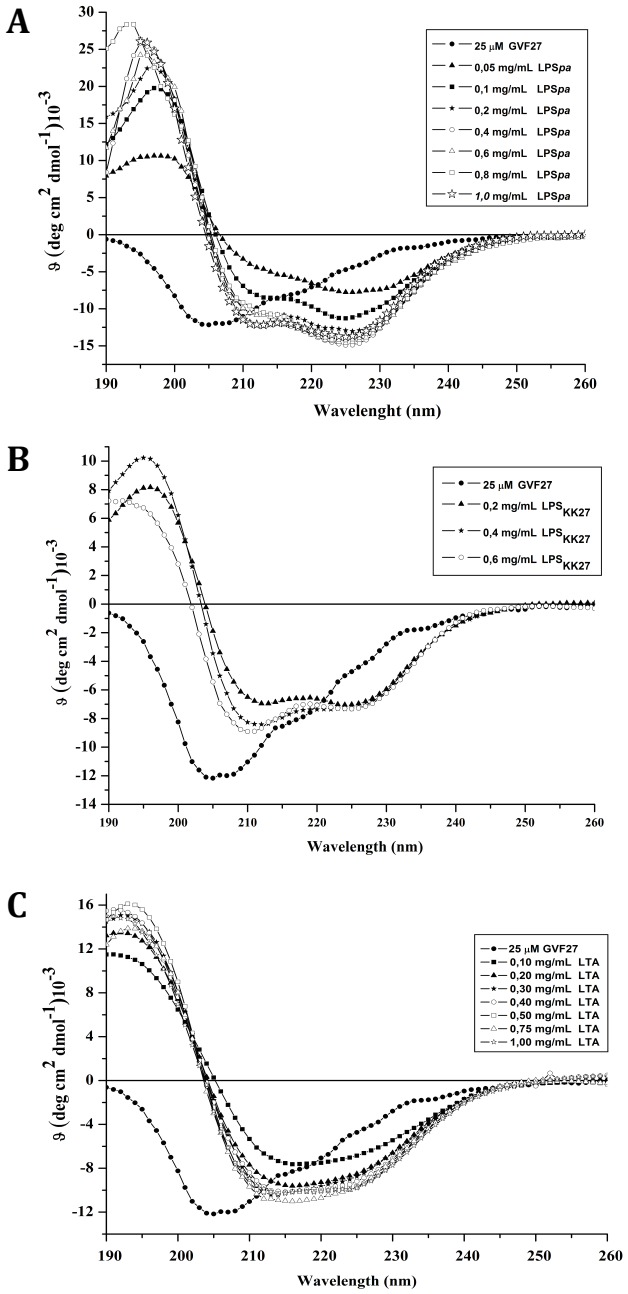

Figure 4 Far UV CD of GVF27 in the presence of increasing concentrations of LPS from *P. aeruginosa* 10 (A), from *P. aeruginosa* KK27 (B) and of LTA from *Staphylococcus aureus* (C)

Spectrofluorimetric data were also collected to investigate if the interaction of GVF27 with LPS and LTA could influence the tertiary structure of the peptide based on the presence in the sequence of three Trp residues (see Fig. S1). Fluorescence spectra were recorded upon excitation at 280 nm and 295 nm and showed (see Fig. S4) that the interaction of the peptide with LPS, LTA, and TFE results in a blue shift of the wavelength of the maximum of emission, indicating that GVF27 folds upon interaction with LPS or LTA, in agreement with CD data. However, in the presence of TFE a less marked effect was observed.

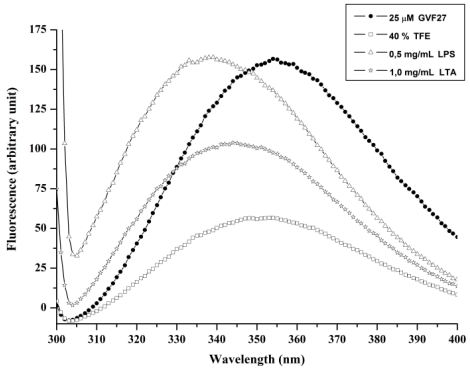

Figure S4 Tryptophan fluorescence spectra for GVF27 in H_2O and in the presence of TFE (40%), LPS (0,5 mg/mL) and LTA (1 mg/mL).

3.3.2 Structural characterization by NMR

A deeper investigation of the conformational preferences of peptide GVF27 was performed by NMR spectroscopy. In order to investigate the influence of the environment experienced by a membrane-interacting peptide on the structure, the NMR study was carried out both in bulk water, simulating the transport fluid, and in 30% TFE-d3/H2O) 30:70 (v/v) mixture, which reduces solvent polarity. The comparison of 1D spectra under these two conditions, reported in Figure 5A (upper and lower trace for water and TFE/water mixture respectively) reveals that in the less polar environment the dispersion of the chemical shift is higher. This is confirmed by the comparison of the 2D NOESY spectra, reported in the panel B and C respectively, showing also a higher number of cross-peaks in the presence of TFE. Then, NMR characterization of GVF27 was performed in TFE-d3/H_2O 30:70 (v/v) mixture at 298K. The standard sequential assignment approach based on homonuclear 2D 1H NMR [42] allowed the complete sequence specific ^{1}H NMR assignment (**Table 3**). Particularly, identification of spin systems and resonance assignment were established by a combination of two-dimensional DQF-COSY and TOCSY spectra, whereas sequence-specific assignment was obtained by NOESY experiments.

Residue	NH	αH	βH	γH	Others
Gly1	7.97	3.70			
Val2	8.10	3.99	1.95	0.96	
Phe3	7.90	4.58	2.92		2,6H 7.32; 3,5H 7.24
Tyr4	7.58	4.48	2.67		2,6H 6.95; 3,5H 6.73
Pro5		4.32	2.13; 1.98	1.89	δCH_2 3. 45
Trp6	7.68	4.32			2H 7.23; 4H 7.57; 6H 7.20; 7H 7.52; NH 10.02
Arg7	8.03	4.09	1.74		δCH_2 2.84
Phe8	7.76	4.59	2.88		2,6H 7.22; 3,5H 7.34
Arg9	7.86	3.85	1.60; 1.48	1.62	δCH_2 2.95
Leu10	7.74	3.96	1.74	1.50	δCH_3 0.85
Leu11	8.37	3.93	1.73	1.45	δCH_3 0.91
Cys12	7.56	4.58	3.00		
Leu13	7.85	3.88	1.65	1.48	δCH_3 0.82
Leu14	7.53	4.08	1.83	1.54	δCH_3 0.93
Arg15	7.57	3.94	1.71		
Arg16	7.55	4.00	1.89	1.71	δCH_2 3.33
Trp17	7.26	4.36	3.24; 3.00		2H 7.13; 4H 7.35; 6H 7.11; 7H 7.22; NH 9.89
Leu18	7.72	3.97	1.58	1.40	δCH_3 0.90
Pro19		4.21	2.40; 2.24	1.88	δCH_2 3. 55
Arg20	8.08	4.13	1.65	1.48	δCH_2 3.03
Pro21		4.23	2.40; 2.19		δCH_2 3. 36
Arg22	7.88	4.27	1.79	1.54	δCH_2 3.06
Ala23	7.25	4.16	1.27		
Trp24	7.46	4.32	3.26; 3.19		2H 7.02; 4H 7.31; 6H 7.07; 7H 7.20; NH 9.99
Phe25		4.41	2.78; 2.64		2,6H 7.00; 3,5H 6.80
Ile26	7.45	4.02	1.67	1.20	γCH_3 0.93; δCH_3 0.78
Arg27	7.32	4.32	1.53;1.28		δCH_2 2.98

Table 3: Proton chemical shifts (ppm) of GVF27 in TFE-d3/H_2O (30:70) at 298 K

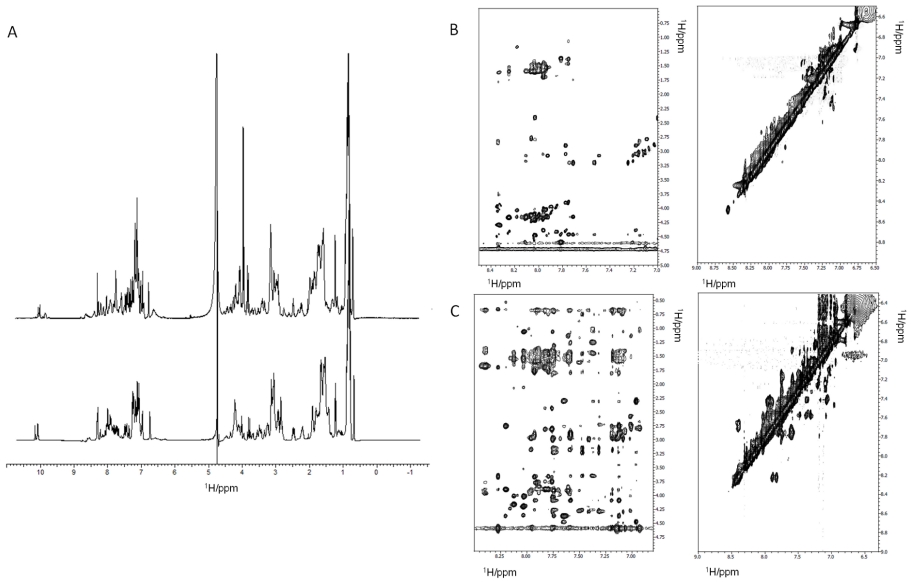

Figure 5. NMR conformational analysis. A) Superposition ^{1}H-NMR spectrum of GVF27 in water (upper) and in water/TFE mixture (lower). B) 2D [^{1}H, ^{1}H] NOESY spectrum of GVF27 in water at 298 K and pH 7.0 and C) in water/TFE mixture at 298 K and pH 7.0

The values of the deviation of Hα chemical shifts (ΔδHα) analysis performed by using Chemical Shift Index (CSI) (**Figure S5**) [43] and the 3JHN-Hα couplings **(Figure S6**) indicate the presence of a random coil structure in aqueous solution. On the other hand, GVF27 shows a significant change in the 1H chemical shifts and in^{3}JHN-Hα coupling values when TFE is added, suggesting that the entire polypeptide chain is involved in a conformational transition. Indeed, the ΔδHα and the ^{3}JHN-Hα coupling values indicate a high helical propensity of the entire polypeptide chain. Further, the 2D **[^{1}H, ^{1}H]** NOESY analysis showed several HN–HN (i, i+1), Hα–HN (i, i+3), and Hα-Hβ (i, i+3) connectivities (see Figure S7), confirming the presence of a helical conformation, in agreement with the trend suggested by the CSI analysis based on Hα and with CD data.

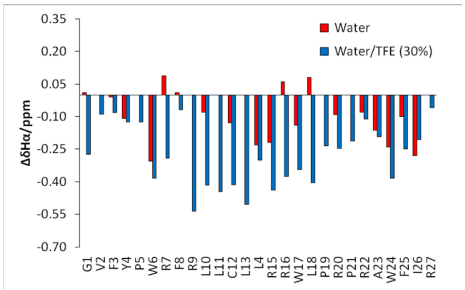

Figure S5. Hα chemical shift difference (ΔδHα) plotted for 27 residues of GVF27 in water (red) and in TFE-d3/H_2O 30:70 (blue) at 298 K and pH 7.0. Negative ΔδHα (ΔδHα ≥ 0.10 ppm) are indicative of helical conformation.

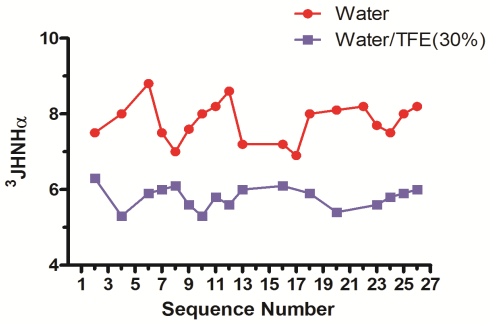

Figure S6. Observed values of the ^{3}JHNHα couplings for the peptide GVF27 in water (red) and TFE-d3/H_2O 30:70 (blue) mixture plotted against the residue number. Typical values of ^{3}JHNHα are 4 Hz for a α-helix, 9 Hz for a sheet and 7 Hz for a random coil structure.

A set of 267 (119 intra-residual, 88 sequential and 66 medium and long-range) experimental NOE constraints (**Table 4**) was used as upper limits of inter-proton distances for structure calculations by CYANA program [34]. The backbone overlay of the best 20 CYANA conformers displays a good convergence confirmed by a backbone and all heavy atoms root-mean-square difference (rmsd) values of 0.19±0.10Å and 1.24±0.15 Å respectively (**Figure 6**). Apart from some dynamic fraying at the N-terminus, the calculated structures comprise a regular α-helix, in agreement with the NOE data, H-bonding (**Table 5**) and the pattern of φ/ψangles (**Figure S7**).

No. of the distance restraints	
Unambiguous NOE	267
Ambiguous NOE	91
Total NOE	358
Divided into	
Intra-residue NOE	119
Sequential NOE	88
Medium- and Long- range NOE	60
Residual NOE violations	
Number>0.1°	±1
Maximum, Å	0.16±0.06
Residual angle violations	
Number>2.0°	0±0
Maximum, Å	0
R.m.s.d (Å) [a] **to a mean structure**	
Backbone (residues (5-20)	0.19 ±0.10
Heavy atoms (residues (5-20)	1.24±0.15
Ramachandran plot residues (%) [b]	
In most favored regions	62.1
In additional allowed regions	27.3
In generously allowed regions	10.6
In disallowed regions	0.0

Table 4: CYANA structural statistic of GVF27 in TFE-d3/H_2O (30:70)

Number	Residue	Atom	Number	Residue	Atom	Distance (Å)
7	Arg	HN	3	Phe	O	1.97
11	Leu	HN	7	Arg	O	2.20
13	Leu	HN	9	Arg	O	1.94
14	Leu	HN	10	Leu	O	1.92
22	Arg	HN	18	Leu	O	2.10
23	Ala	HN	19	Pro	O	1.99
24	Phe	HN	21	Pro	O	1.95

Table 5: Observed and calculated average hydrogen bond lengths for GVF27 in TFE-d3/H_2O (30:70)

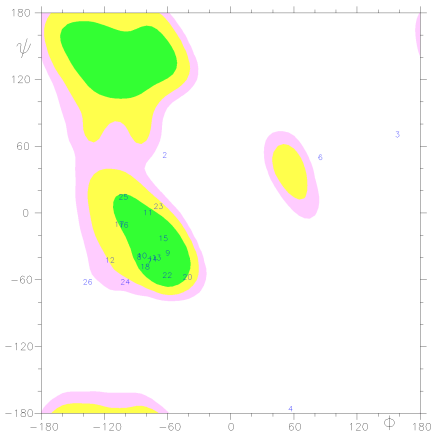

Figure S7: Ramachandran plot for the **GVF27** mean structure in TFE-d3/H_2O 30:70 mixture.

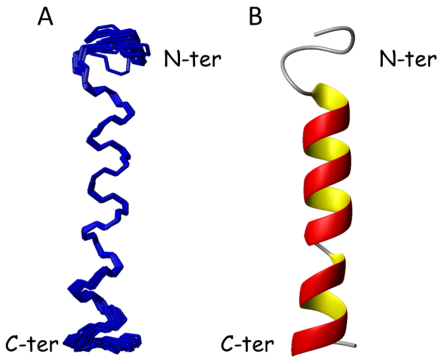

Figure 6: NMR structures of GVF27 in TFE-d3/H_2O 30:70 mixture at 298 K A) Backbone superposition of the 20 energy-minimized structures and B) Ribbon model of a representative structure

3.4 GVF27 assembles LPS aggregates

DLS is a well-known technique used to measure Brownian motion (diffusion) and size distribution of particles in solution. For this reason DLS experiments were used to investigate whether peptide GVF27 may alter the size of micelles of LPS and LTA (above their critical micelle concentration). In both cases GVF27 displayed an associating action, promoting the formation of larger aggregates. In particular, the data indicate that LPS from *Pseudomonas* is poly-dispersed in solution with major size-populations having a hydrodynamic radius centered at about 40 nm (**Figure 7**). Incubation of LPS with GVF27 causes a shift of the average size of LPS micelles to a higher value centered at about 260 nm. On the other hand, when the peptide was incubated with LTA, a mean diameter of 100 nm of the aggregates was observed, indicating a weaker potency of GVF27 in associating LTA aggregates.

It can be hypothesized that this aggregation action, already observed for other antimicrobial peptides [44], may be part of a LPS neutralization mechanism, inhibiting the interaction of LPS with its cell receptors, with the concomitant blocking of cytokine production and release [45].

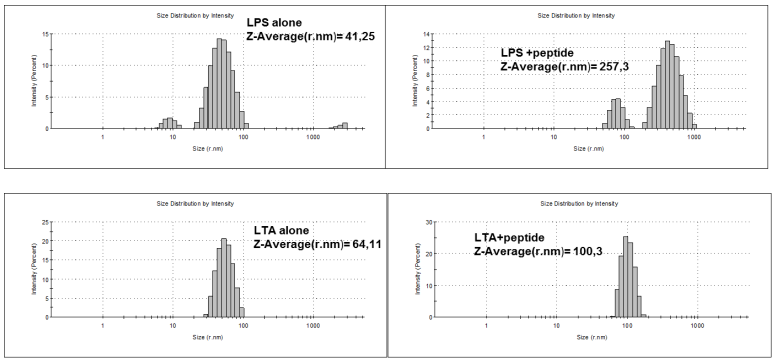

Figure 7: Effect of GVF27 on the structural organization of LPS or LTA micelles. Light scattering of LPS from *aeruginosa* 10 (top) or LTA (bottom) before and after incubation with the peptide

3.5 Anti-inflammatory properties of GVF27

Data above would indicate that GVF27 is able to assume specific conformations in the presence of mimic membrane agents, LPS and LTA, as well as to induce aggregation of LPS, and to a lesser extent of LTA. As it is has been already reported that several HDPs are able to mitigate up-regulation of LPS-induced pro-inflammatory mediators and cytokines [7, 46,47], it seemed interesting to verify if GVF27 could possess also putative anti-inflammatory properties. To collect data on possible anti-inflammatory properties of GVF27, nitric oxide production and interleukin Il-6 release by murine macrophages RAW 264.7 treated with GVF27 and LPS were analyzed.

Nitric oxide (NO) plays diverse roles in biological systems: it is a mediator of vasodilatation, platelet aggregation and neurotransmission, and regulates function, death and survival of various cell types including many of those involved in immunity and inflammation [48, 49].

To study the effect of GVF27 on NO production in LPS activated RAW 264.7 cells, we performed three types of treatments: 1. medium containing a mixture of peptide (5 or 20 μM) and 50 ng/mL LPS; medium containing peptide alone (5 or 20 μM) for an initial incubation of 2 h followed by addition of 50 ng/mL LPS from *Salmonella* Minnesota; 2. medium containing 50 ng/mL LPS for an initial incubation of 2 h followed by addition of peptide (5 or 20 μM). In all the cases, culture supernatants were collected after 24h. As shown in **Figure 8A**, GVF27 exerts a strong dose-dependent attenuation of the production of NO when co-incubated with 50 ng/mL LPS. Conversely, when we performed a pre-incubation of RAW 264.7 cells with peptide and subsequently we induced LPS stimulation, the effect of GVF27 on NO production was not significant (**Figure 8A**). Similarly, when RAW 264.7 cells were pre-incubated with LPS and subsequently treated with 5 or 20 μM of GVF27, we revealed a slight dose dependent reduction of NO production (**Figure 8A**).

Cytokines are small proteins (about 25 kDa) released by many cell types, usually after an activation signal, and they induce a response by binding specific receptors. IL-6 is a monomer produced by T cells,

macrophages and endothelial cells. It is able to determine growth and differentiation of B and T cells, and the production of acute phase proteins, like C-reactive protein [50].

When we analyzed the effect of GVF27 on RAW 264.7 cells by ELISA (see Methods), following the same scheme used in the NO production assay, we revealed a strong inhibitory effect exerted by the peptide on the secretion of IL-6 when the macrophages were co-incubated for 24 h with GVF27 (5 or 20 μM) and 50 ng/ml LPS (see **Figure 8B**). Moreover, we found that GVF27 was also able to exert a significant dose dependent protective effect on cells. Indeed, as shown in **Figure 8B (**on the center**)**, when RAW 264.7 cells were pre-treated for two hours with 5 or 20 μM GVF27 and then incubated for an additional 22h with 50 ng/ml LPS, we observed a reduction of the IL-6 secretion, indicating a prolonged peptide effect. When cells, were pre-incubated with LPS and then subjected to the action of the peptide (see **Figure 8B** – on the right), still we were able to observe a reduction in IL-6 secretion, although the LPS-induced secretion itself was already low due to the very short LPS incubation time in this set-up Collectively, these data indicate that GVF27 is able to exert an intriguing anti-inflammatory effect on LPS treated cells.

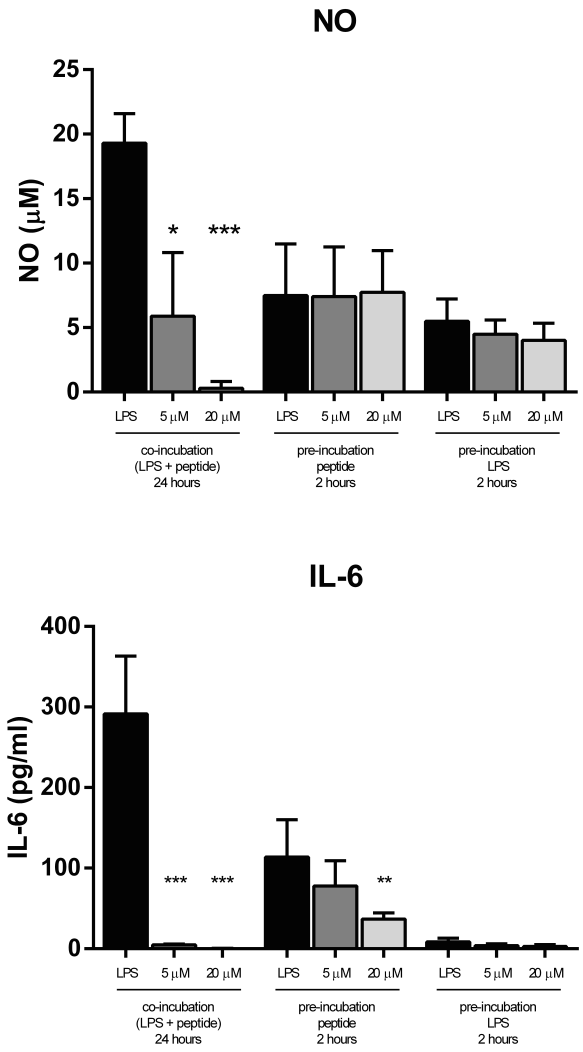

Figure 8 (A) Effect of GVF27 on NO production in LPS induced mouse macrophages RAW 264.7.. (B) Effect of GVF27 on IL-6 release in LPS induced mouse macrophages RAW 264.7 LPS extracted from *Salmonella minnesota* was assayed at a final concentration of 50 ng/mL (see methods). All experiments were carried out for a total incubation time of 24 h.

Finally, the ability of GVF27 to bind LPS, was further confirmed by a different approach using the chromogenic LAL (*Limulus amaebocyte* lysate) assay [51] Three different concentrations of GVF27 (6.25 -

12.5 – 25 μM) were incubated for 30 minutes at 37 °C with LPS from *Escherichia coli* 011:B4 following manufacturer instructions. As shown in **Figure S8**, a concentration of 12.5 μM GVF27 was enough to neutralize about 40% of LPS whereas the presence of 25 μM GVF27 completely neutralized LPS thus supporting the hypothesis that GVF27 might act in a dose-dependent manner as a scavenger of Gram negative's LPS (**Figure S8**).

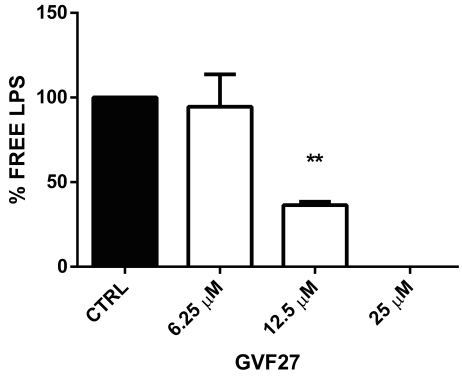

Figure S8 Neutralization LPS in the presence of GVF27. Peptide was incubated with the endotoxin (0.25 units/mL) for 30 min and the amount of free endotoxin quantified by LAL assay (see methods).

4. Discussion

Host defense peptides (HDPs) are important modulators in both mammalian and non-mammalian systems to prevent microbial colonization and tissue damage [52]. In mammals, such peptides constitute the major proportion (over 10% of total protein) among immune cells involved in immediate defense against aggressive microbes as well as in acute inflammatory reactions [53]. HDPs beneficial effects may encompass direct antimicrobial activity, binding to and inactivating endotoxins, such as LPS or LTA, which reduce the detrimental pro-inflammatory response, and one or more direct effects on cellular behaviors, such as enhanced migration and proliferation. The majority of HDPs share common biochemical features, including relatively small size, cationicity and amphipathicity in membrane-mimicking environments. These features allow them to selectively interact with and damage bacterial membranes.

A number of human proteins, whose primary functions are not necessarily related to host defense, contain HDPs hidden inside their sequence [54-55, 40]. Our group has established a bioinformatic procedure (manuscript submitted) through which it is possible to identify host defense peptides in precursor protein sequences and predict their strain dependent antimicrobial propensities. By using this tool to analyze about 4,000 human secreted proteins, a cryptic peptide has been identified in human 11-hydroxysteroid dehydrogenase-1 β-like (accession number UniProtKB: Q7Z5J1), here named GVF27, with potent antimicrobial activity (see Fig. S1).

The experiments described in this paper confirm that GVF27 peptide exhibits antibacterial activities, with MIC values comparable to that of a well studied cathelicidin, against a broad spectrum of both Gram-positive and -negative strains. Interestingly, its antibacterial properties are not limited to planktonic cells but are significant also on sessile bacteria forming biofilm. Indeed, here we provide evidences that GVF27 inhibits biofilm formation, as well as it is able to eradicate existing mature biofilm in a dose dependent manner. In addition, GVF27 is also able to induce a strong reduction of viable sessile bacterial cells. This suggests that our peptide presents affinity for biofilm components, presumably extracellular DNA and/or polysaccharides, but also retains its ability to attack bacterial membranes due to its amphipatic properties.

This clearly confers to the peptide a relevant potential as an anti-biofilm agent alternative to conventional antibiotics, the latter almost totally ineffective against microbes encapsulated in biofilm.

A crucial point regarding the development of membranolytic antimicrobial therapeutics is that they must not destroy the membrane of mammalian cells. We showed here that, although endowed with antimicrobial activity, GVF27 displays virtually no hemolytic and cytotoxic activity on an assortment of murine and human cell lines. This implies that GVF27, probably due its net positive charge composition, has evident high membrane selectivity towards bacterial cells but not mammalian cells.

From a structural point of view, in agreement with the canonical properties of most HDPs, we verified by CD and NMR experiments that GVF27 is unstructured in aqueous buffer whereas it tends to assume a helical conformation in the presence of TFE. Moreover, NMR data clearly indicate that the spatial segregation of polar and apolar amino acids of GVF27 are on opposite faces oriented along the axis of a helical structure. This would indicate that GFV27 is able to assume an optimal conformation to effectively promote strong membrane association.

Further tests by CD and light scattering have also allowed to highlight that the peptide is able to interact both with LPS and LTA, albeit in a less effective manner with the latter, thus suggesting that it can bind to the microbial surfaces via these wall determinants. The ability of GVF27 to interact with LPS has been also confirmed by different approaches, thanks to which it has been possible to show that the peptide is able to inhibit the pro-inflammatory response. Indeed, GVF27 strongly down-regulates the release of NO and the production of IL-6 both in LPS pre-treated murine macrophages cells and upon co-administration of the peptide and the endotoxin. Moreover, it is worth noting that in murine macrophages treated with GVF27 and then subjected to LPS, a decrease of both NO and IL-6 was still detectable, thus suggesting also a protecting action for the peptide. This opens an interesting scenario because GVF27 is a "hidden" peptide in a protein that, although not yet been characterized, could be constitutively present under physiological conditions and able to release, by induced proteolysis, a fragment containing GVF27 in response to pathogen invasion. Our hypothesis is substantiated by an *in silico* prediction of peptides obtainable as a result of hydrolysis, which was carried out on the isoforms in which we identified GVF27 by simulating hydrolysis mediated by neutrophil elastase. Indeed, as shown in Figure S9, possible peptides released by hydrolysis are virtually superimposable to GVF27 and all have high antimicrobial scores, thus clearly supporting our idea that human proteins may fascinatingly be seen as active reservoirs of HDPs.

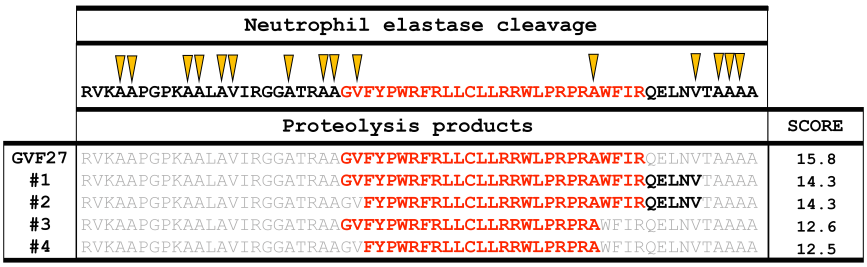

	Proteolysis products	SCORE
GVF27	RVKAAPGPKAALAVIRGGATRAA**GVFYPWRFRLLCLLRRWLPRPRAWFIR**QELNVTAAAA	15.8
#1	RVKAAPGPKAALAVIRGGATRAA**GVFYPWRFRLLCLLRRWLPRPRAWFIRQELNV**TAAAA	14.3
#2	RVKAAPGPKAALAVIRGGATRAAGV**FYPWRFRLLCLLRRWLPRPRAWFIRQELNV**TAAAA	14.3
#3	RVKAAPGPKAALAVIRGGATRAA**GVFYPWRFRLLCLLRRWLPRPRA**WFIRQELNVTAAAA	12.6
#4	RVKAAPGPKAALAVIRGGATRAAGV**FYPWRFRLLCLLRRWLPRPRA**WFIRQELNVTAAAA	12.5

Figure S9 *In silico* prediction, on the C-terminal region of the four isoforms in which we have identified GVF27, of hypothetical peptides released by cleavage mediated by human neutrophil elastase. For each putative peptide (#1, #2, #3 and #4) has been also calculated the antimicrobial score by using the bioinformatics procedure described in Pane et al 2017 (reference n. 23).

Finally, it seems very interesting the ability of GVF27 to attenuate LPS-induced pro-inflammatory response and its apparent ability to protect the cells by mitigating upstream the effects of infection. In both cases it seems plausible to hypothesize for GVF27 different targets.

In our opinion at least three mechanisms could be responsible for GVF27 immune-modulatory properties. First, GVF27 might modulate cellular response to pro-inflammatory mediators by acting as an endotoxin scavenger during initial steps of infection. In this case the peptide could bind to and neutralize the endotoxin directly. Second, GVF27 might reduce inflammatory dysfunction during immune response by interacting with membrane receptors, i.e CD14, that then would activate down regulation of different pro-inflammatory pathways. Third, endogenous GVF27, or internalized from paracrine cells, may contribute to attenuation of the inflammatory response by interacting with intracellular targets. Based on these hypotheses and on the evidences described in this work, it is indisputable that the existence of cryptic HDPs implies that innate immunity is more complex than usually believed and that human proteome is an unexplored and essential source of bioactive agents.

In conclusion, GVF27 may offer several advantages compared to other antimicrobial agents,: (i) it is non-immunogenic given its human origin; (ii) specifically targets bacterial strains, (iii) is not hemolytic and contributes to enhance anti-inflammatory response without altering cell viability.

Thus, we confidentially believe that structural, immunomodulatory and antimicrobial data of GVF27 presented in this work, could serve as leads for the design of human-specific therapeutics.

Acknowledgments

We thank Rita Faella for her skillful technical assistance and drawing skills. This study was supported by the Italian Cystic Fibrosis Foundation (grant number 20/2014). We are deeply indebted to volunteers who devote many efforts in fundraising, in particular delegations from Palermo and Ragusa Vittoria Catania 2.

References

1. P. Bulet, R. Stöcklin, L. Menin, Anti-microbial peptides: from invertebrates to vertebrates, Immunol Rev. 198 (2004) 169-84.
2. J.P. Tam, S. Wang, K.H. Wong, W.L. Tan, Antimicrobial Peptides from Plants, Pharmaceuticals (Basel). 8(4) (2015) 711-57
3. R.E. Hancock, E.F. Haney, E.E. Gill, The immunology of host defence peptides: beyond antimicrobial activity, Nat Rev Immunol. 16(5) (2016) 321-343
4. F. Guilhelmelli, N. Vilela, P. Albuquerque, S. Lda. Derengowski, I. Silva-Pereira, C.M. Kyaw, Antibiotic development challenges: the various mechanisms of action of antimicrobial peptides and of bacterial resistance, Front Microbiol. 4 (2013) 353
5. D. Kraus, A. Peschel, Molecular mechanisms of bacterial resistance to antimicrobial peptides, Curr Top Microbiol Immunol. 306 (2006) 231-50
6. D.I. Andersson, D. Hughes, J.Z. Kubicek-Sutherland, Mechanisms and consequences of bacterial resistance to antimicrobial peptides. Drug Resist Updat. 26 (2016) 43-57
7. G. Diamond, N. Beckloff, A. Weinberg, K.O. Kisich, (2009) The roles of antimicrobial peptides in innate host defense, Curr Pharm Des. 15(21) (2009) 2377-92
8. M. Malmsten, Interactions of Antimicrobial Peptides with Bacterial Membranes and Membrane Components, Curr Top Med Chem. 16(1) (2016) 16-24
9. A. Bhunia, P.N. Domadia, J. Torres, K.J. Hallock, A. Ramamoorthy, S. Bhattacharjya, NMR structure of pardaxin, a pore-forming antimicrobial peptide, in lipopolysaccharide micelles: mechanism of outer membrane permeabilization, J Biol Chem. 285(6) (2010) 3883-95

10. P. Schmitt, R.D. Rosa, D. Destoumieux-Garzón, An intimate link between antimicrobial peptide sequence diversity and binding to essential components of bacterial membranes, Biochim Biophys Acta. 1858(5) (2016) 958-70
11. Y.R. Bommineni, G.H. Pham, L.T. Sunkara, M. Achanta, G. Zhang, Immune regulatory activities of fowlicidin-1, a cathelicidin host defense peptide, Mol Immunol. 59(1) (2014) 55-63
12. M.G. Scott, D.J. Davidson, M.R. Gold, D. Bowdish, R.E. Hancock, The human antimicrobial peptide LL-37 is a multifunctional modulator of innate immune responses, J Immunol. 169(7) (2002) 3883-91
13. N. Mookherjee, K.L. Brown, D.M. Bowdish, S. Doria, R. Falsafi, K. Hokamp, F.M. Roche, R. Mu, G.H. Doho, J. Pistolic, J.P. Powers, J. Bryan, F.S. Brinkman, R.E. Hancock, Modulation of the TLR-mediated inflammatory response by the endogenous human host defense peptide LL-37. J Immunol. 176(4) (2006) 2455-64
14. D. Bowdish, D. J. Davidson, D. P. Speert, and R. E. W. Hancock, The human cationic peptide LL-37 induces activation of the extracellular signal-regulated kinase and p38 kinase pathways in primary human monocytes. J. Immunol. 172 (2004) 3758 –3765
15. M.G. Scott, A.C. Vreugdenhil, W.A. Burman, R.E.W. Hancock, and M. R. Gold, Cutting edge: cationic antimicrobial peptides block the binding of lipopolysaccharide (LPS) to LPS binding protein. J. Immunol. 164 (2000) 549 –553
16. A. Giacometti, O. Cirioni, R. Ghiselli, F. Mocchegiani, F. Orlando, C. Silvestri, A. Bozzi, A. Di Giulio, C. Luzi, M.L. Mangoni, D. Barra, V. Saba, G. Scalise, A.C. Rinaldi, Interaction of antimicrobial peptide temporin L with lipopolysaccharide in vitro and in experimental rat models of septic shock caused by gram-negative bacteria, Antimicrob Agents Chemother. 50(7) (2006) 2478-86
17. J. Agier, M. Efenberger, E. Brzezińska-Błaszczyk, Cathelicidin impact on inflammatory cells. Cent Eur J Immunol. 40(2) (2015) 225-35
18. A.L. Hilchie, K. Wuerth, R.E. Hancock, Immune modulation by multifaceted cationic host defense (antimicrobial) peptides, Nat Chem Biol. 9(12) (2013) 761-8
19. N. Mookherjee, R.E. Hancock, Cationic host defence peptides: innate immune regulatory peptides as a novel approach for treating infections, Cell Mol Life Sci. 64(7-8) (2007) 922-33
20. A. Zanfardino, E. Pizzo, A. Di Maro, M. Varcamonti, G. D'Alessio, The bactericidal action on Escherichia coli of ZF-RNase-3 is triggered by the suicidal action of the bacterium OmpT protease, FEBS J.;277(8) (2010) 1921-8
21. G. D'Alessio, Denatured bactericidal proteins: active per se, or reservoirs of active peptides?, FEBS Lett.;585(15) (2011) 2403-4
22. P. Wang, L. Hu, G. Liu, N. Jiang, X. Chen, J. Xu, W. Zheng, L. Li, M. Tan, Z. Chen, H. Song, Y.D. Cai, K.C. Chou, Prediction of antimicrobial peptides based on sequence alignment and feature selection methods, PLoS One. Apr 13;6(4) (2011) e18476
23. K. Pane, L. Durante, O. Crescenzi, V. Cafaro, E. Pizzo, M. Varcamonti, A. Zanfardino, V. Izzo, A. Di Donato, E. Notomista, Antimicrobial potency of cationic antimicrobial peptides can be predicted from their amino acid composition: Application to the detection of "cryptic" antimicrobial peptides. J Theor Biol. 2017 Feb 17;419:254-265
24. R. Sukhija, P. Kakar, V. Mehta, J.L. Mehta, Enhanced 11beta-hydroxysteroid dehydrogenase activity, the metabolic syndrome, and systemic hypertension, Am J Cardiol. 98(4) (2016) 544-8
25. Y. Kallberg, U. Oppermann, H. Jörnvall, B. Persson, Short-chain dehydrogenases/reductases (SDRs), Eur J Biochem. Sep;269(18) (2002) 4409-17
26. C. Huang, B. Wan, B. Gao, S. Hexige, L. Yu, Isolation and characterization of novel human short-chain dehydrogenase/reductase SCDR10B which is highly expressed in the brain and acts as hydroxysteroid dehydrogenase, Acta Biochim Pol. 56(2) (2009) 279-89

27. Y. Xiao, H. Dai, Y.R. Bommineni, J.L. Soulages, Y.X. Gong, O. Prakash, G. Zhang, Structure-activity relationships of fowlicidin-1, a cathelicidin antimicrobial peptide in chicken, FEBS J. Jun;273(12) (2006) 2581-93
28. I. Wiegand, K. Hilpert, R.E. Hancock, Agar and broth dilution methods to determine the minimal inhibitory concentration (MIC) of antimicrobial substances, Nat Protoc. 3(2) (2008) 163-75
29. R. Cooper, L. Jenkins, S. Hooper, Inhibition of biofilms of *Pseudomonas aeruginosa* by Medihoney in vitro, J Wound Care. Mar;23(3) (2014) 93-6
30. K.H. Park, Y.H. Nan, Y. Park, J.I. Kim, I.S. Park, K.S. Hahm, S.Y. Shin, Cell specificity, anti-inflammatory activity, and plausible bactericidal mechanism of designed Trp-rich model antimicrobial peptides, Biochim Biophys Acta. 1788(5) (2009) 1193-203
31. S. Correale, C. Esposito, L. Pirone, L. Vitagliano, S. Di Gaetano, E. Pedone, A biophysical characterization of the folded domains of KCTD12: insights into interaction with the GABAB2 receptor. J Mol Recognit.;26(10) (2013) 488-95
32. R. Del Giudice, A. Arciello, F. Itri, A. Merlino, M. Monti, M. Buonanno, A. Penco, D. Canetti, G. Petruk, S.M. Monti, A. Relini, P. Pucci, R. Piccoli, D.M. Monti, Protein conformational perturbations in hereditary amyloidosis: Differential impact of single point mutations in ApoAI amyloidogenic variants. Biochim Biophys Acta. 1860 (2) (2016) 434-44
33. M. Leone, P. Di Lello, O. Ohlenschläger, E.M. Pedone, S. Bartolucci, M. Rossi, B. Di Blasio, C. Pedone, M. Saviano, C. Isernia, R. Fattorusso, Solution structure and backbone dynamics of the K18G/R82E *Alicyclobacillus acidocaldarius* thioredoxin mutant: a molecular analysis of its reduced thermal stability, Biochemistry. 43(20) (2004) 6043-58
34. P. Güntert, C. Mumenthaler, K. Wüthrich, Torsion angle dynamics for NMR structure calculation with the new program DYANA, J. Mol. Biol. 273 (1997) 283–298
35. R. Koradi, M. Billeter, K. Wüthrich, MOLMOL: a program for display and analysis of macromolecular structures, J Mol Graph. Feb;14(1) (1996) 51-5, 29-32
36. Schneider VA, Coorens M, Ordonez SR, Tjeerdsma-van Bokhoven JL, Posthuma G, van Dijk A, Haagsman HP, Veldhuizen EJ. (2016) Imaging the antimicrobial mechanism(s) of cathelicidin-2. Sci Rep. 6:32948
37. M. Coorens, M.R. Scheenstra, E.J. Veldhuizen, H.P. Haagsman, Interspecies cathelicidin comparison reveals divergence in antimicrobial activity, TLR modulation, chemokine induction and regulation of phagocytosis. Sci Rep. (2017) 19;7 doi: 10.1038/srep40874
38. E.J. Veldhuizen, V.A. Schneider, H. Agustiandari, A. van Dijk, J.L. Tjeerdsma-van Bokhoven, F.J. Bikker, H.P. Haagsman, Antimicrobial and immunomodulatory activities of PR-39 derived peptides, PLoS One. 9(4) (2014) e95939
39. N. Takei, N. Takahashi, T. Takayanagi, A. Ikeda, K. Hashimoto, M. Takagi, T. Hamada, E. Saitoh, A. Ochiai, T. Tanaka, M. Taniguchi, Antimicrobial activity and mechanism of action of a novel cationic α-helical dodecapeptide, a partial sequence of cyanate lyase from rice, Peptides. 42 (2013) 55-62
40. D. Pletzer, S.R. Coleman, R.E. Hancock, Anti-biofilm peptides as a new weapon in antimicrobial warfare, Curr Opin Microbiol. 33 (2016) 35-40
41. A.I. Herrera, J.M. Tomich, O. Prakash, Membrane Interacting Peptides: A Review, Curr Protein Pept Sci. 17(8) (2016) 827-841
42. E. Notomista, A. Falanga, S. Fusco, L. Pirone, A. Zanfardino, S. Galdiero, M. Varcamonti, E. Pedone, P. Contursi, The identification of a novel Sulfolobus islandicus CAMP-like peptide points to archaeal microorganisms as cell factories for the production of antimicrobial molecules, Microb Cell Fact. 14 (2015) 126
43. D.S. Wishart, B.D. Sykes, Chemical shifts as a tool for structure determination, Methods Enzymol. 239 (1994) 363-92
44. K. Pane, V. Sgambati, A. Zanfardino, G. Smaldone, V. Cafaro, T. Angrisano, E. Pedone, S. Di Gaetano, D. Capasso, E.F. Haney, V. Izzo, M. Varcamonti, E. Notomista, R.E. Hancock, A. Di Donato, E. Pizzo, A new

cryptic cationic antimicrobial peptide from human apolipoprotein E with antibacterial activity and immunomodulatory effects on human cells, FEBS J. 283(11) (2016) 2115-31
45. M.M. Domingues, R.G. Inácio, J.M. Raimundo, M. Martins, M.A. Castanho, N.C. Santos, Biophysical characterization of polymyxin B interaction with LPS aggregates and membrane model systems, Biopolymers. 98(4) (2012) 338-44
46. L. Heinbockel, L. Palacios-Chaves, C. Alexander, E. Rietschel, J. Behrends, W. Correa, S. Fukuoka, T. Gutsmann, A.J. Ulmer, K. Brandenburg, Mechanism of Hbγ-35-induced an increase in the activation of the human immune system by endotoxins, Innate Immun. Apr;21(3) (2015) 305-13
47. M. Hemshekhar, V. Anaparti, N. Mookherjee, Functions of Cationic Host Defense Peptides in Immunity, Pharmaceuticals (Basel). Jul 4 (2016) 9(3)
48. T.J. Guzik, R. Korbut, T. Adamek-Guzik, Nitric oxide and superoxide in inflammation and immune regulation, J Physiol Pharmacol. 54(4) (2003) 469-87
49. C.V. Suschek, O. Schnorr, V. Kolb-Bachofen, The role of iNOS in chronic inflammatory processes in vivo: is it damage-promoting, protective, or active at all?, Curr Mol Med. Nov;4(7) (2003) 763-75
50. J. Scheller, A. Chalaris, D. Schmidt-Arras, S. Rose-John, The pro- and anti-inflammatory properties of the cytokine interleukin-6, Biochim Biophys Acta. May;1813(5) (2011) 878-88
51. J.L. Ding, B. Ho, Endotoxin detection - from limulus amebocyte lysate to recombinant factor C, Subcell Biochem. 53 (2010) 187-208
52. S.C. Mansour, O.M. Pena, R.E. Hancock, Host defense peptides: front-line immunomodulators, Trends Immunol. Sep;35(9) 2014 443-50
53. T. Ganz, The role of antimicrobial peptides in innate immunity, Integr Comp Biol. Apr;43(2) (2003) 300-4
54. P. Papareddy, M. Kalle, G. Kasetty, M. Mörgelin, V. Rydengård, B. Albiger, K. Lundqvist, M. Malmsten, A. Schmidtchen, C-terminal peptides of tissue factor pathway inhibitor are novel host defense molecules, J Biol Chem. Sep 3;285(36) (2010) 28387-98
55. E. Andersson, V. Rydengard, A. Sonesson, M Morgelin, L. Bjorck, A. Schmidtchen, Antimicrobial activities of heparin-binding peptides, Eur J Biochem 271 (2004) 1219–1226.

Insights into the anticancer properties of the first antimicrobial peptide from Archaea

Journal:	*ACS Chemical Biology*
Manuscript ID	Draft
Manuscript Type:	Article
Date Submitted by the Author:	n/a
Complete List of Authors:	Gaglione, Rosa; Universita degli Studi di Napoli Federico II, Dipartimento di Scienze Chimiche Pirone, Luciano; Institute of Biostructures and Bioimaging (CNR), Farina, Biancamaria; Istituto di Biostrutture e Bioimmagini Unita Operativa di Supporto di Napoli Consiglio Nazionale delle Ricerche Fusco, Salvatore; Universita degli Studi di Napoli Federico II Dipartimento di Biologia Smaldone, Giovanni; IRCCS SDN Aulitto, Martina; Universita degli Studi di Napoli Federico II Dipartimento di Biologia Dell'Olmo, Eliana; Universita degli Studi di Napoli Federico II, Dipartimento delle Scienze Chimiche Roscetto, Emanuela; Universita degli Studi di Napoli Federico II Dipartimento di Medicina Molecolare e Biotecnologie Mediche Del Gatto, Annarita; Istituto di Biostrutture e Bioimmagini-CNR, Fattorusso, Roberto; Seconda Università di Napoli, Dipartimento di Scienzee Tecnologie Ambientali, Biologiche e Farmaceutiche Notomista, Eugenio; Università di Napoli Federico II, Dipartimento di Biologia Strutturale e Funzionale Zaccaro, Laura; Istituto di Biostrutture e Bioimmagini-CNR, Arciello, Angela; Università degli Studi di Napoli Federico II, Department of Chemical Sciences Pedone, Emilia; Consiglio Nazionale delle Ricerche, Istituto di Biostrutture e Bioimmagini Contursi, Patrizia; Universita degli Studi di Napoli Federico II, Biologia

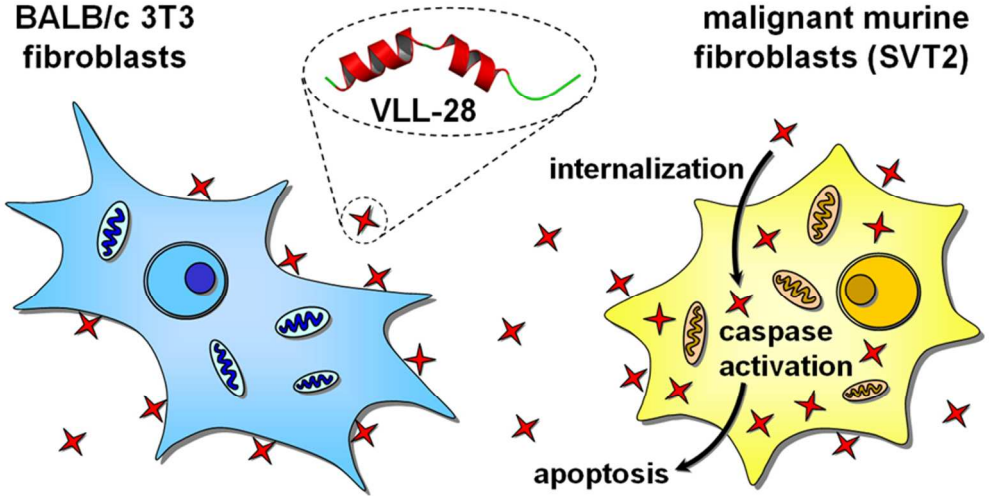

Graphical Abstract

80x39mm (300 x 300 DPI)

Title

Insights into the anticancer properties of the first antimicrobial peptide from Archaea

Rosa Gaglione[1§], Luciano Pirone[2§], Biancamaria Farina[2,3§], Salvatore Fusco[4§], Giovanni Smaldone[5], Martina Aulitto[4], Eliana Dell'Olmo[1], Emanuela Roscetto[6], Annarita Del Gatto[2,7], Roberto Fattorusso[7,8], Eugenio Notomista[4], Laura Zaccaro[2,7], Angela Arciello[1,9*], Emilia Pedone[2,7*#] and Patrizia Contursi[4*#]

[1]Department of Chemical Sciences, University of Naples Federico II, 80126, Naples, Italy
[2] Institute of Biostructures and Bioimaging, Italian Research National Council, Naples, Italy
[3]Advanced Accelerator Applications 81100, Caserta, Italy
[4]Department of Biology, University of Naples Federico II, Complesso Universitario Monte S. Angelo, Via Cinthia, 80126, Naples, Italy.
[5]IRCCS SDN, Via E. Gianturco 113, 80143, Naples, Italy
[6]Department of Molecular Medicine and Medical Biotechnology, Federico II University Medical School
[7]Research Centre on Bioactive Peptides (CIRPeB), University of Naples "Federico II", Via Mezzocannone 16, 80134, Naples, Italy
[8]Department of Environmental, Biological and Pharmaceutical Sciences and Technologies, University of Campania- Luigi Vanvitelli - 81100 Caserta, Italy
[9] National Institute of Biostructures and Biosystems (INBB), Italy

[§]These authors equally contributed.
*Corresponding author: anarciel@unina.it; empedone@unina.it and contursi@unina.it.
[#] These authors equally contributed to the study and are therefore both last names on this manuscript.

Abstract
VLL-28, previously identified and characterized as an antimicrobial peptide from the archaeal kingdom, is here demonstrated to selectively exert cytotoxic activity against murine and human tumor cells. Through a combined approach of NMR spectroscopy, Circular Dichroism and Dynamic Light Scattering, the interaction with the membranes of both parental and malignant cell lines is proven and the binding residues were identified. Importantly, microscopy data show that VLL-28 is internalized only into tumor cells, thus suggesting that the cell membrane is not the main target and that not yet identified intracellular components are involved. Finally, it is shown that cell death is mainly caused by a time-dependent activation of apoptotic pathways.

Keywords:
Antimicrobial Peptide; Anticancer Peptide; *Sulfolobus*, Archaea; peptide-membrane interactions .

Introduction

Antimicrobial peptides (AMPs) are short peptides endowed with direct and broad-spectrum antimicrobial activity and represent essential components of the innate immune system of higher eukaryotes, being the first line of defense against microbial invasions (*1, 2*). In addition to a direct antimicrobial action, AMPs show a wide panel of biological activities including anti-inflammatory, anti-viral, chemoattractive and pro-angiogenic activity (*1, 3-6*). AMPs are very heterogeneous in length, amino-acid composition, secondary structure and mechanism of action; however, the majority of them shows a peculiar abundance of cationic and hydrophobic residues. These AMPs, also called Host Defence Peptides (HDPs)(*7*), kill bacterial cells through a specific mechanism i.e. targeting bacterial membranes (*2, 6, 8*): the net positive charge drives the adsorption of the peptide onto the surface of bacterial membranes which are richer in anionic lipids than eukaryotic membranes, hence the hydrophobic residues mediate the insertion of the peptide into the membrane. The accumulation of peptide molecules in the membrane causes the alteration of its structure/permeability, accompanied by a severe impairment of the membrane functions that eventually lead to the death of bacterial cells, often by cell lysis (*2, 6, 8*). Since eukaryotic plasma membranes show an asymmetric distribution of negatively charged phospholipids, generally present only in the inner leaflet of the membrane, HDPs are not able to effectively adsorb to eukaryotic cells. The presence of cholesterol further prevents the insertion into and the perturbation of the eukaryotic membranes. Nonetheless, it is worth mentioning that at high concentration several HDPs become toxic also for eukaryotic cells.

Intriguingly, several AMPs endowed with anti-cancer activity (*9*) are defined as "anti-cancer peptides" (ACPs), because they show a much stronger toxicity for cancer cells than that towards normal cells. This differential toxicity has been attributed to the fact that transformation of eukaryotic cells is often associated to alterations of the membrane composition (*10*), such as: i) loss of the asymmetric distribution of phospholipids with exposure of phosphatidylserine on the outer leaflet, ii) increased production of anionic lipids (e.g. sulfated lipids), sialic acid containing glycolipids and glycoproteins, and sometimes iii) decreased production of cholesterol. Altogether these events lead to an augmented negative charge at the external surface of tumor cells that, in turn, would favor the binding of ACPs. However, differently from bacterial killing mechanisms, the death of tumor cells is not necessarily due to accumulation of the peptide into the membrane followed by their lysis. Indeed, in several cases it has been demonstrated that ACPs are internalized and the cell death occurs upon the interaction with one or more intracellular targets, such as mitochondria, DNA, cytoplasmic and nuclear proteins (e.g. HSP70(*11*) and DNA polymerase β(*12*), respectively). Moreover, it is worth noting that these ACPs usually induce apoptosis rather than necrosis. (*9*)

Due to the severe side effects of conventional chemotherapeutic agents and the ability of some tumor cells to develop the multidrug resistant phenotype, ACPs have attracted considerable attention. Indeed, these peptides could help to develop a new generation of anti-cancer drugs with a mechanism of action well distinguished from those of conventional chemotherapeutic agents.

As not all the HDPs are ACPs and the killing mechanism seems to differ for each ACP and tumor cell line, the rationale development of new antitumor agents based on CAMPs/ACPs requires further investigations. In particular, the identification and characterization of new ACPs could help to better define the requirements for a strong and selective antitumor activity.

Recently, we have developed an *in silico* tool allowing to identify HDP-like peptides hidden into the sequences of proteins not necessarily involved in host defense (*13*). Using this tool we have already identified three new human HDPs (*14-16*). Furthermore, we have demonstrated that DNA binding proteins can be a convenient source of new HDP-like peptides by identifying the first HDP from an archaeal protein, the transcription factor Stf76 encoded by the hybrid plasmid-virus pSSVx from *Sulfolobus islandicus (17)*. This archaeal HDP, named VLL-28 from its sequence(*16*), has a broad-spectrum antibacterial activity and exhibits selective leakage and fusogenic capability on vesicles with a lipid composition similar to that of bacterial membranes. Moreover, we have shown

that VLL-28 retains the ability of the parental protein to bind nucleic acids (both single and double strand DNA). Using a fluorescent derivative, we have demonstrated that VLL-28 localizes not only on the cell membrane but also in the cytoplasm of *Escherichia coli*, thus suggesting that it could target both membranes and intracellular components of bacterial cells.
Here we report for the first time the characterization of the antitumor activity of VLL-28. By means of a multidisciplinary approach including biochemical, cellular biology and spectroscopic techniques, the action mechanism of VLL-28 has been elucidated. Intriguingly, it has been proved to be an effective ACP able to selectively kill tumor cells by inducing apoptosis.

Results and Discussion

Selective antitumor action of VLL-28 peptide

To assess whether VLL-28 was endowed with anti-cancer activity, cytotoxicity assays were performed on malignant SVT2 mouse fibroblasts and parental non-malignant BALBc 3T3 mouse fibroblasts. Interestingly, these studies have shown that the peptide VLL-28 exerts a dose- and time-dependent inhibition of viability on malignant SVT2 murine fibroblasts (see Figure 1a). Conversely, the peptide was found to be inactive towards the non-malignant line of BALBc 3T3 fibroblasts (Figure 1b). This evidence was also confirmed by morphological analyses through light microscopy, where a severe alteration of cell morphology with the presence of cell debris was observed only in the case of SVT2 cancer cells (Figure S1). Remarkably, this peptide was also found to be effective and selective against human tumor cell lines, as demonstrated by MTT assays performed on transformed HEK-293 cells and human primary renal cortical epithelial (HRCE) cells (Figure S2). In agreement with these results, it has been previously reported that other AMPs, which are toxic for bacteria but not for normal mammalian cells, are instead cytotoxic for cancer cells (*18*).

Internalization of VLL-28 peptide

Most AMPs and ACPs share a common membranolytic mechanism of action that results first either in the selective disruption or permeation of the cancer cell membrane and then in the swelling of mitochondria. Nonetheless, a non-membranolytic mechanism of action is increasingly recognized as an alternative ACPs mechanism. (*19*) To test whether the selective antitumor activity of VLL-28 was associated to a membranolytic mechanism and/or to its internalization, we performed experiments by using the peptide labeled with fluorescein isothiocyanate (FITC). To this purpose, SVT2 and BALBc 3T3 cells were incubated for 12 h with 20 μM FITC-labeled VLL-28, since this concentration of peptide turned out to be the most effective in terms of cytotoxicity. As shown in Figure 2a, in the case of SVT2 cells, VLL-28 fluorescent signal appears to be mostly intracellular already after 12 h of incubation, thus indicating that the peptide is internalized into the target cancer cells. On the other hand, the peptide (green) mainly co-localizes with WGA (red) at the plasma membrane in BALBc 3T3 cells (as indicated by arrows in Figure 2b). The failed internalization of VLL-28 into these latter cells is consistent with the absence of cytotoxicity emerged from viability tests (Figure 1b). Fluorescent staining was found to be specific, as no fluorescent signals were observed in the absence of FITC-labeled peptide (data not shown). Since the internalization has been observed at a time point preceding the cell death (48-72h), the molecular target of VLL-28 might be a not yet identified intracellular component.

VLL-28 CD analyses in the presence of intact eukaryotic cells

Since differences in the plasma membrane composition between normal and cancer cells are supposed to contribute to the selective permeability and toxicity of ACPs towards the latter, we

resolved to examine if the presence of the two different cell lines affect differently the secondary structure of VLL-28. Interestingly, VLL-28 CD spectra registered in the presence of either BALBc 3T3 or SVT2 whole cells revealed a different behavior (Figure 3). In particular, in the presence of BALBc 3T3 cells, VLL-28 seems to gradually get structured over time until a prevalence of helical structure is observed upon 1 h incubation (Figure 3a). Indeed, the spectrum shows two minima, at 208 and 222 nm, typical of helical structure, in agreement with CD data obtained in the presence of n-dodecyl-phosphatidylcholine (DPC), a well-known eukaryotic membrane mimetic agents.(*16*) Differently, in the presence of SVT2 intact cells, a drop in the CD signal is observed suggesting a fast internalization process of VLL-28, occurring already after 10 min (Figure 3b), as confirmed by confocal microscopy data (Figure 2).

NMR conformational analysis of VLL-28

In order to gain insight into the mechanism of action of VLL-28 and provide information on the basis of the different behaviors of VLL-28 with regard to the two studied cell lines, a NMR conformational analysis of the peptide in the absence and in the presence of TFE, a well-known structuring solvent, has been initially carried out. (Figure S3 and S4). According with what previously observed by CD analysis (*16*), VLL-28 does not adopt a well-defined conformation in phosphate neutral solution, as indicated by sharp and low-dispersed resonances in both the amide/aromatic and the aliphatic regions (Figure S3a). Upon addition of TFE (25% v/v), amide, aromatic and aliphatic proton resonances resulted significantly more dispersed (Figure S3b). In particular, the tryptophan side chain H_N, clearly distinguishable at 10.14 ppm in the absence of TFE (Figure S3a, left), exhibits up-field shift at 9.94 ppm upon addition of TFE (Figure S3b, left), possibly induced by an aromatic-aromatic long-range interaction. Moreover, 2D [^{1}H, ^{1}H] NOESY spectrum of VLL-28 peptide contains a consistent higher number of cross-peaks with respect of that recorded in the absence of TFE, indicating a more structured conformation (Figure S4). Almost complete assignment of proton resonances of VLL-28 has been achieved in 25% TFE by using a combination of TOCSY and NOESY spectra, according to the standard procedures (Table S1).
To assess the secondary structure of VLL-28 in 25% TFE, analyses of the H_α chemical shift deviations from random coil values ($\Delta\delta H_\alpha$) and of the NOE patterns were performed. Interestingly, two regions encompassing residues V^{37}- R^{48} andV^{50}-S^{59} showed large negative deviations ($\Delta\delta H_\alpha <$ -0.1 ppm), suggesting that the peptide mostly assumes a helical conformation, which is lost in the last C-terminal amino acids. (Figure 4a). Accordingly, H_N-H_N NOEs, together with $H_{\alpha i}$-H_{Ni+3} and $H_{\alpha i}$-$H_{\beta i+3}$ NOEs, were observed starting from residues V^{37} to S^{59} only in the presence of TFE (Figure 4b and c), further confirming the helical structure of that region in TFE.

STD NMR interaction studies of VLL-28 with tumor and normal cell membranes and definition of its binding epitopes

To identify binding residues of VLL-28 saturation transfer difference (STD) NMR binding experiments of the peptide in the presence of intact SVT2 and BALBc 3T3 cells (*20*), as well as of their isolated membranes, were performed. Unfortunately, ^{1}H NMR VLL-28 proton resonances vanish when in presence of each of the two cell lines, thus hampering a detailed molecular analysis of the VLL-28 interaction with the cellular membranes (data not shown).
Very recently, we described the use of native cell membranes to overcome peptide cell internalization issues in “on-cell” NMR binding experiments(*21*). This approach provides a significant improvement of NMR peptide spectra with respect to those acquired by using intact cells. Particularly, in the presence of isolated membranes, the ^{1}H NMR signals of the peptide are sharper and better resolved, the STD signals appear significantly stronger, and background signals

of the cellular components result much weaker in both the ^{1}H and the STD spectra.(*21*) On the basis of the biochemical evidences of peptide internalization (see above), we carried out STD NMR experiments of the VLL-28 peptide in the presence of isolated membranes.

Interestingly, ^{1}H NMR peptide signals resulted well visible in the presence of both SVT2 and BALBc3T3 cell membranes as in the sole buffer (Figure S5), thus allowing to perform STD NMR binding studies. In particular, we evaluated the binding capability of VLL-28 to the two different components of the cell membrane, proteins and lipids, acquiring STD spectra at two different saturation frequencies, i.e. one to selectively saturate proteins (0.2 ppm) and another one to saturate lipids (5.2 ppm) (*22*) Remarkably, the ^{1}H STD spectra showed that VLL-28 receives a detectable saturation transfer in the presence of cell membranes only when lipids are saturated (Figure 5). This effect, which is negligible in the absence of cell membranes (Figure 5b), provides a direct observation of the binding of VLL-28 to the lipid component of the cell membranes. This finding is in agreement with previous results showing that the peptide is able to interact with lipids mimicking bacterial membranes (*16*). It is worth of note that differences in the STD spectra were observed for BALBc 3T3 and SVT2 cell membranes (Figure 5). In particular, a higher number of STD signals, with stronger intensities, were observed in the presence of BALBc 3T3 cell membranes compared with those of SVT2 (Figure 6A). In particular, all the binding residues of VLL-28 to the SVT2 cell membranes are in common with that of the BALBc 3T3 cell membranes. Specifically, VLL28 residues involved in both BALBc 3T3 and SVT2 interactions are G^{49}, Y^{52} and W^{55} (Figure 6b, highlighted in magenta). Moreover, one or both of the two threonine residues, T^{41} and T^{43}, appear involved in the VLL-28 interaction with both cell lines. On the other hand, Q^{47}, V^{50}, I^{51} and F^{58}, together with the acetyl N-terminal, show protons that are saturated only in the presence of BALBc 3T3 membranes (Figure 6b, highlighted in red). Furthermore, strong STD effects were observed for side-chains of arginine and lysine residues. However, due to the spectral overlap and to the presence of a high number of basic residues in the peptide sequence they could not identified unambiguously. Moreover, methyl of leucine (L) and valine (V) localized in the N-terminal region, seem to be involved as well.

Overall, these data indicate that the interaction of VLL-28 with cell membranes is mediated by the N-terminal and the central regions (V^{37}-F^{58}) (Figure 6), which interestingly correspond to the portions of the peptide that assume helical conformation in presence of TFE. Specifically, the binding to both the cell membranes seems to be mainly mediated by aromatic and basic residues, as could be expected for peptide-lipid interactions

Different STD intensities of the peptide induced by the interaction with BALBc 3T3 and SVT2 cell membranes are likely ascribed to a different interaction mechanism between the peptide and the two membranes. In particular, stronger STD effects observed in the presence of non-tumor BALBc 3T3 membranes indicates that a fast-exchange equilibrium between the free form and a well-recognized bound conformation occurs. Since fast-exchange regime are observed with lower affinity interaction, this could explain the inability of VLL-28 to penetrate these cell membranes. Differently, the reduced STD effects, observed in the presence of SVT2 membranes, can be ascribed to a stronger interaction with the cell membranes possibly being the first step of an internalization process.

Effect of VLL-28 on zeta-potential of cell membranes

Zeta potential of cell membranes has been used as a possible marker for the assessment of membrane damage and could be suitable to study the permeabilizing property of the VLL-28 peptide. (*23*) Zeta potential analyses were performed on *E. coli*, BALBc 3T3 and SVT2 cells. The measured zeta potential in our experimental conditions for the cells in the absence of any peptide is −43.93mV for *E. coli* (Figure S6), -6.91mVfor BALBc 3T3 and -12.91mV for SVT2 cells, respectively, indicating that their surfaces are all negatively charged and, as already known, that the surface of the bacterial membranes is more negatively charged than mammalian cells.(*24, 25*) This

is due to both lipid composition and negatively charged cell surface macromolecules, as described also for other systems(*9*). Furthermore, Z-potential measurements clearly demonstrated that the surface of SVT2 has a more negative charge than BALBc 3T3 cells. The addition of VLL-28 caused an increase of Z-potential values towards neutralization indicating that the peptide is interacting with the surface of all the cells tested (Figure 7 a and b and S6). Given the role of electrostatic interactions in driving the AMPs initial adsorption onto the extracellular surface, it is reasonable to question if VLL-28, as ACP, exerts the same kind of action. In accordance with the general mechanism of action of AMPs, VLL-28 fully neutralizes *E. coli* cell's surface potential to exert its antimicrobial action (Figure S6). Differently, on eukaryotic cells, VLL-28 is able to increase the Z-potential but never reaching full neutralization even at concentrations ≥ 20μM thus indicating that total surface neutralization is not necessary to elicit its anticancer action.(*26*)

Cell death pathway activated by cell treatment with VLL-28

To elucidate cell death pathways selectively activated by cell treatment with VLL-28, we performed western blot analyses by using antibodies specifically recognizing pro-caspase 3 and p62 proteins. The activation of procaspase-3 to caspase-3 is a key event in the apoptotic execution phase, since caspase-3 is considered the most important among executioner caspases and is activated by any of the initiator caspases (caspase-8, caspase-9, or caspase-10).(*27*) p62, instead, is generally used as a marker to study the autophagic flux, since it accumulates when autophagy is inhibited, whereas p62 decreased levels can be observed when autophagy is induced (*28*).

To get insight into cell death pathway induced by VLL-28, western blot analyses were performed on SVT2 cells in comparison with BALBc 3T3 (Figure 8a-d). In SVT2 cells it was found a significant increase of p62 levels upon 6 h treatment with 20 μM VLL-28 (Figure 8a, d), indicative of a stress leading to cell death with a consequent block of autophagy flux (*29*). Accordingly, procaspase-3 levels appear lower than in control cells upon 6 and 12 h treatment (Figure 8a, b), indicating a significant (about 30%) activation of procaspase-3 to caspase-3 associated to apoptosis induction. This activation appears even stronger (about 50%) after 24 h of treatment (Figure 8a, b), and is associated to a significant decrease of p62 levels (Figure 8a, d), in agreement with a time-dependent activation of apoptotic cell pathway.

In the case of non-malignant BALBc 3T3 cells, instead, no significant effects on procaspase-3 levels were observed upon cell treatment with 20 μM VLL-28 peptide at different time intervals (6, 12 and 24 h) (Figure 8B, C), in agreement with the results reported above. This indicates that these cells are not susceptible to VLL-28 peptide toxic effects. Moreover, no significant effects were observed also when p62 levels were analyzed, except for 72 h treatment, where a slight increase of p62 levels was observed (Figure 8b, d). Since no effects on cell viability were detected by MTT assays, this might be indicative of a slight cell perturbation counteracted by autophagy activation.

Hence, experimental data revealed that VLL-28 exerts its action through a time-dependent activation of apoptotic cell pathways as demonstrated by the maturation of procaspase-3 to the caspase-3 (*30*). This is in agreement with data reported in the literature indicating that several potential ACPs are able to induce apoptosis in human cancer cell lines of different origin, such as breast, uterine cervix, liver and prostate (*9*). Apoptosis induction, with some degree of selectivity towards cancer cells, has been described also in the case of ACPs effective on metastatic tumor cells or on cancer endothelial cells (*9*). Since metastases are the main cause of conventional therapy failure, peptides able to specifically interfere with the process of metastases formation by stimulating apoptosis induction in neoplastic cells represent valuable resources in cancer treatment (*9*). These observations associated to the strong and selective toxic effects exerted by VLL-28 peptide towards cancer cells open interesting perspective to future applications of this peptide.

Concluding remarks

The cytotoxic activities of several AMPs turn this group of molecules into an amazing pool of new templates for anticancer drug development (*31*). Accordingly, VLL-28, previously identified as an AMP (*16*), is here found to be endowed also with selective cytotoxic activity towards both murine and human cancer cells, thus pointing to VLL-28 as a potential chemotherapeutic agent. Microorganisms belonging to the archaeal kingdom have been so far considered as source of biotechnologically relevant enzymes and proteins (*32-40*), but there are no reports regarding potential ACPs isolated from this kingdom. This paper represents the first evidence that archaeal microorganisms could bear also an unexplored repertoire of such kind of molecules exerting a trans-kingdom action. Given the intrinsic stability to physical and chemical agents of Stf76, the parental source of VLL-28, it is foreseen that VLL-28 might be a promising "lead compound" for future development of novel drugs, upon chemical modifications, *i.e.* D-amino acids, an all-hydrocarbon bridge, and/or modified amide bounds to further increase its stability to proteases (*41*).

Methods

Peptide Synthesis Reagents

Polypropylene reaction vessels and sintered polyethylene frits were supplied by Alltech Italia (Milan, Italy). NovaSyn TGR resin, 2-(1H-benzotriazole-1-yl)-1,1,3,3-tetramethyluronium hexafluorophosphate (HBTU), cyano-hydroxyimino-acetic acid ethyl ester (Oxyma) and all amino acids were purchased from Novabiochem-Merck (Nottingham, U.K.). N,N′-diisopropylethylamine (DIPEA), piperidine, Kaiser test, trifluoroacetic acid (TFA), scavengers, fluorescein isothiocyanate (FITC) and N-methylmorpholine (NMM) were purchased from Sigma-Aldrich (Milan, Italy). N,N-Dimethylformamide (DMF) was purchased from CARLO ERBA Reagents (Milan, Italy). Acetonitrile (ACN), dichloromethane (DCM) and diethyl ether were purchased from VWR International (Milan, Italy). All aqueous solutions were prepared by using water obtained from a Milli-Q gradient A-10 system (Millipore, 18.2 MΩ·cm, organic carbon content ≥ 4 μg/L).

Peptide Synthesis

VLL-28 and FITC-VLL-28 (VLL-28 derivative with an additional glycine residue at the C-terminus as spacer and a lysin residue for FITC labeling) peptides were manually synthesized using the fluorenylmethyloxycarbonyl (Fmoc) solid-phase strategy (0.2 mmol). The syntheses were performed on NovaSyn TGR resin (loading 0.24 mmol/g), using all standard amino acids. The Fmoc protecting group was removed by treatment with 30% piperidine in DMF (3 × 10 min). The amino acids in 10-fold excess were pre-activated with HBTU (9.8 equiv)/Oxyma (9.8 equiv)/DIPEA (10 equiv) in DMF for 5 min and then added to the resin suspended in DMF. The reaction was performed for 1 h and the coupling efficiency was assessed by the Kaiser test. In the case of FITC-VLL-28 peptide, once synthesis was completed, the ivDde protecting group of Lys(ivDde) residue was selectively removed by treatment of the peptidyl resin with a solution of 2% hydrazine in DMF (20 x 3 min). FITC labeling was then performed with 2 equiv of fluorescein isothiocyanate and 4 equiv of NMM in DMF for 5 h.

The peptides were finally cleaved off the resins by treatment with a mixture of trifluoroacetic acid (TFA)/water/triisopropylsilane (95:2.5:2.5 v/v/v) for 3 h at room temperature. The resins were filtered, the crude peptides were precipitated with diethyl ether, dissolved in H_2O/ACN solution, and lyophilized. The products were purified by preparative RP-HPLC on a Shimadzu system equipped with a UV−visible detector SPD10A using a Phenomenex Jupiter Proteo column (21.2 × 250 mm; 4 μm; 90 Å) and a linear gradient of H_2O (0.1% TFA)/ACN (0.1% TFA) from 10%–55% of ACN (0.1%TFA) in 15 min at a flow rate of 20 mL/min. The collected fractions containing the

peptides were lyophilized giving a final yield of about 35% of each pure product. The identity and purity of the compounds were assessed by the AGILENT Q-TOF LC/MS instrument equipped with a diode array detector combined with a dual ESI source on a Agilent C18 column (2.1 × 50 mm; 1.8 μm; 300 Å) at a flow rate of 200 μL/min and a linear gradient of H_2O (0.01% TFA)/ACN (0.01% TFA) from 5%–70% of ACN (0.01% TFA) in 15 min.

Cell culture

Malignant SVT2 murine fibroblasts (BALBc 3T3 cells transformed by SV40 virus), parental BALBc 3T3 murine cells, and HEK-293 human embryonic kidney cells were cultured in Dulbecco's Modified Eagle's Medium (Sigma-Aldrich), supplemented with 10% fetal bovine serum (HyClone), 2 mM L-glutamine and antibiotics, in a 5% CO_2 humidified atmosphere at 37 ºC. HRCE (Human Renal Cortical Epithelial) cells (Innoprot) were cultured in basal medium, supplemented with 2% fetal bovine serum, epithelial cell growth supplement and antibiotics, all from Innoprot, in a 5% CO_2 humidified atmosphere at 37 °C (*42*).

Cytotoxicity assays

Cells were seeded in 96-well plates (100 μL per well) at a density of $5x10^3$ per well (SVT2, HEK-293, and HRCE cells) or $2.5x10^3$ per well (BALBc 3T3 cells). VLL-28 peptide was added to the cells 24 h after seeding for time- and dose-dependent cytotoxic assays. At the end of incubation, cell viability was assessed by the MTT assay, as previously described(*43*). In brief, MTT reagent, dissolved in DMEM in the absence of phenol red (Sigma-Aldrich), was added to the cells (100 μL per well) to a final concentration of 0.5 mg/mL. After a 4-h incubation at 37 °C, the culture medium was removed and the resulting formazan salts were dissolved by adding isopropanol containing 0.1 N HCl (100 μL per well). Absorbance values of blue formazan were determined at 570 nm using an automatic plate reader (MicrobetaWallac 1420, Perkin Elmer). Cell survival was expressed as percentage of viable cells in the presence of the peptide, with respect to control cells grown in the absence of the peptide. In all of the experiments described in this paper, controls were performed by supplementing the cell cultures with identical volumes of peptide buffer for the same time span. Obtained data represent the mean (± standard deviation) of at least 4 independent experiments, each one carried out with triplicate determinations. Statistical analysis was performed using a Student's t-Test, and significant differences were indicated as *($P < 0.05$), **($P < 0.01$) or ***($P < 0.001$).

Analysis of cell death

Cells were plated in 6-well plates (1mL per well) at a density of $1x10^6$ cells per well in complete medium for 24 h and then exposed to 20 μM VLL-28 for 6, 12 or 24 h To prepare cell lysates, both untreated and treated cells were scraped off in PBS, centrifuged at 1,000 x *g* for 10 min and resuspended in lysis buffer (1% NP-40 in PBS, pH 7.4) containing protease inhibitors. After 30 min of incubation on ice, lysates were centrifuged at 14,000 x *g* for 30 min at 4 °C. Upon determination of total protein concentration in the supernatant by the Bradford assay, samples were analyzed by SDS-PAGE followed by Western blotting using specific antibodies directed towards procaspase-3 (Cell Signaling Technology) or p62 (Novus Biologicals) proteins. For normalization to internal standard signals, antibodies against β-actin (Sigma-Aldrich) were used. In parallel experiments, cells were treated with puromycin (10 μg/mL) for 12 h or with rapamycin (20 μM) for 24 h, which were used as positive controls for apoptosis and autophagy induction, respectively.

For morphological analyses, cells were seeded on glass coverslips in 24-well plates and grown to semi-confluency. Cells were then incubated for 72 h with 20 μM VLL-28 peptide in complete medium, after which cells were washed with PBS, fixed for 10 min at room temperature (RT) with 4% paraformaldehyde in PBS and mounted in 50% glycerol in PBS. Samples were then examined

using a confocal laser-scanner microscope Zeiss LSM 700. All images were taken under identical conditions.

Fluorescence studies

Fluorescence analyses were performed as previously described (*44*). Briefly, cells were seeded on glass coverslips in 24-well plates, grown to semi-confluency, and then incubated for 12 h with 20 μM FITC-labeled VLL-28. Following incubation, cells were washed with PBS and then fixed for 10 min at RT with 4% paraformaldehyde in PBS. Cell membranes were labeled by incubating the cells with Wheat Germ Agglutinin (WGA, 5 μg/mL) Alexa Fluor®594 Conjugate (ThermoFisher Scientific) for 10 min at RT. Cells were then washed twice in PBS following the manufacturer's instructions. Confocal microscopy analyses were performed with a confocal laser-scanner microscope Zeiss LSM 700.

Circular dichroism analyses

Far-UV CD spectra were recorded on a Jasco J-810 spectropolarimeter (JASCO Corp) equipped with a PTC-423S/15 peltier temperature controller in the wavelength interval of 198–260 nm. Experiments were performed using a 20 μM VLL-28 solution (in PBS pH7.4) in a 0.1 cm path-length quartz cuvette as already reported in Notomista et al.(*16*)
CD spectra in the presence of intact cells were registered using 8 10^5 BALBc 3T3 cells or SVT2 cells at different incubation times (0, 10, 30, 60 min and 24 h) in PBS buffer. The baseline was corrected by subtracting the spectrum of the cells alone at the same time of incubation. (*41, 45, 46*)

Membrane preparation

Membranes used in NMR experiments were isolated from BALBc 3T3 or SVT2 cells and obtained as reported in Farina *et al*. (*21*). In details, cells were detached from the flask with trypsin and washed twice with PBS. Then the cells were transferred into homogenization buffer containing PBS and homogenized by means of a pellet pestle (Sigma). Particulate matter was removed by centrifuging at 3,500 rpm for 15 min. The supernatant was then centrifuged at 28000 rpm for 1 h at 4 °C. The pellet was washed and centrifuged at 28000 rpm for 30 min at 4 °C. 180 μL of PBS plus 20 μL D_2O were added to the pellet, and the membrane was re-suspended by 20 passages through a 25 gauge needle.

NMR spectroscopy
All NMR experiments were carried out at 298K using an Inova 600 MHz spectrometer (Varian Inc., Palo Alto, CA, USA), equipped with a cryogenic probe optimized for ^1H detection.
NMR samples were prepared as follows. For chemical shift assignment and conformational analysis, 1 mg of VLL-28 was dissolved either in 500 μL sodium phosphate 20 mM pH 7.0 with 10% v/v D_2O or in 500 μL of the same buffer containing 25% (v/v) TFE (2,2,2-trifluoroethanol-D3 99.5% isotopic purity, Sigma-Aldrich). One-dimensional (1D) ^1H spectra were acquired with a spectral width of 7191.66 Hz, relaxation delay 1.03 s, 7k data points for acquisition and 16k for transformation. Bi-dimensional (2D) [^1H, ^1H] total correlation spectroscopy (TOCSY),(*47*) double quantum filtered correlated spectroscopy (COSY)(*48*) and nuclear Overhauser effect spectroscopy (NOESY) (*49*) were acquired with 32 or 64 scans per t1 increment with a spectral width of 7191.66 Hz along both t1 and t2, 2048 × 256 data points in t2 and t1, respectively, and recycle delay 1.0 s. Water suppression was achieved by means of Double Pulsed Field Gradient Spin Echo (DPFGSE) sequence.(*50, 51*) TOCSY experiments were recorded using a DIPSI-2 mixing scheme of 70 ms with 7.7 kHz spin-lock field strength. NOESY spectra were carried out with a mixing time of 250

ms. Data were typically apodized with a square cosine window function and zero filled to a matrix of size 4096 × 1024 before Fourier transformation and baseline correction.
According to the procedure recently reported (*21*) for interaction studies of VLL-28 with intact cells and isolated membranes of BALBc 3T3 and SVT2 cell lines, pellet of 18 x 10^6 cells and membranes from 18 x 10^6 cells, obtained as reported above, were re-suspended in 150 μL of PBS buffer (pH 7.4) and 10% ^2H_2O, to obtain reference spectra, or of VLL-8 (430 μM) in PBS buffer. STD spectra were acquired with 10000 scans with on-resonance irradiation at 0.2 ppm or 5.2 ppm for saturation of membrane proteins or lipids resonances, respectively, and off-resonance irradiation at 30 ppm. A train of 40 Gaussian shaped pulses of 50 ms with 1 ms delay between pulses were used, for a total saturation time of 2 s. STD spectra were obtained by internal subtraction of saturated spectrum from off-resonance spectrum by phase cycling. STD spectrum of the only peptide was also acquired and did not show any signal. 2D [^{1}H, ^{1}H] TOCSY and NOESY spectra of VLL-28 in presence of isolated membranes were also acquired, similarly to those of the peptide alone.
All NMR data were processed with the software VNMRJ 1.1.D (Varian Inc.). 1D spectra were analyzed using ACD/NMR Processor 12.0 [www.acdlabs.com]. 2D TOCSY, COSY and NOESY spectra for proton chemical shift assignment were analyzed using Homoscope, a tool available in CARA (Computer Aided Resonance Assignment) software. Chemical shift assignments of VLL-28 in the absence of TFE are referred to residual water proton signals, (4.75 ppm), whereas in 25% TFE to residual TFE proton signals (3.88 ppm). Chemical shift deviations from random coil values for Hα were calculated using the ChemShiftDeviationsFile script available in CARA.

Zeta-Potential measurements of bacterial and eukaryotic cells in the presence of VLL-28

BL21 DE3 *E. coli* cells were plated on Luria-Bertani agar overnight at 37 °C. An isolated bacterial colony was used to inoculate Mueller Hinton Broth (MHB; OXOID, Hampshire, UK), and the bacterial culture was allowed to grow overnight at 37 °C. 100 μL of culture was used to freshly inoculate 5 ml of MHB. The suspension was incubated at 37 °C for ~ 2 h, until a final bacterial concentration of ~ 3 × 10^8 colony forming units per ml (CFU/mL) was reached (OD_{600nm} ~ 0.1). Bacterial suspensions were diluted using fresh MHB to 3 × 10^7 CFU/mL for zeta-potential studies. Afterwards, cells were centrifuged at 12,000 × *g* for 5 min, and washed three times using 20 mM sodium phosphates buffer, pH 7.4. The zeta-potential of bacterial cells was determined at 25 °C from the mean of 3 measurements (50 runs each), in the absence and presence of different VLL-28 concentrations (0-10 μM). Zeta-potential values were obtained by phase analysis light scattering (PALS) in a Zetasizer Nano ZS (Malvern Instruments, Malvern, UK), using disposable zeta cells with gold electrodes. Values of viscosity and refractive index were set to 0.8872 cP and 1.330, respectively.
Confluent BALBc 3T3 and SVT2 cells were washed with PBS buffer followed by trypsinization. Zeta potential measurements of eukaryotic cells were performed using the Diffusion Barrier Technique (Malvern, Application Note). 4x10^5 cells were dispensed into the disposable zeta cells with gold electrodes in PBS with and without the peptide (from 0 to 50 μM) and allowed to equilibrate for 30 min at 37°C. One measurement (~70 runs each) was performed with a constant voltage of 40 V. The complete experiment was carried out at least two times using independent cellular suspensions.

Figure legends

Figure 1. Effects of the peptide VLL-28 on the SVT2 (a) and BALBc 3T3 (b) cell viability. MTT assays were performed on cells treated with increasing amounts of the peptide (5, 10 and 20 μM) for different time spans (24, 48 and 72 h). The viability of cell samples was expressed as the percentage of MTT reduction with respect to control cells, tested under the same conditions but in

the absence of the peptide. Data represent the mean (± standard deviation, SD) of at least 4 independent experiments, each one carried out with triplicate determinations. *P < 0.05, **P < 0.01, or ***P < 0.001 were obtained for control versus treated samples in the case of SVT2 cells treated with VLL-28 peptide for 48 and 72 h.

Figure 2. Internalization of VLL-28 peptide in SVT2 (a) and BALBc 3T3 (b) cells. Cells were cultured on coverslips, incubated for 12 h with 20 μM VLL-28 peptide (green) and stained with WGA (5 μg/ml, Alexa Fluor®594 Conjugate). Cells were analyzed by confocal microscopy.

Figure 3. Far UV VLL-28 CD spectra (●) recorded in the presence of a) BALBc 3T3 cells and b) SVT2 cells at 0 (■), 10 (▲), 30 (♦), 60 (∗) min and 24 h (○) of incubation.

Figure 4. (a) Chemical shift deviation from random coil values of Hα backbone atoms (ΔHα) plotted as a function of residue number. Two segments with helical conformation encompassing residues V37-R58, V50-S59, as suggested from the ΔHαs, are indicated above the plot. (b) and (c) Expansions of the H_N-H_N correlation region of the 2D [^{1}H, ^{1}H] NOESY spectra of VLL-28 in phosphate buffer pH 7.0 at 298K in the absence and presence of TFE 25%, respectively. HN_i-HN_{i+1} cross-peaks, observed only in (C), are labeled.

Figure 5. Reference ^{1}H (a) and (STD)-NMR spectra of VLL-28 in the absence (b) and in the presence of SVT2 (C) and BALBc 3T3 (D) cell membranes.

Figure 6. (a) Bar graphs of STD signal intensities (I_{STD}) for the VLL-28 H^N/aromatic and aliphatic protons receiving saturation transfer in the presence of BALBc 3T3 (red bars) and SVT2 (blue bars) cell membranes. In the x-axis label, HNbb=not assigned backbone amide protons, R = R44/R48/R53/R61/R64; K = K54/K64; Y = Y52/Y63; L = L38/L39/L45; T = T41/T43. (b) The VLL-28 sequence is reported. VLL-28 residues showing STD effect in the presence of the both cell membranes are highlighted in magenta, whereas those affected only in the presence of BALBc 3T3 in red. Asterisk indicates that, due to overlapped proton resonances, one or both the threonine are possibly involved in the interaction with BALBc 3T3 and SVT2 cell membranes. Residues that are not involved in the binding or that could not be identified unambiguously are indicated in black.

Figure 7. a) VLL-28 effect on the Z-potential of SVT2 cells. b) VLL-28 effect on the Z-potential of BALBc 3T3 cells. At 4x10^{5}cells/mL cells were incubated and stabilized for 5 min with different peptide concentrations and the potential was measured at 37°C. Data represent the mean (± standard deviation, SD) of 2 independent experiments.

Figure 8. Analysis of cell death pathway activated by the treatment with 20 μM VLL-28 peptide of SVT2 (a) and BALBc 3T3 (c) cells. Lane 1, cell lysate of untreated cells; lane 2, lysate of cells treated with rapamycin; lane 3, lysate of cells treated with puromycin; lane 4, lysate of cells treated with the peptide for 6 h; lane 5, lysate of cells treated with the peptide for 12 h; lane 6, lysate of cells treated with the peptide for 24 h. Western blots were performed by using antibodies directed towards procaspase-3, p62, and endogenous β-actin used as an internal standard (a, c). Densitometric analyses of protein bands specifically recognized by anti-procaspase-3 and anti-p62 antibodies are reported in b and d, respectively, where data represent the mean (± standard deviation, SD) of 3 independent experiments. *P < 0.05, **P < 0.01, or ***P < 0.001 were obtained for control *versus* treated samples.

References

1. Mansour, S. C., Pena, O. M., and Hancock, R. E. (2014) Host defense peptides: front-line immunomodulators, *Trends Immunol 35*, 443-450.
2. Wiesner, J., and Vilcinskas, A. (2010) Antimicrobial peptides: the ancient arm of the human immune system, *Virulence 1*, 440-464.
3. Hilchie, A. L., Wuerth, K., and Hancock, R. E. W. (2013) Immune modulation by multifaceted cationic host defense (antimicrobial) peptides, *Nat Chem Biol 9*, 761-768.
4. Mulder, K. C. L., Lima, L. A., Miranda, V. J., Dias, S. C., and Franco, O. L. (2013) Current scenario of peptide-based drugs: the key roles of cationic antitumor and antiviral peptides, *Front Microbiol 4*.
5. Pushpanathan, M., Gunasekaran, P., and Rajendhran, J. (2013) Antimicrobial peptides: versatile biological properties, *Int J Pept 2013*, 675391.
6. Riedl, S., Zweytick, D., and Lohner, K. (2011) Membrane-active host defense peptides - Challenges and perspectives for the development of novel anticancer drugs, *Chem Phys Lipids 164*, 766-781.
7. Hancock, R. E. W., Haney, E. F., and Gill, E. E. (2016) The immunology of host defence peptides: beyond antimicrobial activity, *Nat Rev Immunol 16*, 321-334.
8. Teixeira, V., Feio, M. J., and Bastos, M. (2012) Role of lipids in the interaction of antimicrobial peptides with membranes, *Prog Lipid Res 51*, 149-177.
9. Gaspar, D., Veiga, A. S., and Castanho, M. R. B. (2013) From antimicrobial to anticancer peptides. A review, *Front Microbiol 4*.
10. Gabernet, G., Muller, A. T., Hiss, J. A., and Schneider, G. (2016) Membranolytic anticancer peptides, *Medchemcomm 7*, 2232-2245.
11. Rerole, A. L., Gobbo, J., De Thonel, A., Schmitt, E., Pais de Barros, J. P., Hammann, A., Lanneau, D., Fourmaux, E., Demidov, O. N., Micheau, O., Lagrost, L., Colas, P., Kroemer, G., and Garrido, C. (2011) Peptides and aptamers targeting HSP70: a novel approach for anticancer chemotherapy, *Cancer Res 71*, 484-495.
12. Kuriyama, I., Miyazaki, A., Tsuda, Y., Yoshida, H., and Mizushina, Y. (2013) Inhibitory effect of novel somatostatin peptide analogues on human cancer cell growth based on the selective inhibition of DNA polymerase beta, *Bioorgan Med Chem 21*, 403-411.
13. Pane, K., Durante, L., Crescenzi, O., Cafaro, V., Pizzo, E., Varcamonti, M., Zanfardino, A., Izzo, V., Di Donato, A., and Notomista, E. (2017) Antimicrobial potency of cationic antimicrobial peptides can be predicted from their amino acid composition: Application to the detection of "cryptic" antimicrobial peptides, *J Theor Biol 419*, 254-265.
14. Gaglione, R., Dell'Olmo, E., Bosso, A., Chino, M., Pane, K., Ascione, F., Itri, F., Caserta, S., Amoresano, A., Lombardi, A., Haagsman, H. P., Piccoli, R., Pizzo, E., Veldhuizen, E. J., Notomista, E., and Arciello, A. (2017) Novel human bioactive peptides identified in apolipoprotein B: evaluation of their therapeutic potential, *Biochem Pharmacol*.
15. Pane, K., Sgambati, V., Zanfardino, A., Smaldone, G., Cafaro, V., Angrisano, T., Pedone, E., Di Gaetano, S., Capasso, D., Haney, E. F., Izzo, V., Varcamonti, M., Notomista, E., Hancock, R. E. W., Di Donato, A., and Pizzo, E. (2016) A new cryptic cationic antimicrobial peptide from human apolipoprotein E with antibacterial activity and immunomodulatory effects on human cells, *Febs Journal 283*, 2115-2131.
16. Notomista, E., Falanga, A., Fusco, S., Pirone, L., Zanfardino, A., Galdiero, S., Varcamonti, M., Pedone, E., and Contursi, P. (2015) The identification of a novel Sulfolobus islandicus CAMP-like peptide points to archaeal microorganisms as cell factories for the production of antimicrobial molecules, *Microb Cell Fact 14*.
17. Contursi, P., Farina, B., Pirone, L., Fusco, S., Russo, L., Bartolucci, S., Fattorusso, R., and Pedone, E. (2014) Structural and functional studies of Stf76 from the Sulfolobus islandicus plasmid-virus pSSVx: a novel peculiar member of the winged helix-turn-helix transcription factor family, *Nucleic Acids Res 42*, 5993-6011.
18. Hoskin, D. W., and Ramamoorthy, A. (2008) Studies on anticancer activities of antimicrobial peptides, *Bba-Biomembranes 1778*, 357-375.
19. Schweizer, F. (2009) Cationic amphiphilic peptides with cancer-selective toxicity, *Eur J Pharmacol 625*, 190-194.

20. Malgieri, G., Avitabile, C., Palmieri, M., D'Andrea, L. D., Isernia, C., Romanelli, A., and Fattorusso, R. (2015) Structural Basis of a Temporin 1b Analogue Antimicrobial Activity against Gram Negative Bacteria Determined by CD and NMR Techniques in Cellular Environment, *Acs Chemical Biology 10*, 965-969.
21. Farina, B., de Paola, I., Russo, L., Capasso, D., Liguoro, A., Del Gatto, A., Saviano, M., Pedone, P. V., Di Gaetano, S., Malgieri, G., Zaccaro, L., and Fattorusso, R. (2016) A Combined NMR and Computational Approach to Determine the RGDechi-hCit-alpha(v)beta(3) Integrin Recognition Mode in Isolated Cell Membranes, *Chem-Eur J 22*, 681-693.
22. Pan, X., Wilson, M., McConville, C., Brundler, M.-A., Arvanitis, T. N., Shockcor, J. P., Griffin, J. L., Kauppinen, R. A., and Peet, A. C. (2012) The lipid composition of isolated cytoplasmic lipid droplets from a human cancer cell line, BE(2)M17, *Mol Biosyst 8*, 1694-1700.
23. Halder, S., Yadav, K. K., Sarkar, R., Mukherjee, S., Saha, P., Haldar, S., Karmakar, S., and Sen, T. (2015) Alteration of Zeta potential and membrane permeability in bacteria: a study with cationic agents, *Springerplus 4*.
24. Hancock, R. E. W., and Sahl, H. G. (2006) Antimicrobial and host-defense peptides as new anti-infective therapeutic strategies, *Nat Biotechnol 24*, 1551-1557.
25. Gaspar, D., Freire, J. M., Pacheco, T. R., Barata, J. T., and Castanho, M. A. R. B. (2015) Apoptotic human neutrophil peptide-1 anti-tumor activity revealed by cellular biomechanics, *Bba-Mol Cell Res 1853*, 308-316.
26. Gaspar, D., Veiga, A. S., Sinthuvanich, C., Schneider, J. P., and Castanho, M. A. R. B. (2012) Anticancer Peptide SVS-1: Efficacy Precedes Membrane Neutralization, *Biochemistry 51*, 6263-6265.
27. Elmore, S. (2007) Apoptosis: A review of programmed cell death, *Toxicol Pathol 35*, 495-516.
28. Bjorkoy, G., Lamark, T., Pankiv, S., Overvatn, A., Brech, A., and Johansen, T. (2009) Monitoring Autophagic Degradation of P62/Sqstm1, *Methods in Enzymology: Autophagy in Mammalian Systems, Vol 452, Pt B 452*, 181-197.
29. Gonzalez-Rodriguez, A., Mayoral, R., Agra, N., Valdecantos, M. P., Pardo, V., Miquilena-Colina, M. E., Vargas-Castrillon, J., Lo Iacono, O., Corazzari, M., Fimia, G. M., Piacentini, M., Muntane, J., Bosca, L., Garcia-Monzon, C., Martin-Sanz, P., and Valverde, A. M. (2014) Impaired autophagic flux is associated with increased endoplasmic reticulum stress during the development of NAFLD, *Cell Death Dis 5*.
30. Huang, Y., Feng, Q., Yan, Q., Hao, X., and Chen, Y. (2015) Alpha-helical cationic anticancer peptides: a promising candidate for novel anticancer drugs, *Mini Rev Med Chem 15*, 73-81.
31. Gaspar D., C. M. A. R. B., (Ed.) (2016) *Host Defense Peptides and Their Potential as Therapeutic Agents*, Springer International Publishing Switzerland R.M. Epand ed.
32. Prato, S., Vitale, R. M., Contursi, P., Lipps, G., Saviano, M., Rossi, M., and Bartolucci, S. (2008) Molecular modeling and functional characterization of the monomeric primase-polymerase domain from the Sulfolobus solfataricus plasmid pIT3, *Febs J 275*, 4389-4402.
33. Fusco, S., She, Q., Bartolucci, S., and Contursi, P. (2013) T(lys), a newly identified Sulfolobus spindle-shaped virus 1 transcript expressed in the lysogenic state, encodes a DNA-binding protein interacting at the promoters of the early genes, *J Virol 87*, 5926-5936.
34. Fusco, S., She, Q. X., Fiorentino, G., Bartolucci, S., and Contursi, P. (2015) Unravelling the Role of the F55 Regulator in the Transition from Lysogeny to UV Induction of Sulfolobus Spindle-Shaped Virus 1, *J Virol 89*, 6453-6461.
35. Fusco, S., Aulitto, M., Bartolucci, S., and Contursi, P. (2015) A standardized protocol for the UV induction of Sulfolobus spindle-shaped virus 1, *Extremophiles 19*, 539-546.
36. Contursi, P., Fusco, S., Cannio, R., and She, Q. X. (2014) Molecular biology of fuselloviruses and their satellites, *Extremophiles 18*, 473-489.
37. Contursi, P., Fusco, S., Limauro, D., and Fiorentino, G. (2013) Host and viral transcriptional regulators in Sulfolobus: an overview, *Extremophiles 17*, 881-895.
38. Bartolucci, S., Contursi, P., Fiorentino, G., Limauro, D., and Pedone, E. (2013) Responding to toxic compounds: a genomic and functional overview of Archaea, *Front Biosci (Landmark Ed) 18*, 165-189.

39. Contursi, P., Cannio, R., and She, Q. X. (2010) Transcription termination in the plasmid/virus hybrid pSSVx from Sulfolobus islandicus, *Extremophiles 14*, 453-463.
40. Prato, S., Cannio, R., Klenk, H. P., Contursi, P., Rossi, M., and Bartolucci, S. (2006) pIT3, a cryptic plasmid isolated from the hyperthermophilic crenarchaeon Sulfolobus solfataricus IT3, *Plasmid 56*, 35-45.
41. de Paola, I., Pirone, L., Palmieri, M., Balasco, N., Esposito, L., Russo, L., Mazza, D., Di Marcotullio, L., Di Gaetano, S., Malgieri, G., Vitagliano, L., Pedone, E., and Zaccaro, L. (2015) Cullin3-BTB Interface: A Novel Target for Stapled Peptides, *PLoS One 10*.
42. Galano, E., Arciello, A., Piccoli, R., Monti, D. M., and Amoresano, A. (2014) A proteomic approach to investigate the effects of cadmium and lead on human primary renal cells, *Metallomics 6*, 587-597.
43. Monti, D. M., Guarnieri, D., Napolitano, G., Piccoli, R., Netti, P., Fusco, S., and Arciello, A. (2015) Biocompatibility, uptake and endocytosis pathways of polystyrene nanoparticles in primary human renal epithelial cells, *J Biotechnol 193*, 3-10.
44. Arciello, A., De Marco, N., Del Giudice, R., Guglielmi, F., Pucci, P., Relini, A., Monti, D. M., and Piccoli, R. (2011) Insights into the fate of the N-terminal amyloidogenic polypeptide of ApoA-I in cultured target cells, *J Cell Mol Med 15*, 2652-2663.
45. Smaldone, G., Diana, D., Pollegioni, L., Di Gaetano, S., Fattorusso, R., and Pedone, E. (2015) Insight into conformational modification of alpha-synuclein in the presence of neuronal whole cells and of their isolated membranes, *FEBS Lett 589*, 798-804.
46. Correale, S., Esposito, C., Pirone, L., Vitagliano, L., Gaetano, S. D., and Pedone, E. (2013) A biophysical characterization of the folded domains of KCTD12: insights into interaction with the GABAB2 receptor, *J Mol Recognit 26*, 488-495.
47. Bax, A., and Davis, D. G. (1985) Mlev-17-Based Two-Dimensional Homonuclear Magnetization Transfer Spectroscopy, *J Magn Reson 65*, 355-360.
48. Rance, M., Sorensen, O. W., Bodenhausen, G., Wagner, G., Ernst, R. R., and Wuthrich, K. (1983) Improved spectral resolution in cosy 1H NMR spectra of proteins via double quantum filtering, *Biochem Biophys Res Commun 117*, 479-485.
49. Kumar, A., Ernst, R. R., and Wuthrich, K. (1980) A two-dimensional nuclear Overhauser enhancement (2D NOE) experiment for the elucidation of complete proton-proton cross-relaxation networks in biological macromolecules, *Biochem Biophys Res Commun 95*, 1-6.
50. Hwang, T. L., and Shaka, A. J. (1995) Water Suppression That Works - Excitation Sculpting Using Arbitrary Wave-Forms and Pulsed-Field Gradients, *J Magn Reson Ser A 112*, 275-279.
51. Dalvit, C. (1998) Efficient multiple-solvent suppression for the study of the interactions of organic solvents with biomolecules, *J Biomol NMR 11*, 437-444.

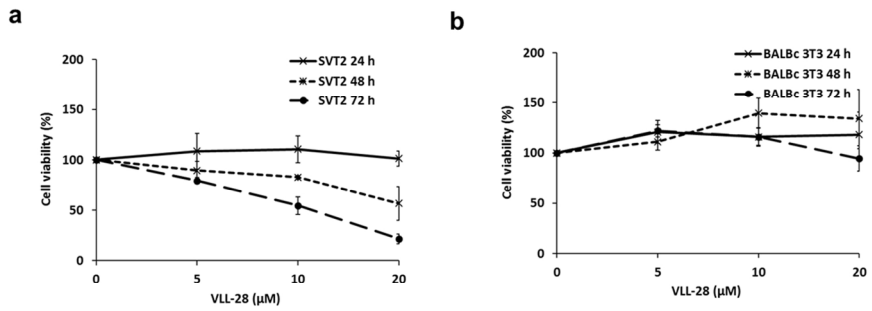

Figure 1

Figure 1

190x107mm (300 x 300 DPI)

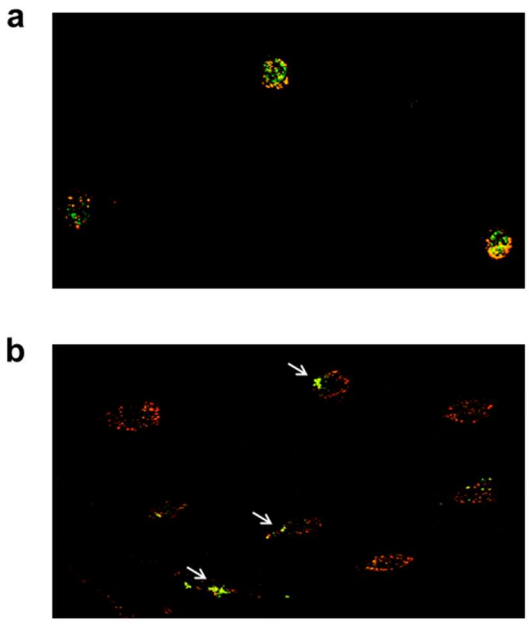

Figure 2

Figure 2

190x142mm (300 x 300 DPI)

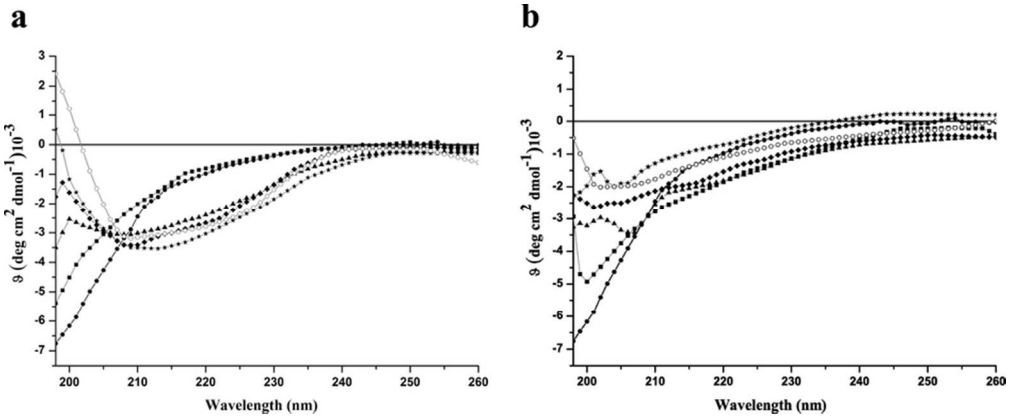

Figure 3

79x32mm (300 x 300 DPI)

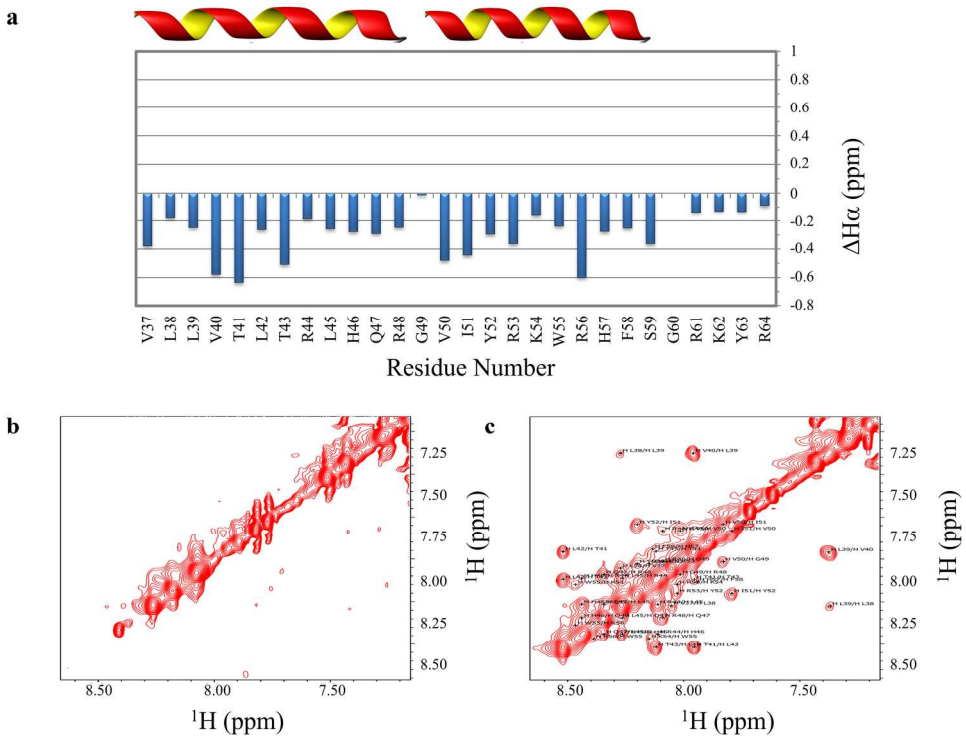

Figure 4

190x142mm (300 x 300 DPI)

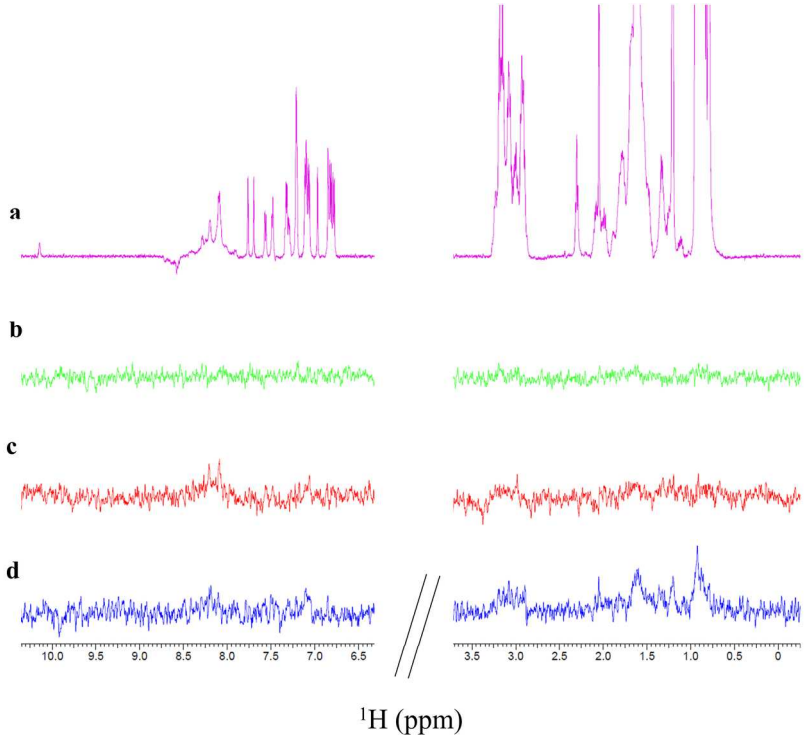

Figure 5

190x142mm (300 x 300 DPI)

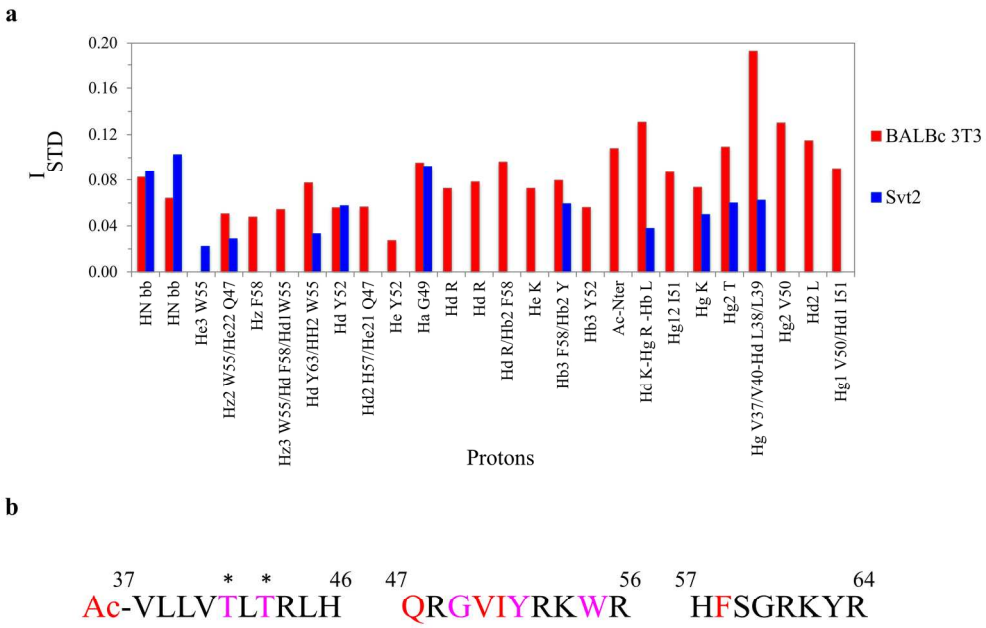

190x142mm (300 x 300 DPI)

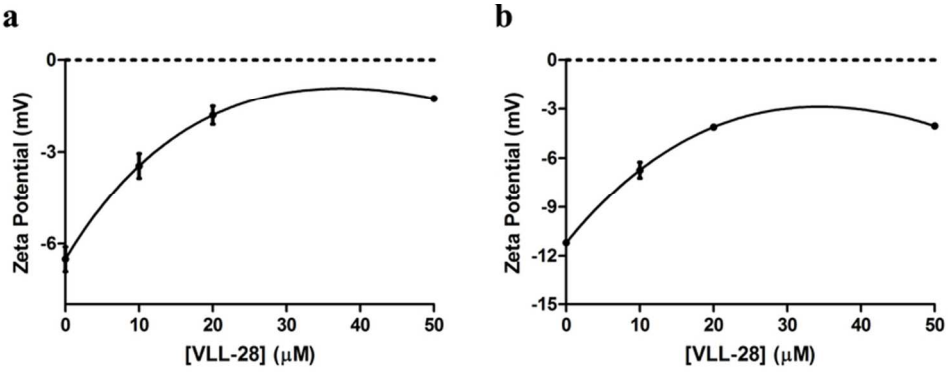

Figure 7

74x28mm (300 x 300 DPI)

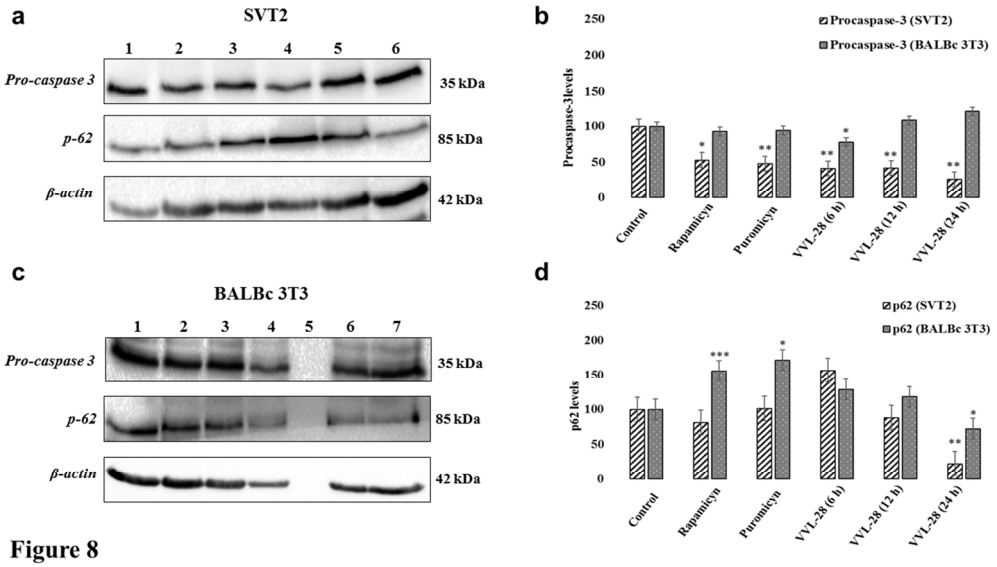

Figure 8

Figure 8

190x107mm (300 x 300 DPI)